

METAL COMPLEXES OF 1,4,7-TRIAZACYCLONONANE WITH PENDANT DONOR ARMS

Paul Alexander Lovatt (B.Sc.)

A thesis submitted for the degree of Doctor of Philosophy



**UNIVERSITY
of
GLASGOW**

ProQuest Number: 13815501

All rights reserved

INFORMATION TO ALL USERS

The quality of this reproduction is dependent upon the quality of the copy submitted.

In the unlikely event that the author did not send a complete manuscript and there are missing pages, these will be noted. Also, if material had to be removed, a note will indicate the deletion.



ProQuest 13815501

Published by ProQuest LLC (2018). Copyright of the Dissertation is held by the Author.

All rights reserved.

This work is protected against unauthorized copying under Title 17, United States Code
Microform Edition © ProQuest LLC.

ProQuest LLC.
789 East Eisenhower Parkway
P.O. Box 1346
Ann Arbor, MI 48106 – 1346

Thesis
10824
Copy 1

“I haven’t lost it, I just don’t know where it is”

Bob Peacock

ACKNOWLEDGEMENTS

A number of people must be thanked, without whom this thesis would not be possible. Foremost, I would like to thank my supervisors, Dr. Robert D. Peacock and Dr Louis J. Farrugia for their patience and encouragement over the last few years. Thanks to Dr Louis J Farrugia for the crystallographic work; Dr. A. Harrison and Dr G. Whittacker (University of Edinburgh) for the squid magnetic measurements; Dr D Ellis who crystallised the phosphine complexes.

I would also like to thank my friends and inmates of A4-30 who helped make the past three years enjoyable; Alan K “Aldo”, Nicola “Nicky”, Elaine, Mark, Colin, Simon M, Alan C “Chambie”, Sarah, Bob H, Dave A, Norman, John, Ron, Iain “Santa”, Campbell “greasy biker dude”, Davie K “Big Dave”, Rosie “Rosie”, Simon W “Fatboy”, Phil “Postman Pat” and Graham “Cairnsy”.

Finally, I must thank my parents for their support and generosity throughout my academic career.

ABBREVIATIONS

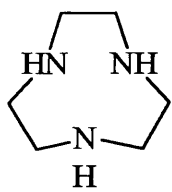
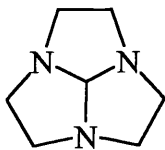
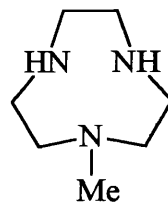
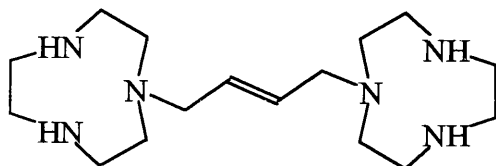
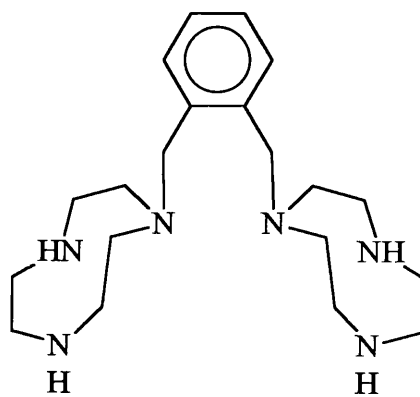
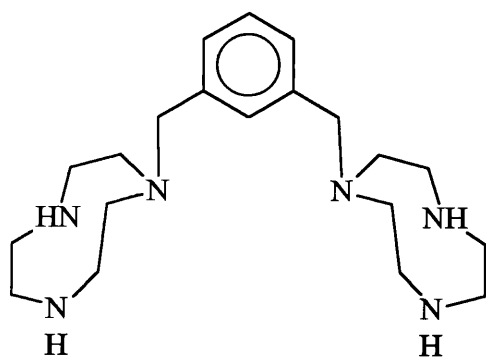
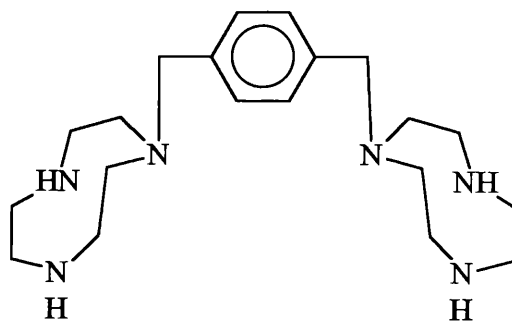
1 ^y	primary
2 ^y	secondary
3 ^y	tertiary
AMP	adenosine monophosphoric acid
b	broad
d	doublet
en	ethylene diamine
EPR	electron paramagnetic resonance
EtOH	ethanol
Et ₂ O	diethyl ether
Hc	haemocyanin
IR	infra-red
LFSE	ligand field stabilisation energy
LMCT	ligand to metal charge transfer
m	multiplet
MeCN	acetonitrile
MeOH	methanol
M.pt.	melting point
nb	norbornene

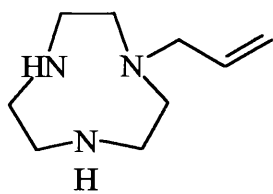
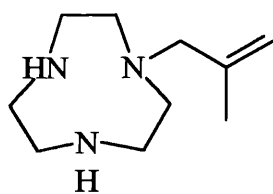
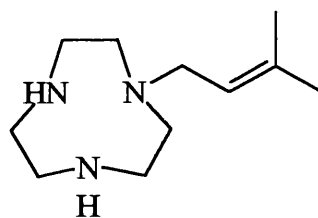
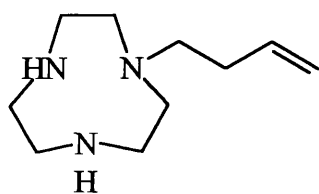
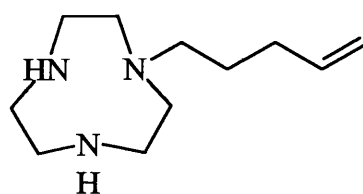
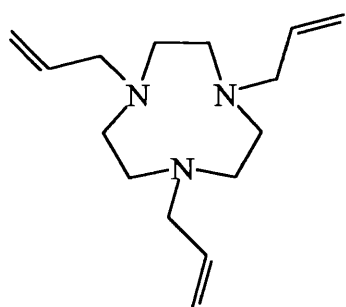
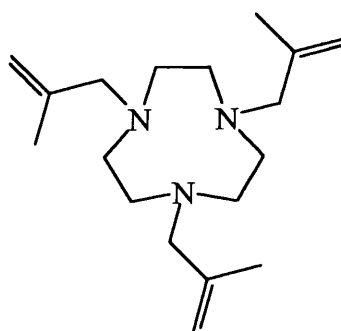
NMR	nuclear magnetic resonance
Oxy-Hc	oxygenated haemocyanin
ppm	parts per million
s	singlet
t	triplet
tosyl (Ts)	p-tolyl sulphonyl
Tr	triphenylmethyl
UV	ultra-violet
VIS	visible

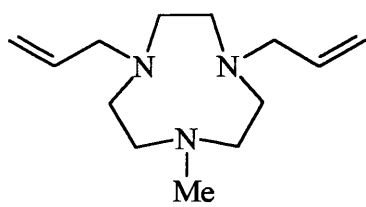
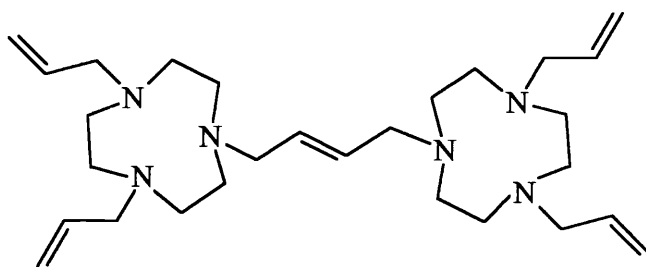
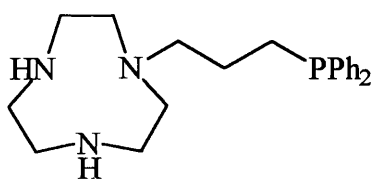
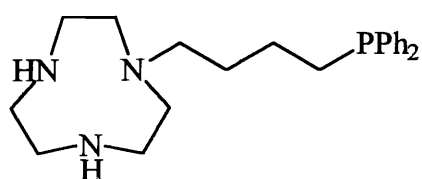
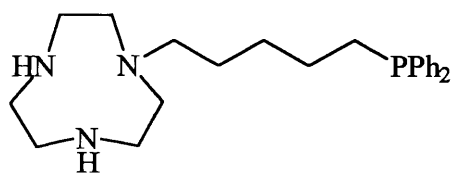
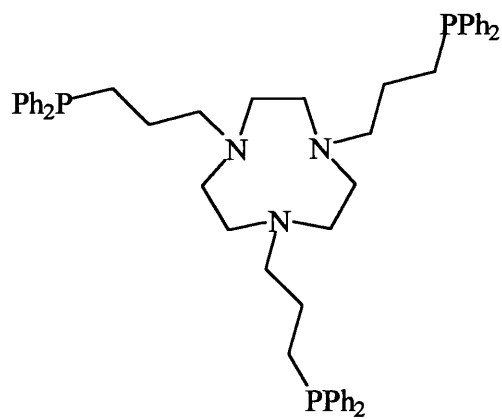
LIGANDS

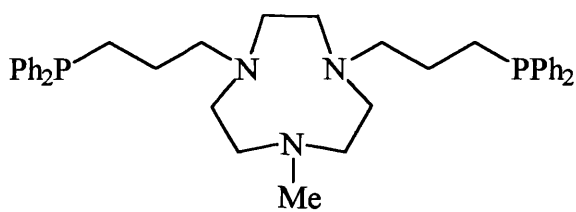
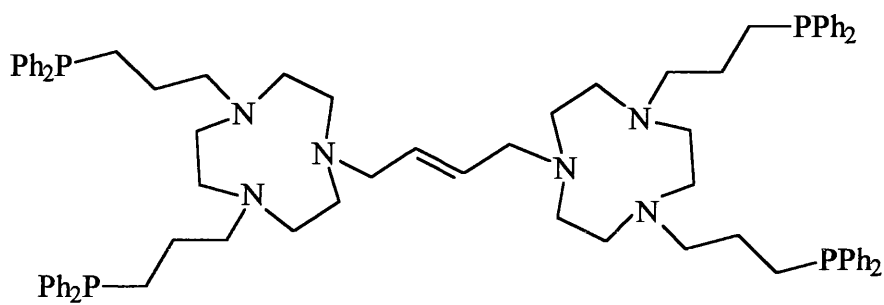
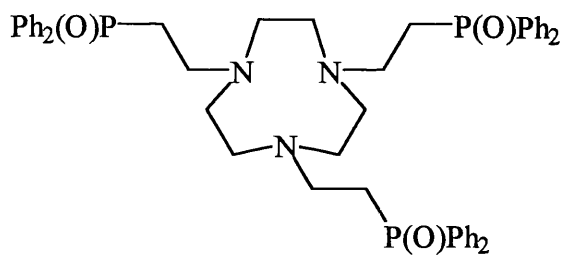
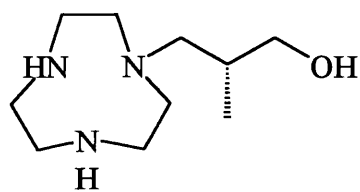
[9]aneN ₃	1,4,7-triazacyclononane
[10]aneN ₃	1,4,7-triazacyclodecane
[11]aneN ₃	1,4,7-triazacycloundecane
[12]aneN ₃	1,5,9-triazacyclododecane
Bn ₃ TACN	<i>N,N',N''</i> -tribenzyl-1,4,7-triazacyclononane
cyclam	1,4,8,11-tetrazacyclotetradecane
L ^{mes}	<i>N</i> -(2-mesitylethyl)-1,4,7-triazacyclononane
mmtp	1,1,1-tris(dimethylphosphinomethyl)ethane
Me ₃ TACN	<i>N,N',N''</i> -trimethyl-1,4,7-triazacyclononane
TACN	1,4,7-triazacyclononane
tmen	<i>N,N,N',N'</i> -tetramethylethylenediamine
teen	<i>N,N,N',N'</i> -tetraethylethylenediamine
L ¹	1,4,7-Triazatricyclo[5.2.1.0 ^{4,10}]decane
L ²	<i>N</i> -Methyl-1,4,7-triazacyclononane
L ³	Trans-1,4-bis(1,4,7-triazacyclononane)but-2-ene
L ⁴	α,α' -Bis(1,4,7-triazacyclononane)- <i>ortho</i> -xylene
L ⁵	α,α' -Bis(1,4,7-triazacyclononane)- <i>meta</i> -xylene
L ⁶	α,α' -Bis(1,4,7-triazacyclononane)- <i>para</i> -xylene
L ⁷	<i>N</i> -Allyl-1,4,7-triazacyclononane

L ⁸	<i>N</i> -3-(2-Methylprop-1-ene)-1,4,7-triazacyclononane
L ⁹	<i>N</i> -4-(2-Methylbut-2-ene)-1,4,7-triazacyclononane
L ¹⁰	<i>N</i> -4-But-1-ene-1,4,7-triazacyclononane
L ¹¹	<i>N</i> -5-Pent-1-ene-1,4,7-triazacyclononane
L ¹²	<i>N,N',N''</i> -Triallyl-1,4,7-triazacyclononane
L ¹³	<i>N,N',N''</i> -Tris(2-methylprop-1-ene)-1,4,7-triazacyclononane
L ¹⁴	<i>N</i> -Methyl- <i>N',N''</i> -diallyl-1,4,7-triazacyclononane
L ¹⁵	Trans-1,4-bis[<i>N,N'</i> -diallyl-1,4,7-triazacyclononane]but-2-ene
L ¹⁶	<i>N</i> -Diphenylphosphinopropyl-1,4,7-triazacyclononane
L ¹⁷	<i>N</i> -Diphenylphosphinobutyl-1,4,7-triazacyclononane
L ¹⁸	<i>N</i> -Diphenylphosphinopentyl-1,4,7-triazacyclononane
L ¹⁹	<i>N,N',N''</i> -Tris(diphenylphosphinopropyl)-1,4,7- triazacyclononane
L ²⁰	<i>N</i> -Methyl- <i>N',N''</i> -di(diphenylphosphinopropyl)-1,4,7- triazacyclononane
L ²¹	Trans-1,4-bis[<i>N,N'</i> -di(diphenylphosphinopropyl)-1,4,7- triazacyclononane]but-2-ene
L ²²	<i>N,N',N''</i> -Tris(diphenylphosphinylethyl)-1,4,7- triazacyclononane
L ²³	<i>N</i> -(<i>S</i>)-2-Methyl-1-propanol-1,4,7-triazacyclononane

**TACN****L¹****L²****L³****L⁴****L⁵****L⁶**

 L^7  L^8  L^9  L^{10}  L^{11}  L^{12}  L^{13}

**L¹⁴****L¹⁵****L¹⁶****L¹⁷****L¹⁸****L¹⁹**

 L^{20}  L^{21}  L^{22}  L^{23}

SUMMARY

This work is centred upon a series of novel N-functionalised macrocycles and their transition metal complexes.

The macrocycles in question are derivatives of 1,4,7-triazacyclononane (TACN) and are functionalised at one, two or all three nitrogens. The pendant arms contain alkene, phosphine and activated aryl donor groups. In some cases the pendant arm acts as a bridge between two macrocyclic rings producing a potential dinucleating ligand.

The single alkene pendant arm macrocycles L^{10} & L^{11} contain both hard N_3 and soft olefin donor sets. Complexation of L^{10} to Cu(I) results in a complex that has a coordinated alkene and N_3 donor set, this causes considerable strain in the short C_4 pendant arm. Rapid oxidation of the Cu(I) to Cu(II) releases the co-ordinated olefin releasing strain on the pendant arm. The Cu(II) complex formed is Jahn-Teller distorted $[Cu(L^{10})_2]^{2+}$ and contains an elongated Cu- N_{ax} bond length of 2.5Å. The C_5 pendant arm macrocycle L^{11} forms a more stable Cu(I) complex and has been studied by 1H and ^{13}C NMR spectroscopy, results show that π -back bonding is present in the complex. The Ag(I) complex of L^{11} to silver(I) has been studied by NMR, the degree of π -back bonding is reduced in this complex.

A series of dimers with a planar $\{\text{Cu}(\mu\text{-OH})_2\text{Cu}\}^{2+}$ core has been structurally characterised by X-ray crystallography, with the macrocyclic ligands bound to the copper centres having either one (L^{10}), two (L^{14}) or three (L^{12}) alkene pendant arms. The dinucleating macrocyclic ligands (L^{4-6}) also form a series of copper dimers in which the TACN units are linked by either *ortho*-, *meta*- or *para*-xylene spacer units. The *meta*-xylene linked macrocycle was ideal for the spatial requirements for a $\{\text{Cu}(\mu\text{-OH})_2\text{Cu}\}^{2+}$ core, the dimeric complex $[\text{Cu}_2(\mu\text{-OH})_2\text{L}^5]^{2+}$ has been structurally characterised showing the complex to have a bent $\{\text{Cu}(\mu\text{-OH})_2\text{Cu}\}^{2+}$ core.

The Cu(I) complex of L^{12} can “activate” molecular CO_2 in the presence of trace amounts of water to produce the dimeric Cu(II) oxalate complex $[\text{Cu}(\text{L}^{12})(\mu\text{-C}_2\text{O}_4)\text{Cu}(\text{L}^{12})]^{2+}$. Results indicate that the mechanism of complexation is not simple and an intermediate copper(I) hydrogen carbonate complex $[\text{Cu}(\text{L}^{12})(\mu\text{-HCO}_3)_2\text{Cu}(\text{L}^{12})]$ is believed to be involved in oxalate formation.

The novel phosphine pendant arm macrocycles L^{16-21} were prepared by photolytic addition of diphenylphosphine across their olefin analogous. The potentially hexadentate ligand *N,N',N''*-tris(diphenylphosphinylethyl)-1,4,7-triazacyclononane (L^{22}) was prepared from the addition reaction of TACN with vinyl diphenylphosphine oxide. The ligands have been complexed to several metals in low or zero valence states. The Zn(II) complex of L^{16} has been structurally characterised and shows the complex to be an asymmetric

dimer in which both zinc atoms are coordinated by the three amine groups and the phosphine. In both halves of the dimer each zinc atom is further coordinated by a chloride ion and an asymmetrically bridging chloride ion giving pseudo-octahedral geometry at each centre. L^{16} forms a pseudo-octahedral complex with Ni(II) in which the metal centre is further coordinated by a chloride ion and an ethanol molecule. The addition of KSCN to $[NiL^{16}Cl(EtOH)]^+$ displaced the coordinated chloride and ethanol to give a new Ni(II) complex which contained coordinated thiocyanate. Other complexes have been prepared and their spectroscopic studies are presented.

Chirality has been introduced into the ligand system via the chiral alcohol pendant arm macrocycle *N*-(*S*)-2-methyl-1-propanol-1,4,7-triazacyclononane (L^{23}). This macrocycle complexes to Co(II) forming an air sensitive tetrahedral complex that rapidly oxidises to a Co(III) species. Complexation of L^{23} with $Cu(NO_3)_2$ produces an octahedral complex with bound nitrate, the second nitrate ion is hydrogen bonded to the coordinated alcohol of the ligand. The Zn(II) complex of L^{23} has been studied by 1H and ^{13}C NMR and the spectroscopic studies are presented.

The *C*-functionalised triamine (*5S*)-6-methyl-3-azaheptane-1,5-diamine has been synthesised with the aim of being converted to a chiral triazamacrocycle using the Richmann-Atkins synthetic route. This would allow chirality to be introduced into all hexadentate ligand systems.

CONTENTS

	<i>Page</i>
Acknowledgements	iii
Abbreviations	iv
Ligands	vi
Summary	xii
Contents	xv
<u>CHAPTER 1</u> INTRODUCTION	1
1.1 Introduction to macrocycles	2
1.2 Triazamacrocycles	4
1.2.1 Synthesis of triazamacrocycles	4
1.2.2 Properties of 1,4,7-triazacyclononane	7
1.2.3 Trisubstituted derivatives of 1,4,7-triazacyclononane	8
1.2.4 Monosubstituted and disubstituted ligands of 1,4,7-triazacyclononane	11
1.3 Transition metal complexes of macrocycles	16
1.3.1 Conformations of chelate rings	16
1.3.2 Complexes with TACN	17

1.3.3	Complexes with pendant arm macrocyclic ligands	20
1.4	Biocoordination chemistry	36
1.4.1	Metals in biological systems	36
1.4.2	Model systems for metallobiosites	37
1.4.3	Copper proteins	38
1.4.4	Haemocyanin	41
1.4.5	Carbonic anhydrase	46
1.5	Objectives	48
1.6	References	49
 <u>CHAPTER 2</u> EXPERIMENTAL		55
2.1	Instrumentation	56
2.2	Magnetic susceptibility measurements	57
2.3	X-ray crystallographic data collection	57
2.4	Chemicals and solvents	58
2.5	Ligand syntheses	62
2.5.1	1,4,7-Triazacyclononane and its precursors	62
2.5.2	C-Functionalised diethylenetriamine	68
2.5.3	N-Functionalised macrocycles	72
2.6	Metal complexes	98

2.6.1	Olefin binding to Cu(I) and Ag(I) complexes	98
2.6.2	Hydroxyl bridged copper(II) complexes	101
2.6.3	Low temperature oxygenation of copper(I) complexes	105
2.6.4	CO ₂ activation By [Cu(L ¹²)] [BPh ₄]	107
2.6.5	Complexes of L ¹⁸ , L ¹⁹ , L ²⁰ and L ²²	109
2.6.6	Complexes of L ²³	115
2.7	References	117
 <u>CHAPTER 3</u> CUPPER & SILVER COMPLEXES OF L¹⁰ & L¹¹		118
3.1	Introduction	119
3.2	Copper complexes of L ¹⁰ and L ¹¹	120
3.2.1	Synthesis the complexes	120
3.2.2	IR spectrum of [CuL ¹⁰] [BPh ₄]	122
3.2.3	NMR spectra of [CuL ¹¹] [BF ₄]	125
3.2.4	Structure of [Cu(L ¹⁰) ₂] [BPh ₄] ₂	132
3.2.5	Structure of [CuL ¹⁰ (μ-OH) ₂ CuL ¹⁰] [BPh ₄] ₂	137
3.3	Silver(I) Complex of L ¹¹	141
3.4	References	146

CHAPTER 4 HYDROXIDE BRIDGED COPPER COMPLEXES 148

4.1	Introduction	149
4.2	Ligand preparation	150
4.3	Preparation of the complexes	152
4.4	Crystal structure of $[\text{Cu}_2\text{L}^5(\mu\text{-OH})_2]^{2+}$	153
4.5	Crystal structure of $[\text{CuL}^{12}(\mu\text{-OH})_2\text{CuL}^{12}]^{2+}$	159
4.6	Crystal structure of $[\text{CuL}^{14}(\mu\text{-OH})_2\text{CuL}^{14}]^{2+}$	161
4.7	Comparison of copper dimer structures	164
4.8	Magnetic susceptibility measurements	170
4.9	^1H NMR spectra of $[\text{CuL}^{12}(\mu\text{-OH})_2\text{CuL}^{12}][\text{BPh}_4]_2$	171
4.10	Low temperature oxygen studies	172
4.11	References	180

CHAPTER 5 COPPER(II) OXALATE COMPLEX OF L^{12} 182

5.1	Introduction	183
5.2	Crystal structure of $[\text{CuL}^{12}(\text{C}_2\text{O}_4)\text{CuL}^{12}][\text{BPh}_4]_2$	186
5.3	Preparation of $[\text{CuL}^{12}(\text{C}_2\text{O}_4)\text{CuL}^{12}][\text{BPh}_4]_2$	188
5.4	Reaction of $[\text{CuL}^{12}]^+$ with CO_2 and CsHCO_3	189
5.5	IR spectra of the copper(II) complexes	191
5.6	Mechanism to oxalate formation	193

5.7	References	199
------------	-------------------	------------

CHAPTER 6 PHOSPHINE PENDANT ARM MACROCYCLES

	& THEIR TRANSITION METAL COMPLEXES	201
6.1	Introduction	202
6.2	Ligand preparation	206
6.3	Metal complexes of L¹⁹	208
6.3.1	Cobalt(-I/I) complex	208
6.3.2	Nickel(II) complex	210
6.3.3	Molybdenum(0) complex	214
6.4	Metal complexes of L²⁰	219
6.4.1	Platinum complex	219
6.4.2	Gold(I) complex	225
6.5	Metal complexes of L¹⁶	226
6.5.1	Zinc(II) complex	226
6.5.2	Nickel(II) complexes	230
6.6	Metal complexes of L¹⁸	234
6.6.1	Cobalt(II) complex	234
6.6.2	Copper(I) complex	235
6.7	References	236

CHAPTER 7 CHIRAL LIGANDS & HARD PENDANT

DONOR ARM MACROCYCLES	239
7.1 Introduction	240
7.2 C-Functionalised TACN derivatives	241
7.3 Chiral alcohol pendant arm macrocycles	244
7.4 Complexes of L^{23}	246
7.4.1 Cobalt complexes of L^{23}	246
7.4.2 Copper complex of L^{23}	251
7.4.3 Zinc complex of L^{23}	256
7.5 L^{22} and its cobalt(II) complex	261
7.6 References	266

CHAPTER 8 GENERAL CONCLUSIONS **268**

CHAPTER 1

INTRODUCTION

1.1 INTRODUCTION TO MACROCYCLES

Macrocycles and their metal complexes have been of great interest to chemists for many years. The presence of unsaturated macrocyclic ligand complexes in many fundamental biological processes has stimulated the study of macrocyclic complexes in a search for useful model systems. In more recent years, the involvement of macrocyclic systems in the disciplines of host-guest chemistry and molecular recognition, have resulted in the subject area expanding to include supramolecular chemistry. In particular concepts such as molecular recognition and signalling have opened up a particularly exciting dimension to macrocyclic chemistry (1). Macrocyclic complexes have many different properties from their non-cyclic analogues, and the probing of these properties by the large number of physical and chemical techniques now available have prompted intense investigations into natural, and the ever increasing number of synthetic, macrocyclic systems.

The basic definition of a macrocycle is a heterocyclic ring, comprising of nine or more atoms, of which, at least three are non-carbon atoms such as N, O, P, S etc.

Naturally occurring complexes incorporating unsaturated macrocyclic ligands have been known for many years. These include porphyrins and corrins which, in the form of haem and chlorophyll, play an essential part in the biological processes of oxygen transport in mammals and photosynthesis in plants respectively. Synthetic macrocycles are to a large extent new

additions to the chemical scene. Prior to 1960, the only synthetic macrocycles were a number of derivatives of phthalocyanine obtained by the interaction of phthalonitrile with metal halides. Phthalocyanine complexes have exceptionally high thermal stabilities and their intense colour make them an important class of commercial pigments.

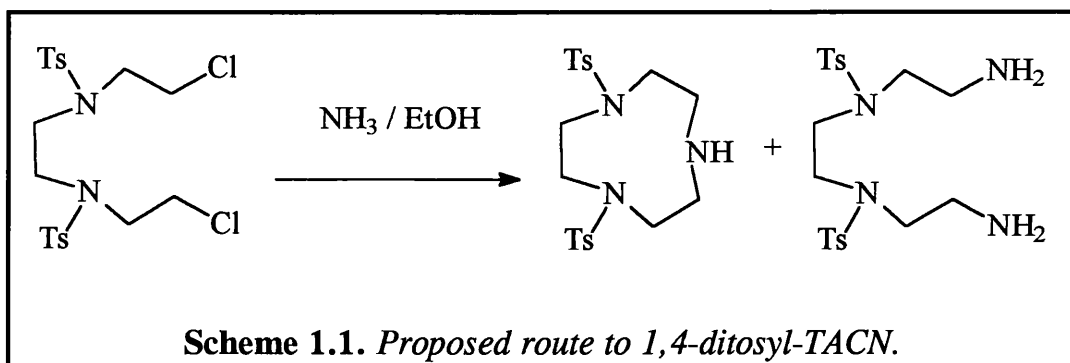
A template type process first pioneered by Curtis (2) assembled a C-substituted 14 membered ring with 4 nitrogen donors. A number of template syntheses followed producing tetra-aza macrocycles of various ring sizes and degrees of unsaturation.

In the late 1960's the macrocyclic polyethers, known as crown ethers were synthesised by Pedersen (3), later work by Lehn & Sauvage extended the range of macrocycles to include cage-like macrobicycles otherwise known as cryptands (4). These ligands, as a result of their oxygen donor functions, prefer to complex alkali and alkaline earth metals, as opposed to the transition metals favoured by aza-macrocycles, in effect opening up a whole new area of macrocyclic chemistry.

1.2 TRIAZAMACROCYCLES

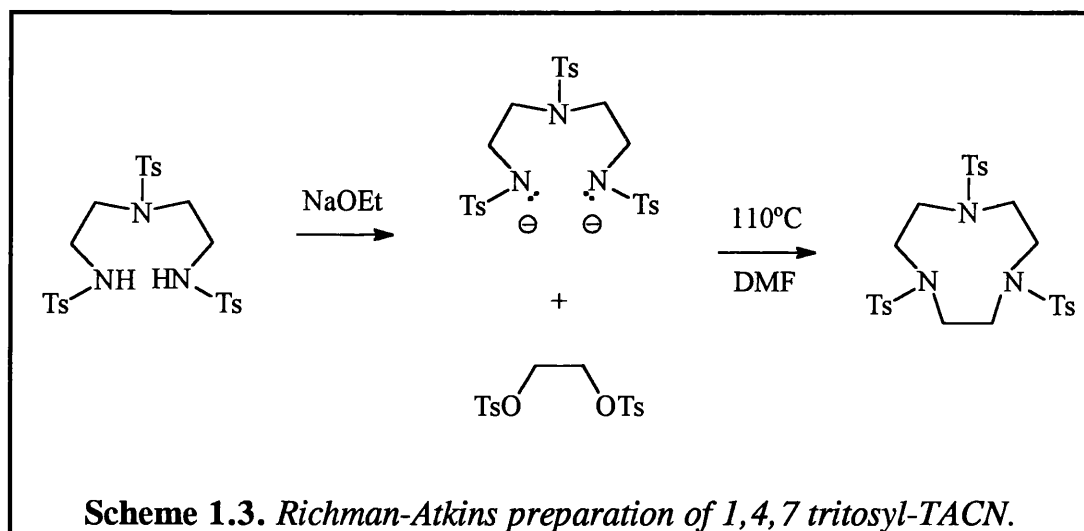
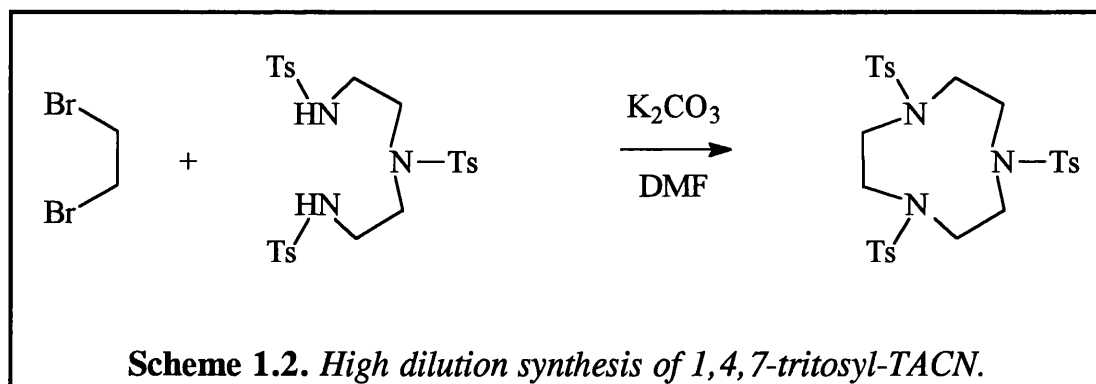
1.2.1 Synthesis Of Triazamacrocycles

In 1937 Peacock and Gwan (5) reported the first triaza macrocyclic compound 1,4-ditosyl-1,4,7-triazacyclononane, they proposed the ditosylate of TACN as a by-product from the reaction (scheme 1.1) between *N,N'*-di(*p*-tolylsulphonyl)-*N,N'*-bis(β -chloroethyl)ethylene diamine and alcoholic ammonia.



In 1972 Koyama and Yoshino (6) reported the first synthesis of 1,4,7-triazacyclononane. They presented a high dilution route to triazamacrocycles via the cyclisation of tritosyl triamine salts and dibromo alkanes in DMF (scheme 1.2). Richman and Atkins (7) modified this synthesis (scheme 1.3) to provide a simple route to 9 to 21 membered macrocycles containing 3 to 7 nitrogen atoms. Their strategy utilised sulphonate ester leaving groups as

opposed to the previous halide moieties, improving overall yields of cyclic products.

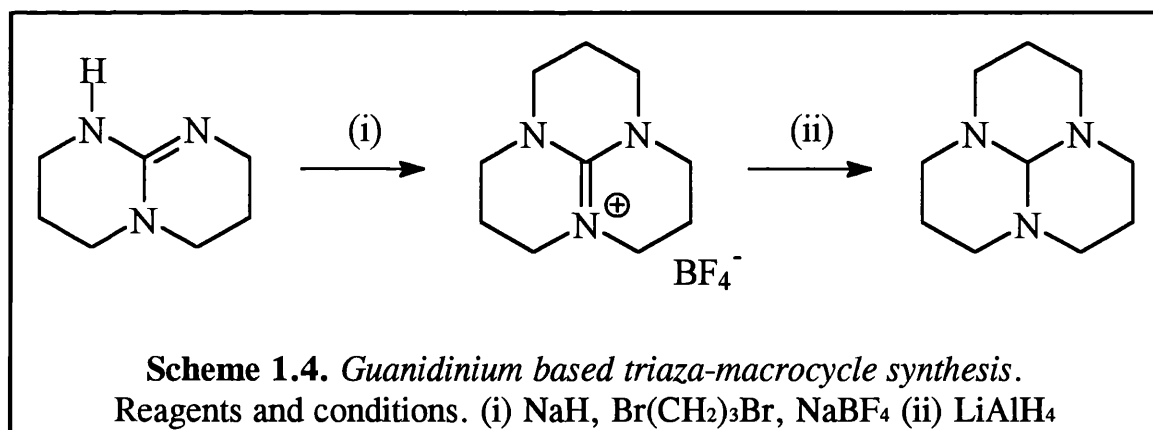


The tosyl groups in this preparation have three functions:

- (i) Activation of the primary amino function, by increasing the acidity of the amino protons and stabilising the resulting anion.
- (ii) Protection of the secondary amine function.
- (iii) Conversion of the hydroxyl functions of diols to good leaving groups.

Hydrolysis of tosylated cyclic polyamines may be achieved by several methods including electrochemical reduction, reduction with either sodium amalgam in buffered methanol solution or lithium aluminium hydride. The most common methods of detosylation for cyclic triamines are reductive cleavage of the tosyl group with HBr in acetic acid or simply heating in concentrated sulphuric acid at 100-110°C for 2-3 days. Lázár (8) has recently published a method for rapid, high yielding detosylation of linear and macrocyclic p-toluene-sulphonamides using concentrated sulphuric acid at 180°C for 8 minutes. The process gives yields of 90%+ for polyaza macrocycles and yields of 50%+ for oxapolyaza type macrocycles.

A novel preparation of medium sized tri-azamacrocycles has been published (9), which uses a guanidinium based template (scheme 1.4).



The final orthoamide may be treated with acid to yield the parent macrocycle or with alkylating agents to afford single pendant arm macrocycles. This synthesis proceeds in high yield giving triamines with 11,

12 or 13 membered rings, attempts at a 9 membered ring failed due to excessive strain in the intermediate guanidinium ion.

1.2.2 Properties of 1,4,7-Triazacyclononane

TACN and other triazamacrocycles tend to be more basic than their linear counterparts, this is exemplified by comparison of the first protonation constants of TACN ($pK_1=10.6$) and diethylene triamine $H_2N(CH_2)_2NH(CH_2)_2NH_2$ ($pK_1=9.7$). The second and third protonation constants are lower for the cyclic species, believed to be a consequence of the increased repulsion towards an incoming proton by the mono and di protonated macrocycle. The conformation of TACN results in the lone pairs of the three amine functions pointing inwards towards the macrocycle cavity, effectively creating an electron rich hole which increases the rate of uptake of the first proton. This is observed in the crystal structure (12) of Me_3TACN and a bound proton (figure 1.1). The proton is bound to one nitrogen donor and hydrogen bonded to the other two. TACN coordinates in a facial manner, as exemplified by the complexation of H^+ . Increasing the triazamacrocycle ring size to 15 atoms or larger allows equatorial coordination which is observed in larger macrocycles such as cyclam.

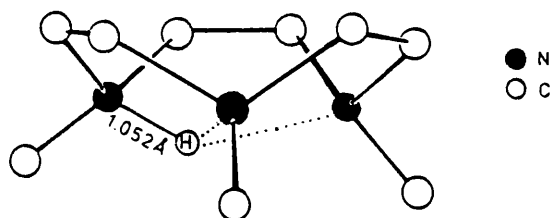


Figure 1.1. *Crystal structure of [Me₃9-aneN₃H][ClO₄].*

1.2.3 Trisubstituted Derivatives of 1,4,7-Triazacyclononane

Direct alkylation of the secondary amine functions of 1,4,7-triazacyclononane is a very common process and has provided a starting point to many *N*-functionalised ligands (10-12). These appended moieties, known as pendant arms, modify the coordination properties and abilities of the ligand, primarily making the ligand hexadentate. A quite diverse array of pendant groups has been reported with TACN (table 1.1) mostly utilising hard donor groups such as amines, alcohols and carboxylates, very few examples have been reported with soft donor groups such as phosphines and thiols. Introducing non-coordinating donor groups such as simple alkyl groups creates a tridentate macrocycle which promotes piano stool type complexes or more often binuclear complexes.

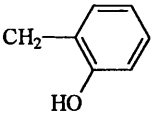
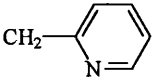
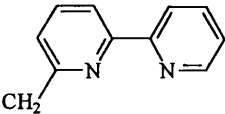
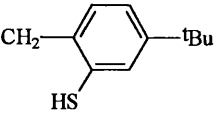
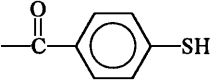
	Pendant Arm Group	Reference
Oxygen Donors	$\text{CH}_2\text{CO}_2\text{H}$	13
	$\text{CH}_2\text{CH}_2\text{OH}$	14
	$\text{CH}_2\text{CH}(\text{Me})\text{OH}$	15
	$\text{CH}_2\text{CH}(\text{iPr})\text{OH}$	16
		17
	$\text{CH}_2\text{P}(\text{O})\text{PhOH}$	18
	$\text{CH}_2\text{P}(\text{O})\text{Ph}_2$	19
	$\text{CH}_2\text{CH}_2\text{P}(\text{O})\text{Ph}_2$	this work
Nitrogen Donors	$\text{CH}_2\text{CH}_2\text{NH}_2$	20
		21
		22
Sulphur Donors	$\text{CH}_2\text{CH}_2\text{SH}$	23
		24
		25
Phosphine Donors	$\text{CH}_2\text{CH}_2\text{CH}_2\text{PPh}_2$	this work
Alkyl Groups	Me	26
	iPr	27
	$\text{CH}_2\text{C}_6\text{H}_5$	28
	$\text{CH}_2\text{CH}=\text{CH}_2$	this work

Table 1.1 *Selected pendant arm types*

Various methods have been employed to introduce these additional groups to the parent macrocycle:

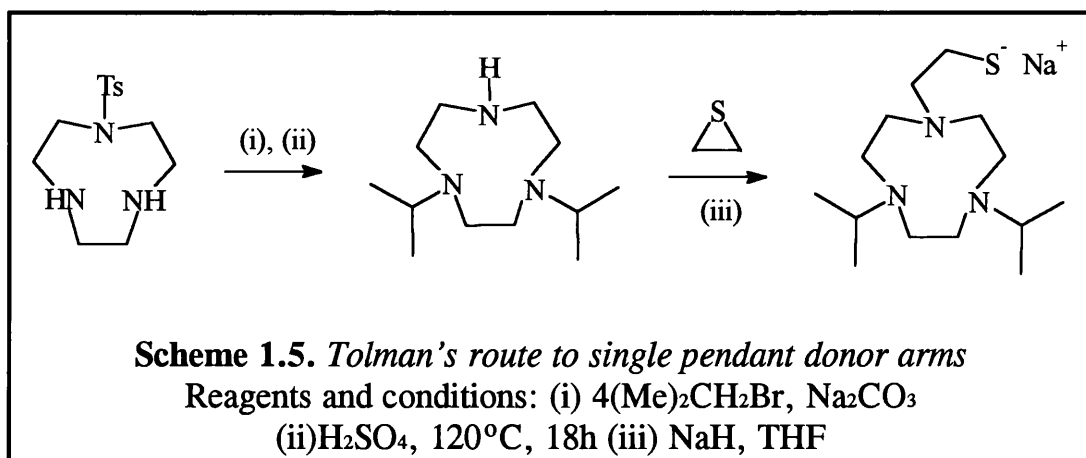
- (i) S_N2 or S_N2' Reactions. Nucleophilic attack by the secondary nitrogen to displace halogens of appropriate alkyl halides. This is the simplest and the most common form of *N*-functionalisation, but there may be the complication of quaternary ammonium ion formation (TACN and MeI) or a mixture of products containing one, two or three pendant donor arms (TACN and i PrBr). The synthetic route can not be extended to dihalo-alkylating agents without the proper protection of two of the amine functions.
- (ii) Mannich type reaction. This is the common method for the methylation of macrocycles using formaldehyde and formic acid. The method has also been used for the preparation of phosphinic acid (**18**), phosphinyl (**19**) and phosphino (**29**) derivatives by the reaction of the parent macrocycle with formaldehyde and PhP(OMe)_2 , $\text{Ph}_2\text{P(O)H}$ or Ph_2PH respectively. The only draw back to this route is that the pendant arm length is limited to one carbon.
- (iii) Ring opening reactions. The ring opening of epoxides by amines is a well characterised reaction and provides a route to alkyl ethyl hydroxy substituted aza-macrocycles (**14**). The regiospecific attack at the least hindered carbon under basic or neutral conditions allows the introduction of chiral centres to the ligand (**15**, **16**). A number of optically active

epoxides are commercially available or can be prepared from commercially available amino acids.

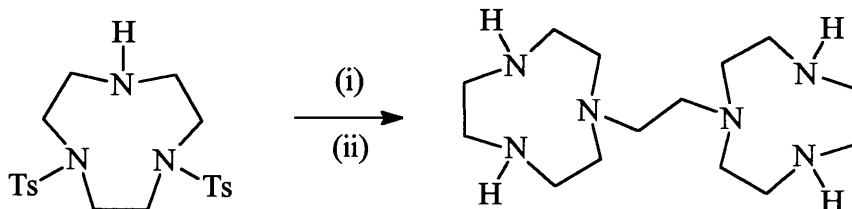
1.2.4 Monosubstituted and Disubstituted Ligands of 1,4,7-

Triazacyclononane

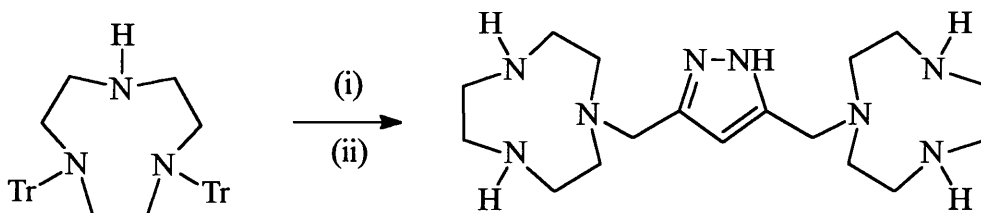
Synthetic routes towards monosubstituted and disubstituted ligands based on TACN are somewhat complicated with several steps involving protection and deprotection often being required to avoid the trisubstituted macrocycles. 1-Tosyl-1,4,7-triazacyclononane (**30**) has been used to synthesis 1,4-dimethyl-1,4,7-triazacyclononane, which can be further *N*-functionalised to produce a single pendant arm macrocycle. A recent report by Tolman *et al.* (**31**) used 1-Tosyl-1,4,7-triazacyclononane in the synthesis of a macrocycle with a single pendant thiolate arm (Scheme 1.5).



The ditosyl derivative of TACN 1,4-ditosyl-1,4,7-triazacyclononane was used by Wieghardt (32) to synthesise the dinucleating ligand 1,2-bis(1,4,7-triazacyclononyl)ethane (scheme 1.6). Removal of the tosyl group using concentrated sulphuric makes these synthetic routes unsuitable for acid sensitive donor groups. A modification of this method using the trityl group as a mode of *N*-protection was used by Kaden (33) to link two TACN units with a bridging pyrazole moiety (Scheme 1.7). The conditions for deprotection are milder than using concentrated sulphuric acid, but the route is still not suitable for acid sensitive donor groups.



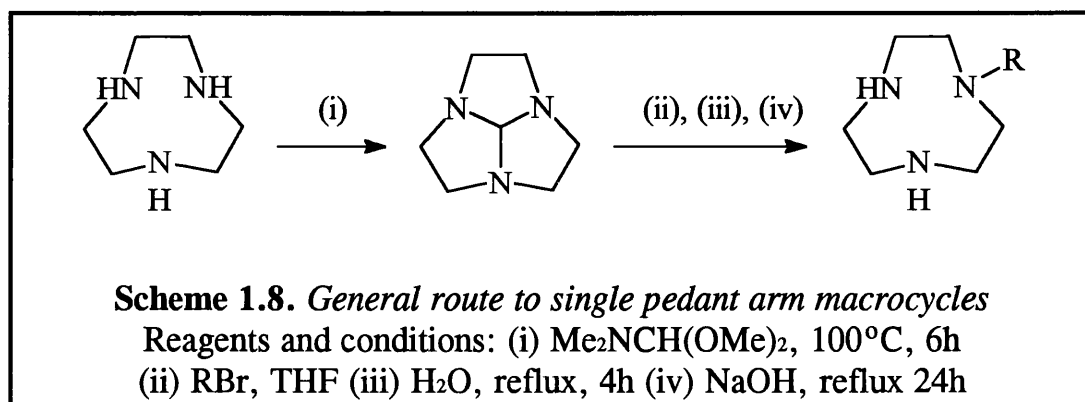
Scheme 1.6. Wieghardt's route to 1,2-bis(1,4,7-triazacyclononyl)ethane
Reagents and conditions: (i) TsO(CH₂)₂OTs, Na₂CO₃, DMF
(ii) H₂SO₄, 110°C, 48h



Tr = triphenylmethyl

Scheme 1.7. Kaden's use of trityl protecting groups
Reagents: (i) 3,5-bis(chloromethyl)pyrazole.HCl (ii) HCl / MeOH

The facile synthesis of 1,4,7-triazatricyclo[5.2.1.0^{4,10}]decane by Atkins (34) and subsequent alkylation reactions by Weisman *et al.* (35) heralded a new era in single pendant arm triaza macrocyclic ligands (scheme 1.8). The only limitations to the synthetic route is that the pendant arm (or its precursor) must be introduced as a primary alkyl bromide or iodide.



The crystal structure of the quaternary ammonium bromide salt, formed as an intermediate in a reaction similar to the above scheme was reported by Farrugia *et al.* in 1993 (36) (figure 1.2). The structure shows that the bond length of the capping C atom and quaternary N atom [1.67Å] is significantly longer than the other two C-N bond lengths [1.42 and 1.40Å]. Comparison with the C-N bond lengths [1.47Å] published by Blake *et al.* (37) for 1,4,7-triazatricyclo[5.2.1.0^{4,10}]decane (figure 1.3), showed that significant delocalisation of the nitrogen lone pairs was present making the structure more like a bicyclic amidinium salt (figure 1.4).

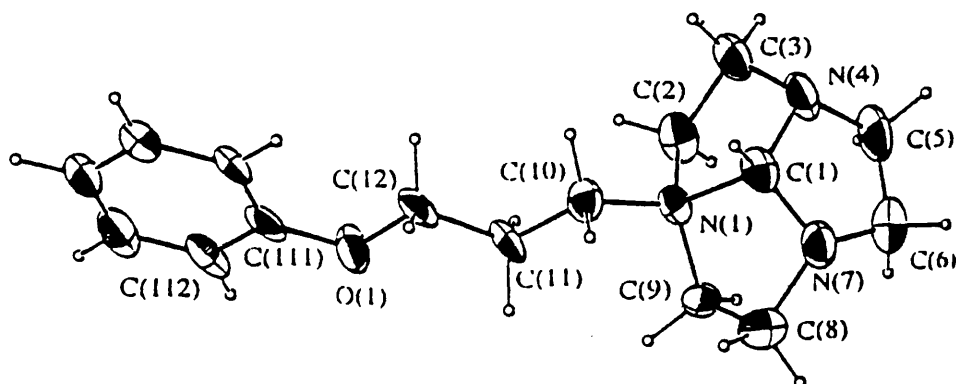


Figure 1.2. *Crystal structure of the quaternary ammonium ion*

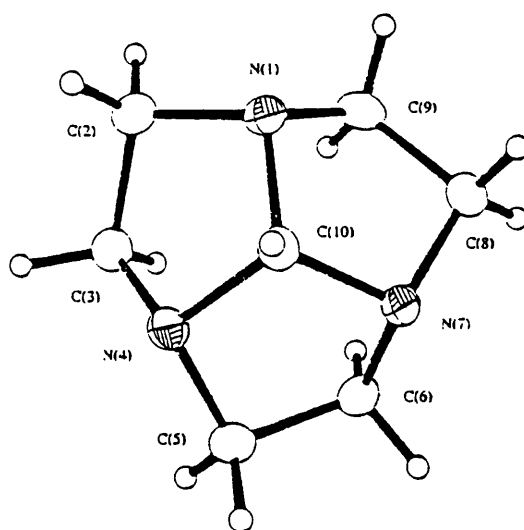


Figure 1.3. *Crystal structure of 1,4,7-triazatricyclo[5.2.1.0^{4.10}]decane*

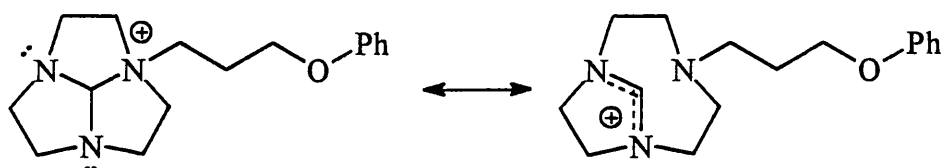
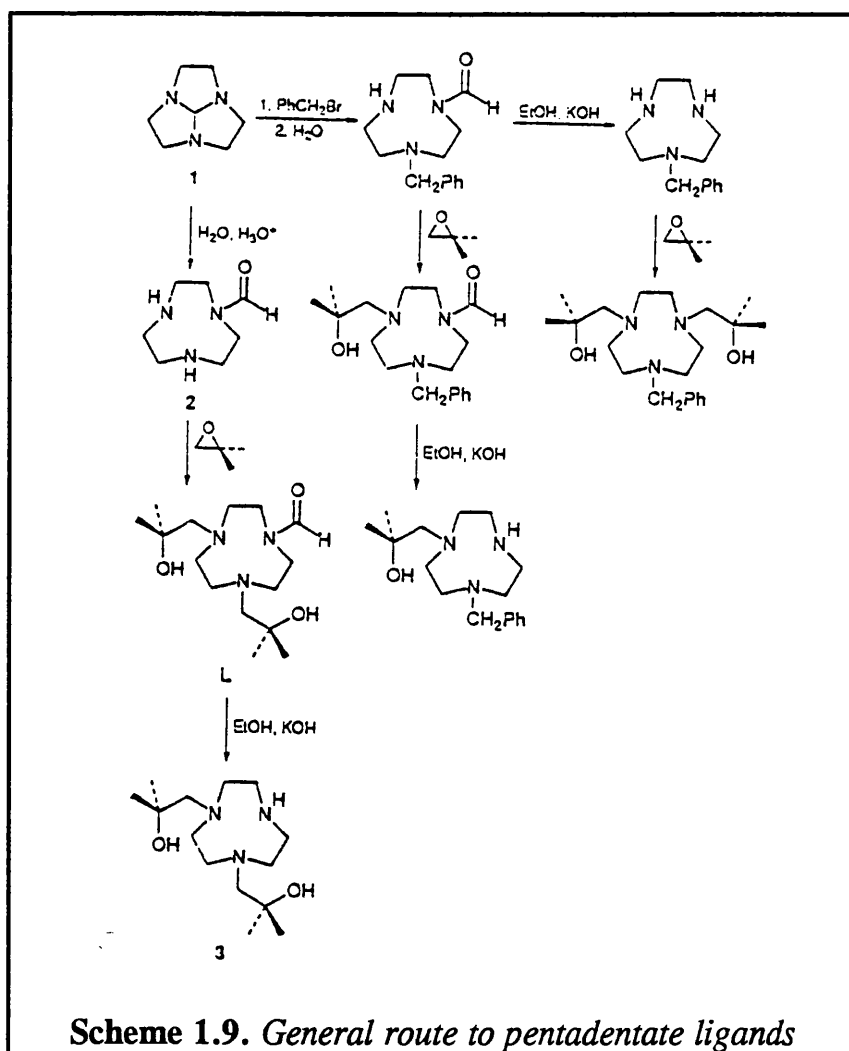


Figure 1.4. *Delocalisation of the nitrogen lone pairs showing the quaternary amine and amidinium forms*

Wieghardt (38) improved on his original synthesis of 1,2-bis(1,4,7-triazacyclononyl)ethane using the synthetic route pioneered by Weisman. The method proved to be less complex synthetically, less time consuming and improved the yield of the final product.

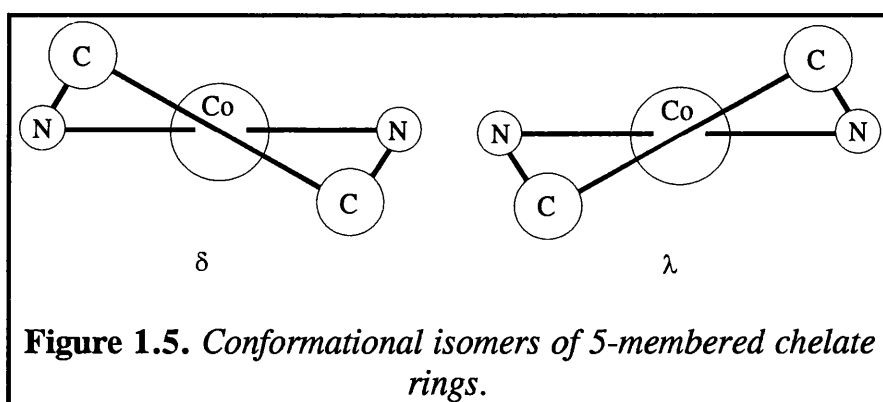
Modifications of Weisman's synthetic route by Schröder *et al.* (39) has lead to a facile synthesis of pentadentate macrocycles (scheme 1.9). The key step to the synthetic route being permanent protection of one nitrogen by a non-coordinating benzyl group or by a *N*-formyl group which can be removed by base hydrolysis.



1.3 TRANSITION METAL COMPLEXES OF MACROCYCLES

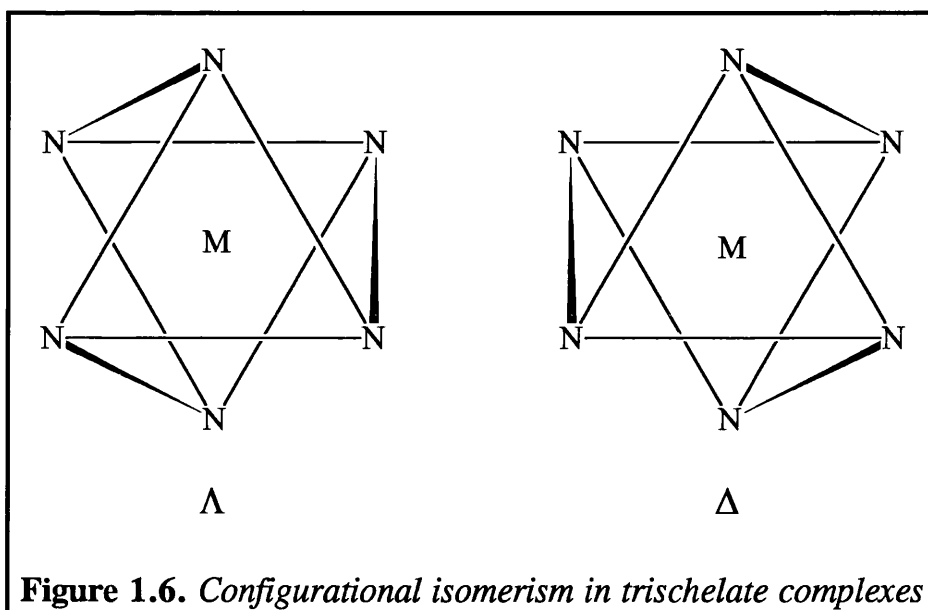
1.3.1 Conformations of Chelate Rings

Often complexes containing chelate rings show dissymmetry in the solid state. The dissymmetry results from two sources; conformational and configurational isomerism. The first source of dissymmetry is the chelate rings which may adopt either of two possible chiral conformations δ and λ (figure 1.5).



The conformation has the δ form if the C-C bond forms a segment of a right handed helix with respect to the N-N direction in the chelate ring. The λ conformation involves a similar left handed helix. The second source of dissymmetry is the orientation of the chelate rings about the metal atom (figure 1.7). This is observed as the twist of the propeller blades, looking down the C_3 axis of the molecule. Concentrating on one of the three near

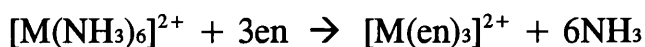
nitrogens it's seen to be connected to one of the rear nitrogens. If the connected rear nitrogen is to the right of the front nitrogen, then the Δ configuration is present. On the other hand, if this connection is to the left of the nitrogen, Λ symmetry results.



1.3.2 Complexes with TACN

1,4,7-Triazacyclononane has been coordinated to all of the first row transition metals and many of the second and third row elements, establishing it as an excellent metal chelator. The complexes formed have an enhanced stability over their straight chain analogue or unidentate donors, this increased stability arising from the chelate and macrocyclic effects.

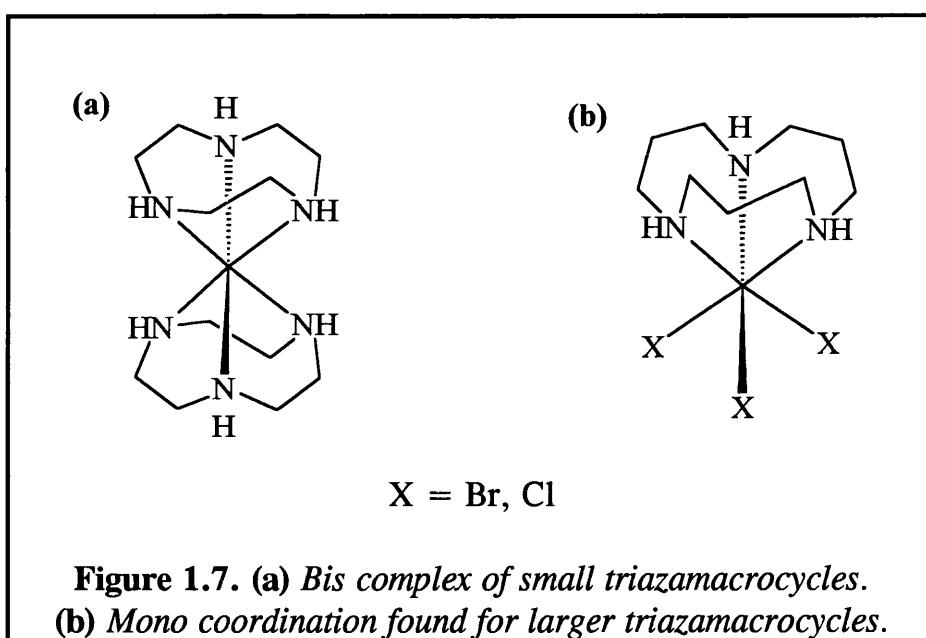
The chelate effect refers to the enhanced stability of a complex system containing chelate rings as compared to a similar system containing no rings, the effect is largely entropic as shown below:



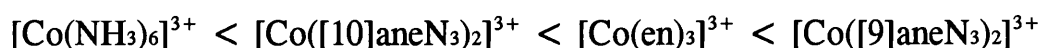
The entropic term arises from the simple fact that on complexation of a chelating ligand, there are more species or individual elements on the right hand side of the equation giving an overall positive entropy for the reaction.

The macrocyclic effect, an increased stability of complexes of cyclic polydentate ligands compared with complexes of linear analogues, was first discovered in studies of tetraaza-macrocycles (40). Considerable debate has taken place as to whether the origins of this effect are due to more favourable enthalpy or entropy changes in the complex formation, with triaza-macrocycles the effect has been attributed to entropy effects (41). The entropy effect arises because the macrocycle is preformed into a particular configuration, the loss of entropy on complexation is less than that experienced for a non-cyclic system. A favourable enthalpy change also arises from this preformed configuration; the donor atoms of the macrocycle are already in roughly the desired position for complex formation, as a result the macrocycle requires less energy than its linear analogue to complex a metal ion.

Koyama and Yoshino (6) carried out the initial work on transition metal complexes with triazamacrocycles. They prepared a series of Co(III) complexes with [9]aneN₃, [10]aneN₃, [11]aneN₃ and [12]aneN₃, each of the macrocycles coordinating in a facial manner. The smaller macrocycles [9]aneN₃ and [10]aneN₃ were assigned as having bis-ligand sandwich like structures (figure 1.7a), whereas the larger macrocycles were assigned as piano stool like structures (figure 1.7b).



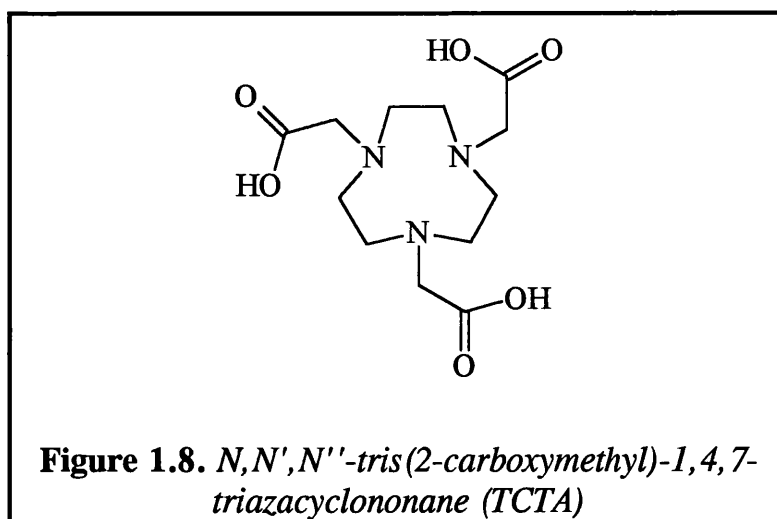
From their spectroscopic investigations of the various complexes, Koyama and Yoshino were able to suggest the following spectrochemical series (arranged in order of increasing ligand field strength from left to right):



Thus it can be seen that smaller ring sizes produce larger ligand field strengths and can stabilise higher oxidation states (smaller ions). Larger macrocycles result in weaker ligand fields with a resultant lengthening of metal-ligand bonds. This is further exemplified in the Fe(II) complexes of *N,N',N''*-tris(2-pyridylmethyl)-1,4,7-triazacyclononane (TPTACN) (21) and of *N,N',N''*-tris(2-pyridylmethyl)-1,5,9-triazacyclododecane (TPTACDD) (42). The small nine-membered ring of TPTACN results in a ligand field sufficiently strong enough to enforce spin pairing and a diamagnetic complex results, the larger ring of TPTACDD results in an extension of the Fe-N bond length i.e. a weaker field and a high spin complex is formed.

1.3.3 Complexes with Pendant Arm Macrocyclic Ligands

The transition metal chemistry of TACN and its *N*-functionalised derivatives is very extensive and will only be touched upon here. Historically the first pendant arm triazamacrocycle to be synthesised was *N,N',N''*-tris(2-carboxymethyl)-1,4,7-triazacyclononane (TCTA) by Takamoto and co-workers (13). The versatility of this hexadentate donor was demonstrated by Wieghardt *et al.* in the synthesis of mononuclear complexes of V(IV), Cr(III), Mn(II), Mn(III), Fe(III), Co(II), Co(III), Ni(II), Cu(II) and Al(III) (43).

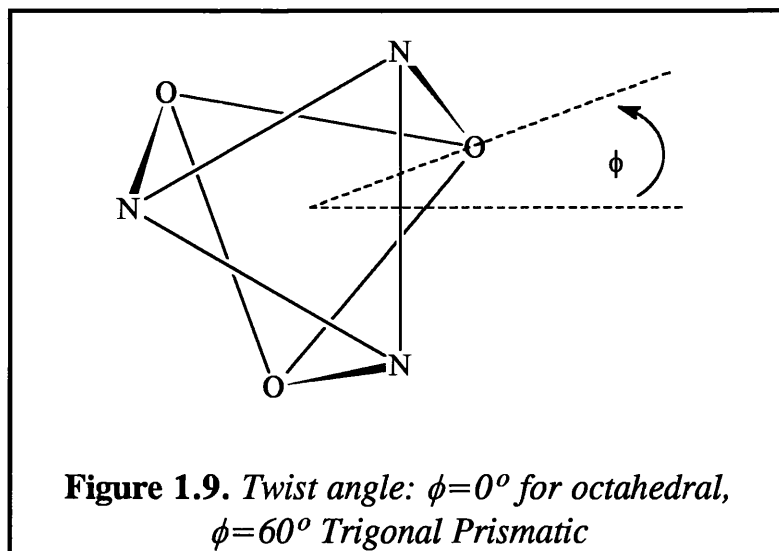


The most interesting feature of these complexes was the degree of trigonal twist (figure 1.9) observed in the crystal structures (table 1.2).

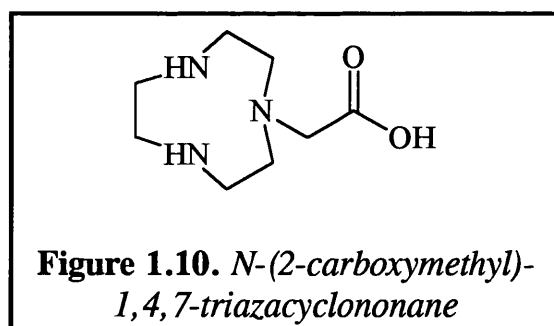
		Twist Angle ϕ	Ref.
Cr(III)	d ³	11.0°	43
Ni(II)	d ⁸	12.0°	44
Cu(II)	d ⁹	33.4°	43
Fe(III)	d ⁵	35.0°	43

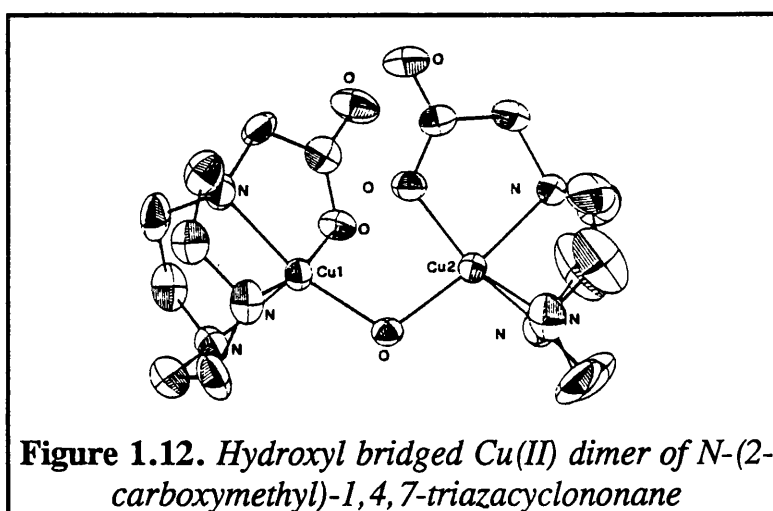
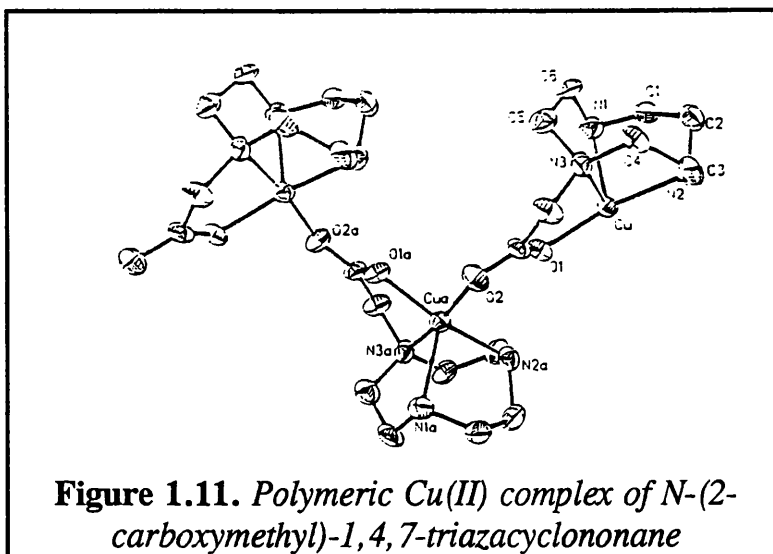
Table 1.2. *Twist angles for TCTA complexes.*

From these values it can be seen that while the Cr(III) and Ni(II) complexes are only slightly distorted from octahedral geometry, the Fe(III) and Cu(II) complexes approach trigonal prismatic geometry. The observed twists are determined by the magnitude of LFSE required by each metal ion, since the ligand is the same in all cases.

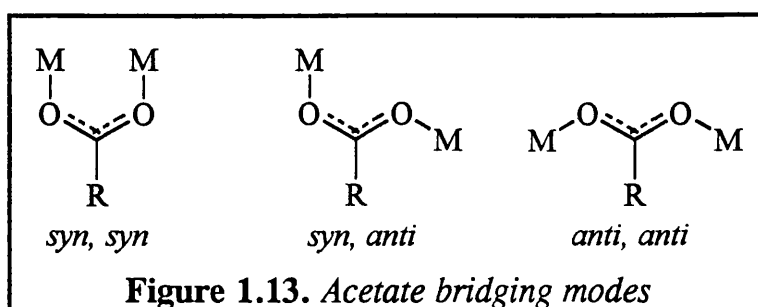


The tetradentate macrocycle *N*-(2-carboxymethyl)-1,4,7-triazacyclononane was prepared by reaction of chloroacetic acid with excess TACN by Kaden (45). Two distinct Cu(II) complexes have been reported (46), both isolated from the same reaction but at different pH. One structure consists of a helical array of Cu(II) centres (figure 1.11), the coordination sphere consisting of the N_3O of the macrocycle and a bridging carboxylate from an adjacent complex. The other complex (figure 1.12) was isolated at higher pH and consists of a hydroxyl bridged Cu(II) dimer.





A more recent publication by Wieghardt *et al.* (47) showed that the addition of chloride ions breaks up the syn, anti bridging mode (figure 1.13) of the acetates in the helical array and the formation of a monomeric Cu(II) complex results (figure 1.14).



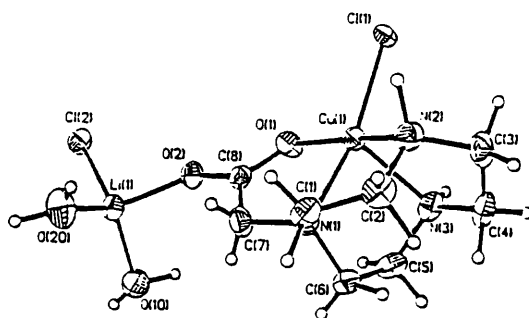


Figure 1.14. *Monomeric Cu(II) complex of N-(2-carboxymethyl)-1,4,7-triazacyclononane*

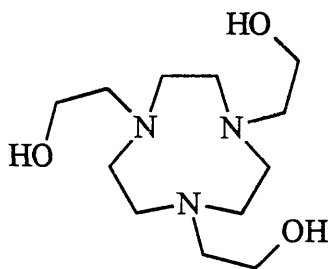
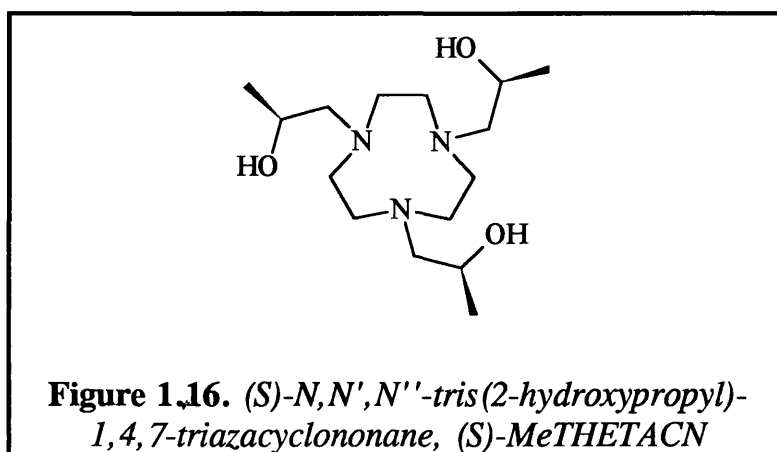


Figure 1.15. *N,N',N''-tris(2-hydroxyethyl)-1,4,7-triazacyclononane (THETACN)*

In 1983 Hancock *et al.* (14) prepared *N,N',N''*-tris(2-hydroxyethyl)-1,4,7-triazacyclononane (THETACN) and determined the stability constants of its Cu(II) and Zn(II) complexes. The complexes had the same or larger stability constants than the analogous TACN complexes. This was usual as the addition of hydroxyethyl groups to amines normally leads to a lowering of the stability. This larger stability lead the authors to believe that all three arms were coordinated to the metal.

Protonation studies showed that THETACN had an unexpected higher pK_1 (11.5) value than that measured for TACN (10.6), this was unusual due

to the electron withdrawing nature of the hydroxyl functions, which would suggest a lower pK_1 value for the pendant arm macrocycle. The second protonation constant was lower than that of TACN as expected i.e. the electron withdrawing alcohol groups would decrease the basicity of the ring donors. The reason for this observation was, according to the authors, that at higher pH there is intramolecular hydrogen bonding between the first incoming proton and the hydroxyl donor groups, this behaviour breaks down at lower pH giving a much lower pK_2 value.



Some three years later Peacock and Robb (15) reported the synthesis of *(S)* *N,N',N''*-tris(2-hydroxypropyl)-1,4,7-triazacyclononane abbreviated *(S)*-MeTHETACN and its Co(III) complexes. The structure of the Co(III) complex (48) was shown to be a hydrogen bridged dimer. The ligand remains protonated in one half of the dimer and deprotonates in the other half to give alkoxide ligands. The electronic spectra obtained for the Co(III) complex is pH sensitive, suggesting that the dimeric structure dissociates in

acid or alkaline solutions and is only maintained under neutral conditions. Reaction of (*S*)-MeTHETACN with Cr(III) gives a complex isostructural to the Co(III) dimer, whereas manganese (**49**) gives a novel mixed valent dimer $[\text{Mn(II)LH}_3\text{LMn(IV)}]^{3+}$ (figure 1.17). The structure contains a Mn(II) centre with trigonal-prismatic coordination and a Mn(IV) centre with pseudooctahedral coordination with the alkoxide ligators bound to the smaller Mn(IV) ion. The mixed metal dimer $[\text{Zn(II)LH}_3\text{LV(IV)}]^{3+}$ (**50**) contains a Zn(II) centre with trigonal-prismatic coordination and a V(IV) centre with pseudooctahedral coordination. The Ni(II) complex of (*S*)-MeTHETACN (**51**) is a mononuclear complex in which the alcohol ligators remain protonated. The electronic spectrum of the Ni(II) complex is pH independent, indicating that the complex is monomeric in solution as well as the solid state.

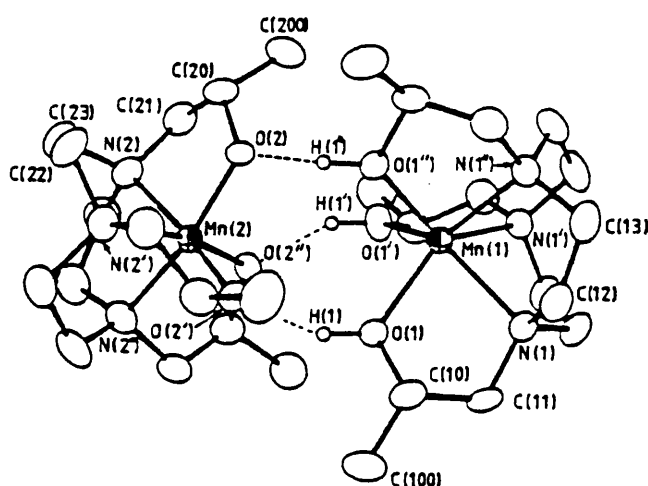
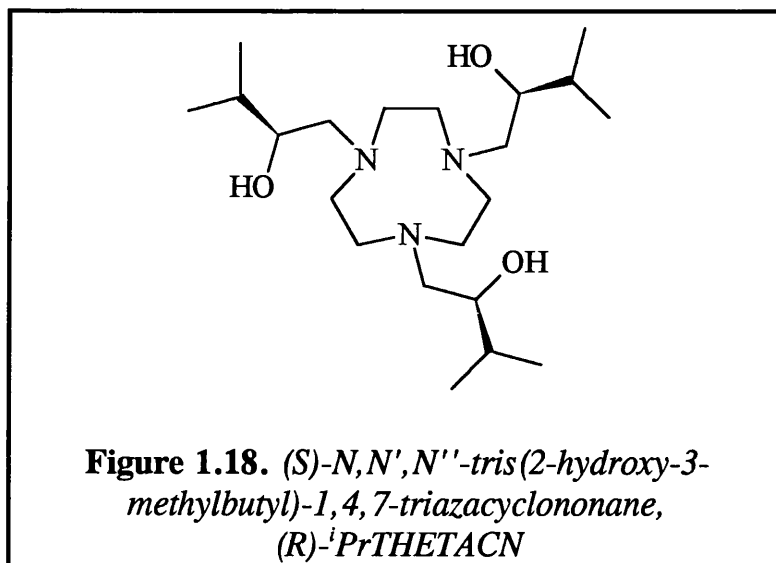


Figure 1.17. Crystal structure of $[\text{Mn(II)LH}_3\text{Mn(IV)L}]^{3+}$,
 $L = (\textit{S})\text{-MeTHETACN}$

A bulky alcohol appended triazamacrocycle, namely (*R*)-*N,N',N''*-tris(2-hydroxy-3-methylbutyl)-1,4,7-triazacyclononane (*R*)-^{*i*}PrTHETACN was synthesised by Fallis and Peacock (16) in an attempt to prevent the dimerisation that was observed in (*S*)-MeTHETACN complexes.



The monomeric Mn(IV) complex of (*R*)-^{*i*}PrTHETACN was prepared under similar conditions to the previously mentioned Mn(II)/Mn(IV) dimer of (*S*)-MeTHETACN. It can be seen from the crystal structure (figure 1.19) that the bulky isopropyl groups on the pendant arm block of the O,O',O'' face of the complex, preventing dimerisation. The ligand also forms monomeric complexes with V(IV), Cr(III), Ni(II), Cu(II) and Zn(II).

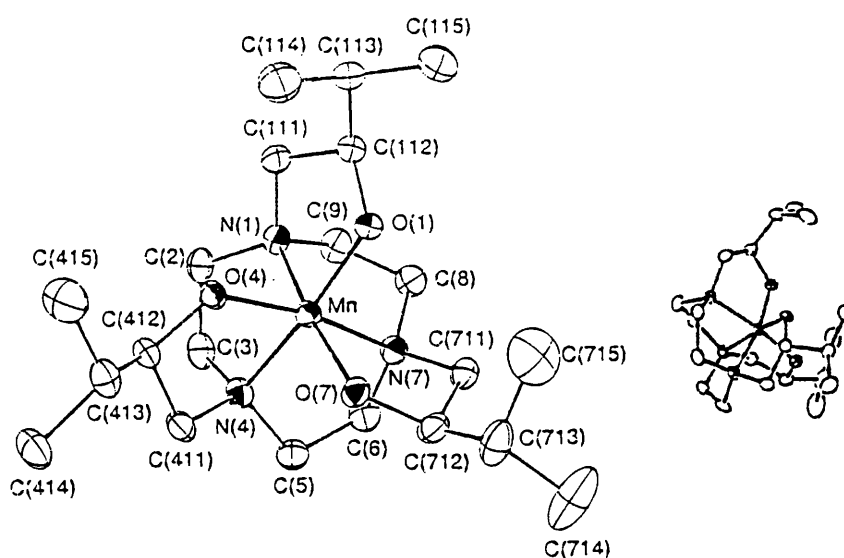


Figure 1.19. Crystal structure of $[Mn(IV)L]^+$,
 $L = (r)\text{-}i\text{PrTHETACN}$

A potential 10 coordinate ligand (figure 1.20) obtained by the reaction of 1,2-bis(1,4,7-triazacyclononyl)ethane with 2,2-dimethyl oxirane was reported by Schröder *et al.* (52) in 1994. The ligand forms dinuclear complexes with Co(II), Zn(II), Ni(II) and Cu(II).

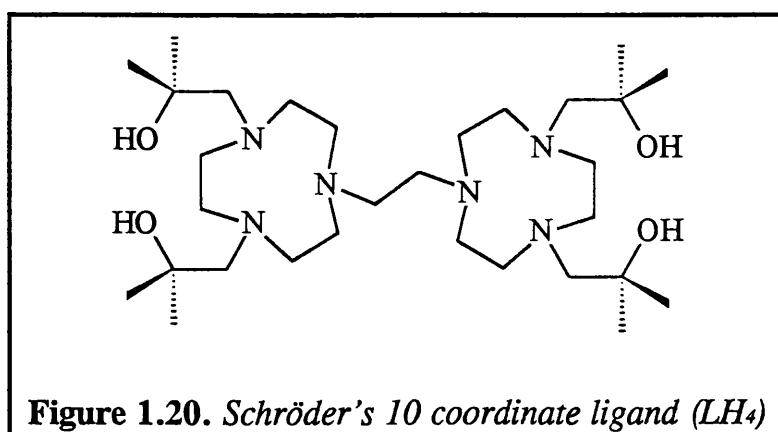
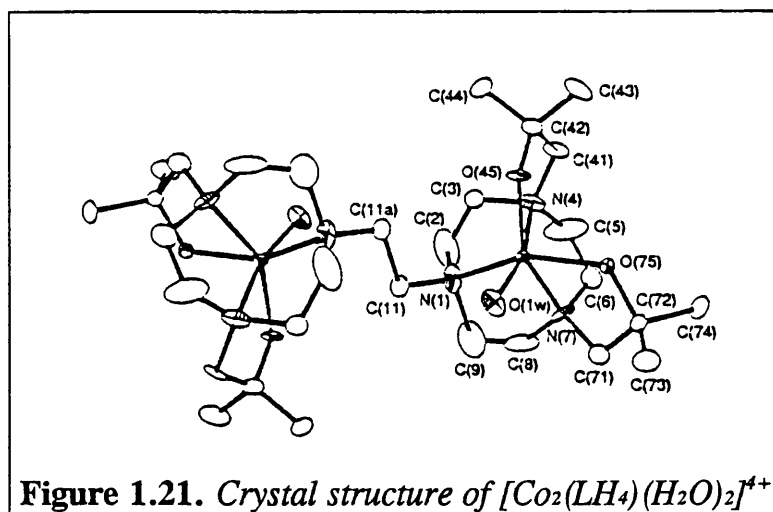


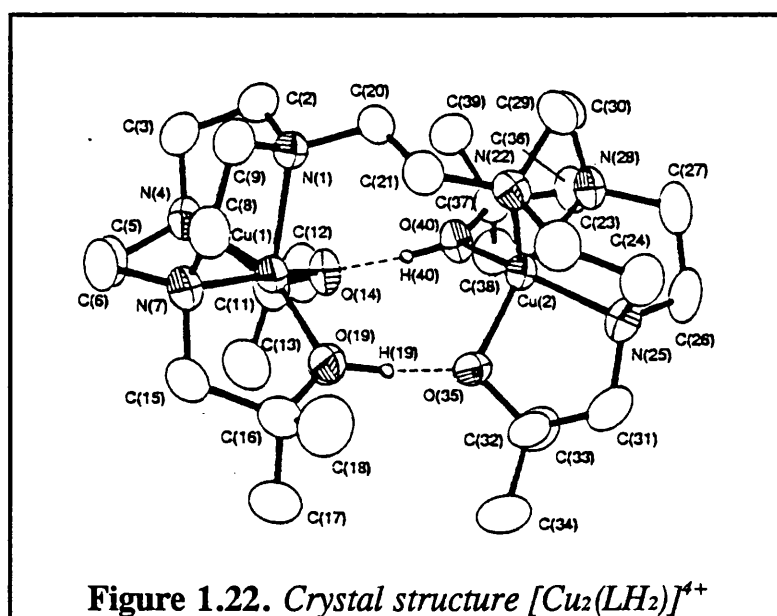
Figure 1.20. Schröder's 10 coordinate ligand (LH_4)

No oxidation to Co(III) was observed in the preparation of the Co(II) complex dimer (figure 1.21), this was unusual for such a system with a N_3O_3

donor set. The stabilisation of Co(II) in the presence of hydroxyl arms usually required a larger triaza ring size of 10 or more (53).



The Cu(II) complex (figure 1.22) was also unusual in that deprotonation of two of the pendant alcohol groups occurred, forming two hydrogen bridges between the two halves of the ligand. This loss of a proton to form an alkoxide species is uncommon for divalent cations and is usually observed in tri- or tetravalent cations.



There are few examples of soft pendant arm derivatives of TACN, the first system to functionalise TACN with soft pendant donor arms was reported by Welch *et al.* (23). The paper outlined the synthesis of 1,4,7-tris(2-mercaptoethyl)-1,4,7-triazacyclononane (TS-TACNH₃) and its Ga³⁺ complex, no other work regarding this ligand or its complexes has been published since. The Ga³⁺ complex (figure 1.23) formed showed some deviation from octahedral geometry with a small trigonal twist $\phi=10.4^\circ$. The authors expected a similar twist to that of Fe(TCTA) ($\phi=35.0^\circ$), since Fe(III) and Ga(III) generally display similar coordination chemistries. However, since Ga³⁺ has a greater affinity for nitrogen over Fe³⁺, the result is shorter M-N bond lengths and a complex with a less distorted octahedral geometry.

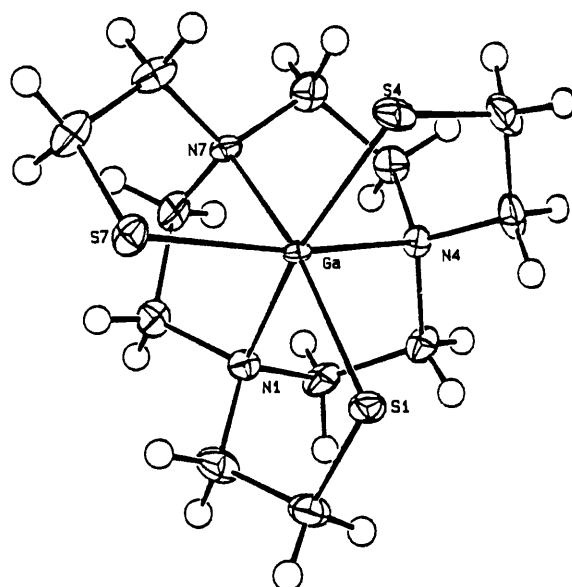
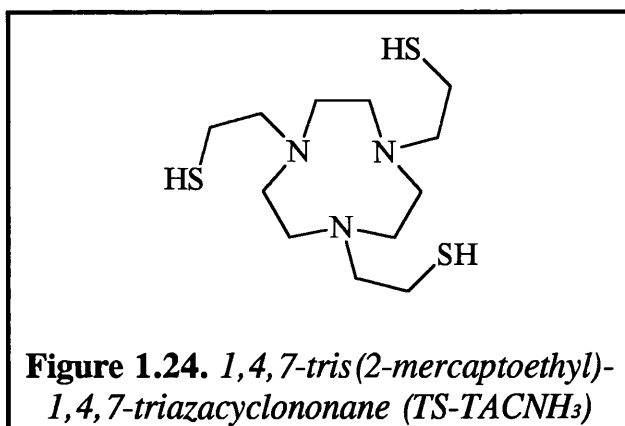
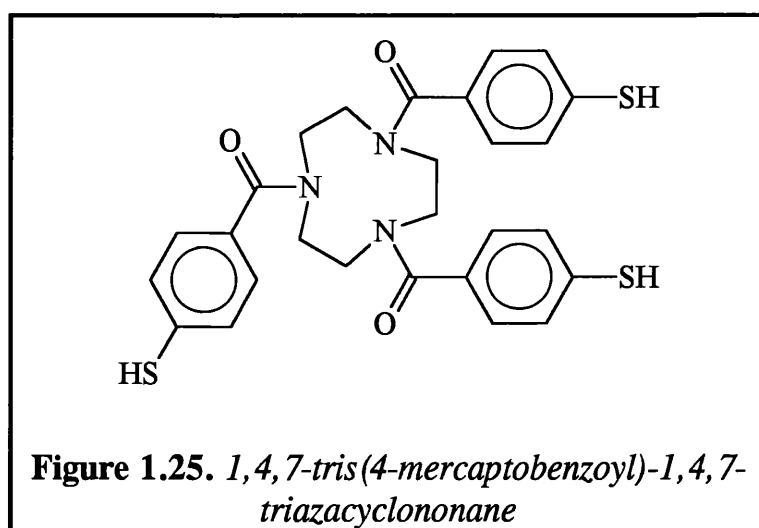
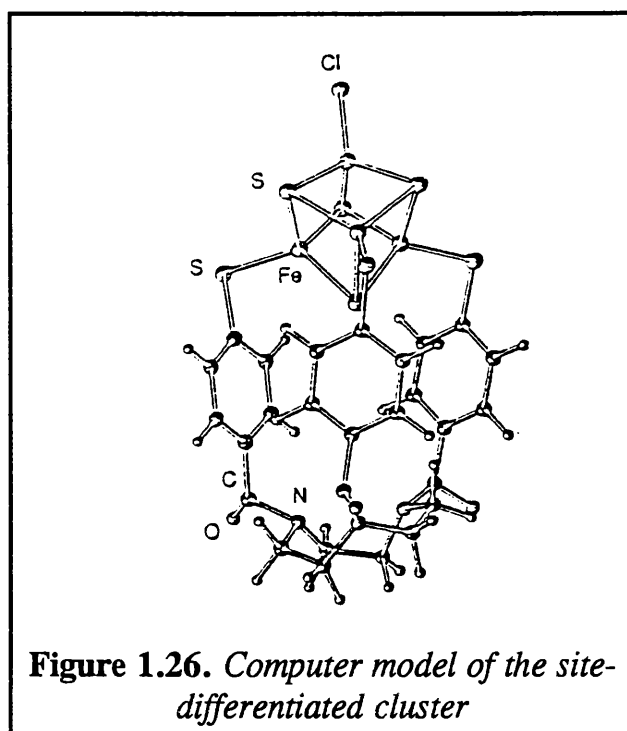


Figure 1.22. Crystal structure of Ga(TS-TACN)

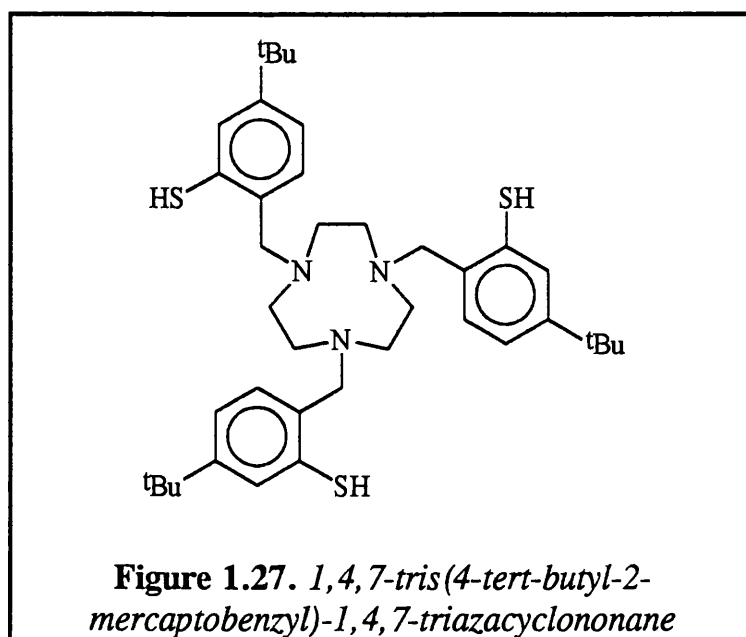


The tripodal thiol ligand 1,4,7-tris(4-mercaptobenzoyl)-1,4,7-triazacyclononane was synthesised by Evans (25) to bind a $[\text{Fe}_4\text{S}_4]^{2+}$ core producing a “site differentiated” iron atom (figure 1.26). Characterisation of the resulting $[\text{Fe}_4\text{S}_4\text{L}(\text{SR})]^{2-}$ complexes by NMR and Mössbauer spectroscopy showed that the ligand does complex the $[\text{Fe}_4\text{S}_4]^{2+}$ core in the required fashion and not as a random 3-D polymer. The authors have stated that ultimate proof of the “site differentiated” species will require crystallographic analysis of suitable crystalline material, which has eluded them to date.



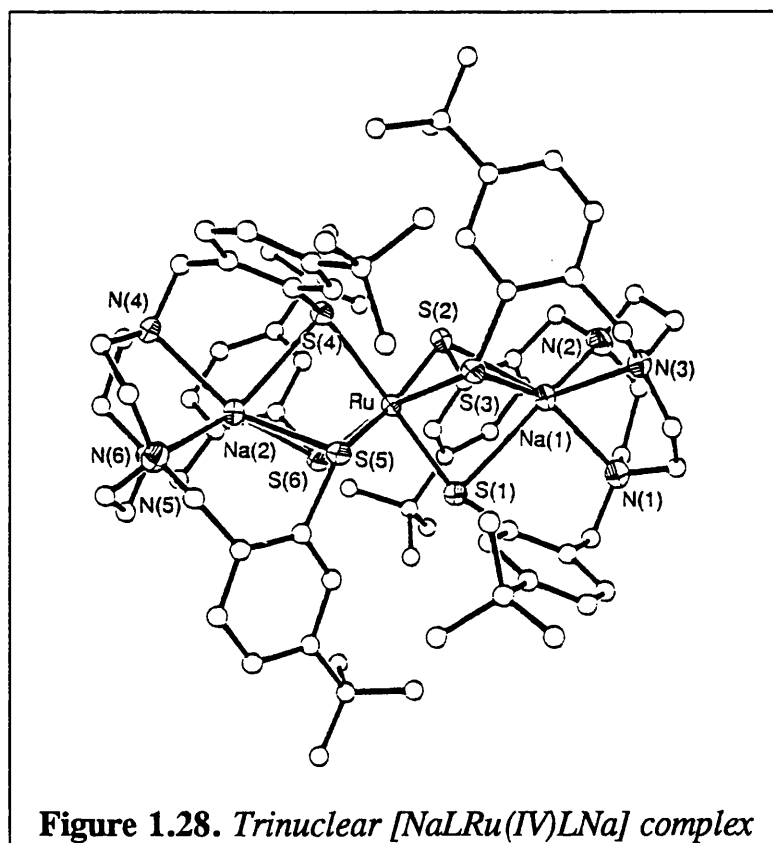


Wieghardt *et al.* has prepared two thiolate ligands based on TACN, namely 1,4,7-tris(4-*tert*-butyl-2-mercaptobenzyl)-1,4,7-triazacyclononane and 1,4,7-tris(2-mercaptopropyl)-1,4,7-triazacyclononane (**24**), although no detailed synthetic route to the latter has been published.

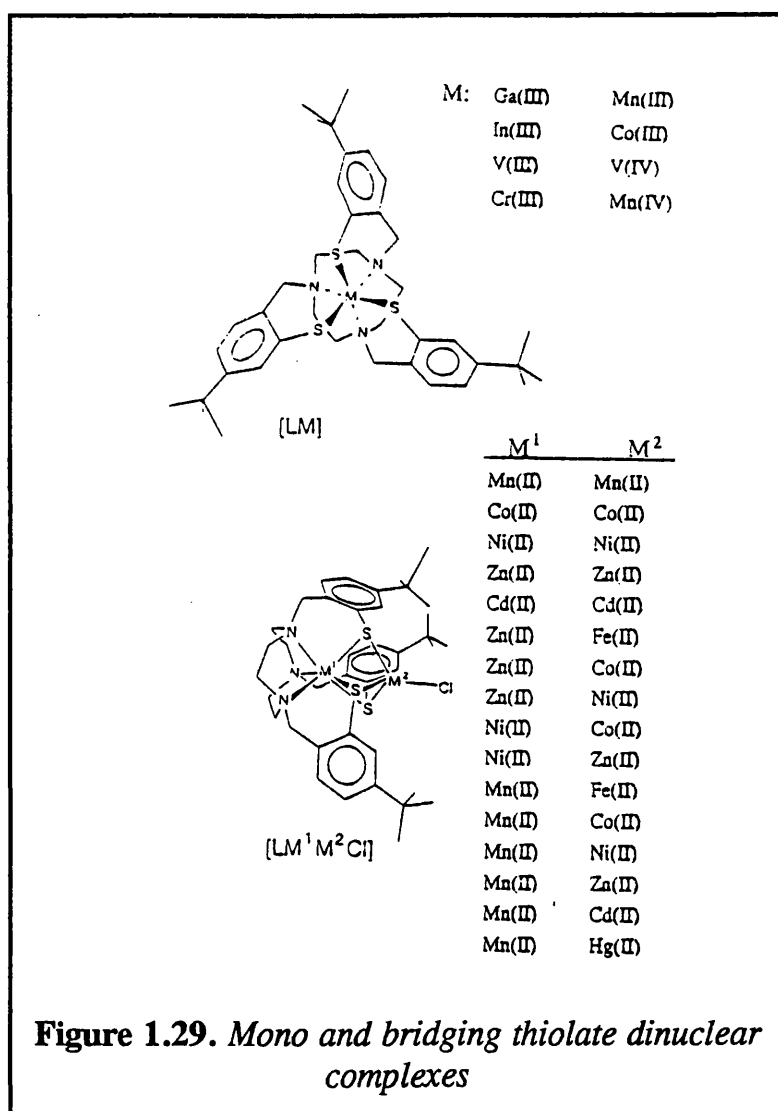


The ligand prepared by Evans was essentially an S_3 donor, whereas Wieghardt's ligand is a true N_3S_3 donor ligand capable of mononuclear and more interestingly multinuclear complexes. Wieghardt's original paper centred on the structural and magnetic analysis of a mononuclear octahedral Fe(III) complex as a model for a iron-sulphur centre in nitrile hydratase.

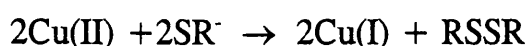
Thiolate groups are well known to form bridges between transition metal ions and this was shown in a series of trinuclear (**54**) and dinuclear (**55**) complexes of Wieghardt's ligand. The trinuclear complex $[LNaRu(IV)LNa]$ (figure 1.28) contains two sodium ions coordinated to the N_3S_3 donor set in a trigonal prismatic geometry, the thiolate groups then further coordinate a central ruthenium ion in an octahedral geometry.



Subsequent publications showed that mononuclear complexes were formed with tri- and tetravalent ions, whereas dinuclear complexes were formed with divalent metal ions (figure 1.29). In the dinuclear complexes one metal is six coordinate (N_3MS_3) while the other is four coordinate (N_3MCl); the two polyhedra are linked by μ_2 -thiolate bridges. Heterodinuclear complexes were obtained from the $[LM_2Cl]$ species by abstraction of the four coordinate metal ion with TACN and replacement by a different metal ion.



The sterically hindered single pendant thiolate armed macrocycle synthesised by Tolman (**31**) (scheme 1.5) forms a thiolate bridged dimer with Cu(II) (figure 1.30). As mentioned previously, thiolates are well known to bridge transition metal ions, indeed Cu(I)-(μ -SR)-Cu(I) are common. With Cu(II) a redox coupling to a disulphide is usually observed as shown below:



The complex was unusual in that it has the proper stoichiometry to undergo such a redox reaction shown above, yet no coupling is observed. The long S...S distance [3.09Å] was shorter than that required for a van der Waals contact [3.7Å], but by no means was it a disulphide bond. It is unusual properties like this that has stimulated the interests of chemists' in the macrocyclic field over the past few decades.

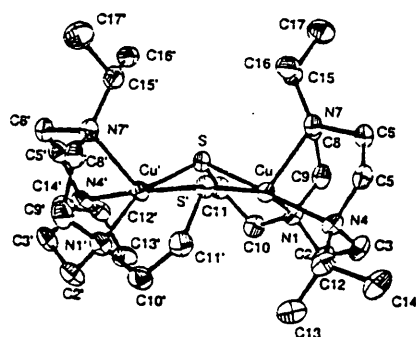


Figure 1.30. *Tolman's thiolate bridged Cu(II) dimer*

1.4 BIOCOORDINATION CHEMISTRY (56)

1.4.1 Metals in Biological Systems

Although biology involves extremely complicated organic molecules and their reactions, it is important to recognise that without the participation of metallic elements, life would not exist (table 1.3). At present it is known that 13 metals are essential for plants and animals. Four of these metals, Na, K, Mg and Ca are required in bulk by essentially all forms of life; the remaining nine metals are from the d-block occurring in small quantities. Fe, Cu, Zn are essential to most life forms and are known as the trace metals, whereas the ultratrace metals (Mn, Mo, Co, Ni and V) are required by a few life forms.

Metal	g/75Kg
Ca	1100
K	160-200
Na	70-120
Mg	25
Fe	4-5
Zn	2-3
Cu	0.8-1.2
Mn	1
V	0.015
Mo	0.01
Cr	0.002
Co	0.0012

Table 1.3. Metals in man

One of the major roles played by metallic elements in biology is in metalloproteins, i.e. proteins that incorporate one or more metal atoms as a normal part of their structure. An important subclass of metalloproteins is metalloenzymes where the metal is not only a part of the protein structure, but also plays an important role in the active biosite. There are a great number of metalloproteins known, only haemocyanin and carbonic anhydrase which have some relevance to this work will be mentioned in this chapter.

1.4.2 Model Systems for Metallobiosites

It is generally believed that the function of a biological system depends on its structure. For the past few decades single X-ray diffraction studies have determined biological structure, although there is question as to whether the structure in the crystalline form is the same as the structure *in vivo*. Often the precise nature of an active metallobiosite is structurally unknown and comparison of spectroscopic data with that of a small molecular model is required. Models have been classified as one of three types:

- (i) Speculative, where the structure is not known but is anticipated from accumulated spectroscopic data and so the model is used to mimic these properties in order to produce a predictive comparison.
- (ii) Corroborative, where the structure of the metalloprotein is known and the model is built to determine if the properties of the metalloprotein are dominated by the first coordination sphere of the metal.
- (iii) Functional, where the actual functioning of the site is reproduced by a model system.

A protein contains large folded chains which play an important role in the active biosite. Therefore, reproduction of the spectroscopic and structural properties of a protein by a small molecular model does not mean that the model can mimic the protein in a truly functional manner.

1.4.3 Copper Proteins

Copper is an essential element in biology found in many enzymes and in the hemolymph of arthropods and molluscs (57). The most notable features of protein bound active copper are in the metabolism of O₂ and N/O compounds and its frequent association with oxidising organic substrates. The classical division of copper proteins into Type I, II, and III (table 1.4)

was a consequence of correlating the spectroscopic and magnetic properties of the protein with its function.

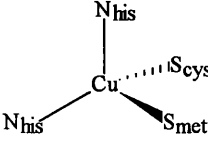
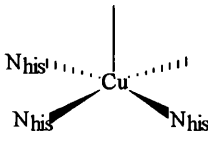
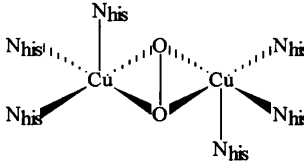
	<p>EPR spectra have abnormally small hyper fine splitting ($A_{ }$)</p> <p>Type I copper (blue)</p> <p>Function - electron transfer</p> <p><i>plastocyanin, azurin, laccases</i></p>	<p>absorption spectra have a very intense band ($\sim 600\text{nm}$, $\epsilon \sim 5000$), due to LMCT ($\text{Cys}^- \rightarrow \text{Cu}^{2+}$)</p>
	<p>EPR spectra typical of small Cu(II) complexes</p> <p>Type II copper (non-blue)</p> <p>Function - catalysis and redox reactivity</p> <p><i>galactose oxidase, superoxide dismutase, cytochrome c oxidase</i></p>	<p>normal Cu(II) absorption spectra with no intense LMCT</p>
	<p>EPR silent, diamagnetic, $2J > 600\text{cm}^{-1}$</p> <p>Type III copper</p> <p>Function - O_2 activation for oxygenation and transport</p> <p><i>haemocyanin, tyrosinase</i></p>	<p>intense absorption spectra (580nm, $\epsilon 1000$, $340 \epsilon 20000$), due to $\text{O}_2^{2-} \rightarrow \text{Cu}^{2+}$</p>

Table 1.4. Classical Copper Types

Subsequent discovery of additional copper biosites, which do not fall into the above categories has lead to the definition of further types of copper

centres in biological systems (table 1.5). Future structure determinations may well lead to corrections of the aforementioned types or even further alternatives.

	<p>normal Cu(II) EPR spectra</p> <p>intense absorption spectra due to LMCT ($O_2^{2-} \rightarrow Cu^{2+}$)</p>
<p>Type II+III Trimer</p> <p>Function - O_2 activation for oxidase function</p> <p><i>ascorbate oxidase,, laccases</i></p>	
	<p>EPR spectra have very small $A_{ }$ due to two equivalent $Cu^{1.5+}$</p> <p>absorption in the near infrared due to metal-metal charge transfer</p>
<p>Cu_A</p> <p>Function - electron transfer</p> <p><i>N₂O reductase, cytochrome c oxidase</i></p>	
	<p>Metallothioneins (~ 61 amino acids) are cystine-rich proteins able to bind metals (Cu^I) with a high affinity for thiolates</p>
<p>MT-Cu</p> <p>Function - copper storage, regulation and transport</p>	

Table 1.5. New Types of Copper Centres in Biology

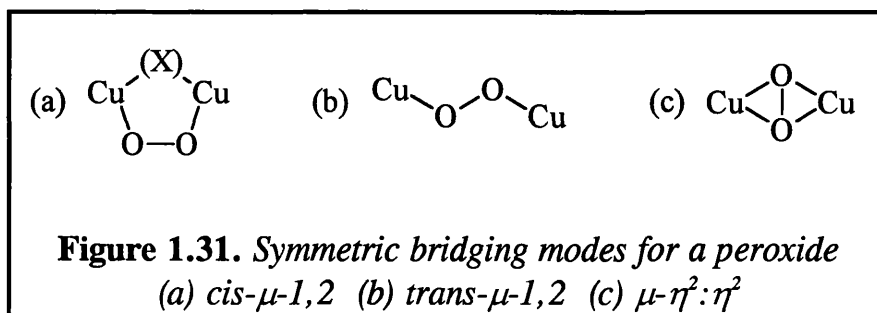
1.4.4. Haemocyanin

Dioxygen interactions with dinuclear Cu(I) species occur in both biological and inorganic chemistry (58). A dicopper(I) centre is readily amenable to $2e^-$ oxidation by O_2 to generate a dicopper(II) species with simultaneous $2e^-$ reduction of dioxygen to peroxide. The resulting $Cu(II)_2(O_2^{2-})$ species is recognised as an active intermediate or product in at least two Cu enzymes, namely haemocyanin and tyrosinase. Haemocyanin is an O_2 carrier protein in arthropods and molluscs; the deoxy dicopper(I) form reversibly binds O_2 via its $2e^-$ reduction to O_2^{2-} . A similar active site has been identified for tyrosinase, a monooxygenase that catalyses ortho hydroxylation of phenols to catechols with further oxidation to quinones.

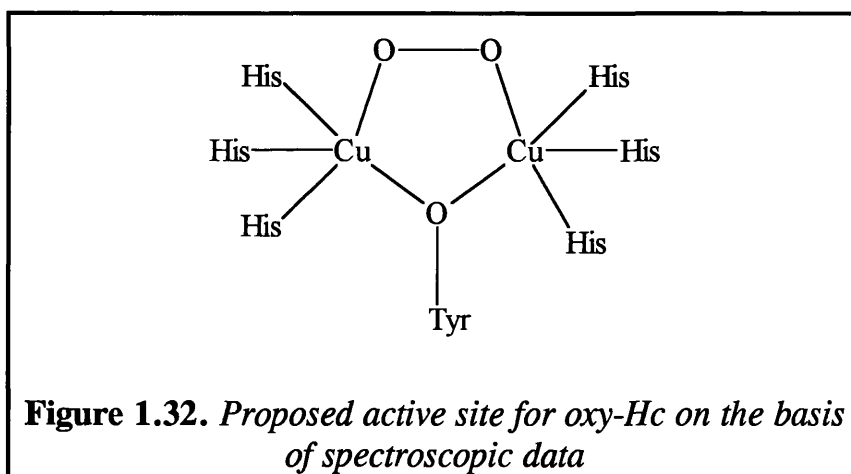
The active site in oxy-haemocyanin was initially proposed from spectroscopic data:

- (i) Intense blue colour of oxy-haemocyanin (345nm , 570nm) assigned as $O_2^{2-} \rightarrow Cu^{2+}$ charge transfer (59).
- (ii) Resonance Raman studies found $\nu(O-O)$ at $750cm^{-1}$, indicative of a peroxide species. Use of $^{16}O^{18}O$ showed the peroxide species to bind in a symmetrical fashion (60).
- (iii) EXAFS studies showed the $Cu \cdots Cu$ distance to be *ca.* 3.6-3.7Å with three histidine ligands per Cu(II) centre (61).
- (iv) Oxy-haemocyanin is diamagnetic at room temp ($-2J > 600cm^{-1}$) (62).

From the Raman studies the coordination mode of the peroxide species must be symmetric and therefore could be one of three possibilities (Figure 1.31).

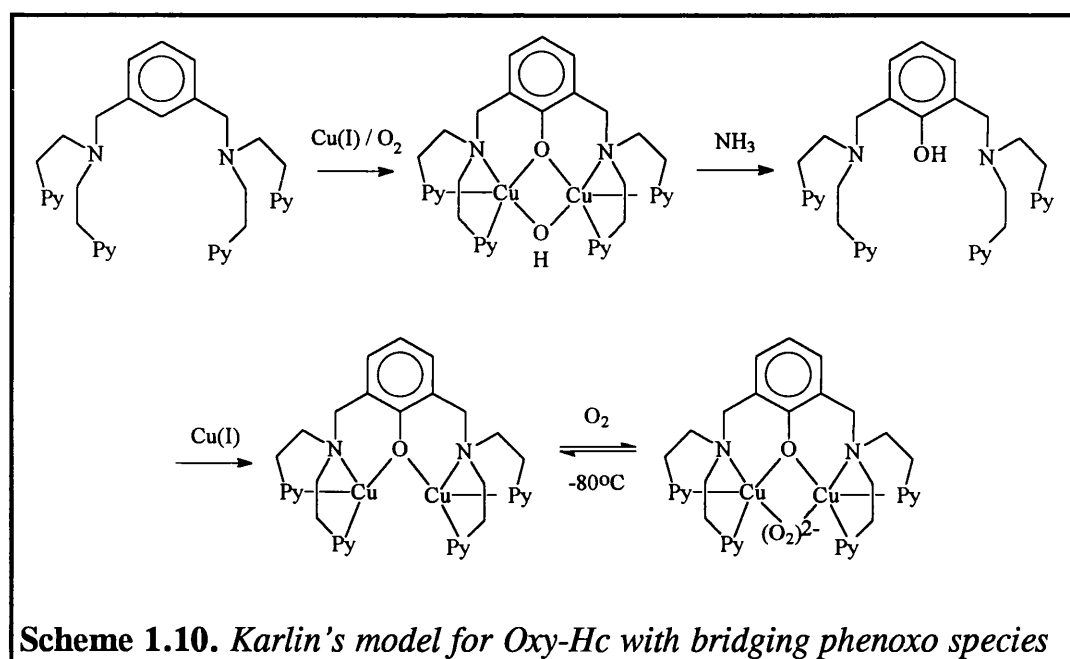


The diamagnetic nature of oxy-haemocyanin was believed to be a consequence of an endogenous bridging ligand, it was therefore believed that the active site consisted of a *cis-μ-1,2* peroxide and the bridging ligand was tyrosine (figure 1.32).



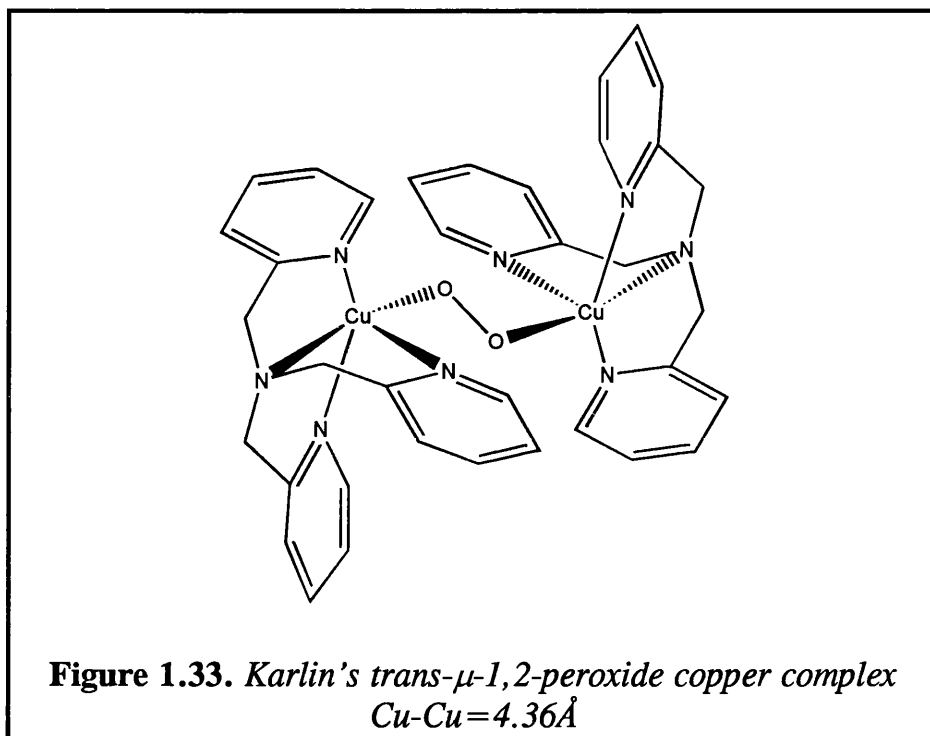
This proposed active site generated many model studies aimed at producing a dicopper system which could reversibly bind O₂ (63). In 1984 Karlin *et al.* (64) reported the synthesis and structure of a dinuclear

copper(I) complex containing a bridging phenoxo group, the complex also reacted with O_2 quasireversibly giving a peroxo dinuclear copper(II) complex (Scheme 1.10). The basis of the peroxide species was determined by resonance Raman spectroscopy ($\nu(O-O)$ 803cm^{-1}) and UV/VIS spectroscopy (385, 610nm). The subsequent detailed Raman study (65), however showed the peroxide to be bound unsymmetrically and therefore in a different fashion to oxy-haemocyanin.



In 1989 the solution of the crystal structure of deoxy-haemocyanin from the spiny lobster (*Panulirus interruptus*) confirmed the dinuclear nature of the active site, but eliminated the concept of an endogenous bridge as there was no amino acid residue within 6\AA capable of bridging the dicopper site (66). The coordination mode of the peroxide species could now only be

trans- μ -1,2 or μ - $\eta^2:\eta^2$. Crystallographic characterisation of a trans- μ -1,2 peroxide species was published by Karlin (67) in 1988 (figure 1.33), yet the complex did not mimic the spectroscopic properties of oxy-haemocyanin.

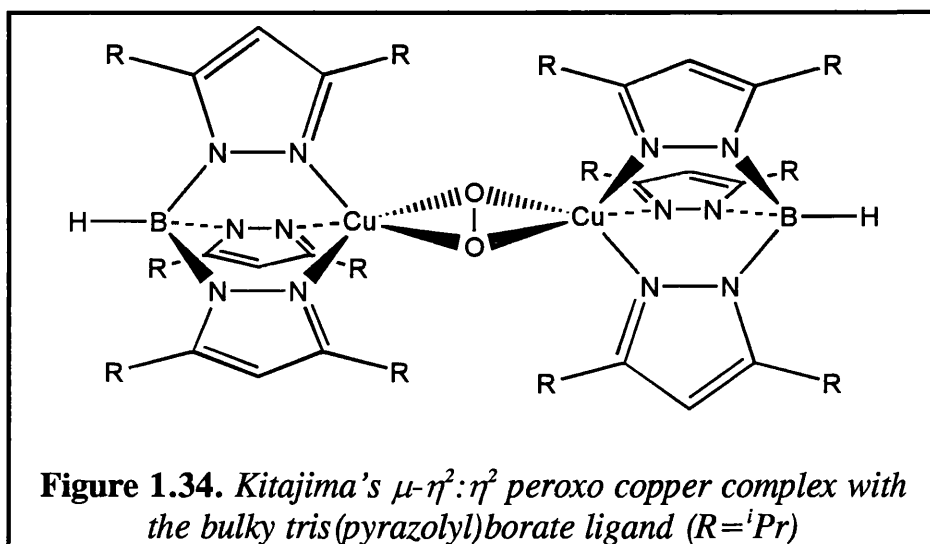


The μ - $\eta^2:\eta^2$ coordination mode of peroxide was not considered seriously due to the lack of structurally characterised complexes, but in 1989 Kitajima *et al.* (68) published the structure of a μ - $\eta^2:\eta^2$ peroxo dinuclear copper(II) complex (figure 1.34). The complex exhibited remarkably similar characteristics to those of oxy-haemocyanin:

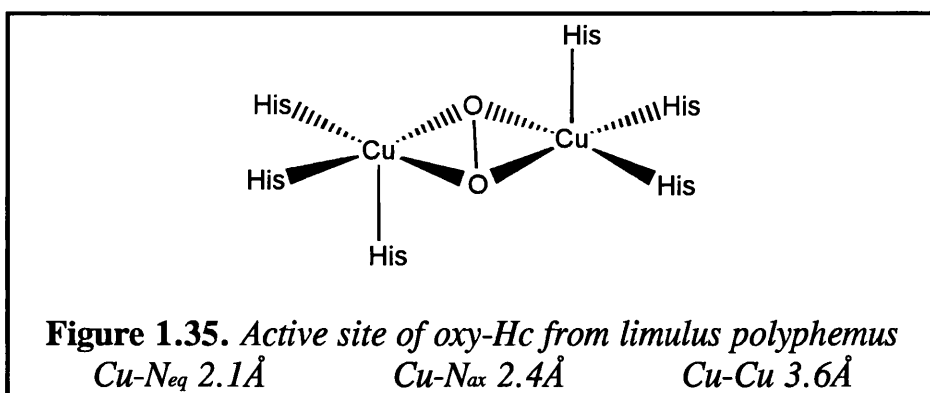
- (i) Absorption spectra contained bands at 345nm (ϵ 20000) and 550nm (ϵ 1000)
- (ii) EPR silent and diamagnetic ($-2J > 900\text{cm}^{-1}$)

(iii) Resonance Raman studies found $\nu(\text{O-O})$ at $725\text{-}760\text{cm}^{-1}$

(iv) The crystal structure showed the $\text{Cu}\cdots\text{Cu}$ distance to be *ca.* 3.56\AA



In 1994 the dilemma concerning the actual mode of bonding was resolved with the crystal structure of oxy-haemocyanin from the horseshoe crab (*limulus polyphemus*) (69). The peroxide was found in a $\mu\text{-}\eta^2\text{:}\eta^2$ mode with three histidines attached to each copper (figure 1.35).

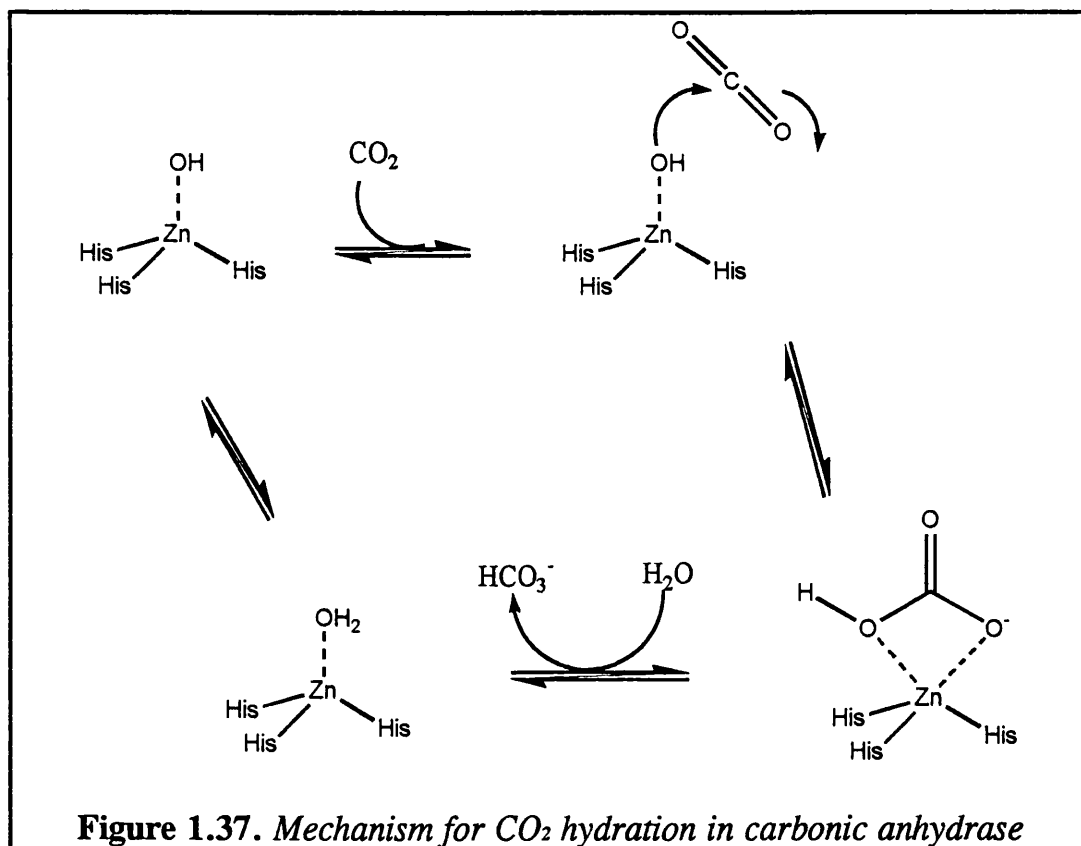
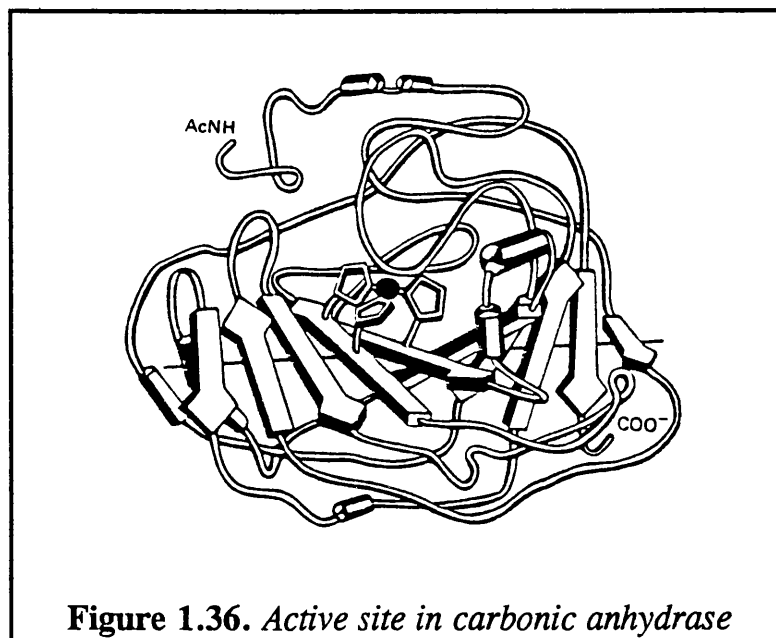


1.4.5. Carbonic Anhydrase

Zinc is the second most abundant trace element in man and is required as an integral component in many enzymes (70). It can play an active catalytic role or it can act in a structural role. A unique feature of all structurally characterised active mononuclear zinc sites is a water molecule which can be activated by ionization or by polarization.

Carbonic anhydrase was first recognised as a zinc enzyme in 1940 and is found in nearly all phyla. Its role is to catalyse the reversible hydration of carbon dioxide to form bicarbonate and a proton. In the absence of the enzyme, hydration is somewhat 10^7 times slower. Human carbonic anhydrase is found in red blood cells and has a molecular weight of about $\sim 30,000$ D. There are two similar human forms and both have been characterised by X-ray crystallography. The zinc atom is ligated by three histidine imidazole groups (figure 1.36) and a water molecule in a distorted tetrahedral geometry. A general mechanism to the formation of HCO_3^- is shown in figure 1.37. The first sequence involves nucleophilic attack at the carbon atom of the CO_2 , it is assumed that hydrogen bonding to the oxygen atoms of the CO_2 molecule enhances the positive character of the carbon atom. The positioning of the CO_2 prior to nucleophilic attack is believed to be by interactions other than that from the Zn^{2+} i.e. interactions from the surrounding protein chains. The final sequence in the mechanism is the

regeneration of the catalytically active species ZnOH^+ in which a neighbouring histidine acts as a proton acceptor.



1.5 OBJECTIVES

At the time of commencement of this work there was considerable activity in the field of hard pendant arm macrocycles based on TACN. The number of publications of TACN macrocycles containing soft pendant donor groups in the pendant arm was limited to three publications, all on trisubstituted rings containing thiolate pendant arms. The number of single pendant arm derivatives of TACN was also limited and few groups were exploiting the route to single pendant arms using the method pioneered by Atkins and Weisman.

The primary aim of this work was to study the coordination chemistry of TACN based macrocycles containing one, two or three soft pendant donor arms, thus allowing the fusion of macrocyclic with organometallic chemistry. The soft donor groups to be considered were phosphines, alkenes, alkynes and activated arenes. If possible it was desired to make the macrocycle chiral or be dinucleating in nature. It was envisaged that these mixed donor ligands would have a different chemistry to their more studied hard counterparts.

1.6 REFERENCES

1. J.M Lehn, *Angew. Chem., Int. Ed. Engl.*, 1988, **27**, 89.
2. N.F. Curtis, *J. Chem. Soc.*, 1960, 4409.
3. C.J. Pedersen, *J. Am. Chem. Soc.*, 1967, **89**, 7017.
4. B. Deiderich, J-M. Lehn, J-P. Sauvage, *Tetrahedron Letters.*, 1969, **34**, 2885.
5. Y.S. Gwan, D.H. Peacock, *J. Chem. Soc.*, 1937, 1468.
6. H. Koyama, T. Yoshino, *Bull. Chem. Soc. Jpn.*, 1972, **45**, 481.
7. T.J. Atkins, J.E. Richman, *J. Am. Chem. Soc.*, 1974, **96**, 2268.
8. I. Lázár, *Synth. Comm.*, 1995, **25**, 3181.
9. R.W. Alder, R.W. Mowiam, D.J. Vachon, G.R. Weisman, *J. Chem. Soc., Chem. Comm.*, 1991, 507.
10. R. Bhula, P. Osvath, C. Weatherburn, *Coord. Chem. Rev.*, 1988, **91**, 89.
11. P.V. Bernhardt, G.A. Lawrance, *Coord. Chem. Rev.*, 1990, **104**, 297.
12. P. Chaudhuri, K. Wiegardt, *Prog. Inorg. Chem.*, 1987, **35**, 329.
13. T. Arishima, K. Hamada, S. Takamoto, *Nippon Kagaku Kaishi*, 1973, 1119.
14. R.D. Hancock, J.P. Micheal, B.A. Sayer, *Inorg. Chim. Acta.*, 1983, **77**, L63.

15. R.D. Peacock, J. Robb, *Inorg. Chim. Acta.*, 1986, **121**, L15.
16. I.A. Fallis, L.J. Farrugia, N.M. MacDonald, R.D. Peacock, *J. Chem. Soc., Dalton Trans.*, 1993, 2759.
17. U. Auerbach, U. Eckert, B. Nuber, J. Weiss, K. Wieghardt, *Inorg. Chem.*, 1990, **29**, 938.
18. E. Cole, G. Ferguson, J.F. Gallagher, B. Kaitner, D. Parker, *J. Chem. Soc., Chem. Comm.*, 1991, 1473.
19. M.I. Kabachnik, T.Ya. Medved, B.K. Shcherbakov, E.I. Sinyavskaya, M.Yu. Polikarpov, K.B. Yatsimirskii, *Zhur. Neorg. Khim.*, 1984, **29**, 884. [*Russ. J. Inorg. Chem.*, 1985, **30**, 1463].
20. L.R. Gahan, G.A. Lawrence, A.M. Sargeson, *Aust. J. Chem.*, 1982, **35**, 1119.
21. B. Nuber, E. Schöffmann, J. Weiss, K. Wieghardt, *Inorg. Chem.*, 1986, **25**, 4877.
22. N.W. Alcock, F. McLaren, P. Moore, G.A. Pike and S.M. Roe, *J. Chem. Soc., Chem. Comm.*, 1989, 629.
23. P.E. Fanwick, D.A. Moore, M.J. Welch, *Inorg. Chem.*, 1990, **29**, 672.
24. T. Biessel, K.S. Bürger, C. Butzlaff, A.X. Trautwein, G. Voigt, K. Wieghardt, *Inorg. Chem.*, 1993, **32**, 124.
25. D.J. Evans, G. Garcia, G.J. Leigh, M.S. Newton, M.D. Santana, *J. Chem. Soc., Dalton Trans.*, 1992, 3229.
26. P. Chaudhuri, B. Nuber, J. Weiss, K. Wieghardt, *Inorg. Chem.*, 1982, **21**, 3086.
27. G. Haselhorst, B. Nuber, S. Stoezel, A. Strassburger, W. Walz, K. Wieghardt, *J. Chem. Soc., Dalton Trans.*, 1993, 93.

28. T. Beissel, R. Boese, B.S.P.C.D. Vedova, K. Wieghardt, *Inorg. Chem.*, 1990, **29**, 1736.
29. H. Hope, B. Moezzi, P.P. Power, M. Viggiano, *Inorg. Chem.*, 1984, **23**, 2550.
30. V. Lynch, J.L. Sessler, J.W. Sibert, *Inorg. Chem.*, 1990, **29**, 4143.
31. R.P. Houser, J.A. Halfen, V.G. Young, N.J. Blackburn, W.B. Tolman, *J. Am. Chem. Soc.*, 1995, **117**, 10745.
32. K. Wieghardt, I. Tolksdorf, W. Herrmann, *Inorg. Chem.*, 1985, **24**, 1230.
33. L. Behle, M. Neuburger, M. Zehnder, T. Kaden, *Helv. Chim. Acta.*, 1995, **78**, 693.
34. T.J. Atkins, *J. Am. Chem. Soc.*, 1980, **102**, 6364.
35. G.R. Weisman, D.J. Vachon, V.B. Johnson, D.A. Gronbeck, *J. Chem. Soc., Chem. Comm.*, 1987, 886.
36. L.J. Farrugia, P.A. Lovatt, R.D. Peacock, *Acta Cryst.*, 1993, **C49**, 2164.
37. A.J. Blake, I.A. Fallis, R.O. Gould, S.G. Harris, S. Parsons, S.A. Ross, M. Schröder, *Acta Cryst.*, 1995, **C51**, 738.
38. D. Hanke, K. Wieghardt, B. Nuber, R-S. Lu, R.K. McMullan, T.F. Koetzle, R. Bau, *Inorg. Chem.*, 1993, **32**, 4300.
39. A.J. Blake, I.A. Fallis, R.O. Gould, S. Parsons, S.A. Ross, M. Schröder, *J. Chem. Soc., Chem. Comm.*, 1994, 2467.

40. D.K. Cabbiness and D.W. Margerum, *J. Am. Chem. Soc.*, 1969, **91**, 6540.
41. M. Kodama, E. Kimura, *J. Chem. Soc., Dalton Trans.*, 1978, 1081.
42. L. Christiansen, D.N. Hendrickson, H. Toftlund, S.R. Wilson, C-L. Xie, *Inorg. Chem.*, 1986, **25**, 2813.
43. U. Bossek, P. Chaudhuri, W. Herrmann, B.C. Menke, J. Weiss, K. Wiegardt, *Inorg. Chem.*, 1982, **21**, 4308.
44. M.J. van der Merwe, J.C.A. Boeyens and R.D. Hancock, *Inorg. Chem.*, 1985, **24**, 1208.
45. M. Studer, T.A. Kaden, *Helv. Chim. Acta.*, 1986, **68**, 2081.
46. M. Studer, A. Riesen, T.A. Kaden, *Helv. Chim. Acta.*, 1989, **72**, 307.
47. D. Schulz, T. Weyhermüller, K. Wiegardt, C. Butzlaff, A.X. Trautwein, *Inorg. Chim. Acta.*, 1996, **246**, 387.
48. A.A. Belal, L.J. Farrugia, R.D. Peacock and J. Robb, *J. Chem. Soc., Dalton Trans.*, 1989, 931.
49. A.A. Belal, P. Chaudhuri, I.A. Fallis, L.J. Farrugia, R. Hartung, N.M. MacDonald, R.D. Peacock, B. Nuber, J. Weiss and K. Wiegardt, *Inorg. Chem.*, 1991, **30**, 4397.
50. I.A. Fallis, L.J. Farrugia, N.M. MacDonald, R.D. Peacock, *Inorg. Chem.*, 1993, **32**, 779.
51. L.J. Farrugia, R.D. Peacock, *Acta. Cryst.*, 1991, **C47**, 1312.
52. A.J. Blake, T.M. Donlevy, P.A. England, I.A. Fallis, S. Parsons, S.A. Ross, M. Schröder, *J. Chem. Soc., Chem. Comm.*, 1994, 1981.

53. H. Al-Sagher, I.A Fallis, L.J. Farrugia, R.D. Peacock, *J. Chem. Soc., Chem. Comm.*, 1993, 1499.
54. K. Mochizuki, F. Kesting, T. Weyhermüller, K. Wiegardt, C. Butzlaff, A.X. Trautwein, *J. Chem. Soc., Chem. Comm.*, 1994, 909.
55. T. Beissel, T. Glaser, F. Kesting, K. Wiegardt, B. Nuber, *Inorg. Chem.*, 1996, **35**, 3936.
56. *Biocoordination Chemistry*, D.E. Fenton, Oxford University Press: Oxford, 1995.
57. *Bioinorganic Chemistry of Copper*, ed. K.D. Karlin, Z. Tyeklár, Chapman and Hall: London, 1993.
58. *Biological and Inorganic Copper Chemistry*, ed. K.D Karlin, J. Zubieta, Adenine: Guilderland, NY, 1986.
59. T.B. Freedman, J.S. Loehr, T.M. Loehr, *J. Am. Chem. Soc.*, 1976, **98**, 2809.
60. T.B. Freedman, J.S. Loehr, T.M. Loehr, *J. Am. Chem. Soc.*, 1977, **99**, 4187.
61. *J. Am. Chem. Soc.*, 1980, **102**, 4212.
62. T.H. Moss, D.C. Gould, A. Ehrenberg, J.S. Loehr, H.S. Mason, *Biochemistry*, 1973, **12**, 2444.
63. K.D. Karlin, Y. Gultneh, *Prog. Inorg. Chem.*, 1987, **35**, 219.
64. K.D. Karlin, R.W. Cruse, Y. Gultneh, J.C. Hayes, J. Zubieta, *J. Am. Chem. Soc.*, 1984, **106**, 3372.
65. J.E. Pate, R.W. Cruse, K.D. Karlin, E.I. Solomon, *J. Am. Chem. Soc.*, 1987, **109**, 2668.
66. A. Volbeda, W.G. J. Hol, *J. Mol. Biol.*, 1989, **209**, 249.
67. R.R. Jacobson, Z. Tyeklár, A. Farooq, K.D. Karlin, S. Liu, J. Zubeta, *J. Am. Chem. Soc.*, 1988, **110**, 3690.
68. N. Kitajima, K. Fujisawa, Y. Moro-oka, K. Toriumi, *J. Am. Chem. Soc.*, 1989, **111**, 8975.

69. K.A. Magnus, H. Ton-That, J.E. Carpenter, *Chem. Rev.*, 1994, **94**, 727.
70. E. Kimura, *Prog. Inorg. Chem.*, 1994, **41**, 443.

CHAPTER 2

EXPERIMENTAL

2.1 INSTRUMENTATION

UV/VIS spectra were obtained on Perkin-Elmer Lambda 9 and Shimadzu UV-3101PC spectrophotometers. Reference and sample spectra were obtained in a 1cm quartz cuvette. Corrected spectra were produced by sample-reference subtraction using the Perkin-Elmer PECSS and Shimadzu UVPC software programs.

NMR spectra were obtained on AM200 and WP200 200MHz FT-NMR spectrometers using the Bruker Dis-NMR suite of programs. Carbon spectra were obtained at 50MHz using a DEPT sequence. Phosphorus spectra were obtained at 81MHz and were broad-band proton decoupled. All samples were referenced internally to solvent resonances. Deuterated solvents were purified by freeze-thaw degassing and stored under a nitrogen atmosphere.

Infra-red spectra were obtained on Philips PU9800, Perkin-Elmer 16PC & P1000 FT-IR spectrometers. Samples were prepared as 8 mm diameter KBr discs using 300 mg of KBr and a press force of 8 tons or as thin films between NaCl plates. Solution spectra were obtained using matched CaF_2 cells and the corrected spectra were produced by sample-reference subtraction.

Melting points were recorded in air using a Gallenkamp melting point apparatus and were uncorrected.

2.2 MAGNETIC SUSCEPTIBILITY MEASUREMENTS

Magnetic measurements were determined by Drs A. Harrison and G. Whittaker (University of Edinburgh) using a SQUID magnetometer. Single crystals were attached to a silica fibre and the magnetic susceptibility run over the range 1.8-300K. The data between 50 and 300K was fitted with a Bleaney-Bowers expression.

2.3 X-RAY CRYSTALLOGRAPHIC DATA COLLECTION.

Crystallographic data was obtained by Dr Louis J. Farrugia; crystals were mounted on a glass fibre and data collected at ambient temperature on an Enraf-Nonius Turbo CAD4 automated diffractometer, running under CAD4-Express software and using graphite monochromated X-radiation ($\lambda = 0.71069\text{\AA}$). An ω - 2θ scan mode was used.

Unit cell parameters were determined by refinement of the setting angles of 25 reflections using the SET 4 routine. All structure solution calculations were performed on a IBM compatible PC using the Glasgow WINGX suite of programs.

2.4 CHEMICALS AND SOLVENTS.

Chemicals, their suppliers and purity used in preparative work are listed in table 2.1. Solvents and purification methods are listed in table 2.2.

Table 2.1 Chemicals and suppliers.

Allyl Bromide (Aldrich)	99%
Ammonium hexafluorophosphate (Fluka)	98+ %
α,α' -Azoisobutyronitrile (Janssen)	98%
4-Bromo-1-butene (Aldrich)	97%
4-Bromo-2-methyl-2-butene (Aldrich)	96%
S(+)-3-Bromo-2-methyl-1-propanol (Fluka)	97+ %
3-Bromo-2-methyl-1-propene (Aldrich)	97%
5-Bromo-1-pentene (Lancaster)	97%
Caesium hydrogencarbonate (Aldrich)	99.9%
Chloroauric acid (Matthey Chemicals)	
Cobaltous chloride hexahydrate (BDH)	97%
⁶³ Copper(II) tetrafluoroborate hydrate (Aldrich)	19-22%
Cupric nitrate trihydrate (Riedel de Haen)	99%
<i>trans</i> -1,4-Dibromobut-2-ene (Aldrich)	99%

α,α' -Dibromo- <i>meta</i> -xylene (Aldrich)	97%
α,α' -Dibromo- <i>ortho</i> -xylene (Aldrich)	96%
α,α' -Dibromo- <i>para</i> -xylene (Aldrich)	97%
Diethylenetriamine (Aldrich)	99%
<i>N,N</i> -Dimethylformamide-dimethylacetal (Avocado)	95%
Diphenyl phosphine (Fluka)	95+ %
Ethylene Glycol (Aldrich)	99+ %
Lithium aluminium hydride (Aldrich)	95%
Methyl iodide (Fluka)	99%
Nickel chloride hexahydrate (BDH)	98%
⁸ Ruthenium(III) chloride hydrate (herraesus)	40.79%
Silver tetrafluoroborate anhydrous (Avocado)	98%
Sodium in liquid paraffin (Fisons)	99+ %
Sodium carbonate (BDH)	99.9%
Sodium Hydroxide (BDH)	98%
Tetraphenylboron sodium (Aldrich)	99.5+ %
Thionyl chloride (Fluka)	97+ %
<i>p</i> -Toluene sulphonyl chloride (Aldrich)	98%
L-Valine (Avocado)	99%
Zinc chloride anhydrous(BDH)	97+ %

^s Purity stated as % metal in salt

All reagents were used without further purification unless otherwise stated.

Table 2.2. Solvents and purification methods.

Ethanol	Twice distilled from magnesium turnings and iodine, under N ₂ . Stored over 4Å sieves.
Acetonitrile	Distilled from calcium hydride under N ₂ .
Di-n-butyl ether	Analytical grade.
Dichloromethane	Distilled from calcium hydride under N ₂ .
Diethyl ether	Distilled from sodium benzophenone under N ₂ .

Dimethyl formamide	Stored over dried magnesium sulphate overnight, filtered and stored over 4Å sieves.
Ethylene diamine	Dried over sodium hydroxide, then distilled from sodium under N ₂ .
Methanol	Stored over activated 3Å sieves.
40-60°C Petroleum Ether	Distilled under N ₂ from sodium/potassium alloy.
Tetrahydrofuran	Distilled under N ₂ from sodium benzophenone.
Toluene	Distilled from sodium under N ₂ and stored over 4Å molecular sieves.

All other solvents were used without further purification.

2.5 LIGAND SYNTHESSES

2.5.1 1,4,7-TRIAZACYCLONONANE AND ITS PRECURSORS.

The preparations outlined below are based upon the Richman-Atkins (1) procedure.

(1) *N,N',N''*-Tris(*p*-tolylsulphonyl)diethylene triamine.



A 5L three necked round bottom flask equipped with mechanical stirrer and thermometer was charged with diethylene triamine (165g, 1.6mol) dissolved in distilled water (1L). Sodium hydroxide (192g, 4.8mol) was added slowly keeping the temperature below 40°C. The solution was cooled to 15°C and diethyl ether (1L) was added with vigorous stirring to ensure complete mixing of the two phases. *p*-Toluene sulphonyl chloride (916g, 4.8mol) was added slowly, while keeping the temperature below 20°C. When all the *p*-toluene sulphonyl chloride had been added, the solution was cooled to 0°C and stirring maintained for 1hr. The solid product was filtered off, washed with water (4L), ethanol (1L), diethyl ether (1L) and dried at 90°C overnight. The pure product was obtained by filtration from boiling ethanol and was air dried.

FW: 565gmol⁻¹

Yield 653g (72%)

Found: C 52.0% H 5.4% N 7.3% Calc. for C₂₅H₃₁N₃O₆S₃ C 53.1%
H 5.5% N 7.4%.

¹H NMR (200MHz, CDCl₃, δ): 2.40 (s, 9H, Ar-CH₃); 3.13 (m, 8H, N-CH₂); 7.28 (d, 6H, Ar-H); 7.74 (d, 6H, Ar-H).

M.Pt. 180-183°C.

(2) 1,2-Bis[(*p*-tolylsulphonyl)oxy]ethane.

TsO(CH₂)₂OTs

A 3L three necked round bottom flask equipped with a mechanical stirrer, dropping funnel and thermometer was charged with *p*-toluene sulphonyl chloride (916g, 4.8mol) dissolved in acetone (1L). Ethylene glycol (149g, 2.4mol) was added to the solution and the mixture was cooled to 15°C. Meanwhile sodium hydroxide (192g, 4.8mol) was dissolved in distilled water (500mL) and the solution cooled to room temperature. The cooled sodium hydroxide solution was added dropwise to the mixture keeping the temperature below 20°C. When the last sodium hydroxide had been added the mixture was stirred for a further 1hr, then added to 3L of ice water with vigorous stirring. The solid product was filtered, washed with water (4L), cold ethanol (1L), diethyl ether (1L) and dried at 90°C

overnight. The product was recrystallised by dissolution in the minimum volume of boiling chloroform followed by the addition of three volumes of ethanol. The solution was cooled to 0°C. Crystallisation commenced after 1hr and was completed by refrigeration overnight. The product was collected by filtration, washed with ethanol and air dried.

FW: 370gmol⁻¹

Yield 410g (46%)

Found: C 51.2% H 4.75% Calc. for C₁₆H₁₈O₆S₂ C 51.9% H 4.9%.

¹H NMR (200MHz, CDCl₃, δ): 2.37 (s, 6H, Ar-CH₃); 4.10 (s, 4H, -CH₂-); 7.25 (d, 4H, Ar-H); -; 7.65 (d, 4H, Ar-H).

¹³C NMR (51MHz, CDCl₃, δ): 21.63 (Ar-CH₃); 66.74 (-CH₂-); 127.90, 129.94, 132.14, 145.30 (aromatic).

M.Pt. 121-124°C.

(2) *N,N',N''*-Tris(*p*-tolylsulphonyl)diethylene triamine disodium salt.

(TsN(CH₂)₂NTs(CH₂)₂NHTs)Na₂

A 5L beaker was fitted with a thermometer, magnetic stirring bar and an ice bath. The beaker was then charged with *N,N',N''*-tris(*p*-tolylsulphonyl)diethylene triamine (310g, 0.55mol) suspended in dry ethanol (2.5L). Sodium metal (45g, 1.96mol) was then added to the suspension in sugar cube sizes, while keeping the temperature between 60-70°C. When the

last sodium cubes were added (50°C) the solution was clear and on cooling (30°C) the disodium salt precipitated. The mixture was covered and refrigerated overnight to complete the precipitation. The product was obtained by filtration, then dried at 120°C for 12hr.

FW: 609gmol⁻¹

Yield 319g (95%)

(4) *N,N',N''*-Tris(*p*-tolylsulphonyl)-1,4,7-triazacyclononane.

A 5L three necked round bottomed flask was fitted with a nitrogen inlet/outlet, mechanical stirrer, air condenser and an oil bath. The flask was purged with nitrogen and charged with *N,N',N''*-tris(*p*-tolylsulphonyl)diethylene triamine disodium salt (638g, 1.05mol) dissolved in dry dimethyl formamide (3.75L). The mixture was heated to 60°C and 1,2-bis[(*p*-tolylsulphonyl)oxy]ethane (387g, 1.05mol) was added with efficient stirring. The solution was then heated to 105°C and stirred for a further 12hr. The solution was allowed to cool to room temperature, then added slowly to ice water (30L) with vigorous stirring. The precipitated solid product was filtered, washed with water (8L), ethanol (2L), diethyl ether (1L) and dried at 120°C for 2-3 days. The product was recrystallised by dissolution in the minimum volume of hot chloroform followed by addition of three volumes of ethanol. The solution was cooled to 0°C, crystallisation

commenced after 1hr and was completed by refrigeration overnight. The product was collected by filtration and washed with ethanol (500mL). The product was recrystallised once more and air dried.

FW: 591gmol⁻¹

Yield 445g (71%)

Found: C 53.9% H 5.4% N 6.75% Calc. for C₂₇H₃₃N₃O₆S₃ C 54.8%
H 5.6% N 7.1%.

¹H NMR (200MHz, CDCl₃, δ): 2.41 (s, 9H, Ar-CH₃); 3.40 (s, 12H, N-CH₂); 7.30 (d, 6H, Ar-H); 7.69 (d, 6H, Ar-H).

¹³C NMR (51MHz, CDCl₃, δ): 21.48 (Ar-CH₃); 51.80 (-CH₂-); 127.43, 129.83, 134.46, 143.86 (aromatic).

M.Pt. 216-219°C.

(5) 1,4,7-Triazacyclononane trihydrobromide.

A 2L three necked round bottomed flask was equipped with a magnetic stirring bar, an air condenser, drying tube (CaCl₂) and an oil bath. The flask was charged with concentrated sulphuric acid (1.2L) and *N,N',N''*-tris(*p*-tolylsulphonyl)-1,4,7-triazacyclononane (400g, 0.68mol) was added to the flask with stirring. The mixture was heated maintaining an oil bath temperature of 110°C using a thermocouple controlled stirring hot plate for 2-3 days. The flask was allowed to cool and the reaction mixture was split

into two equal portions. The first portion was added dropwise with overhead stirring to a 5L beaker containing ethanol (2L) and diethyl ether (400mL), keeping the temperature below 20°C. After the last addition of the mixture, diethyl ether (1L) was added and the mixture cooled to 0°C. The precipitated grey/brown solid was filtered using glass microfibre paper and washed with ether (500mL). The process was repeated for the other portion. The solid was dissolved in the minimum volume of hot distilled water and the temperature was raised to 85°C for 2hr to remove any ether/ethanol. 47% Hydrobromic acid (500-1000mL) was added to the solution until no more trihydrobromide salt precipitated. The salt was collected by filtration and washed with cold HBr (100mL) and ethanol (500ml).

FW: 372gmol⁻¹

Yield 278g (110%)

(6) 1,4,7-Triazacyclononane.

A 2L three necked round bottomed flask was equipped with a magnetic stirring bar, oil bath and Dean-Stark trap with condenser. The flask was charged with 1,4,7-triazacyclononane trihydrobromide (278g, 0.75mol) dissolved in distilled water (250mL). Sodium hydroxide (95g, 2.375mol) was dissolved in distilled water (250mL) and added slowly to the flask, if the pH was below 11 more sodium hydroxide was added. Toluene (750mL) was added to the flask and the mixture was refluxed until no more water collected

in the trap. The trap was emptied, filled with silica gel and the solution refluxed for a further 2hr. The solution was filtered and the solvent removed on the rotary evaporator to leave the product as a viscous yellow oil that crystallised on cooling. Redissolving the solid residue in distilled water and repeating the procedure yielded a further 5-10g of the product.

FW: 129gmol⁻¹

Yield 64g (74% based on **4**)

Found: C 55.65% H 11.7% N 32.3% Calc. for C₆H₁₅N₃ C 55.8%
H 11.6% N 32.6%.

¹H NMR (200MHz, CDCl₃, δ): 1.61 (b, 3H, N-H); 2.59 (s, 12H, -CH₂-).

¹³C NMR (51MHz, CDCl₃, δ): 47.42 (-CH₂-).

M.Pt. 41-43°C.

2.5.2 C-FUNCTIONALISED DIETHYLENE TRIAMINE

The following procedure is a modification of the published procedure for (5*S*)-3-azanonane-1,5,9-triamine by Parker *et al.* (2).

(1) L-Valine ethyl ester hydrochloride.

A 2L three necked round bottom flask equipped with a nitrogen inlet/outlet, magnetic stirring bar, water condenser and an oil bath was charged with L-valine (30g, 0.255mol) suspended in dry ethanol (800mL).

Thionyl chloride (45g, 27mL, 0.38mol) was added dropwise with vigorous stirring, without bringing the solution to reflux. After the last addition of SOCl_2 the solution was refluxed for 7hr under a dry atmosphere. The solvent was removed on the rotary evaporator to leave the product as a white moisture sensitive crystalline mass.

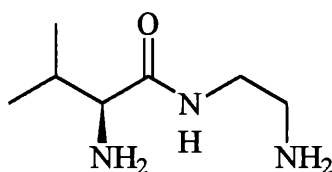
FW: 182g mol^{-1}

Yield 47g (115%)

^1H NMR (200MHz, CDCl_3 , δ): 1.07 (dd, 6H, $-\text{CH}(\text{CH}_3)_2$); 1.25 (t, 3H, $-\text{OCH}_2\text{CH}_3$); 2.04 (m, 1H, $-\text{CH}(\text{CH}_3)_2$); 3.90 (m, 1H, $\text{H}_2\text{NCH}(\text{iPr})\text{CO}_2\text{Et}$); 4.25 (m, 2H, $-\text{OCH}_2\text{CH}_3$); 8.73 (b, 3H, $-\text{NH}_3\text{Cl}$).

^{13}C NMR (51MHz, CDCl_3 , δ): 14.02 ($-\text{OCH}_2\text{CH}_3$); 18.10, 18.33 ($-\text{CH}(\text{CH}_3)_2$); 29.75 ($-\text{CH}(\text{CH}_3)_2$); 58.43 ($\text{H}_2\text{NCH}(\text{iPr})\text{CO}_2\text{Et}$); 62.17 ($-\text{OCH}_2\text{CH}_3$); 168.24 ($-\text{CO}_2\text{Et}$).

(2) (2S)-N-(2-Aminoethyl)-2-amino-3-methyl-butyramide.



A 2L three necked round bottom flask equipped with a drying tube (CaCl_2), magnetic stirring bar, water condenser and an oil bath was charged with ethylene diamine (500mL) in ethanol (500mL). The solution was heated

to 60°C and L-valine ethyl ester hydrochloride (47g) was added in small portions with vigorous stirring over 2hr. After the last addition of L-valine ethyl ester hydrochloride the mixture was refluxed overnight under a dry atmosphere. The bulk of the solvent was removed by distillation at reduced pressure. The last traces of solvent and excess ethylene diamine were removed on the rotary evaporator and the resulting oily brown mass was taken up in distilled water (200mL). Sodium carbonate (20g) was added to the acidic mixture until the $\text{pH} > 11$. The water was removed on the rotary evaporator and the resulting yellow mass taken up in methanol (200mL). The methanol solution was filtered and the solid residue was taken into more methanol (200mL) and filtered. The methanol solutions were combined and the solvent removed on the rotary evaporator. The process was repeated using CH_2Cl_2 as the solvent to leave the product as an extremely viscous brown oil.

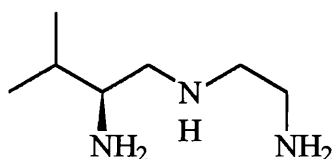
FW: 159g mol^{-1}

Yield 28g

^1H NMR (200MHz, CDCl_3 , δ): 0.6 (dd, 6H, $-\text{CH}(\text{CH}_3)_2$); 1.54 (b, 4H, $-\text{NH}_2$); 1.89 (m, 1H, $-\text{CH}(\text{CH}_3)_2$); 2.52 (t, 2H, $-\text{CONHCH}_2\text{CH}_2\text{NH}_2$); 2.90 (d, 1H, $\text{H}_2\text{NCH}(\text{Pr})\text{CONH}-$); 3.05 (q, 2H, $-\text{CONHCH}_2\text{CH}_2\text{NH}_2$); 7.48 (b, 1H, $-\text{CONH}-$).

^{13}C NMR (51MHz, CDCl_3 , δ): 16.11, 19.49 ($-\text{CH}(\text{CH}_3)_2$); 30.88 ($-\text{CH}(\text{CH}_3)_2$); 41.34, 41.49 ($-\text{CONHCH}_2\text{CH}_2\text{NH}_2$); 60.16 ($\text{H}_2\text{NCH}(\text{tPr})\text{CONH}-$); 174.79 ($-\text{CONH}-$).

(3) (5S)-6-Methyl-3-azaheptane-1,5-diamine.



A 2L three necked round bottom flask equipped with nitrogen inlet/outlet, magnetic stirring bar, water condenser and an ice bath was charged with dry THF (1L). Lithium aluminium hydride (16.7g, 0.4mol) was added slowly to the THF and the suspension cooled to 0°C . (2S)-N-(2-Aminoethyl)-2-amino-3-methyl-butyramide (**2**) (25g, 0.157mol) dissolved in THF (250mL) was added with vigorous stirring and cooling. After the last addition of (**2**) the solution was refluxed for 5days under a dry inert atmosphere. The mixture was cooled to 0°C using an ice bath and the LiAlH_4 was destroyed with the addition of water (16.7mL), 15% NaOH solution (16.7mL) and water (50.1mL). The granular precipitate was removed by filtration, washed with THF (2x100mL) and the THF solutions combined. The solvent was removed on the rotary evaporator to leave the product as a viscous yellow liquid.

FW: 145gmol⁻¹

Yield 17g (74%)

¹H NMR (200MHz, CDCl₃, δ): 0.7 (dd, 6H, -CH(CH₃)₂); 1.29 (b, 5H, -NH); 1.42 (m, 1H, -CH(CH₃)₂); 2.1-2.7 (m, 7H, N-CH₂- & N-CH-).

¹³C NMR (51MHz, CDCl₃, δ): 17.61, 19.17 (-CH(CH₃)₂); 32.18 (-CH(CH₃)₂); 41.62 (-NHCH₂CH₂NH₂); 52.48 (-NHCH₂CH₂NH₂); 53.74 (H₂NCH(ⁱPr)CH₂NH); 56.34 (H₂NCH(ⁱPr)CH₂NH-).

2.5.3 N-FUNCTIONALISED MACROCYCLES

[Note on the preparation of ligands L² - L¹¹ & L²³]

It was subsequently discovered that improved yields of the free ligand could be achieved using chloroform extraction[†] of the basic solution compared to the described method using Dean-Stark azeotrope apparatus. This method also required considerably less time.

[†] pH > 11, CHCl₃ (3x100mL), brine (1x50mL), dried (Na₂CO₃).

(1) 1,4,7-Triazatricyclo[5.2.1.0^{4,10}]decane (L¹).

The preparation outlined below is based upon the Atkins method (3).

In a 25mL round bottom flask 1,4,7-triazacyclononane (8.99g, 69.9mmol) was dissolved in *N,N*-dimethylformamide-dimethylacetal (8.12g, 69.9mmol) and refluxed under nitrogen for 5hr in a well ventilated fumehood as the evolving dimethylamine does not condense in a water cooled condenser. The mixture was then heated to 50°C on the rotary evaporator to remove any unreacted acetal and methanol that formed during the reaction. The product was distilled under reduced pressure (120°C, 12mmHg) to give a clear viscous oil that crystallised when stored at -18°C.

FW: 139gmol⁻¹

yield 8.73g (91%)

¹H NMR (200MHz, CDCl₃, δ): 2.30-2.90 (m, 12H, -CH₂-); 4.68 (s, 1H, -CH-).

¹³C NMR (51MHz, CDCl₃, δ): 51.07 (-CH₂-); 103.27 (-CH-).

(2) *N*-Methyl-1,4,7-triazacyclononane (L²).

A 50mL conical flask equipped with a magnetic stirring bar was charged with 1,4,7-triazatricyclo[5.2.1.0^{4,10}]decane (2.8g, 20.1mmol) dissolved in dry THF (30mL) and cooled to 0°C (ice bath). Methyl iodide

(3g, 20.1mmol) was added slowly with cooling and the product precipitated almost immediately. The flask was covered with aluminium foil and the solution was stirred overnight. The precipitated ammonium iodide salt was filtered, washed with dry THF (10mL), dissolved in distilled water (40mL) and refluxed for 4hr. On cooling sodium hydroxide (2.8g, 70mmol) was added to the solution and the reflux continued for at least 8hr. Meanwhile a 500mL round bottomed flask was equipped with a magnetic stirring bar, oil bath and Dean-Stark trap with condenser. The solution was transferred to the 500mL flask and toluene (350mL) was added. The mixture was then refluxed until nearly all the water was removed. More sodium hydroxide (1g, 25mmol) was added and the reflux continued until no more water collected in the Dean-Stark trap. The product was obtained as a clear viscous oil by filtering the solution and removing the solvent on the rotary evaporator. Dry acetonitrile (100mL) was used to extract the remaining ligand from the solid residue.

FW: 143gmol⁻¹

yield 1.5g (52%)

¹H NMR (200MHz, CDCl₃, δ): 1.85 (s, 2H, -NH); 2.14 (s, 3H, N-CH₃); 2.25-2.33 (m, 4H, N-CH₂-); 2.40-2.51 (m, 4H, N-CH₂-); 2.48 (s, 4H, -NH-CH₂-CH₂-NH-).

¹³C NMR (51MHz, CDCl₃, δ): 44.88 (N-CH₃); 45.96, 46.35, 54.38 (N-CH₂-)

Note: When *N*-methyl-1,4,7-triazacyclononane was dissolved in dichloromethane, crystalline material was observed after 0.5hr which had a similar ^1H NMR spectrum to *N*-methyl-1,4,7-triazacyclononane. $\cdot\text{xHCl}$.

$\text{L}^2 \cdot \text{xHCl}$.

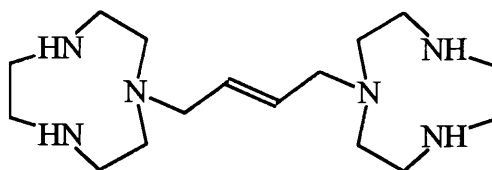
^1H NMR (200MHz, D_2O , δ): 2.51 (s, 3H, N-CH_3); 3.05-3.17 (m, 4H, N-CH_2 -); 3.22-3.35 (m, 4H, N-CH_2 -); 3.38 (s, 4H, $-\text{NH-CH}_2\text{-CH}_2\text{-NH-}$).

$\text{L}^2 + \text{CH}_2\text{Cl}_2$.

^1H NMR (200MHz, D_2O , δ): 2.32 (s, 3H, N-CH_3); 2.77 (t, 4H, N-CH_2 -); 3.07 (t, 4H, N-CH_2 -); 3.24 (s, 4H, $-\text{NH-CH}_2\text{-CH}_2\text{-NH-}$).

^{13}C NMR (51MHz, D_2O , δ): 44.20, 45.03 (N-CH_2 -); 45.22 (N-CH_3); 52.67 (N-CH_2 -).

(3) Trans-1,4-bis(1,4,7-triazacyclononane)but-2-ene (L^3).



A 50mL conical flask equipped with a magnetic stirring bar was charged with 1,4,7-triazatricyclo[5.2.1.0^{4,10}]decane (1.5g, 10.79mmol) dissolved in dry acetonitrile (100mL). Trans-1,4-dibromobut-2-ene (1.15g,

5.37mmol) dissolved in dry acetonitrile (30mL) was added dropwise to the flask over 1hr. The mixture was stoppered, covered in aluminium foil and stirred overnight. The precipitated diammonium salt was collected by filtration, washed with dry acetonitrile (10mL), dissolved in distilled water (30mL) and refluxed for 4h. On cooling sodium hydroxide (1.5g, 37.5mmol) was added to the solution and the reflux continued for at least 8h. Meanwhile a 500mL round bottomed flask was equipped with a magnetic stirring bar, oil bath and Dean-Stark trap with condenser. The solution was transferred to the 500mL flask and toluene (300mL) was added. The mixture was then refluxed until nearly all the water was removed. More sodium hydroxide (0.5g, 12.5mmol) was added and the reflux continued until no more water collected in the Dean-Stark trap. The free amine was obtained by filtering the solution and removing the solvent on the rotary evaporator. Dry acetonitrile (100mL) was used to extract the remaining ligand from the solid residue. The product obtained was an off white solid and stored in the refrigerator.

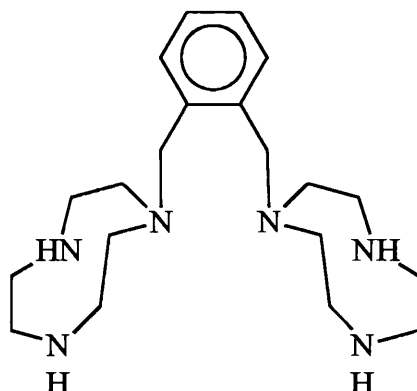
FW: 310gmol⁻¹

Yield 0.63g (56%)

¹H NMR (200MHz, CDCl₃, δ): 1.82 (b, 4H, N-H); 2.4-2.6 (m, 24H, N-CH₂- ring); 2.98 (d, 4H, N-CH₂- arm); 5.57 (b, 2H, -CH=CH-).

¹³C NMR (51MHz, CDCl₃, δ): 46.61, 46.76, 52.40 (N-CH₂- ring); 59.00 (N-CH₂- arm); 130.58 (-CH=CH-).

(4) α,α' -Bis(1,4,7-triazacyclononane)-*ortho*-xylene (L^4).



The same procedure was used as for trans-1,4-bis(1,4,7-triazacyclononane)but-2-ene, with the except of the addition time which was 2hr. Weights used were 1.54g (11.1mmol) 1,4,7-triazatricyclo[5.2.1.0^{4,10}]decane in acetonitrile (100mL) and 1.46g (5.53mmol) α,α' -dibromo-*ortho*-xylene in acetonitrile (75mL). The product obtained was a viscous yellow oil and stored at -18°C.

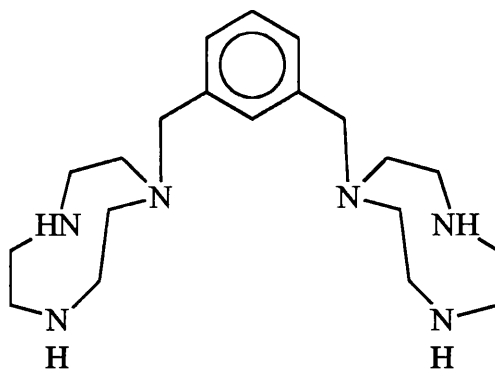
FW: 360gmol⁻¹

Yield 0.95g (48%)

¹H NMR (200MHz, CDCl₃, δ): 2.07 (b, 4H, N-H); 2.47-2.64 (m, 24H, N-CH₂- ring); 3.81 (s, 4H, N-CH₂- arm); 7.07-7.17 (m, 4H, Ar-H).

¹³C NMR (51MHz, CDCl₃, δ): 46.51, 52.93 (N-CH₂- ring); 59.16 (N-CH₂- arm); 126.76, 129.95, 138.43 (aromatic).

(5) α,α' -Bis(1,4,7-triazacyclononane)-*meta*-xylene (L^5).



The same procedure was used as for trans-1,4-bis(1,4,7-triazacyclononane)but-2-ene, with the exception of the addition time which was 2hr. Weights used were 1.63g (11.72mmol) 1,4,7-triazatricyclo[5.2.1.0^{4,10}]decane in acetonitrile (100mL) and 1.55g (5.86mmol) α,α' -dibromo-*meta*-xylene in acetonitrile (100mL). The product obtained was a viscous yellow oil and stored at -18°C .

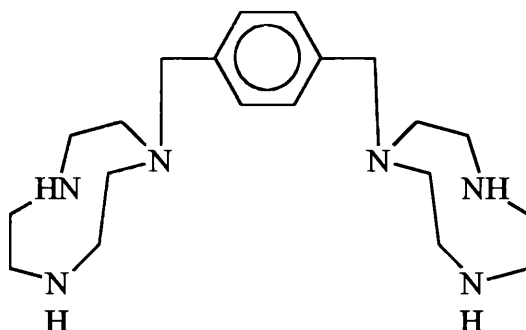
FW: 360g mol^{-1}

Yield 1.23g (58%)

^1H NMR (200MHz, CDCl_3 , δ): 2.14 (b, 4H, N-H); 2.54 (s, 16H, N-CH₂-ring); 2.67 (s, 8H, N-CH₂ ring); 3.62 (s, 4H, N-CH₂- arm); 7.06-7.21 (m, 4H, Ar-H).

^{13}C NMR (51MHz, CDCl_3 , δ): 46.37, 46.65, 52.62 (N-CH₂- ring); 61.52 (N-CH₂- arm); 127.59, 128.07, 129.51, 139.71 (aromatic).

(6) α,α' -Bis(1,4,7-triazacyclononane)-*para*-xylene (L^6).



The same procedure was used as for *trans*-1,4-bis(1,4,7-triazacyclononane)but-2-ene, with the exception of the addition time which was 2hr and the solvent used was a THF / acetonitrile mixture. Weights used were 0.98g (7.05mmol) 1,4,7-triazatricyclo[5.2.1.0^{4,10}]decane in dry acetonitrile (150mL) and 0.93g (3.53mmol) α,α' -dibromo-*para*-xylene in dry THF (50mL). The product obtained was a viscous yellow oil and stored at -18°C.

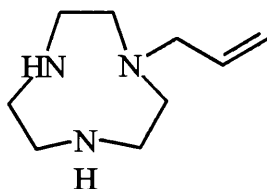
FW: 360gmol⁻¹

Yield 0.58g (46%)

¹H NMR (200MHz, CDCl₃, δ): 2.08 (b, 4H, N-H); 2.53 (s, 16H, N-CH₂-ring); 2.66 (s, 8H, N-CH₂ ring); 3.59 (s, 4H, N-CH₂- arm); 7.18 (s, 4H, Ar-H).

¹³C NMR (51MHz, CDCl₃, δ): 46.44, 46.75, 52.70 (N-CH₂- ring); 61.33 (N-CH₂- arm); 128.85, 138.51 (aromatic).

(7) *N*-Allyl-1,4,7-triazacyclononane (L**⁷).**



A 50mL conical flask equipped with a magnetic stirring bar was charged with 1,4,7-triazatricyclo[5.2.1.0^{4,10}]decane (1.27g, 9.1mmol) dissolved in dry THF (20mL). Allyl bromide (2.18g, 18.2mmol) was added to the flask and the solution was stirred for 2 days. The precipitated ammonium bromide salt was filtered, washed with dry THF (10mL), dissolved in distilled water (40mL) and worked up to the free amine using the same procedure used for trans-1,4-bis(1,4,7-triazacyclononane)but-2-ene. The product obtained was a clear viscous oil.

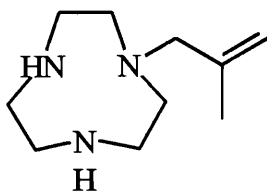
FW: 169gmol⁻¹

yield 0.5g (33%)

¹H NMR (200MHz, CDCl₃, δ): 1.99 (b, 2H, N-H); 2.40-2.58 (m, 12H, -CH₂-N- ring); 3.03 (d, 2H, -CH₂CH=CH₂); 4.9-5.03 (m, 2H, -CH=CH₂); 5.7 (m, 1H, -CH=CH₂).

¹³C NMR (51MHz, CDCl₃, δ): 46.6 46.8 52.47 (-CH₂-N- ring); 60.2 (N-CH₂CH=CH₂); 116.7 (-CH=CH₂); 136.1 (-CH=CH₂).

(8) *N*-3-(2-Methylprop-1-ene)-1,4,7-triazacyclononane (L**⁸).**



The same procedure was used as for *N*-allyl-1,4,7-triazacyclononane.

Weights used were 3g (22.2mmol) 3-bromo 2-methyl propene and 2.5g (18mmol) 1,4,7-triazatricyclo[5.2.1.0^{4,10}]decane.

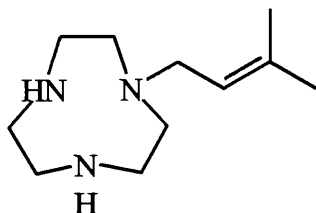
FW: 183gmol⁻¹

Yield 2.2g (67%)

¹H NMR (200MHz, CDCl₃, δ): 1.62 (t, 3H, -CH₂C(CH₃)=CH₂); 1.97 (b, 2H, N-H); 2.36-2.60 (m, 12H, -CH₂-N- ring); 2.90 (s, 2H, -CH₂C(CH₃)=CH₂); 4.70 (d, 2H, -CH₂C(CH₃)=CH₂).

¹³C NMR (51MHz, CDCl₃, δ): 20.69 (-CH₂C(CH₃)=CH₂); 46.66, 46.86, 52.88 (-CH₂-N- ring); 64.26 (N-CH₂C(CH₃)=CH₂); 112.66 (N-CH₂C(CH₃)=CH₂); 143.93 (N-CH₂C(CH₃)=CH₂).

(9) *N*-4-(2-Methylbut-2-ene)-1,4,7-triazacyclononane (L⁹).



The same procedure was used as for *N*-allyl-1,4,7-triazacyclononane.

Weights used were 3g (20.1mmol) 4-bromo 2-methyl but-2-ene and 2.5g (18mmol) 1,4,7-triazatricyclo[5.2.1.0^{4,10}]decane.

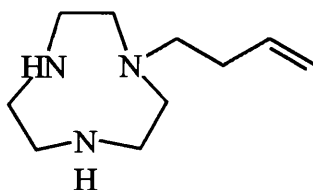
FW: 197gmol⁻¹

Yield 1.8g (51%)

¹H NMR (200MHz, CDCl₃, δ): 1.60 (d, 6H, -CH₂CH=CMe₂); 2.21 (b, 2H, N-H); 2.45-2.70 (m, 12H, -CH₂-N- ring); 2.90 (d, 2H, -CH₂CH=CMe₂); 5.18 (m, 1H, -CH₂CH=CMe₂).

¹³C NMR (51MHz, CDCl₃, δ): 17.86, 25.76 (-CH₂CH=CMe₂); 46.28, 46.38, 51.95 (-CH₂-N- ring); 54.18 (N-CH₂CH=CMe₂); 121.98 (N-CH₂CH=CMe₂); 134.36 (N-CH₂CH=CMe₂).

(10) *N*-4-But-1-ene-1,4,7-triazacyclononane (L¹⁰).



The same procedure was used as *N*-allyl-1,4,7-triazacyclononane.

Weights used were 3.7g (28mmol) 4-bromo but-1-ene and 1.9g (14mmol)

1,4,7-triazatricyclo[5.2.1.0^{4,10}]decane.

Note: After filtration of the ammonium salt, the reaction mixture was left for a further 2 days to yield a second crop of the intermediate ammonium salt.

FW: 183gmol⁻¹

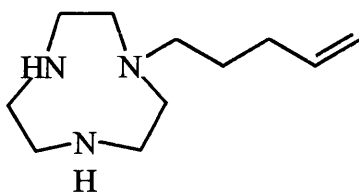
Yield 0.8g (32%)

IR (thin film): $\nu(\text{C}=\text{C})$ 1640cm⁻¹.

¹H NMR (200MHz, CDCl₃, δ): 1.95 (b, 2H, N-H); 2.15 (m, 2H, -CH₂CH₂CH=CH₂); 2.45-2.70 (m, 14H, N-CH₂-); 4.8-5.1 (m, 2H, -CH=CH₂); 5.75 (m, 1H, -CH=CH₂).

¹³C NMR (51MHz, CDCl₃, δ): 32.25 (-CH₂CH=CH₂); 46.36, 46.46, 52.49 (-CH₂-N- ring); 56.41 (N-CH₂CH₂CH=CH₂); 114.9 (-CH=CH₂); 136.2 (-CH=CH₂).

(11) *N*-5-Pent-1-ene-1,4,7-triazacyclononane (L¹¹).



The same procedure was used as *N*-4-but-1-ene-1,4,7-triazacyclononane. Weights used were 2.92g (19.6mmol) 5-bromo pent-1-ene and 2.1g (15.1mmol) 1,4,7-triazatricyclo[5.2.1.0^{4,10}]decane.

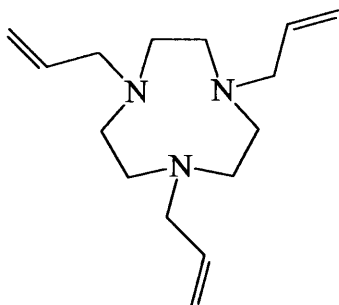
FW: 197gmol⁻¹

Yield 1.81g (61 %)

¹H NMR (200MHz, CDCl₃, δ): 1.45 (*quintet*, 2H, -CH₂CH₂CH₂CH=CH₂); 1.95 (*quartet*, 2H, -CH₂CH₂CH₂-CH=CH₂); 2.09 (b, 2H, N-H); 2.35-2.65 (m, 14H, N-CH₂-); 4.75-5.05 (m, 2H, -CH=CH₂); 5.70 (m, 1H, -CH=CH₂).

¹³C NMR (51MHz, CDCl₃, δ): 26.91 (-CH₂CH₂CH₂CH=CH₂); 31.41 (-CH₂CH₂CH₂CH=CH₂); 46.45, 46.58, 52.78 (-CH₂-N- ring); 56.96 (N-CH₂CH₂CH₂CH=CH₂); 114.44 (-CH=CH₂); 138.39 (-CH=CH₂).

(12) *N,N',N''*-Triallyl-1,4,7-triazacyclononane (L¹²**).**



A 50mL conical flask equipped with a magnetic stirring bar was charged with 1,4,7-triazacyclononane (1g, 7.75mmol) and allyl bromide (2.83g, 23.5mmol) dissolved in dry ethanol (25mL). A sodium ethoxide solution was prepared by the addition of sodium metal (0.54g, 23.5mmol) to dry ethanol (15mL), the solution was then added to the reaction mixture over a period of 1hr with stirring. The mixture was then stirred overnight and the precipitated sodium bromide was removed by filtration and the ethanol was removed on the rotary evaporator. Dry toluene (20mL) was added to the residue and stirring continued for a further 2hr to precipitate any remaining sodium bromide. The solution was filtered through glass micro-fibre filter paper and the solvent removed on the rotary evaporator to leave the product as a yellow light sensitive oil.

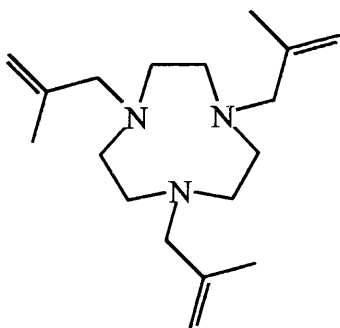
FW: 249gmol⁻¹

yield 1.39g (72%)

^1H NMR (200MHz, CDCl_3 , δ): 2.66 (s, 12H, $-\text{CH}_2\text{-N-}$ ring); 3.05 (d, 6H, $\text{N-CH}_2\text{CH=CH}_2$); 4.9-5.2 (m, 6H, $-\text{CH=CH}_2$); 5.7-5.9 (m, 3H, $-\text{CH=CH}_2$).

^{13}C NMR (51MHz, CDCl_3 , δ): 55.2 ($-\text{CH}_2\text{-N-}$ ring); 61.8 ($\text{N-CH}_2\text{CH=CH}_2$); 116.5 ($-\text{CH=CH}_2$); 136.8 ($-\text{CH=CH}_2$).

(13) *N,N',N''*-Tris(2-methylprop-1-ene)-1,4,7-triazacyclononane (L^{13}).



The same procedure was used as for *N,N',N''*-triallyl-1,4,7-triazacyclononane. Weights used were 2.94g (22.8mmol) 1,4,7-triazacyclononane, 9.23g (68.4mmol) 3-bromo 2-methyl propene in ethanol (100mL) and 1.57g (68.4mmol) of sodium metal in ethanol (50mL).

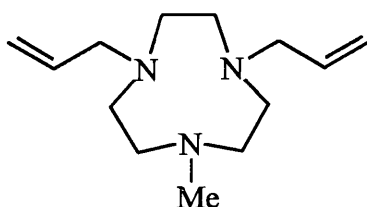
FW: 291g mol^{-1}

Yield 5.2g (78%)

^1H NMR (200MHz, CDCl_3 , δ): 1.75 (s, 9H, $-\text{CH}_2\text{C}(\text{CH}_3)=\text{CH}_2$); 2.68 (s, 12H, $-\text{CH}_2\text{-N-}$ ring); 2.97 (s, 6H, $\text{N-CH}_2\text{C}(\text{CH}_3)=\text{CH}_2$); 4.80 (d, 6H, $-\text{C}(\text{CH}_3)=\text{CH}_2$).

^{13}C NMR (51MHz, CDCl_3 , δ): 21.01 ($-\text{CH}_2\text{C}(\underline{\text{CH}}_3)=\text{CH}_2$); 55.48 ($-\underline{\text{CH}}_2\text{-N}$ -ring); 65.79 ($\text{N}-\underline{\text{CH}}_2\text{C}(\text{CH}_3)=\text{CH}_2$); 112.29 ($-\text{C}(\text{CH}_3)=\underline{\text{CH}}_2$); 144.618 ($-\underline{\text{C}}(\text{CH}_3)=\text{CH}_2$).

(14) *N*-Methyl-*N',N''*-diallyl-1,4,7-triazacyclononane (L^{14}).



The same procedure was used as for *N,N',N''*-triallyl-1,4,7-triazacyclononane. Weights used were 0.83g (5.8mmol) *N*-methyl-1,4,7-triazacyclononane, 1.4g (11.6mmol) allyl bromide and 0.27g (11.6mmol) of sodium metal in ethanol (15mL).

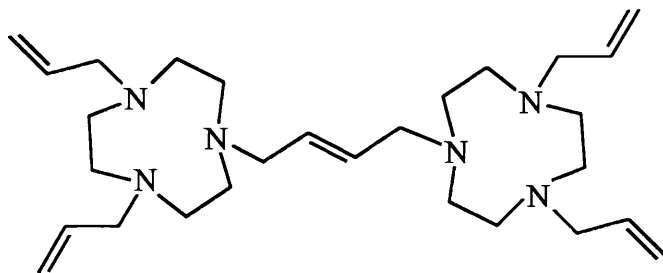
FW: 223g mol^{-1}

Yield 0.87g (67%)

^1H NMR (200MHz, CDCl_3 , δ): 2.29 (s, 3H, $\text{N}-\underline{\text{CH}}_3$); 2.61, (s, 4H, $\text{N}-\underline{\text{CH}}_2$); 2.67 (s, 8H, $\text{N}-\underline{\text{CH}}_2$); 3.07 (d, 4H, $\text{N}-\underline{\text{CH}}_2\text{CH}=\text{CH}_2$); 4.96-5.12 (m, 4H, $-\text{CH}=\underline{\text{CH}}_2$); 5.72-5.92 (m, 2H, $-\underline{\text{CH}}=\text{CH}_2$).

^{13}C NMR (51MHz, CDCl_3 , δ): 46.60 ($\text{N}-\underline{\text{CH}}_3$); 55.17, 55.44, 57.07 ($\text{N}-\underline{\text{CH}}_2$); 61.94 ($\text{N}-\underline{\text{CH}}_2\text{CH}=\text{CH}_2$); 116.54 ($-\text{CH}=\underline{\text{CH}}_2$); 136.84 ($-\underline{\text{CH}}=\text{CH}_2$).

(15) Trans-1,4-bis[*N,N'*-diallyl-1,4,7-triazacyclononane]but-2-ene (L¹⁵**).**



The same procedure was used as for *N,N',N''*-triallyl-1,4,7-triazacyclononane. Weights used were 1.23g (3.96mmol) trans-1,4-bis(1,4,7-triazacyclononane)but-2-ene, 1.92g (15.87mmol) allyl bromide and 0.37g (16.1mmol) sodium metal in ethanol (20mL).

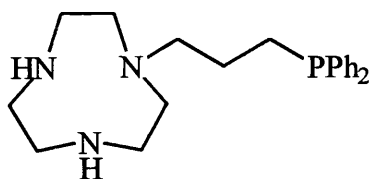
FW: 470gmol⁻¹

Yield 1.27g (68%)

¹H NMR (200MHz, CDCl₃, δ): 2.66 (s, 24H, N-CH₂ ring); 3.05 (d, 12H, N-CH₂ arm); 4.98-5.1 (m, 8H, -CH=CH₂); 5.56 (m, 2H, -CH₂CH=CHCH₂-) 5.76-5.84 (m, 4H, -CH=CH₂).

¹³C NMR (51MHz, CDCl₃, δ): 55.11, 55.21 (N-CH₂ ring); 60.57 (N-CH₂ bridge); 61.82 (N-CH₂ arm); 116.54 (-CH=CH₂); 130.95 (-CH₂CH=CHCH₂-); 136.84 (-CH=CH₂).

(16) *N*-Diphenylphosphinopropyl-1,4,7-triazacyclononane (L¹⁶).



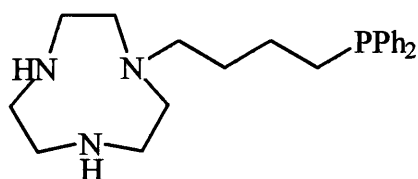
A Schlenk tube was equipped with a magnetic stirring bar and charged with *N*-allyl-1,4,7-triazacyclononane (1g, 5.92mmol) dissolved in dry degassed dichloromethane (5mL). The Schlenk tube was evacuated and purged with nitrogen, diphenyl phosphine (1.29g, 1.2ml, 6.93mmol) was transferred to the Schlenk tube using a syringe under a strong flow of nitrogen. The contents of the flask were mixed and the dichloromethane was removed under reduced pressure. The flask was then irradiated with a high pressure mercury UV lamp with stirring under a nitrogen atmosphere for 72hrs. Excess diphenyl phosphine was removed by washing with dry degassed 40-60° petrol (2x5ml). The remaining viscous oil was then left under vacuum overnight to remove any solvent and volatiles. The product was obtained as a very viscous yellow oil.

FW: 355gmol⁻¹

¹³C NMR (51MHz, CDCl₃, δ): 24.25 (d, N-CH₂CH₂CH₂-P, *J*_{PC}=16Hz); 25.69 (d, N-CH₂CH₂CH₂-P, *J*_{PC}=11.5Hz); 46.73, 46.82, 53.06 (N-CH₂-, ring); 58.73 (d, N-CH₂CH₂CH₂-P, *J*_{PC}=13Hz); 128.36, 132.68, 133.95, 138.94 (all d, aromatic).

^{31}P NMR (81MHz, CDCl_3 , δ): -16.2.

(17) *N*-Diphenylphosphinobutyl-1,4,7-triazacyclononane (L^{17}).



The same procedure was used as for *N*-diphenylphosphinopropyl-1,4,7-triazacyclononane. Weights used were 1.5g (8.2mmol) *N*-4-but-1-ene-1,4,7-triazacyclononane, 1.68g (1.56mL, 9.1mmol) diphenyl phosphine and an irradiation time of 96hr.

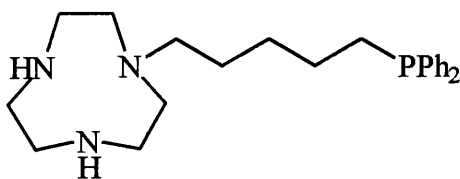
FW: 369g mol^{-1}

^1H NMR (200MHz, CDCl_3 , δ): 1.52 (m, 4H, $\text{N-CH}_2\text{CH}_2\text{CH}_2\text{CH}_2\text{-P}$); 2.05 (m, 2H, $\text{N-CH}_2\text{CH}_2\text{CH}_2\text{CH}_2\text{-P}$); 2.47-2.70 (m, 14H, $\text{N-CH}_2\text{-}$); 2.85 (b, 2H, N-H); 7.25-7.55 (m, 10H, Ar-H).

^{13}C NMR (51MHz, CDCl_3 , δ): 23.63 (d, $\text{P-CH}_2\text{-}$, $J_{\text{PC}}=16.3\text{Hz}$); 27.83 (d, $\text{N-CH}_2\text{CH}_2\text{CH}_2\text{CH}_2\text{-P}$, $J_{\text{PC}}=11.6\text{Hz}$); 28.86 (d, $\text{N-CH}_2\text{CH}_2\text{CH}_2\text{CH}_2\text{-P}$, $J_{\text{PC}}=12.1\text{Hz}$); 43.83, 45.14, 50.67 ($\text{N-CH}_2\text{-}$, ring); 56.42 ($\text{N-CH}_2\text{-}$, arm); 128.47, 132.63, 133.85, 138.51 (all d, aromatic).

^{31}P NMR (81MHz, CDCl_3 , δ): -16.43.

(18) *N*-Diphenylphosphinopentyl-1,4,7-triazacyclononane (L**¹⁸).**



The same procedure was used as for *N*-diphenylphosphinopropyl-1,4,7-triazacyclononane. Weights used were 0.83g (4.2mmol) *N*-5-pent-1-ene-1,4,7-triazacyclononane, 1.18g (1.1mL, 6.35mmol) diphenyl phosphine and an irradiation time of 120hr.

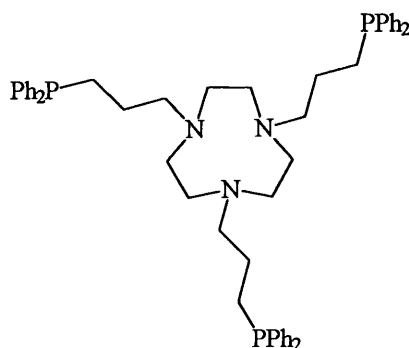
FW: 383gmol⁻¹

¹H NMR (200MHz, CDCl₃, δ): 1.41 (b, 6H, N-CH₂CH₂CH₂CH₂CH₂-P); 2.05 (m, 2H, N-CH₂CH₂CH₂CH₂CH₂-P); 2.41-2.85 (m, 14H, N-CH₂-); 4.12 (b, 2H, N-H); 7.26-7.55 (m, 10H, Ar-H).

¹³C NMR (51MHz, CDCl₃, δ): 25.83 (d, P-CH₂-, *J*_{PC}=16.3Hz); 27.29 (N-CH₂CH₂CH₂CH₂CH₂-P); 27.94 (d, N-CH₂CH₂CH₂CH₂CH₂-P, *J*_{PC}=11.4Hz); 28.85 (d, N-CH₂CH₂CH₂CH₂CH₂-P, *J*_{PC}=13Hz); 45.36, 45.99, 51.81 (N-CH₂-, ring); 57.06 (N-CH₂-, arm); 128.39, 132.62, 133.85, 138.82 (all d, aromatic).

³¹P NMR (81MHz, CDCl₃, δ); -16.31.

(19) *N,N',N''*-Tris(diphenylphosphinopropyl)-1,4,7-triazacyclononane (**L¹⁹**).



The same procedure was used as for *N*-diphenylphosphinopropyl-1,4,7-triazacyclononane. Weights used were 1.73g (6.95mmol) *N,N',N''*-triallyl-1,4,7-triazacyclononane, 4.3g (4mL, 23.2mmol) diphenyl phosphine and an irradiation time of 72hr.

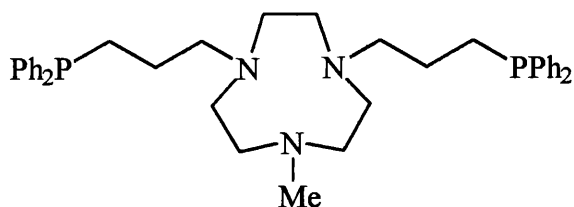
FW: 807gmol⁻¹

¹H NMR (200MHz, CDCl₃, δ): 1.6 (m, 6H, N-CH₂CH₂CH₂-P); 2.1 (m, 6H, N-CH₂CH₂CH₂-P); 2.45-2.8 (m, 18H, N-CH₂- ring); 7.25-7.53 (m, 30H, Ar-H).

¹³C NMR (51MHz, CDCl₃, δ): 24.41 (d, N-CH₂CH₂CH₂-P, *J*_{PC}=16.2Hz); 25.88 (d, N-CH₂CH₂CH₂-P, *J*_{PC}=11.3Hz); 55.79 (N-CH₂- ring); 59.86 (d, N-CH₂CH₂CH₂-P, *J*_{PC}=13.5Hz); 128.36, 132.68, 133.95, 138.94 (all d, aromatic).

³¹P NMR (81MHz, CDCl₃, δ): -15.92.

(20) *N*-Methyl-*N'*,*N''*-di(diphenylphosphinopropyl)-1,4,7-triazacyclononane (L**²⁰).**



The same procedure was used as for *N*-diphenylphosphinopropyl-1,4,7-triazacyclononane. Weights used were 0.53g (2.38mmol) *N*-methyl, *N'*,*N''*-diallyl-1,4,7-triazacyclononane, 0.97g (0.9mL, 5.22mmol) diphenyl phosphine and an irradiation time of 96hr.

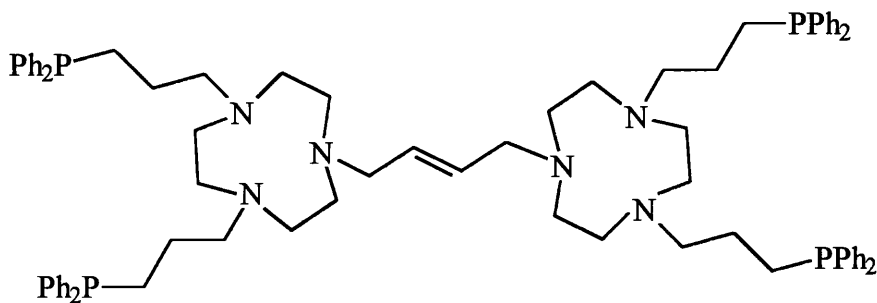
FW: 595gmol⁻¹

¹H NMR (200MHz, CDCl₃, δ): 1.52 (m, 4H, N-CH₂CH₂CH₂-P); 2.02 (m, 4H, N-CH₂CH₂CH₂-P); 2.21-3.05 (m, 16H, N-CH₂-); 2.42 (s, 3H, N-CH₃); 7.25-7.53 (m, 20H, Ar-H).

¹³C NMR (51MHz, CDCl₃, δ): 24.02 (d, N-CH₂CH₂CH₂-P, *J*_{PC}=16.4Hz); 25.72 (d, N-CH₂CH₂CH₂-P, *J*_{PC}=11.6Hz); 45.22 (N-CH₃); 54.69, 55.48 (N-CH₂- ring); 59.77 (d, N-CH₂CH₂CH₂-P, *J*_{PC}=14.3Hz); 128.45, 132.62, 133.88, 138.63 (all d, aromatic).

³¹P NMR (81MHz, CDCl₃, δ): -16.74.

(21) Trans-1,4-bis[*N,N'*-di(diphenylphosphinopropyl)-1,4,7-triazacyclononane]but-2-ene (L**²¹).**



The same procedure was used as for *N*-diphenylphosphinopropyl-1,4,7-triazacyclononane. Weights used were 0.86g (1.83mmol) trans-1,4-bis[*N,N'*-diallyl-1,4,7-triazacyclononane]but-2-ene, 1.8g (1.7mL, 9.68mmol) diphenyl phosphine and an irradiation time of 168hr.

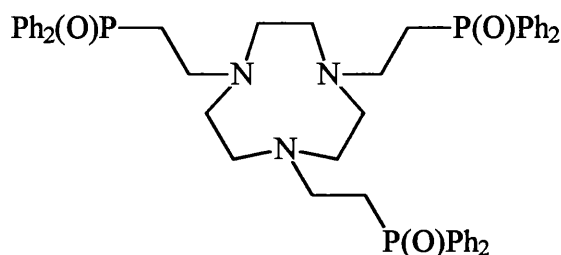
FW: 1214g mol^{-1}

¹H NMR (200MHz, CDCl₃, δ): 1.6 (m, 8H, N-CH₂CH₂CH₂-P); 2.1 (m, 8H, N-CH₂CH₂CH₂-P); 2.45-2.95 (m, 32H, N-CH₂-); 3.15 (b, 4H, N-CH₂CH=CHCH₂-N); 5.63 (b, 2H, -CH₂CH=CHCH₂-); 7.2-7.6 (m, 40H, Ar-H).

¹³C NMR (51MHz, CDCl₃, δ): 24.42 (d, N-CH₂CH₂CH₂-P, $J_{\text{PC}}=16.2\text{Hz}$); 25.90 (d, N-CH₂CH₂CH₂-P, $J_{\text{PC}}=11.5\text{Hz}$); 54.76, 55.97 (N-CH₂- ring); 60.03 (d, N-CH₂CH₂CH₂-P, $J_{\text{PC}}=13.4\text{Hz}$); 60.34 (-CH₂CH=CHCH₂-); 130.71 (-CH₂CH=CHCH₂-); 128.40, 132.69, 133.46, 138.91 (all d, aromatic).

^{31}P NMR (81MHz, CDCl_3 , δ): -15.91.

(22) *N,N',N''*-Tris(diphenylphosphinyloethyl)-1,4,7-triazacyclononane (L^{22}).



A 100ml round bottomed flask equipped with a condenser and drying tube (CaCl_2) was charged with diphenyl vinyl phosphine oxide (5.3g, 23.25mmol). 1,4,7-triazacyclononane (1g, 7.75mmol) dissolved in dry toluene (50mL) was added to the flask and the contents were refluxed for 48hr. On cooling the product precipitated and was collected by filtration, washed with cold toluene (2x10ml) and diethyl ether (2x10ml). The product was recrystallised by dissolving in hot toluene (50mL), cooled to room temperature, filtered and washed with toluene and ether.

FW: 813gmol^{-1}

Yield 3g (48%)

Found: C 70.1% H 6.3% N 4.8% Calc. for $\text{C}_{48}\text{H}_{54}\text{N}_3\text{P}_3\text{O}_3$ C 70.8%
H 6.6% N 5.2%.

^1H NMR (200MHz, CDCl_3 , δ): 2.26-2.39 (m, 6H, P- $\underline{\text{CH}_2}$ -); 2.5 (s, 12H, N- $\underline{\text{CH}_2}$ - ring); 2.69-2.80 (m, 6H, N- $\underline{\text{CH}_2}$ - arm); 7.05-7.69 (m, 30H, Ar- $\underline{\text{H}}$).

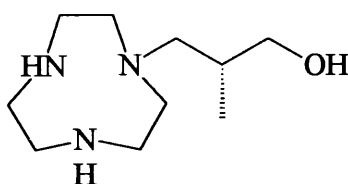
^{13}C NMR (51MHz, CDCl_3 , δ): 27.43 (d, P- $\underline{\text{CH}_2}$ -, $J_{\text{PC}}=68.53\text{Hz}$); 50.69 (P- CH_2 - $\underline{\text{CH}_2}$ -); 55.02 (N- $\underline{\text{CH}_2}$ - ring); 128.64, 130.58, 131.82, 133.87 (aromatic).

^{31}P NMR (81MHz, CDCl_3 , δ): 31.04

IR (KBr): $\nu(\text{P}=\text{O})$ 1188cm^{-1} .

M.Pt. $161\text{-}163^\circ\text{C}$.

(23) *N*-(*S*)-2-Methyl-1-propanol-1,4,7-triazacyclononane (L^{23}).



The same procedure was used as for *N*-allyl-1,4,7-triazacyclononane.

Weights used were 1.9g (12.4mmol) (*R*)-3-bromo-2-methyl-1-propanol and 1.4g (10mmol) 1,4,7-triazatricyclo[5.2.1.0^{4,10}]decane.

Note: After removing the ammonium salt by filtration, the reaction mixture was left for a further 2 days to yield a second crop of the intermediate ammonium salt. This was repeated up to 4 times, until no more salt precipitated.

FW: 225g mol^{-1}

Yield 0.70g (31%)

^1H NMR (200MHz, CDCl_3 , δ); 0.58 (d, 3H, $-\text{CH}_2\text{CH}(\underline{\text{CH}_3})\text{CH}_2\text{OH}$); 1.78 (m, 1H, $-\text{CH}_2\text{CH}(\underline{\text{CH}_3})\text{CH}_2\text{OH}$); 2.1-2.65 (m, 12H, N- $\underline{\text{CH}_2}$ -, ring); 3.1-3.4 (broad d, 4H, $-\text{CH}_2\text{CH}(\underline{\text{CH}_3})\underline{\text{CH}_2}\text{OH}$).

^{13}C NMR (51MHz, CDCl_3 , δ); 15.44 ($-\text{CH}_2\text{CH}(\underline{\text{CH}_3})\text{CH}_2\text{OH}$); 33.31 ($-\text{CH}_2\underline{\text{CH}}(\text{CH}_3)\text{CH}_2\text{OH}$); 46.04, 46.47, 54.81 (N- $\underline{\text{CH}_2}$ -, ring); 64.69 ($-\underline{\text{CH}_2}\text{CH}(\text{CH}_3)\text{CH}_2\text{OH}$); 68.86 ($-\text{CH}_2\text{CH}(\text{CH}_3)\underline{\text{CH}_2}\text{OH}$).

2.6 METAL COMPLEXES

2.6.1 OLEFIN BINDING TO Cu(I) AND Ag(I) COMPLEXES.

(1) [Cu(L¹⁰)] [BPh₄].

A Schlenk tube was equipped with a magnetic stirring bar and charged with CuI (62mg, 0.325mmol) suspended in dry degassed methanol (15mL). Tetraphenylboron sodium (0.1127g, 0.33mmol) was added to the suspension and the mixture was stirred for 0.5hr under reduced pressure. *N*-4-but-1-ene-1,4,7-triazacyclononane (60mg, 0.33mmol) dissolved in toluene (20mL) was added to the mixture and the Cu(I) complex precipitated almost immediately as an off white air sensitive solid. The solvent was then removed under reduced pressure.

IR (nujol mull): $\nu(\text{C}=\text{C})$ 1525cm⁻¹.

(2) [Cu(L¹¹)]I.

An air sensitive NMR tube charged with CuI (96mg, 0.498mmol) was placed inside a long Schlenk tube and left under reduced pressure for 0.25hr. *N*-5-pent-1-ene-1,4,7-triazacyclononane (98mg, 0.497mmol) was dissolved in degassed d₆-DMSO and added to the NMR tube under a strong flow of

nitrogen. The complex oxidised slightly to produce a pale green solution. The cap was fitted to the NMR tube immediately and the sample was transferred to the spectrometer.

^{13}C NMR (51MHz, $\text{d}_6\text{-DMSO}$, δ): 31.09 ($-\text{CH}_2\text{CH}_2\text{CH}_2\text{CH}=\text{CH}_2$); 37.99 ($-\text{CH}_2\text{CH}_2\text{CH}_2\text{CH}=\text{CH}_2$); 48.26, 49.09, 51.63, 52.45, 57.93, 58.41 ($-\text{CH}_2\text{-N- ring}$); 64.29 ($\text{N-CH}_2\text{CH}_2\text{CH}_2\text{CH}=\text{CH}_2$); 73.83 ($-\text{CH}=\text{CH}_2$); 98.74 ($-\text{CH}=\text{CH}_2$).

(3) $[\text{Cu}(\text{L}^{11})][\text{BF}_4].4\text{MeCN}$.

An air sensitive NMR tube charged with $[\text{Cu}(\text{MeCN})_4][\text{BF}_4]$ (205mg, 0.652mmol) was placed inside a long Schlenk tube and purged with a strong flow of nitrogen for 5 minutes. *N*-5-pent-1-ene-1,4,7-triazacyclononane (129mg, 0.655mmol) was dissolved in degassed $\text{d}_6\text{-acetone}$ and added to the NMR tube under a strong flow of nitrogen. The cap was fitted to the NMR tube immediately and the sample was transferred to the spectrometer.

^1H NMR (200MHz, $\text{d}_6\text{-Acetone}$, δ): 1.45-1.9 (m, $-\text{CH}_2\text{CH}_2\text{CH}_2\text{CH}=\text{CH}_2$); 2.25-3.4 (m, $\text{N-CH}_2\text{-}$); 3.5-3.7 (m, $-\text{CH}=\text{CH}_2$); 4.45-4.7 (m, $-\text{CH}=\text{CH}_2$).

^{13}C NMR (51MHz, $\text{d}_6\text{-acetone}$, δ): 1.36 (CH_3CN); 27.04 ($-\text{CH}_2\text{CH}_2\text{CH}_2\text{CH}=\text{CH}_2$); 34.09 ($-\text{CH}_2\text{CH}_2\text{CH}_2\text{CH}=\text{CH}_2$); 44.12, 44.89,

47.74, 48.56, 53.67, 54.41 ($-\underline{\text{CH}}_2\text{-N-}$ ring); 60.44 ($\text{N-}\underline{\text{CH}}_2\text{CH}_2\text{CH}_2\text{CH=CH}_2$); 70.20 ($-\text{CH}=\underline{\text{CH}}_2$); 95.67 ($-\underline{\text{CH}}=\text{CH}_2$); 118 (broad, $\text{CH}_3\underline{\text{CN}}$).

(4) $[\text{Ag}(\text{L}^{11})][\text{BF}_4]$.

A conical flask equipped with a stirring bar was covered with aluminium foil and charged with $\text{Ag}(\text{BF}_4)$ (103mg, 0.53mmol). A d_3 -acetonitrile solution (0.8mL) of *N*-5-pent-1-ene-1,4,7-triazacyclononane (107mg, 0.54mmol) was added, initially producing a light sensitive, clear yellow solution which decomposed over a period of 1-2h to give a black insoluble precipitate. A clean NMR sample was prepared by filtration through glass microfilter paper.

^1H NMR (200MHz, CD_3CN , δ): 1.85 (m, 2H, $-\text{CH}_2\underline{\text{CH}}_2\text{CH}_2\text{CH=CH}_2$); 2.09 (b, 2H, $\text{N-}\underline{\text{H}}$); 2.25 (m, 2H, $-\text{CH}_2\text{CH}_2\underline{\text{CH}}_2\text{-CH=CH}_2$); 2.4-3.2 (m, 14H, $\text{N-}\underline{\text{CH}}_2$ -); 4.9 (m, 2H, $-\text{CH}=\underline{\text{CH}}_2$); 6.0 (m, 1H, $-\underline{\text{CH}}=\text{CH}_2$).

^{13}C NMR (51MHz, CD_3CN , δ): 28.74 ($-\text{CH}_2\underline{\text{CH}}_2\text{CH}_2\text{CH=CH}_2$); 33.87 ($-\text{CH}_2\text{CH}_2\underline{\text{CH}}_2\text{CH=CH}_2$); 45.40, 46.27, 53.31 ($-\underline{\text{CH}}_2\text{-N-}$ ring); 61.35 ($\text{N-}\underline{\text{CH}}_2\text{CH}_2\text{CH}_2\text{CH=CH}_2$); 100.56 ($-\text{CH}=\underline{\text{CH}}_2$); 130.42 ($-\underline{\text{CH}}=\text{CH}_2$).

2.6.2 HYDROXYL BRIDGED COPPER (II) COMPLEXES.

(1) $[\text{Cu}_2(\text{L}^4)(\mu\text{-OH})_2][\text{BPh}_4]_2$.

A Schlenk tube equipped with a magnetic stirring bar was charged with CuI (111mg, 0.584mmol) suspended in dry methanol (30mL). Tetraphenylboron sodium (200mg, 0.584mmol) was added to the suspension and the mixture was stirred under reduced pressure for 0.5hr. α,α' -Bis(1,4,7-triazacyclononane)-*ortho*-xylene (105mg, 0.292mmol) dissolved in dry degassed methanol (10mL) was added to the mixture under a strong flow of nitrogen. The white Cu(I) salt which initially precipitated, rapidly oxidised in air to give a blue solution. Complete oxidation was achieved by stirring the solution overnight. The resulting blue Cu(II) complex was collected by filtration and washed with methanol (20mL). Dissolution in hot acetonitrile followed by refrigeration, precipitated small green crystals.

(2) $[\text{Cu}_2(\text{L}^5)(\mu\text{-OH})_2][\text{BPh}_4]_2$.

The same procedure used for (1) was carried out. Weights used were 365mg (1.01mmol) α,α' -bis(1,4,7-triazacyclononane)-*meta*-xylene, 386mg (2.02mmol) CuI and 694mg (2.02mmol) tetraphenylboron sodium. Dissolution in hot acetonitrile followed by slow evaporation to dryness produced small green crystals suitable for X-ray structure analysis.

(3) $[\text{Cu}_2(\text{L}^6)(\mu\text{-OH})_2][\text{BPh}_4]_2$.

The same procedure used for (1) was carried out, except the initial Cu(I) complex was extremely slow to oxidise (10days). Weights used were 104mg (0.289mmol) α,α' -bis(1,4,7-triazacyclononane)-*para*-xylene, 110mg (0.579mmol) CuI and 200mg (0.584mmol) tetraphenylboron sodium. Dissolution in hot acetonitrile followed by slow evaporation produced an amorphous green solid.

(4) $[\text{Cu}(\text{L}^{10})(\mu\text{-OH})_2\text{Cu}(\text{L}^{10})][\text{BPh}_4]_2 \cdot 2\text{MeCN}$.

The same procedure used for (1) was carried out, except *N*-4-but-1-ene-1,4,7-triazacyclononane (60mg, 0.33mmol) was dissolved in dry degassed toluene (20mL). Weights used were 62mg (0.325mmol) CuI, 113mg (0.33mmol) Tetraphenylboron sodium and 15mL methanol. Dissolution in hot acetonitrile followed by refrigeration, precipitated small blue-green crystals suitable for X-ray structure analysis.

(5) $[\text{Cu}(\text{L}^{10})_2][\text{BPh}_4]_2$.

The same procedure was followed as in (4), except a violet complex precipitated when the Cu(I) complex was exposed to the air. Dissolution in

hot ethanol followed by slow evaporation precipitated small violet crystals suitable for X-ray structure analysis.

UV/VIS (Methanol solution, λ_{\max}): 580nm ($\epsilon = 57 \text{ dm}^3 \text{ mol}^{-1} \text{ cm}^{-1}$); 820nm ($\epsilon = 17 \text{ dm}^3 \text{ mol}^{-1} \text{ cm}^{-1}$).

(6) $[\text{Cu}(\text{L}^{12})(\mu\text{-OH})_2\text{Cu}(\text{L}^{12})][\text{BPh}_4]_2 \cdot 2(\text{CH}_3\text{OH})$.

The initial Cu(I) complex was precipitated using the same procedure used for (4). The Cu(I) complex slowly oxidised when exposed to air to form a green solution. After 1hr stirring ceased and the deep green solution was allowed to stand overnight, during which time small green needles of crystallographic quality formed. The crystals were collected by filtration, washed with water (10mL) and methanol (10mL). Weights used were 0.8g (3.2mmol) *N,N',N''*-triallyl-1,4,7-triazacyclononane, 0.61g (3.2mmol) CuI, 1.1g (3.2mmol) tetraphenylboron sodium, 50mL methanol and 100mL toluene.

Found: C 71.4% H 7.5 % N 6.35% Calc. for $\text{B}_2\text{C}_{80}\text{H}_{104}\text{N}_6\text{O}_4\text{Cu}_2$ C 70.6% H 7.6% N 6.2%.

(7) $[\text{Cu}(\text{L}^{14})(\mu\text{-OH})_2\text{Cu}(\text{L}^{14})][\text{BPh}_4]_2 \cdot 2(\text{MeCN})$.

The same procedure was followed as in (4), except dissolution in hot acetonitrile followed by slow evaporation precipitated small green crystals suitable for X-ray structure analysis. Weights used were 100mg (0.488mmol) *N*-methyl-*N',N''*-diallyl-1,4,7-triazacyclononane, 92mg (0.488mmol) CuI, 153mg (0.488mmol) tetraphenylboron sodium, 15mL methanol and 15mL toluene.

(8) $[\text{Cu}_2(\text{L}^{15})(\mu\text{-OH})_2][\text{BPh}_4]_2$.

The same procedure was followed as in (1), except the initial Cu(I) complex was allowed to oxidise for 2days. Dissolution in hot acetonitrile followed by slow evaporation precipitated small green crystals. Weights used were 240mg (0.51mmol) *trans*-1,4-bis[*N,N'*-diallyl-1,4,7-triazacyclononane]but-2-ene, 194mg (1.02mmol) CuI, 350mg (1.02mmol) tetraphenylboron sodium and 30mL methanol.

2.6.3 LOW TEMPERATURE OXYGENATION OF COPPER(I) COMPLEXES.

$\text{Cu}(\text{MeCN})_4\text{BF}_4$ was prepared according to literature methods (4).

(1) $[\text{Cu}_2(\text{L}^3)(\mu\text{-OH})_2][\text{BF}_4]_2$.

A Schlenk tube equipped with a magnetic stirring bar was charged with $\text{Cu}(\text{MeCN})_4\text{BF}_4$ (284mg, 0.903mmol) suspended in dry degassed dichloromethane (10mL). Trans-1,4-bis(1,4,7-triazacyclononane)but-2-ene (140mg, 0.451mmol) dissolved in dry degassed dichloromethane (20mL) was added to the suspension under a strong flow of nitrogen. The resulting clear yellow solution was cooled to -78°C using an acetone/dry ice bath and O_2 was bubbled into the solution producing an almost instant colour change to deep green. After 20mins the O_2 supply was shut off and the Schlenk tube was sealed and warmed to room temperature. The solvent was reduced in volume (5mL) and layered with diethyl ether. The Cu(II) complex precipitated the following day as an amorphous green solid. Further attempts at crystallisation using different solvents and crystallisation methods failed to yield crystals of crystallographic quality.

(2) $[\text{Cu}_2(\text{L}^4)(\mu\text{-OH})_2][\text{BF}_4]_2$.

The procedure followed was analogous to that in (1), except after 15mins of O_2 uptake the solution was a very intense green colour. Weights used were 315mg (1mmol) $\text{Cu}(\text{MeCN})_4\text{BF}_4$ in 15mL CH_2Cl_2 and 180mg (0.5mmol) α,α' -bis(1,4,7-triazacyclononane)-*ortho*-xylene in 15mL CH_2Cl_2 .

(3) $[\text{Cu}_2(\text{L}^5)(\mu\text{-OH})_2][\text{BF}_4]_2$.

The procedure followed was analogous to that in (1). Weights used were 415mg (1.32mmol) $\text{Cu}(\text{MeCN})_4\text{BF}_4$ in 20mL CH_2Cl_2 and 238mg (0.66mmol) α,α' -bis(1,4,7-triazacyclononane)-*meta*-xylene in 20mL CH_2Cl_2 .

(4) $[\text{Cu}_2(\text{L}^6)(\mu\text{-OH})_2][\text{BF}_4]$.

The procedure followed was analogous to that in (1), except after mixing the ligand and $\text{Cu}(\text{I})$ solutions a colour change to pale green is observed. After 15mins of O_2 uptake the solution did not change colour. THF (15mL) was added to the oxygenated mixture and an instant colour change to intense green was observed. Weights used were 265mg (0.843mmol) $\text{Cu}(\text{MeCN})_4\text{BF}_4$ in 15mL CH_2Cl_2 and 148mg (0.411mmol) α,α' -bis(1,4,7-triazacyclononane)-*para*-xylene in 15mL CH_2Cl_2 .

(5) $[\text{Cu}(\text{L}^{12})(\mu\text{-OH})_2\text{Cu}(\text{L}^{12})][\text{BF}_4]_2$.

The procedure followed was analogous to that in (1). Weights used were 210mg (0.84mmol) *N,N',N''*-triallyl-1,4,7-triazacyclononane in 10mL CH_2Cl_2 and 265mg (0.84mmol) $\text{Cu}(\text{MeCN})_4\text{BF}_4$ in 15mL CH_2Cl_2 .

(6) $[\text{Cu}_2(\text{L}^{15})(\mu\text{-OH})_2][\text{BF}_4]_2$.

The procedure followed was analogous to that in (1). Weights used were 130mg (0.28mmol) *trans*-1,4-bis[*N,N'*-diallyl-1,4,7-triazacyclononane]but-2-ene in 10mL CH_2Cl_2 and 174mg (0.56mmol) $\text{Cu}(\text{MeCN})_4\text{BF}_4$ in 15ml CH_2Cl_2 .

2.6.4 CO_2 ACTIVATION BY $[\text{Cu}(\text{L}^{12})][\text{BPh}_4]$.

(1) $[\text{Cu}(\text{L}^{12})(\mu\text{-C}_2\text{O}_4)\text{Cu}(\text{L}^{12})][\text{BPh}_4]_2 \cdot 2(\text{CD}_3\text{CN})$.

The intermediate Cu(I) complex $[\text{Cu}(\text{L}^{12})][\text{BPh}_4]$ was prepared as described in Section 2.6.2 (6). The oxidation of the Cu(I) complex was aided by exhaling air into the Schlenk tube several times during the first 15-30 minutes of oxidation. During this time the solution precipitated a deep green solid, the solution was left stirring overnight, filtered and dissolved in

acetonitrile. Evaporation of this acetonitrile solution to dryness produced large green opaque crystals. An NMR sample was prepared by dissolution of 80mg of the opaque crystals in boiling d_3 -acetonitrile, the following day green crystals suitable for X-ray structure analysis precipitated in the NMR tube.

IR $\nu(C_2O_4^{2-})$: 1660cm^{-1} .

(2) Reaction of $[Cu(L^{12})][BPh_4] + CO_2$.

The intermediate Cu(I) complex $[Cu(L^{12})][BPh_4]$ was prepared as described in **Section 2.6.2 (6)**. Weights used were 0.330mg (1.32mmol) N,N',N'' -triallyl-1,4,7-triazacyclononane, 253mg (1.32mmol) CuI, 453mg (1.32mmol) tetraphenylboron sodium in 40mL degassed bulk methanol. A steady flow of dry CO_2 gas was produced from a sealed flask of solid dry ice fitted with a piece of tubing containing $CaCl_2$. Bubbling CO_2 gas into the intermediate Cu(I) complex solution caused a colour change from yellow to green after 1-2hr, CO_2 was bubbled overnight to ensure complete reaction. The resulting green precipitate was collected by filtration, dissolution in hot acetonitrile, followed by slow evaporation to complete dryness yielded large green chunks of crystalline mass.

IR (KBr disc): $\nu(\text{C}_2\text{O}_4^{2-})$ 1660cm^{-1} ; $\nu(\text{CO}_3^{2-})$ 1578cm^{-1} .

(3) Reaction of $[\text{Cu}(\text{L}^{12})]\text{I} + \text{CsHCO}_3$.

A Schlenk tube equipped with a magnetic stirring bar was charged with CuI (260mg, 1.37mmol) and CsHCO_3 (270mg, 1.39mmol) suspended in dry degassed methanol (30mL). Addition of *N,N',N''*-triallyl-1,4,7-triazacyclononane (245mg, 1.385mmol) dissolved in dry degassed methanol (10mL) caused the white suspension to dissolve and an almost instant colour change to blue. The blue solution was filtered and the solvent removed on the rotary evaporator. Dissolution in hot acetonitrile followed by slow evaporation precipitated a green amorphous solid.

IR (KBr disc): $\nu(\text{C}_2\text{O}_4^{2-})$ 1660cm^{-1} ; $\nu(\text{CO}_3^{2-})$ 1580cm^{-1} .

2.6.5 COMPLEXES OF L^{18} , L^{19} , L^{20} AND L^{22} .

(1) Cobalt(II) complex of L^{18} .

A Schlenk tube equipped with a magnetic stirring bar was charged with $\text{CoCl}_2 \cdot 6\text{H}_2\text{O}$ (204mg, 0.86mmol) dissolved in dry degassed methanol (20mL). *N*-Diphenylphosphinopentyl-1,4,7-triazacyclononane (329mg,

0.86mmol) dissolved in methanol (5mL) was added under a strong flow of nitrogen gas and the colour of the solution deepened to a dark shade of pink. The pink solution was stirred for 0.5h and the solvent reduced in volume. Overnight vapour diffusion of diethyl ether precipitated the complex as an amorphous blue solid. Unfortunately further attempts to crystallise the complex using different solvent and different methods were unsuccessful.

(2) Copper(I) complex of L¹⁸.

A Schlenk tube equipped with a magnetic stirring bar was charged with $\text{Cu}(\text{MeCN})_4\text{BF}_4$ (67mg, 0.21mmol) dissolved in dry degassed CH_2Cl_2 (15mL). Under a strong flow of nitrogen gas, *N*-diphenylphosphinopentyl-1,4,7-triazacyclononane (82mg, 0.22mmol) dissolved in CH_2Cl_2 (5mL) was added and the initially colourless solution changed almost instantly to pale yellow. Overnight vapour diffusion of diethyl ether precipitated the green Copper(II) complex as an amorphous solid.

(3) Cobalt(-I / I) complex of L¹⁹.

A Schlenk tube equipped with a magnetic stirring bar was charged with $\text{Co}_2(\text{CO})_8$ (224mg, 0.655mmol) dissolved in dry degassed dichloromethane (45mL). *N,N',N''*-Tris(diphenylphosphinopropyl)-1,4,7-

triazacyclononane (529mg, 0.655mmol) dissolved in dry degassed dichloromethane (5mL) was added to the solution. Effervescence of CO occurred immediately after the addition and an almost instant colour change from intense brown to red was observed. The reaction was monitored using infra-red spectroscopy and after 1day of stirring the solution was deep brown, the solvent was reduced in volume (10mL), 40/60 petrol (10mL) was added and the mixture was stored at -18°C for 3 days to aid crystallisation. Unfortunately crystallisation did not occur and further attempts were unsuccessful.

IR (dichloromethane solution): $\nu(\text{C}=\text{O})$ 1889, 1951, 2005 cm^{-1} .

(4) Nickel(II) complex of L¹⁹.

A Schlenk tube equipped with a magnetic stirring bar was charged with $\text{NiCl}_2 \cdot 6\text{H}_2\text{O}$ (58mg, 0.244mmol) dissolved in dry degassed ethanol (10mL). *N,N',N''*-Tris(diphenylphosphinopropyl)-1,4,7-triazacyclononane (197mg, 0.244mmol) dissolved in dichloromethane (10mL) was added to the solution producing an almost instant colour change from green to intense red/purple. Addition of NaBPh_4 (167mg 0.488mmol) in ethanol (10mL) precipitated the complex as a red/brown amorphous solid, this was collected by filtration and washed with dry degassed ethanol (10mL).

^{31}P NMR (81MHz, CDCl_3 , δ): 76.8 (2P); 83.7 (1P).

UV/VIS (CH_2Cl_2 solution, λ_{max}): 380nm, 545nm

(5) Molybdenum(0) complex of L^{19} .

A Schlenk tube equipped with a magnetic stirring bar was charged with $\text{Mo}(\text{CO})_3(\text{MeCN})_3$ (197mg, 0.65mmol) dissolved in a mixture of dry degassed acetonitrile (15mL) and dichloromethane (15mL). N,N',N'' -Tris(diphenylphosphinopropyl)-1,4,7-triazacyclononane (526mg, 0.65mmol) dissolved in dry degassed acetonitrile (5mL) / dichloromethane (5mL) was added to the solution producing no observable colour change from pale yellow. The reaction was monitored using infra-red spectroscopy and after 1day of stirring the solvent was removed under reduced pressure to leave the complex as an extremely air sensitive brown solid.

IR (acetonitrile/dichloromethane solution): $\nu(\text{C}=\text{O})$ 1808, 1831, 1928cm^{-1} .

(6) Platinum(0) complex of L^{20} .

A Schlenk tube equipped with a magnetic stirring bar was charged with $\text{Pt}(\text{nb})_3$ (46mg, 96 μmol). N -methyl- N',N'' -di(diphenylphosphinopropyl)-1,4,7-triazacyclononane (58mg, 97 μmol) dissolved in degassed CDCl_3

(0.8mL) was added to the Schlenk tube under a strong flow of nitrogen producing an instant colour change from pale yellow to orange. The solvent was removed under reduced pressure to leave an orange/brown solid, washing with 40/60 petrol (2x5mL) and drying under reduced pressure removed any released norbornene.

(7) Gold(I) complex of L²⁰.

A gold(I) solution was prepared by the slow addition of thiodiglycol (0.28mL, 2.8mmol) to an acetone/water (5/5mL) solution of chloroauric acid (0.5 g, 1.4mmol). Complete reduction was obtained when the colour of the solution changed from yellow to colourless. *N*-methyl-*N'*,*N''*-di(diphenylphosphinopropyl)-1,4,7-triazacyclononane (833mg, 1.4mmol) dissolved in acetone/dichloromethane (5/5mL) was added to the colourless gold(I) solution with no apparent colour change. The organic layer containing the complex was separated and the solvent removed under reduced pressure to leave the complex as an off white light sensitive solid. Dissolution in chloroform (1mL), addition of diethyl ether (2mL) and overnight storage at -18°C precipitated the complex as a white microcrystalline solid.

FW: 1060gmol⁻¹

^{31}P NMR (81 MHz, CDCl_3 , δ): 28.27 (P-Au-Cl).

(8) Cobalt(II) complex of L^{22} .

A 50mL conical flask equipped with a magnetic stirring bar was charged with $\text{CoCl}_2 \cdot 6\text{H}_2\text{O}$ (68.7mg, 0.289mmol) dissolved in dry ethanol (20mL). *N,N',N''*-Tris(diphenylphosphinylethyl)-1,4,7-triazacyclononane (235mg, 0.289mmol) dissolved in ethanol/dichloromethane (10/5mL) was added slowly to the blue solution with no observable colour change. When a slight excess of ligand was added, the colour changed from blue to pink, addition of ammonium hexafluorophosphate (94mg, 0.576mmol) in ethanol (10mL) precipitated the complex as a pink microcrystalline solid. The complex was collected by filtration and washed with ethanol (10mL). Dissolution in hot acetonitrile followed by vapour diffusion of diethyl ether at room temperature produced a large single pink crystal which lost solvent once removed from solution. Unfortunately further attempts to crystallise the complex using the above and different methods were unsuccessful.

UV/VIS (Acetonitrile solution, λ_{max}): 515nm, 1135nm.

IR (KBr): $\nu(\text{P=O})$ 1141 cm^{-1} .

2.6.6 COMPLEXES OF L^{23} .

(1) Cobalt complexes of L^{23} .

CoCl_2 (183mg, 0.77mmol) was dissolved in dry degassed ethanol (20mL) and placed in a Schlenk tube equipped with a magnetic stirring under a strong flow of nitrogen gas. Addition of *N*-(*S*)-2-methyl-1-propanol-1,4,7-triazacyclononane (173mg, 0.77mmol) as an absolute ethanol solution (10mL) gave an almost instant colour change from blue to intense blue. In an attempt to precipitate the PF_6^- salt, solid NH_4PF_6 (251mg, 1.54mmol) was added, but no solid precipitated. On exposure to air the solution turned deep purple, evaporation of the solution yielded an amorphous purple solid. Further attempts at crystallisation using different solvents and crystallisation methods failed to yield crystals of crystallographic quality.

UV/VIS (Acetonitrile solution, λ_{max}): 565nm ($\epsilon = 140\text{dm}^3\text{mol}^{-1}\text{cm}^{-1}$).

(2) $[\text{Cu}(L^{23})(\text{NO}_3)][\text{NO}_3]$

$\text{Cu}(\text{NO}_3)_2 \cdot 3\text{H}_2\text{O}$ (118mg, 0.49mmol) was dissolved in absolute ethanol (10mL) and placed in a 50mL conical flask equipped with a magnetic stirring bar. Addition of *N*-(*S*)-2-methyl-1-propanol-1,4,7-triazacyclononane (110g, 0.49mmol) in absolute ethanol (10mL) gave an immediate colour change

from pale to intense blue. The flask was stored at room temperature overnight to yield crystallographic quality crystals of the complex.

FW: 412.5 g mol⁻¹

UV/VIS (Acetonitrile solution, λ_{max}): 650 nm ($\epsilon = 97 \text{ dm}^3 \text{ mol}^{-1} \text{ cm}^{-1}$); 1160 nm ($\epsilon = 34 \text{ dm}^3 \text{ mol}^{-1} \text{ cm}^{-1}$).

(3) Zinc(II) complex of L²³.

Anhydrous zinc chloride (58.8 mg, 0.43 mmol) was dissolved in absolute ethanol (10 mL) in a 50 mL conical flask equipped with a magnetic stirring bar. *N*-(*S*)-2-Methyl-1-propanol-1,4,7-triazacyclononane (97 mg, 0.43 mmol) was added as an absolute ethanol solution (10 mL). Addition of NH_4PF_6 was unsuccessful in precipitating the complex and slow evaporation of the solution produced an amorphous white solid.

¹H NMR (200 MHz, D₂O, δ): 0.58 (d, 3H, $-\text{CH}_2\text{CH}(\underline{\text{CH}_3})\text{CH}_2\text{OH}$); 2.03 (m, 1H, $-\text{CH}_2\text{CH}(\underline{\text{CH}_3})\text{CH}_2\text{OH}$); 2.2-3.0 (m, 12H, N- $\underline{\text{CH}_2}$ -, ring); 3.35 (m, 2H, $-\text{CH}_2\text{CH}(\text{CH}_3)\text{CH}_2\text{OH}$); 3.65 (m, 2H, $-\text{CH}_2\text{CH}(\text{CH}_3)\underline{\text{CH}_2}\text{OH}$).

¹³C NMR (51 MHz, D₂O, δ): 17.10 ($-\text{CH}_2\text{CH}(\underline{\text{CH}_3})\text{CH}_2\text{OH}$); 33.44 ($-\text{CH}_2\underline{\text{CH}}(\text{CH}_3)\text{CH}_2\text{OH}$); 42.33, 42.72, 47.64, 49.21, 50.80, 59.18 (N- $\underline{\text{CH}_2}$ -, ring); 69.26 ($-\underline{\text{CH}_2}\text{CH}(\text{CH}_3)\text{CH}_2\text{OH}$); 62.22 ($-\text{CH}_2\text{CH}(\text{CH}_3)\underline{\text{CH}_2}\text{OH}$).

REFERENCES

1. J.E. Richman, T.J. Atkins, *J. Am. Chem. Soc.*, 1974, **96**, 2268.
2. J.P.L. Cox, A.S. Craig, I.M. Helps, K.J. Jankowski, D. Parker, M.A.W. Eaton, A.T. Millican, K. Millar, N.R.A. Beeley, B.A. Boyce, *J. Chem. Soc. Perkin Trans. 1*, 1990, 2567.
3. T.J. Atkins, *J. Am. Chem. Soc.*, 1980, **102**, 6364.
4. B.J. Hathaway, D.G. Holah, J.D. Postlethwaite, *J. Chem. Soc.*, 1961, 3215

CHAPTER 3

COPPER AND SILVER COMPLEXES OF

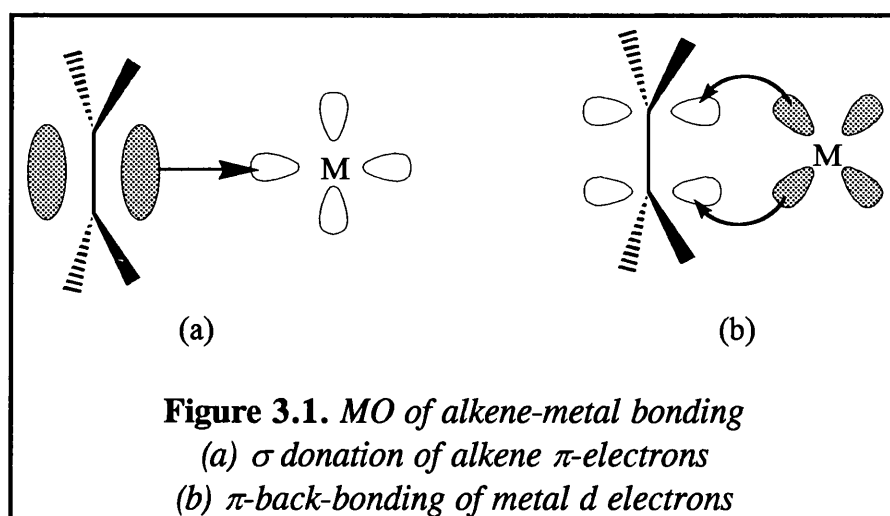
L^{10} and L^{11}

3.1 INTRODUCTION

The binding of unsaturated hydrocarbons to transition metals has been an area of interest to organometallic chemists for many years. The earliest known organotransition metal complex was the ethylene complex $\text{K}[\text{Pt}(\text{C}_2\text{H}_4)\text{Cl}_3]$, discovered in 1827 by W.C. Zeise (1), although the true constitution was not known until over a century later. The metal-alkene bond has received intense investigation in connection with the $\text{C}=\text{C}$ bond distance, NMR of the coordinated olefin and activation of the $\text{C}=\text{C}$ bond for polymerisation. The Dewar-Chatt-Duncanson (2, 3) concept (figure 3.1) of olefins being σ donors and π acceptors has been used to explain most of the features observed in olefin binding to transition metals. For d^{10} metal-olefin complexes the contribution from σ donation was found to be most important for $\text{Ag}(\text{I})$, for $\text{Ni}(\text{O})$ π back donation was found to be the most important, whereas for $\text{Cu}(\text{I})$ complexes the contribution from σ donation and π back donation varies.

Ethylene is a plant hormone that causes seeds to sprout, flowers to bloom, fruit to ripen, petals to shrivel and leaves turn brown. The source of the gas in nature appears to be carbons 3 and 4 of methionine although the ethylene effect can be induced by exogenously applying the gas. Other unsaturated gases such as acetylene, propane and carbon monoxide can induce the effect, but with lower activity. The ethylene receptor site is not

known, but a metal ion is believed to be involved at the site. Consideration of the organometallic chemistry of biologically important transition metals suggests the copper ion as the metal at the ethylene site. Thompson (4, 5) has prepared and structurally characterised copper(I)-amine complexes that tightly bind ethylene and are stable to olefin loss.

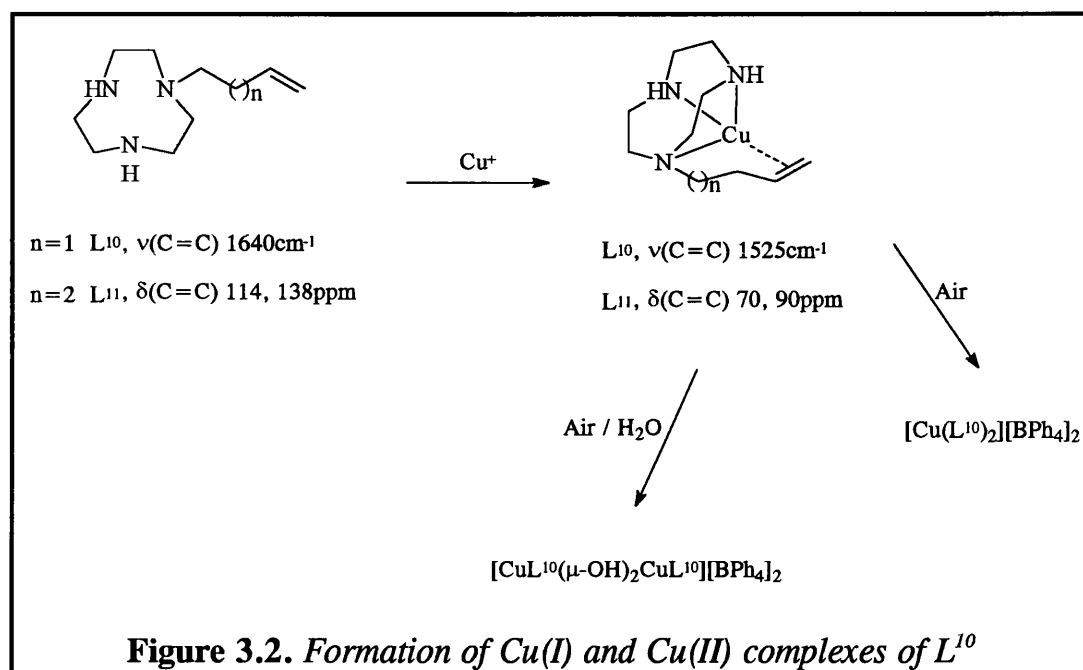


3.2 COPPER COMPLEXES OF L^{10} AND L^{11}

3.2.1 Synthesis of Complexes

The copper(I) complex with L^{10} was prepared using the same method reported for copper(I) complexes with TACN (and Me_3TACN) and ethylene gas, reported by Chaudhuri in 1989 (6). The method utilises CuI and NaBPh_4 as starting materials. It was found by Chaudhuri that CuI was the

preferred Cu(I) salt, as CuCl formed a complex which disproportionated; it was also noted that the more stable complexes were found for the BPh_4^- anion. The Cu(I) complex of L^{10} was extremely air sensitive and rapidly oxidised in air to produce one of two possible copper(II) complexes (figure.3.2).



The blue-green hydroxide bridged dimer $[\text{CuL}^{10}(\mu\text{-OH})_2\text{CuL}^{10}][\text{BPh}_4]_2$ was formed the most often, but the violet bis ligand complex $[\text{CuL}_2^{10}][\text{BPh}_4]_2$ was isolated on two occasions for L^{10} and once for L^7 and L^{11} . It is believed that the bis ligand complex formed when the system was free from moisture; a disproportionation reaction was not responsible for the formation of Cu(II) as no copper metal was isolated from the reaction mixture.

The rapid oxidation of the $[\text{CuL}^{10}]^+$ species is believed to be a consequence of excessive strain on the short C_4 pendant arm. It was anticipated that L^{11} which has one more carbon atom in the pendant arm would be less strained and form more stable Cu(I) complexes. Although BPh_4^- was the preferred counterion in terms of stability, BF_4^- and I^- were more suitable for characterising the $[\text{CuL}^{11}]^+$ species using ^1H and ^{13}C NMR experiments.

3.2.2 Infrared Spectrum of $[\text{CuL}^{10}][\text{BPh}_4]$

The infrared spectra of $[\text{CuL}^{10}][\text{BPh}_4]$ and $[\text{Cu}(\text{L}^{10})_2][\text{BPh}_4]_2$ are shown in figure 3.3, the band at 1525cm^{-1} has been assigned to coordinated $\nu(\text{C}=\text{C})$ and the band at 1640cm^{-1} has been assigned to uncoordinated $\nu(\text{C}=\text{C})$. Thus a reduction of 115cm^{-1} is observed in $\nu(\text{C}=\text{C})$, indicating a weakening in the $\text{C}=\text{C}$ bond due to a π -backbonding interaction from the metal. A list of copper(I) olefin complexes with nitrogen donor ligands is shown in Table 3.1. A ligand with a large number of basic nitrogens would transfer more electron density to a metal centre than a ligand with less basic or a smaller number of nitrogens. The more electron density on a metal, the stronger the π -backbond to a π -acceptor ligand such as an olefin. From these considerations, Me_3TACN would be expected to have the strongest

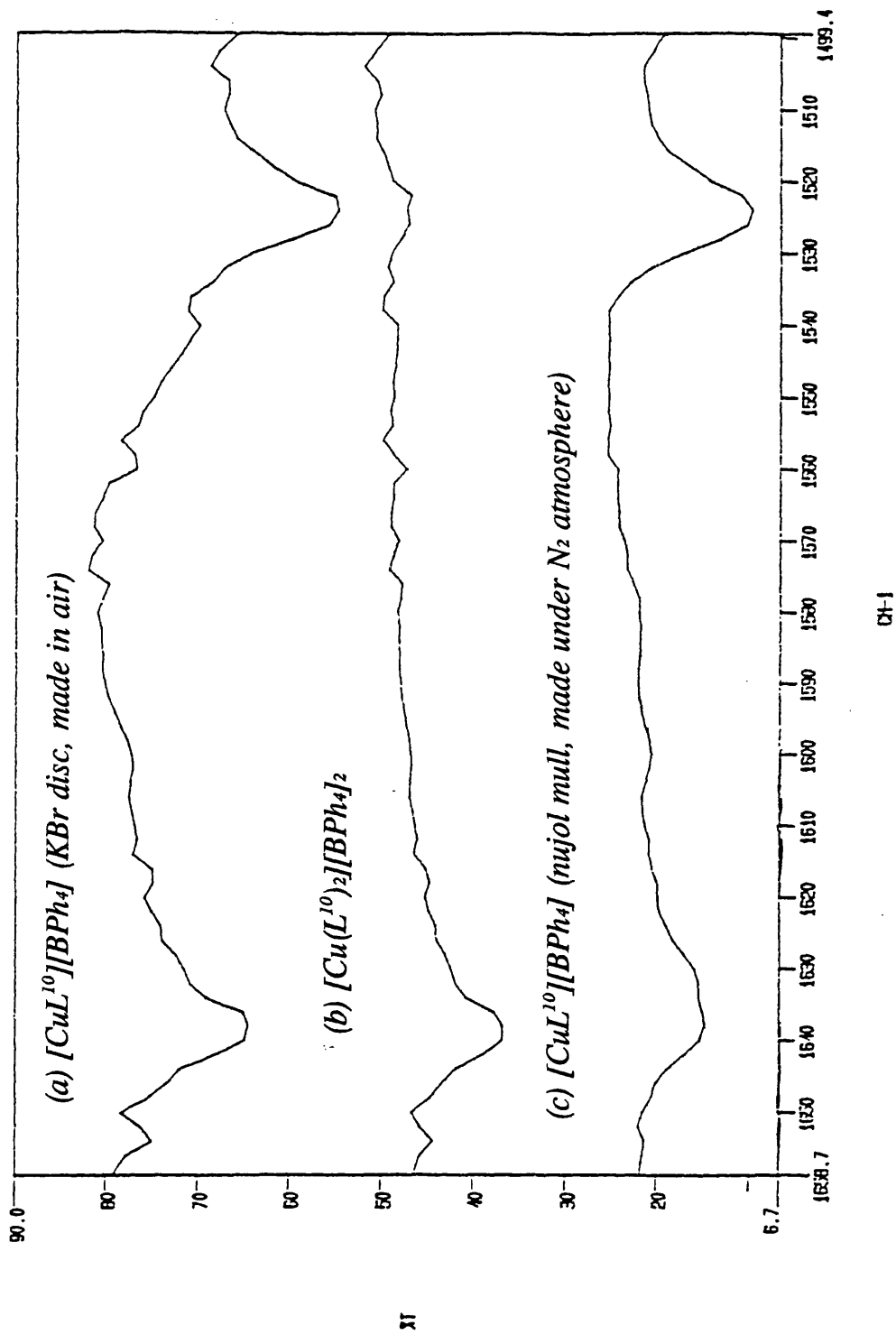


Figure 3.3 IR Spectra of copper complexes

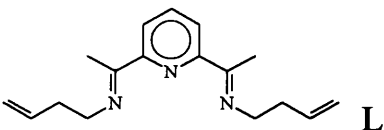
Complex or ligand	$\nu(\text{C}=\text{C}) \text{ cm}^{-1}$	change in $\nu(\text{C}=\text{C})$	Ref.
C_2H_4	1623		6, 7
$[\text{Cu}(\text{TACN})(\text{C}_2\text{H}_4)]^+$	1580	-43	7
$[\text{Cu}(\text{Me}_3\text{TACN})(\text{C}_2\text{H}_4)]^+$	1570	-53	7
$[\text{Cu}(\text{tmen})(\text{C}_2\text{H}_4)]^+$	1525	-98	8
$[\text{Cu}(\text{teen})(\text{C}_2\text{H}_4)]^+$	1525	-98	8
cyclohexene	1646		7
cyclooctene	1648		7
$[\text{Cu}(\text{TACN})(\text{cyclohexene})]^+$	1580	-66	7
$[\text{Cu}(\text{Me}_3\text{TACN})(\text{cyclohexene})]^+$	1565	-81	7
$[\text{Cu}(\text{TACN})(\text{cyclooctene})]^+$	1570	-78	7
$[\text{Cu}(\text{Me}_3\text{TACN})(\text{cyclooctene})]^+$	1575	-73	7
	1636		9
$[\text{Cu}_2\text{L}_2]^{2+}$	1565	-71	9
L^{10}	1640		this work
$[\text{CuL}^{10}]^+$	1525	-115	this work

Table 3.1. *IR data on selected compounds*

tmen = *N,N,N',N'*-tetramethylethylenediamine

teen = *N,N,N',N'*-tetraethylethylenediamine

π -backbond and hence the largest shift in $\nu(\text{C}=\text{C})$ in table 3.1, but this appears to be untrue. The largest shift of $\nu(\text{C}=\text{C})$ is observed for L^{10} , which would be expected to come after Me_3TACN , but before the other bidentate ligands. The smallest shifts in $\nu(\text{C}=\text{C})$ are actually observed for Me_3TACN and TACN , which is the converse to what would be expected. The large shift observed for L^{10} may be attributed to the fact that the macrocyclic ring is attached to the copper(I) and holds the olefin pendant arm in close proximity to the metal centre where it is tightly bound, whereas the other systems contain ethylene which is not tethered to the macrocycle.

3.2.3 NMR Spectra of $[\text{CuL}^{11}][\text{BF}_4]$

The ^1H and ^{13}C NMR spectra of the longer pendant arm macrocycle L^{11} and $[\text{CuL}^{11}][\text{BF}_4]$ are shown on figures 3.4, 3.5 and 3.6, 3.7. The most noticeable feature of the spectra is the loss of symmetry in the ligand upon complexation, the methylene region is more complicated in the ^1H NMR of the complex and each macrocyclic ring carbon is distinct in the ^{13}C NMR of the complex. The olefin ^1H and ^{13}C resonances are seen to shift upfield for $[\text{CuL}^{11}][\text{BF}_4]$, a feature not uncommon in copper(I) complexes and is an indication of the amount of π -backbonding in the complex. Table 3.2 shows the relative ^1H and ^{13}C shifts of selected olefin-copper(I) complexes.

~~XXXX~~
 HNSBPL1.728
 DATE 30-11-96
 TIME 14:23
 SOLVENT CDCl3
 CF 300.132
 Q1 3500.000
 HZ/F1 .133
 PX 5.0
 CQ 10.756
 WU 16.756
 MS 16
 Q2 63L PD
 LB 8.8
 LY 18.88
 PPM/CH .350
 SR 2342.78

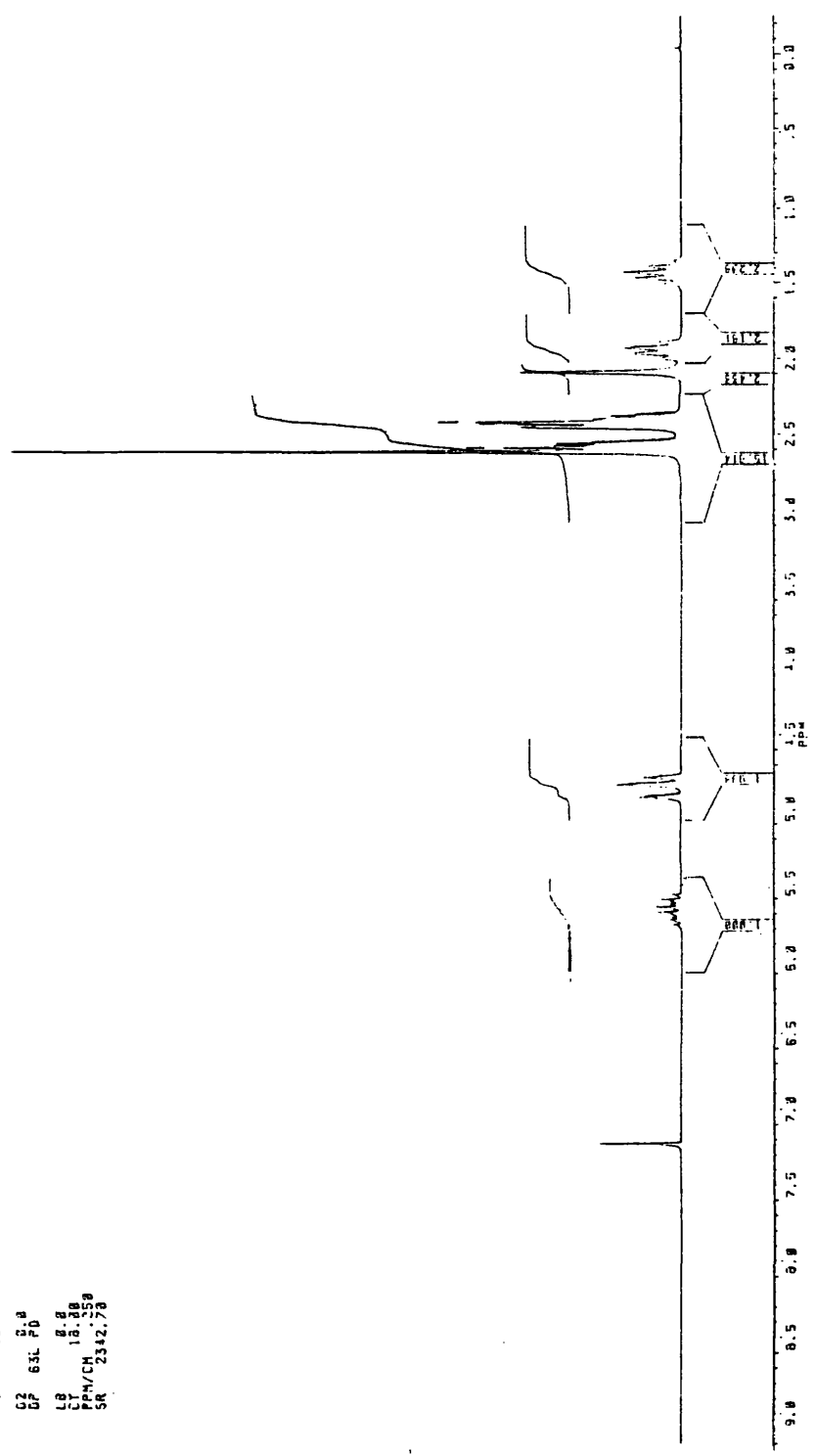


Figure 3.4. ¹H NMR Spectrum of L¹¹ in CDCl₃

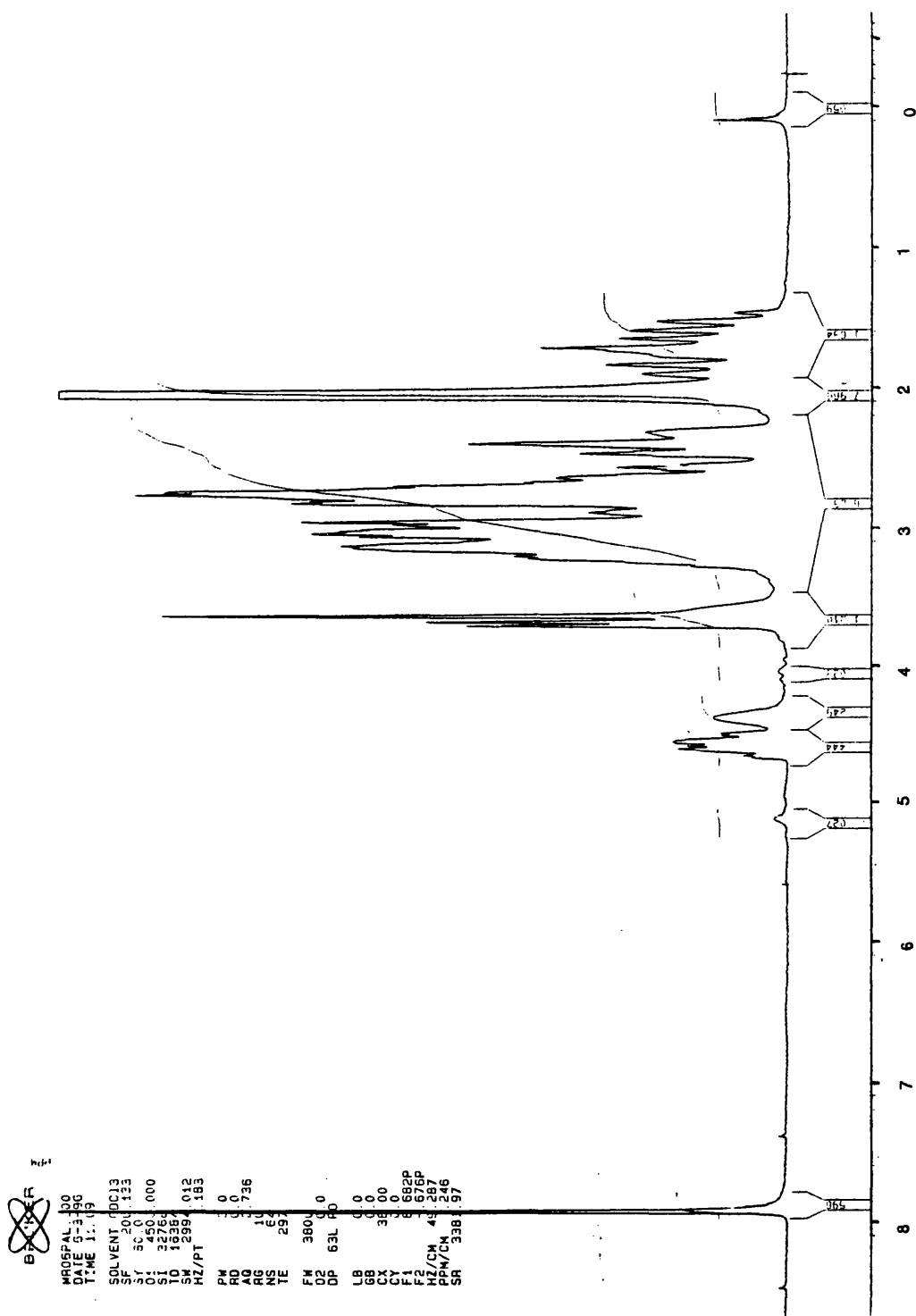


Figure 3.6. ^1H NMR Spectrum of $\text{Cu}(\text{L}^{11})\text{BF}_4$ in d_6 -Acetone



MR06AL.031
AU PRO3
DEPTAGNP
DATE 5-3-95
TIME 11.25
SOLVENT CDCl3
SP 500.13
SY 5L 0300000
O1 29750.000
SI 32768
TD 16384
SW 11304.792
HZ/P1 .727
PM 0.0
RD 0.0
AQ .688
RG 400
NS 128
TE 300.2
FW 14900
D2 3500.000
DP 26H CPD
LB 5.000
GB 0.0
CX 32.00
CY 5.00
F1 222.036P
F2 -14.513P
HZ/CN 312.254
SMA/C 55
SR 2339.93

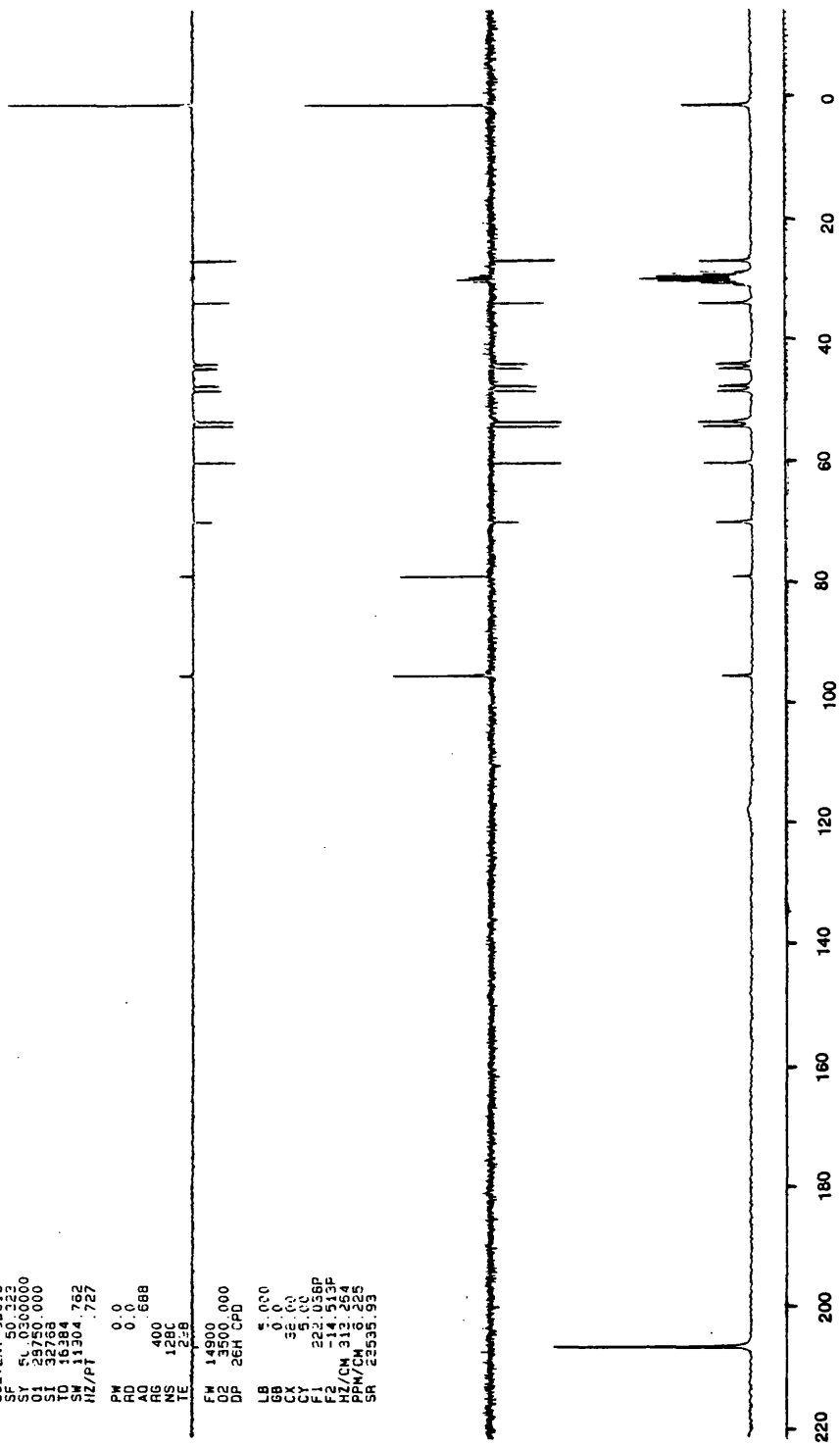


Figure 3.7. ^{13}C NMR Spectrum of $\text{Cu}(\text{L}^{11})\text{BF}_4$ in d_6 -Acetone

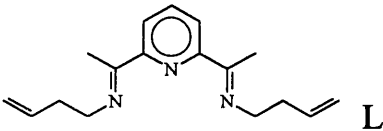
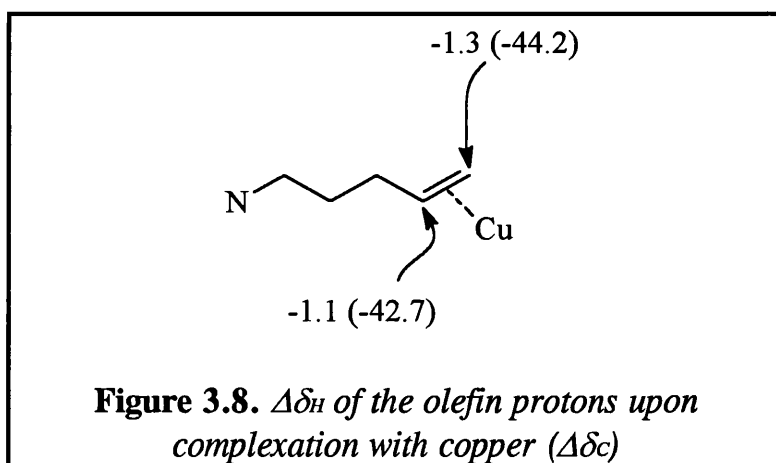
Complex or ligand	δ_H of olefin ppm	change in δ_H	δ_C of olefin ppm	change in δ_C
C_2H_4	5.44		123	
$[Cu(TACN)(C_2H_4)]^+$			51	-72
			55	-68
$[Cu(Me_3TACN)(C_2H_4)]^+$			54	-69
			55	-68
$[Cu(tmen)(C_2H_4)]^+$	4.31	-1.13		
$[Cu(teen)(C_2H_4)]^+$	4.43	-1.01		
	5.1			
	6.0			
$[Cu_2L_2]^{2+}$	4.7	-0.4		
	5.6	-0.4		
L^{11}	4.9		114.4	
	5.7		138.4	
$[CuL^{11}]^+$	3.6	-1.3	70.2	-44.2
	4.6	-1.1	95.7	-42.7

Table 3.2. 1H and ^{13}C NMR data on selected compounds

$[\text{CuL}^{11}]^+$ exhibits significant shielding of the olefin when compared to the other complexes in table 3.2, only the complexes of TACN and Me_3TACN show larger shielding. The methylenes of the ring and pendant arm show little shifts in their ^1H ($\sim 0.5\text{ppm}$) and ^{13}C ($\sim 1\text{-}3\text{ppm}$) NMR spectra upon coordination. The shifts observed for the olefin protons (and carbons) are unequal (figure 3.8) and suggest that there is an unsymmetrical positioning of the copper ion with respect to the olefin. This positioning is not uncommon in unsymmetrical olefins (**10**) and the copper ion is pictured as being closer to the terminal carbon, resulting in a more effective π -backbond and hence a more shielded environment compared to the substituted carbon.



The NMR and IR data confirms that the olefin is coordinated to the copper(I) centre and the structure of the complex is probably tetrahedral Cu(I) with the remaining three sites occupied by the nitrogens of the macrocyclic ring. Although the complex exhibits a reasonably large degree

of π -backbonding, the length of the C=C bond cannot be predicated from the IR and NMR data and will have to be established by X-ray analysis, since significant lengthening of C=C bonds is generally not observed in Cu(I)-alkene complexes (4, 5), irrespective of the magnitude of π -backbonding observed in IR and NMR spectra.

3.2.4 Structure of $[\text{Cu}(\text{L}^{10})_2][\text{BPh}_4]_2$

The complex was isolated on more than one occasion when $[\text{CuL}^{10}][\text{BPh}_4]$ was allowed to oxidise in air. The complex was crystallised from hot ethanol and the structure of the cation is shown in figure 3.8. The most striking feature of the structure is the degree of tetragonal distortion from octahedral symmetry, the two axial Cu-N bonds are $\sim 0.5\text{\AA}$ longer than the four shorter equatorial Cu-N bonds, the copper ion also sits in a centre of inversion. The olefin is uncoordinated and the $\nu(\text{C}=\text{C})$ for the complex is found at 1640cm^{-1} (figure 3.3), the same frequency as the free ligand. A selection of bond lengths and bond angles is presented in table 3.3.

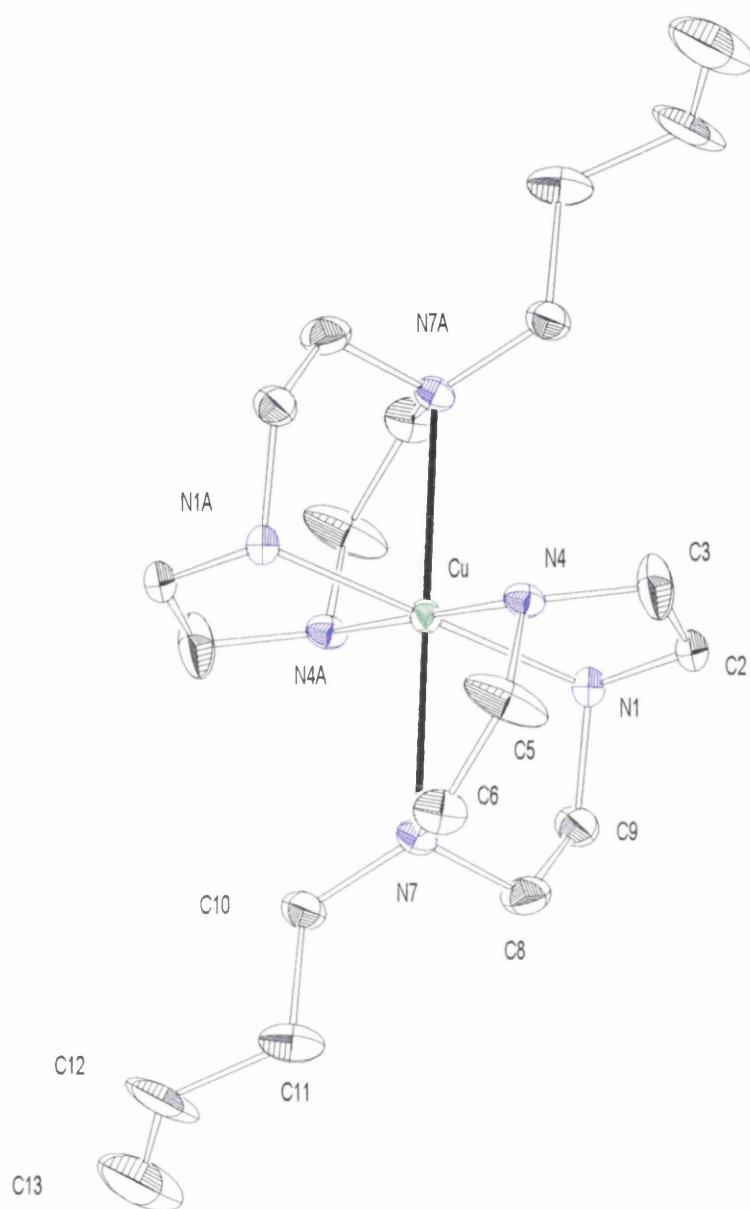


Figure 3.8. *Crystal Structure of the $[\text{Cu}(\text{L}^{10})_2]^{2+}$ cation*

Crystal data for $\text{C}_{68}\text{H}_{82}\text{B}_2\text{CuN}_6$: $M = 1068.6$; Monoclinic; Space Group $P2_1/n$;

$a = 13.0529(8)\text{\AA}$; $b = 18.008(1)$; $c = 13.423(1)\text{\AA}$; $\beta = 111.720(6)^\circ$;

$U = 2931.2(4)\text{\AA}^3$; $Z = 2$; $D_{\text{calc.}} = 1.21\text{gcm}^{-3}$; $F(000) = 1142$;

$\mu(\text{MoK}_\alpha) = 4.17\text{cm}^{-1}$; $R(R') = 0.078(0.077)$.

Cu-N1	2.020(8)Å	N1-Cu-N4	82.7(5)°
Cu-N4	2.043(8)Å	N1-Cu-N7	103.0(4)°
Cu-N7	2.527(9)Å	N4-Cu-N7	79.4(4)°

Table 3.3. *Selected bond lengths and angles for $[\text{Cu}(\text{L}^{10})_2]^{2+}$*

While the equatorial Cu-N bonds are unexceptional, the axial Cu-N bonds are very long, much longer than the mean of Cu-N^{3ry} bond lengths (2.260Å) and well above the upper quartile (2.229Å) (11). The electronic spectrum (figure 3.9) of $[\text{Cu}(\text{L}^{10})_2][\text{BPh}_4]_2$ consists of two bands at 580nm ($\epsilon=57\text{dm}^3\text{mol}^{-1}\text{cm}^{-1}$) and 817nm ($\epsilon=17\text{dm}^3\text{mol}^{-1}\text{cm}^{-1}$) reflecting the essentially square planar Cu(II) coordination. The Jahn-Teller distortion observed in $[\text{Cu}(\text{L}^{10})_2]^{2+}$ is very noticeable when a comparison of Cu-N bond lengths is made with $[\text{Cu}(\text{TACN})_2]^{2+}$ (12) (table 3.4).

	Cu-N _{ax}	Cu-N _{eq}
$[\text{Cu}(\text{L}^{10})_2]^{2+}$	2.527Å	2.032Å (average)
$[\text{Cu}(\text{TACN})_2]^{2+}$	2.321Å (average)	2.062Å (average)

Table 3.4. *Comparison of Cu-N Bond lengths*

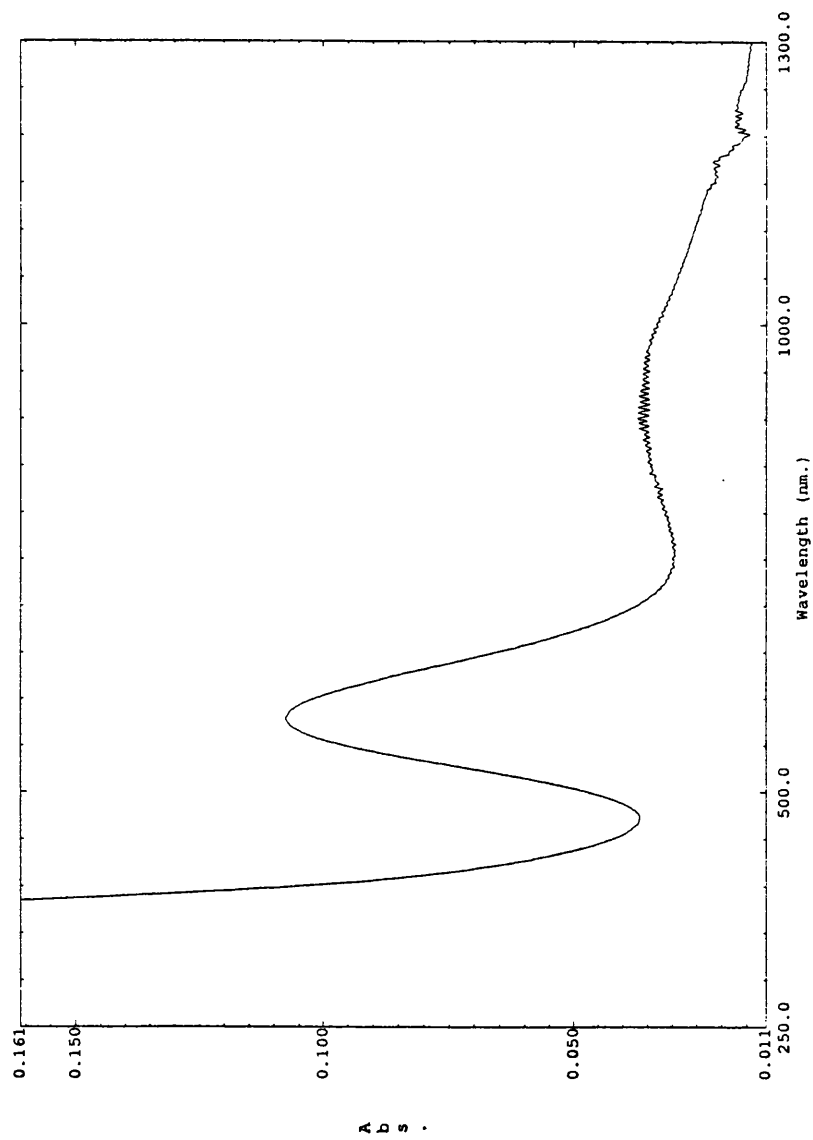


Figure 3.9. Electronic spectrum of $[\text{Cu}(\text{L}^{10})_2]^{2+}$ in methanol

The reason for this extremely long axial Cu-N bond is unknown and has been observed in a similar bis ligand copper(II) complex $[\text{Cu}(\text{L}^{\text{mes}})_2]^{2+}$, where L^{mes} is a single mesityl pendant arm ligand based on TACN (**13**). Perhaps a combination of the reduced basicity of the tertiary amine and the *trans* arrangement of two such weaker σ -donors gives rise to the unusual elongation. A second more plausible reason for this unusual elongation could be due to steric crowding round the metal centre. From the space filling model (figure 3.10) it can be seen that the distance between the pendant arm and the second macrocyclic ring is very small, a shorter axial bond would result in the pendant arm lying even closer to the ring increasing the amount of steric crowding round the metal ion. Therefore a long axial bond is favoured, giving the maximum separation of the arm and macrocycle.

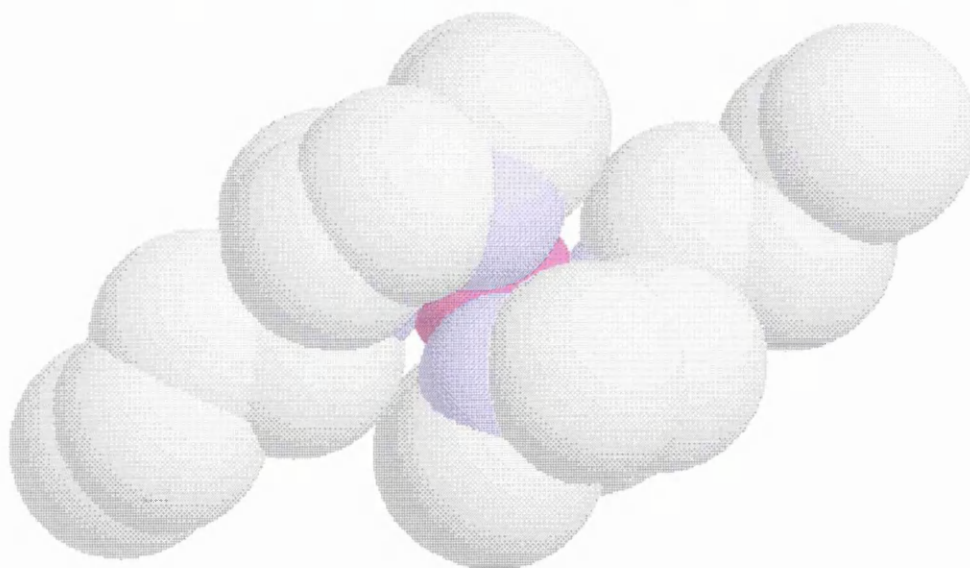


Figure 3.10. Space filling model of $[\text{Cu}(\text{L}^{10})_2]^{2+}$ looking down the equatorial plane, the axial bonds are drawn horizontal

3.2.5 Structure of $[\text{CuL}^{10}(\mu\text{-OH})_2\text{CuL}^{10}][\text{BPh}_4]_2$

The hydroxide bridged dimer $[\text{CuL}^{10}(\mu\text{-OH})_2\text{CuL}^{10}]^{2+}$ was a product of almost all of the atmospheric oxidations of $[\text{CuL}^{10}]^+$. The formation of hydroxide bridged dimers is not uncommon in the oxidation of Cu(I) to Cu(II) by O_2 and is a consequence of ever-present moisture in reaction systems and of course the atmosphere. The complex was recrystallised by dissolution in hot acetonitrile followed by refrigeration, the crystal structure of the cation is shown in figure 3.11. The structure is best described as a distorted square pyramid with a $\sim 0.2\text{\AA}$ elongation of the Cu- N_{ax} bond. The bridging $\text{Cu}_2(\text{OH})_2$ unit is planar and a selection of bond lengths and angles is presented in table 3.5.

Cu1-N1	2.028(2) \AA	Cu1-Cu1A	2.9778(8) \AA
Cu1-N2	2.029(2) \AA	Cu1-O1	1.929(2) \AA
Cu1-N3	2.258(3) \AA	Cu1-O1A	1.928(2) \AA
N1-Cu1-Cu1A	137.74(7) $^\circ$	Cu1-O1-Cu1A	101.01(9) $^\circ$
N2-Cu1-Cu1A	134.77(8) $^\circ$	O1-Cu1-O1A	78.99(9) $^\circ$
N3-Cu1-Cu1A	113.10(7) $^\circ$	N1-Cu1-N2	83.86(10) $^\circ$
N1-Cu1-O1	176.90(9) $^\circ$	N1-Cu1-N3	83.09(10) $^\circ$
N2-Cu1-O1	98.29(9) $^\circ$	N2-Cu1-N3	83.12(10) $^\circ$
N3-Cu1-O1	99.35(9) $^\circ$		

Table 3.5. Selected bond lengths and angles for $[\text{CuL}^{10}(\mu\text{-OH})_2\text{CuL}^{10}]^{2+}$

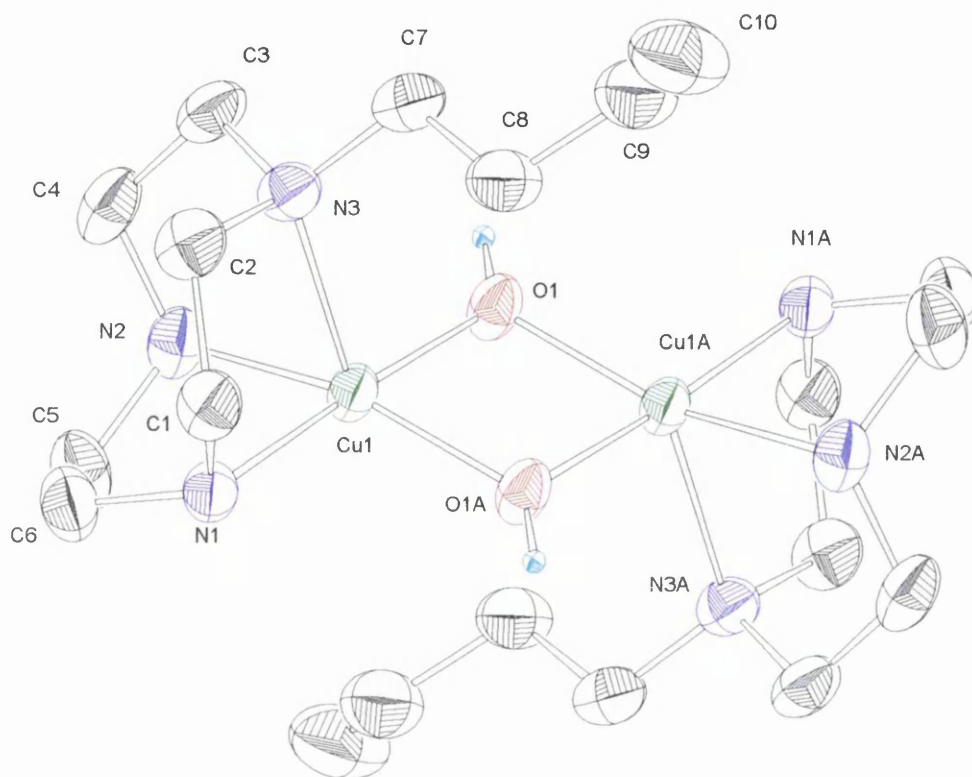


Figure 3.11. *Crystal Structure of the $[\text{CuL}^{10}(\mu\text{-OH})_2\text{L}^{10}]^{2+}$ cation*

Crystal data for $\text{C}_{72}\text{H}_{90}\text{B}_2\text{Cu}_2\text{N}_8\text{O}_2$: $M = 1248.22$; Triclinic; Space Group $P\bar{1}$;
 $a = 11.487(1)\text{\AA}$; $b = 12.870(1)$; $c = 12.867(1)\text{\AA}$; $\alpha = 106.807(6)^\circ$;
 $\beta = 101.833(6)^\circ$; $\gamma = 105.859(6)^\circ$; $U = 1666.2(2)\text{\AA}^3$; $Z = 1$; $D_{\text{calc.}} = 1.244\text{gcm}^{-3}$;
 $F(000) = 622$; $\mu(\text{MoK}_\alpha) = 6.89\text{cm}^{-1}$; $R(R_w^2) = 0.0416(0.1096)$.

There is nothing exceptional about the bond lengths of the hydroxide bridged dimer and a comparison of Cu-N bond lengths is made with $[\text{CuL}'(\mu\text{-OH})_2\text{CuL}']^{2+}$ $\text{L}' = \text{Me}_3\text{TACN}$ (**14**) and $[\text{Cu}(\text{L}^{10})_2]^{2+}$ in table 3.6.

	Cu-N _{ax}	Cu-N _{eq} (average)
$[\text{CuL}^{10}(\mu\text{-OH})_2\text{CuL}^{10}]^{2+}$	2.258Å	2.029Å
$[\text{CuL}'(\mu\text{-OH})_2\text{CuL}']^{2+}$	2.238Å	2.071Å
$[\text{Cu}(\text{L}^{10})_2]^{2+}$	2.527Å	2.032Å

Table 3.4. *Comparison of Cu-N Bond lengths*

The Cu-N bond lengths and Cu-Cu distances are very similar for the hydroxide bridged dimers, but the Cu-O-Cu angle is 1° larger in $[\text{CuL}^{10}(\mu\text{-OH})_2\text{CuL}^{10}]^{2+}$ and this can have a significant effect on the magnetic properties of the complex (**15**) and will be discussed in more detail in the next chapter. The length of the axial Cu-N bond in the dimer is somewhat shorter than that in the bis ligand complex. The copper dimer has two hydroxides where the bis ligand complex would have a bulky TACN ring, resulting in a less sterically congested Cu centre. The space filling model of the dimer (figure 3.12) shows that there is no steric interaction between the pendant arm and hydroxides, reinforcing the idea that abnormal elongation of the Cu-N bond in $[\text{Cu}(\text{L}^{10})_2]^{2+}$ is due an interaction between the pendant arm and the C-backbone of the second macrocyclic ring in $[\text{Cu}(\text{L}^{10})_2]^{2+}$.

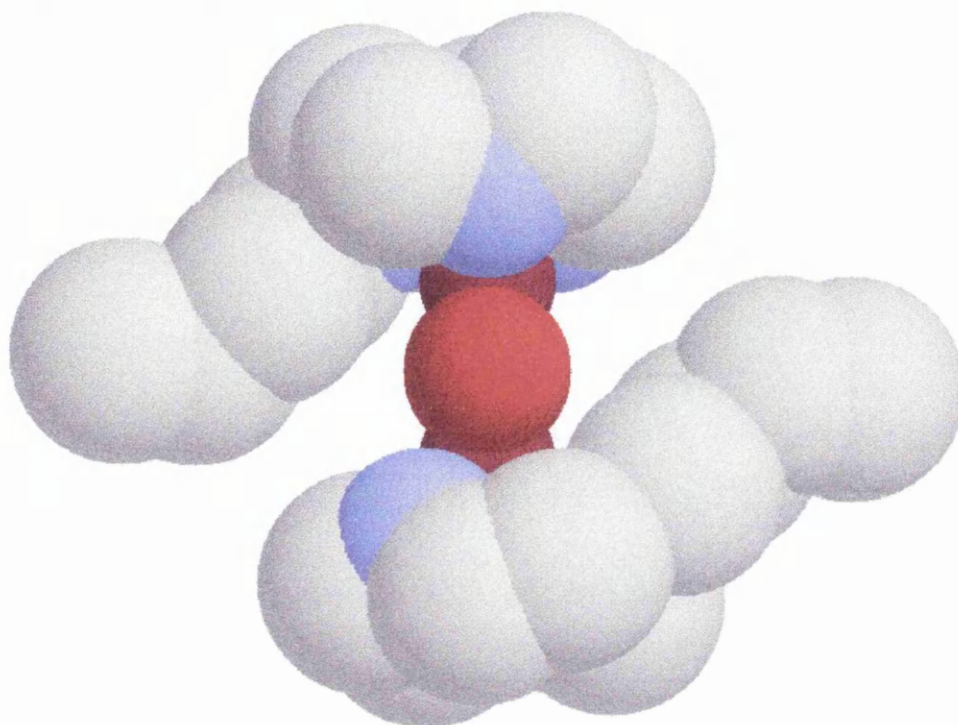


Figure 3.12. *Space filling model of $[Cu(L^{10})(\mu-OH)_2CuL^{10}]^{2+}$, the axial bonds are drawn horizontal*

3.3 SILVER(I) COMPLEX OF L¹¹

The Cu(I) complexes of L¹¹ were extremely air sensitive and difficult to work with, whereas silver(I) complexes with olefin or nitrogen donors are quite stable to aerobic oxidation. It was therefore anticipated that the silver(I) complex of L¹¹ would be easier to prepare and characterise by IR, NMR and X-ray crystallography. The complexes formed with AgBF₄ and L¹¹ decomposed rapidly producing insoluble black precipitates or silver mirrors. Ligand induced disproportionation of Ag(I) is known for tetraazamacrocycles (16), but at the present time it is not known if disproportionation is responsible for the decomposition of the complex. Exclusion of moisture and oxygen from the system did not prevent decomposition, but the rate of decomposition was slower in acetonitrile and acetone. It must be noted however, that at the present time the Cambridge Structural Database contains no silver(I) complex which contains both a coordinated olefin and amine.

¹H and ¹³C NMR spectra were obtained for [AgL¹¹][BF₄] (figures 3.13, 3.14). Poor resolution in the spectra was due to precipitation of decomposition products during data accumulation. Table 3.5 shows selected NMR shifts for L¹⁰ and its Ag(I) complex.

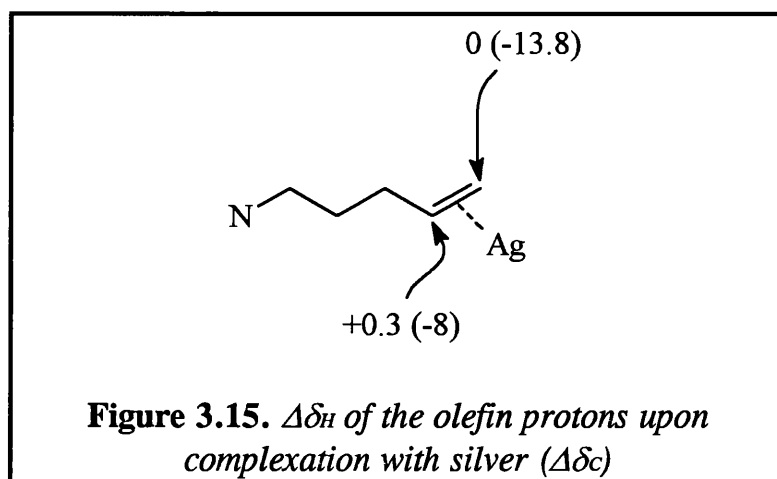
	δ_{H} (δ_{C}) for $-\text{CH}=\text{CH}_2$	δ_{H} (δ_{C}) for $-\text{CH}=\text{CH}_2$
L^{11}	4.9 (114.4)	5.7 (138.4)
$[\text{AgL}^{11}][\text{BF}_4]$	4.9 (100.6)	6.0 (130.4)

Table 3.5. *Selected NMR shifts for L^{11} and $[\text{AgL}^{11}][\text{BF}_4]$*

The resonance of the methine proton in the olefin shifts down field upon complexation, this deshielding effect is commonly observed in silver(I)-olefin complexes (**7**, **10**), whereas the ^{13}C NMR resonances of the coordinated olefin are shifted slightly upfield. This small shift upfield in the ^{13}C NMR is expected in silver(I) complexes where σ -donation is the dominant factor in the silver-olefin bond i.e. little π -backbonding is observed. Like the copper(I) system, unequal $\Delta\delta_{\text{H}}$ and $\Delta\delta_{\text{C}}$ upon complexation (figure 3.15) suggest an unsymmetrical positioning of the silver ion with respect to the olefin. The silver ion is closer to the terminal carbon, resulting in a more effective π -backbond and a more shielded environment.

The NMR data confirms that the olefin is coordinated to the silver ion and the small upfield shifts in the ^{13}C NMR suggest that a small amount of π -backbonding may be present. The ^1H and ^{13}C resonances of the pendant arm are shifted downfield slightly, whereas the resonances of the macrocyclic ring are relatively unshifted and appear to have lost little symmetry,

suggesting that only one of the three nitrogens in the ring is coordinated to the silver ion.



~~8184~~
 HY38PUL2.381
 FU PROCL 2.381
 DEPT16CP
 DATE 92-11-06
 TIME 15:29
 SOLVENT CUC15
 CP 58.323
 Q1 28753.800
 WZ/PT 1.227
 PW 3.3
 ZG 488.633
 NS 483
 Q2 3588.808
 DP 26H CPD
 LB 1.000
 LB 1.000
 PM/CM 1.968
 SR 23535.93

PPH

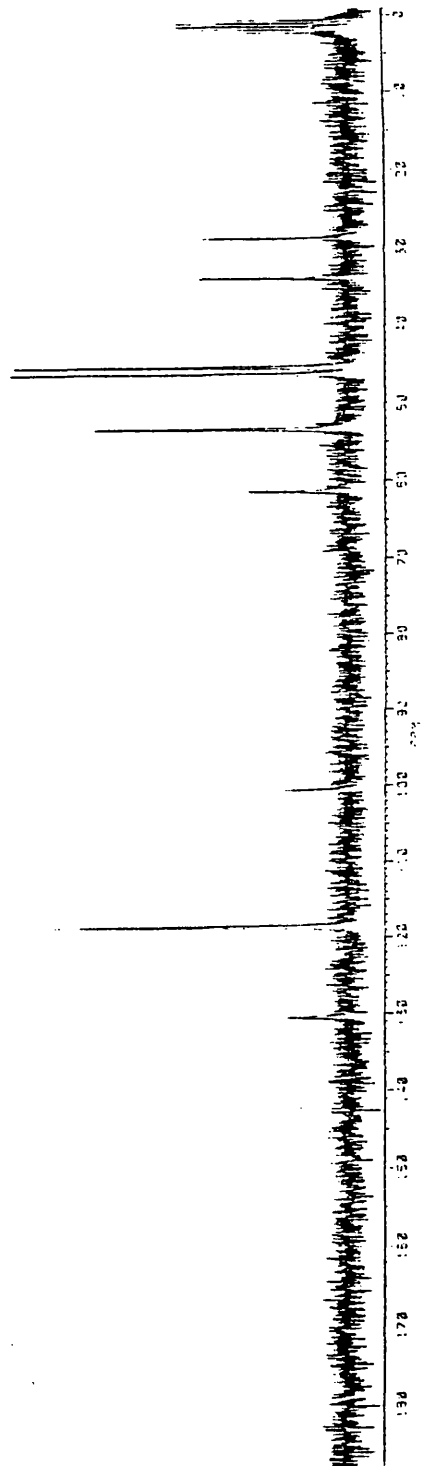


Figure 3.14. ^{13}C NMR spectrum of $[\text{AgL}^{11}][\text{BF}_4]$ in d_3 -acetonitrile

3.4 REFERENCES

1. W.C. Zeise, *Poggendorfs Ann. Phys. Chem.*, 1827, **9**, 632.
2. M.J.S. Dewar, *Bull. Spc. Chim. Fr.*, 1951, **18**, C79.
3. J. Chatt, L.A. Duncanson, *J. Chem. Soc.*, 1953, 2939.
4. J.S Thompson, R.L. Harlow, J.F Whitney, *J. Am. Chem. Soc.*, 1983, **105**, 3522.
5. J.S Thompson, J.F Whitney, *Inorg. Chem.*, 1984, **23**, 2813.
6. P. Chaundhuri, K. Oder, *J. Organomet. Chem.*, 1989, **367**, 249.
7. M. Munkata, S. Kitagawa, S. Kosome, A. Asahara, *Inorg. Chem.*, 1985, **25**, 2622.
8. J.S. Thompson, R.M. Swiatek, *Inorg. Chem.*, 1985, **24**, 110.
9. S.M. Nelson, A. Lavery, M.G.B. Drew, *J. Chem. Soc., Dalton Trans.*, 1986, 911.
10. R.G. Salomon, J. Kochi, *J. Am. Chem. Soc.*, 1973, **95**, 1889.
11. A.G. Orpen, L. Brammer, F.H. Allen, O. Kennard, D.G. Watson, R. Taylor, *J. Chem. Soc., Dalton Trans.*, 1989, S1.
12. P. Chaudhuri, K. Oder, K. Wiegardt, J. Weiss, J. Reedijk, W. Hinrichs, J. Wood, A. Ozarowski, H. Stratemaier, D. Reinen, *Inorg. Chem.*, 1986, **25**, 2951.
13. D. Ellis, L.J. Farrugia, R.D. Peacock, *Personal communication*.

- 14.P. Chaudhuri, D. Ventur, K. Wieghardt, E Peters, K. Peters, A. Simon,
Angew. Chem. Int. Ed. Engl., 1985, **24**,57.
- 15.D.J. Hodgson, *Prog. Inorg. Chem.*, 1975, **19**, 173.
- 16.M.O. Kestner, A.L. Allred, *J. Am. Chem. Soc.*, 1972, **94**, 7189.

CHAPTER 4

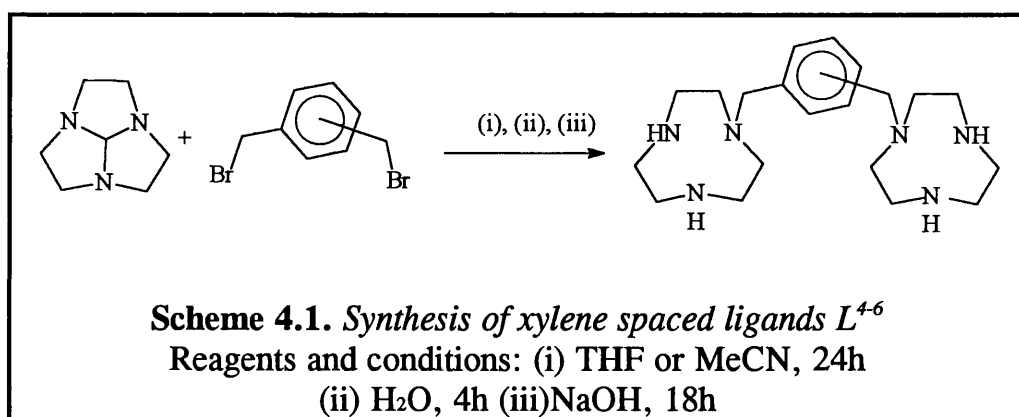
HYDROXIDE BRIDGED COPPER COMPLEXES

4.1 INTRODUCTION

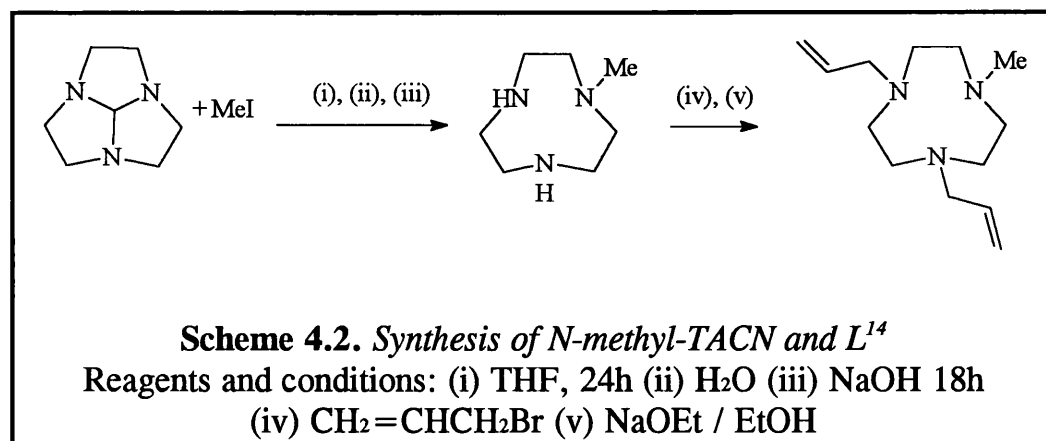
A variety of ligand systems have been devised which give mononuclear to polynuclear copper complexes, the copper ion usually adopting an irregular geometry due to Jahn-Teller distortions. Many of these complexes have been synthesised to model the polynuclear copper containing proteins found in nature, in particular the dinuclear copper proteins such as tyrosinase and haemocyanin responsible for oxygen activation and transportation (1). Reversible binding of molecular oxygen by model compounds only occurs at low temperature; at higher temperatures the bound peroxo species decompose to form hydroxide bridged copper dimers or less commonly activate a C-H bond in the ligand or bound substrate (1-4). Hydroxide bridged copper dimer systems show interesting magnetic behaviour and have been the focus of extensive magnetic studies (5,6). The more recent use of ^1H NMR in the characterisation of ferro- and antiferromagnetically coupled copper(II) dimers has shown that sharp resonances can be obtained for systems with unpaired electrons (7).

4.2 LIGAND PREPARATION

The ligands L^4 , L^5 and L^6 contain two TACN rings separated by varying lengths and were prepared by reaction of α,α' -dibromo-*o*, *m* or *p*-xylene with 1,4,7-triazatricyclo[5.2.1.0^{4,10}]decane in THF or acetonitrile (scheme 4.1). All the ligands were obtained as viscous oils and stored at -18°C since L^5 formed an insoluble solid if left at room temperature for any prolonged period of time.



The tris-allyl pendant arm ligand L^{12} was prepared quantitatively by reaction of allyl bromide with TACN in an ethanol/ethoxide solution. The single olefin pendant arm macrocycle L^{10} was prepared using scheme 4.1 above, whereas the bis-allyl pendant arm ligand L^{14} was prepared from *N*-methyl-TACN (L^2) using the same method as L^{12} (scheme 4.2).



Further attempts at synthesising L¹⁴ using scheme 4.2 were unsuccessful, even when the base was changed from ethoxide to KOH or NaHCO₃. Dichloromethane solutions of *N*-methyl-TACN precipitate microcrystalline material after just 30 minutes from solvation of the parent macrocycle, the ¹H NMR spectrum of the crystalline material showed the *N*-methyl group to shift downfield by +0.18ppm. The hydrochloride salt of *N*-methyl-TACN displays a similar spectrum to the precipitate although the shift downfield is +0.35ppm compared to L². This suggests that *N*-methyl-TACN is sufficiently basic to deprotonate dichloromethane producing a mono-protonated macrocycle. Therefore in scheme 4.2 above the *N*-methyl nitrogen is more basic than the secondary amine functions, so the addition of allyl bromide will result in irreversible quaternary ammonium ion formation at the methylated nitrogen.

The replacement of the electron donating *N*-methyl group with an electron withdrawing group should produce a tertiary nitrogen which is less

basic than the free secondary amine functions, thus allowing easy alkylation of the free amines. This was achieved in L^3 which contains an electron withdrawing bridging alkene group and was alkylated at the secondary nitrogens using allyl bromide and ethoxide solution to form L^{15} .

4.3 PREPARATION OF THE COMPLEXES

It was mentioned in the previous chapter that methanol suspensions of $[CuL^{10}][BPh_4]$ were susceptible to aerial oxidation, forming predominantly hydroxide bridged copper(II) dimers. The initial formation of Cu^+/BPh_4^- complexes in methanol was therefore used as a starting point to all the hydroxide bridged dimers. The rate at which the complexes oxidised was different depending on which ligand was coordinated to the Cu(I), the best example of this was observed for the xylene bridged ligands L^{4-5} . The Cu(I) complex of the *ortho*-xylene ligand (L^4) oxidised over a period of 15-30 minutes, whereas the complex of the *meta*-xylene ligand (L^5) required 1-2 hours for complete oxidation. The closer the copper(I) centres are to each other the faster the rate of oxidation, thus for the Cu(I) complex of the *para*-xylene ligand (L^6) an oxidation time of more than two hours would be expected. The Cu(I) complex was actually air-stable as a methanol suspension for several days, after 4 days only a slight green coloration could

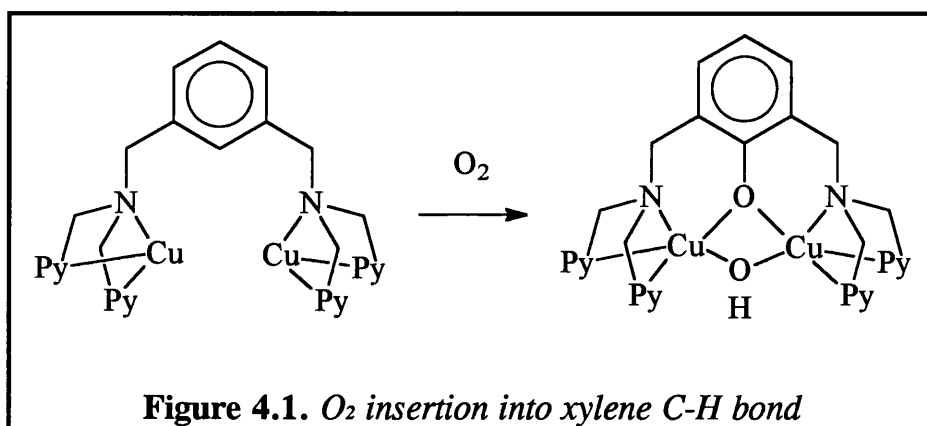
be observed and only after 10 days was complete oxidation achieved. The mononuclear Cu(I) complexes of L¹² and L¹⁴ oxidised over a period of 1-2 hours, much faster than the similar dinuclear Cu(I) complex of L¹⁵ which was expected to oxidise rapidly, but required 2 days for complete oxidation.

Recrystallisation from acetonitrile produced crystals suitable for X-ray structure analysis for the complexes of L⁵, L¹⁰ and L¹⁴. Crystals were obtained for the copper(II) complexes of L⁴ and L¹⁵, but loss of solvent prevented these crystals from being mounted on the diffractometer, only the copper(II) complex of the para-xylene ligand L⁶ failed to crystallise. The structure of each dimer will be discussed individually before a general comparison is made.

4.4 CRYSTAL STRUCTURE OF [Cu₂L⁵(μ-OH)₂]²⁺

Dinucleating aza-ligands using *meta*-xylene spacer units are numerous in the literature, the nitrogen donor groups of the ligand usually originating from pyridine or benzimidazole groups (1, 8). These ligands have been used to model the active sites in haemocyanin and tyrosinase, all the ligands bind oxygen but only the ligand reported by Karlin *et al.* (figure 4.1) is able to effect hydroxylation of the aromatic xylene ring of the ligand by reaction

with dioxygen. Replacement of a single pyridyl group with an amine of similar basicity, completely depresses the monooxygenase reactivity on the ligand and only the hydroxide bridged copper dimers are obtained from reaction with dioxygen.



The copper(I) complex of L^5 reacts with dioxygen to produce a hydroxyl bridged dimer (figure 4.2), no hydroxylation of the xylene was observed. The complex consists of two copper centres in a square pyramidal environment and are not related by symmetry, although the bond lengths and angles are very similar in both halves of the dimer (table 4.1). The axial copper-nitrogen bond is $\sim 0.3\text{\AA}$ longer than the equatorial bonds with the bridging $\text{Cu}(\text{OH})_2\text{Cu}$ unit bent out of the plane by 6.5° in the direction of the *meta*-xylene ring (figure 4.3). The hydroxide bridges impose a copper-copper distance of $\sim 3\text{\AA}$. This separation is shorter than the ideal spacing for the xylene spacer, resulting in geometric strain when the ligand coordinates to the copper centres. Elongation of the axial Cu-N bond and the tilting of the xylene ring (figure 4.3) helps to relieve the strain in the xylene spacer.

To achieve a more ideal spacing, the xylene ring pushes the axial nitrogens apart resulting in the apex of the square based pyramid being non-perpendicular to the base. To maintain square pyramidal geometry, the base of the pyramid orientates itself as close to perpendicular to the axial Cu-N bond as possible, resulting in the hydroxides being pushed towards the xylene ring, giving a bent bridge.

Cu1-N11	2.351(3)Å	Cu2-N21	2.366(2)Å
Cu1-N14	2.024(3)Å	Cu2-N24	2.018(3)Å
Cu1-N17	2.022(3)Å	Cu2-N27	2.039(3)Å
Cu1-O1	1.931(2)Å	Cu2-O1	1.928(3)Å
Cu1-O2	1.928(2)Å	Cu2-O2	1.931(2)Å
Cu1-Cu2	2.9464(5)Å		
Cu1-O1-Cu2	99.56(12)°	O1-Cu1-O2	79.00(10)°
Cu1-O2-Cu2	99.55(12)°	O1-Cu2-O2	79.01(10)°
N11-Cu1-N14	81.82(11)°	N21-Cu2-N24	81.52(10)°
N11-Cu1-N17	81.69(11)°	N21-Cu2-N27	79.64(10)°
N14-Cu1-N17	84.32(11)°	N14-Cu2-N17	84.76(13)°
N11-Cu1-O1	110.73(10)°	N21-Cu2-O1	115.30(10)°
N14-Cu1-O1	97.33(11)°	N24-Cu2-O1	163.15(11)°
N17-Cu1-O1	167.58(11)°	N27-Cu2-O1	96.95(12)°
N11-Cu1-O2	111.78(11)°	N21-Cu2-O2	114.96(10)°
N14-Cu1-O2	166.38(12)°	N24-Cu2-O2	95.08(11)°
N17-Cu1-O2	96.52(11)°	N27-Cu2-O2	165.26(12)°

Table 4.1. *Selected bond lengths and angles for $[\text{Cu}_2\text{L}^5(\mu\text{-OH})_2]^{2+}$*

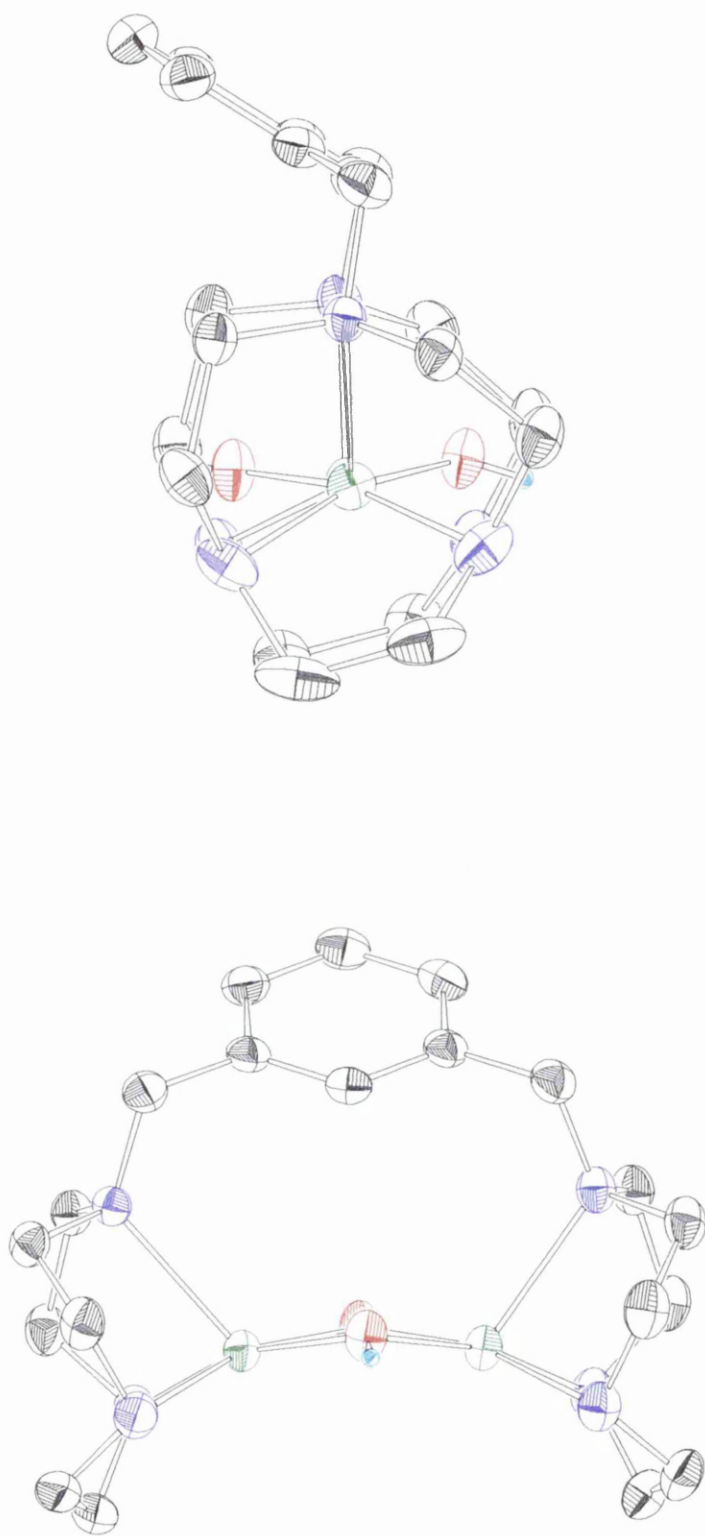


Figure 4.3. Views showing the bent $\{\text{Cu}(\mu\text{-OH})_2\}^{2+}$ core of $[\text{CuL}^5(\mu\text{-OH})_2]^{2+}$

Ligands similar to L^5 are not limited to modelling oxygen transport and activation. Phosphoesterases usually contain two or three metal centres which act as catalysts in the hydrolytic cleavage of phosphate esters, therefore complexes with ligands such as L^5 are well suited to act as model systems. Chin *et al.* (9) reported a dinuclear copper complex (figure 4.4a) which catalysed the hydrolysis of several AMPs to adenosine (figure 4.4b), the rate of hydrolysis being several hundred times faster than the mononuclear $[Cu(TACN)]^{2+}$ complex. It was proposed that the monohydroxy form of the dinuclear complex was the active species for hydrolysing the phosphate ester in the AMPs. Molecular modelling using the MM+ forcefield of hyperchem showed that the bis(μ -OH) form of Chin's ligand adopted a similar geometry to the structure of $[Cu_2L^5(\mu-OH)_2]^{2+}$. It is therefore presumed that the hydrated dinuclear copper(II) complex of L^5 would have approximately the same geometry as Chin's complex and act as a catalyst in the hydrolysis of AMPs.

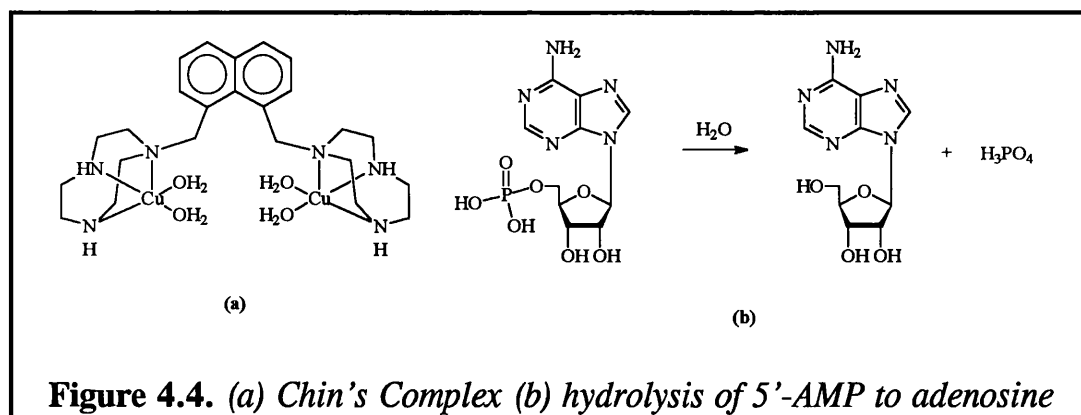


Figure 4.4. (a) Chin's Complex (b) hydrolysis of 5'-AMP to adenosine

A subsequent paper by Chin reported the crystal structure of $[\text{Co}_2(\text{TACN})_2(\mu\text{-OH})_2\{\text{O}_2\text{P}(\text{OCH}_3)_2\}]^{3+}$, a complex with a $\text{Co}_2(\text{OH})_2\text{Co}$ core containing a bound phosphate diester. The cobalt atoms were in a very similar geometry to the copper atoms of $[\text{Cu}_2\text{L}^5(\mu\text{-OH})_2]^{2+}$, the Co··Co separation was 2.9 Å compared to the 2.95 Å spacing of the coppers in $[\text{Cu}_2\text{L}^5(\mu\text{-OH})_2]^{2+}$.

4.5 CRYSTAL STRUCTURE OF $[\text{CuL}^{12}(\mu\text{-OH})_2\text{CuL}^{12}]^{2+}$

The structure of the cation (figure 4.5) is similar to the copper dimer in the previous chapter and to Wieghardt's copper dimer $[\text{CuL}'(\text{OH})_2\text{CuL}']^{2+}$ where L' is Me_3TACN (**10**). The copper atoms are related by a centre of symmetry and are in a square pyramidal environment with the apical Cu-N bond ~ 0.2 Å longer than the equatorial Cu-N bonds (table 4.2). The hydroxide bridges form a plane with the two copper atoms and the secondary amine functions deviate slightly from the plane of the $\text{Cu}_2(\text{OH})_2$ core.

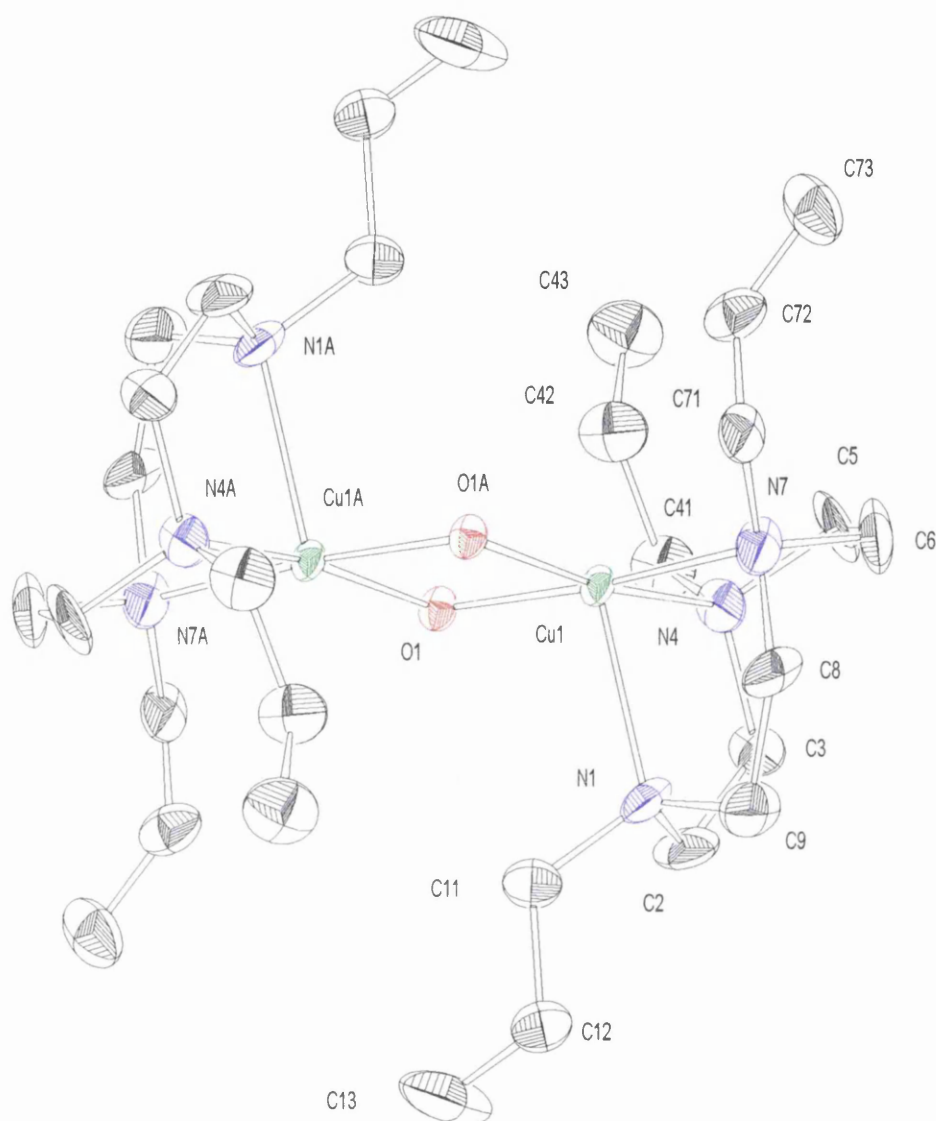


Figure 4.5. *Crystal Structure of $[\text{CuL}^{12}(\mu\text{-OH})_2\text{CuL}^{12}]^{2+}$*

Crystal data for $\text{C}_{80}\text{H}_{104}\text{B}_2\text{Cu}_2\text{N}_6\text{O}_4$: $M = 1362.29$; Triclinic; Space Group $P\bar{1}$;
 $a = 12.907(2)\text{\AA}$; $b = 13.795(2)\text{\AA}$; $c = 13.949(1)\text{\AA}$; $\alpha = 96.313(8)^\circ$;
 $\beta = 114.567(7)^\circ$; $\gamma = 115.060(9)^\circ$; $U = 1918.9(4)\text{\AA}^3$; $Z = 1$; $D_{\text{calc.}} = 1.179\text{gcm}^{-3}$;
 $F(000) = 726$; $\mu(\text{MoK}\alpha) = 6.05\text{cm}^{-1}$; $R(R_w^2) = 0.1127(0.3045)$.

Cu1-N1	2.298(10)Å	Cu1-Cu1A	2.988(2)Å
Cu1-N4	2.084(11)Å	Cu1-O1	1.912(6)Å
Cu1-N7	2.073(11)Å	Cu1-O1A	1.937(6)Å
N1-Cu1-Cu1A	105.8(3)°	Cu1-O1-Cu1A	101.9(3)°
N4-Cu1-Cu1A	134.8(4)°	O1-Cu1-O1A	78.1(3)°
N7-Cu1-Cu1A	134.9(3)°	N1-Cu1-N4	87.1(4)°
N1-Cu1-O1	100.6(3)°	N1-Cu1-N7	83.0(4)°
N4-Cu1-O1	96.2(4)°	N4-Cu1-N7	89.0(5)°
N7-Cu1-O1	173.8(3)°		

Table 4.2. *Selected bond lengths and angles for $[\text{CuL}^{12}(\mu\text{-OH})_2\text{CuL}^{12}]^{2+}$*

4.6 CRYSTAL STRUCTURE OF $[\text{CuL}^{14}(\mu\text{-OH})_2\text{CuL}^{14}]^{2+}$

With two different pedant arms in L^{14} there are two possibilities for a square pyramidal copper geometry. The axial Cu-N bond could be to the *N*-methyl or *N*-allyl nitrogen of the macrocycle, the methylated nitrogen is more basic than the other two *N*-allyl nitrogens, therefore the long Cu-N bond would be expected to involve the less basic *N*-allyl nitrogen. The crystal structure (figure 4.6) confirmed this prediction with one of the *N*-allyl groups in the axial position and the *N*-methyl group in the equatorial position. The copper centres are related by a centre of symmetry and are in a square pyramidal environment with the axial Cu-N bond $\sim 0.2\text{\AA}$ longer than

the equatorial Cu-N bonds (table 4.3). The shortest equatorial Cu-N bond belongs to the other *N*-allyl group and not the methylated nitrogen, which is surprising since the *N*-methyl nitrogen was expected to be the most basic of the two. The hydroxides form a plane with the two coppers and the deviation of the equatorial nitrogens from the $\{\text{Cu}_2(\text{OH})_2\}^{2+}$ plane is more pronounced when compared to $[\text{CuL}^{12}(\mu\text{-OH})_2\text{CuL}^{12}]^{2+}$.

Cu1-N11	2.040(4)Å	Cu1-Cu1A	3.016(1)Å
Cu1-N14	2.267(5)Å	Cu1-O1	1.942(4)Å
Cu1-N17	2.068(5)Å	Cu1-O1A	1.914(3)Å
N11-Cu1-Cu1A	135.58(17)°	Cu1-O1-Cu1A	102.93(18)°
N14-Cu1-Cu1A	111.25(17)°	O1-Cu1-O1A	77.07(16)°
N17-Cu1-Cu1A	99.15(18)°	N11-Cu1-N14	84.66(18)°
N11-Cu1-O1	97.47(17)°	N11-Cu1-N17	85.18(19)°
N14-Cu1-O1	112.49(18)°	N14-Cu1-N17	83.32(19)°
N17-Cu1-O1	164.11(18)°		

Table 4.3. Selected bond lengths and angles for $[\text{CuL}^{14}(\mu\text{-OH})_2\text{CuL}^{14}]^{2+}$

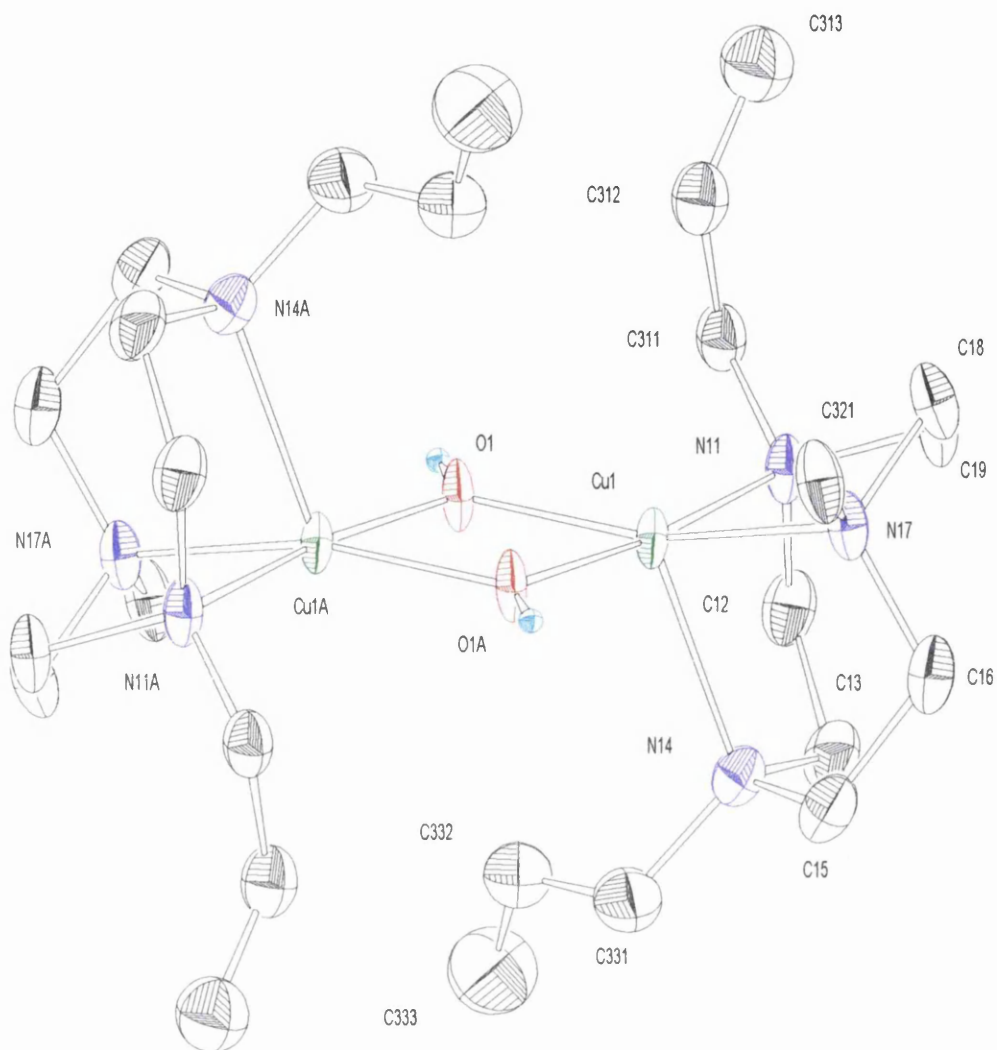


Figure 4.6. Crystal Structure of $[\text{CuL}^{14}(\mu\text{-OH})_2\text{CuL}^{14}]^{2+}$

Crystal data for $\text{C}_{74}\text{H}_{92}\text{B}_2\text{Cu}_2\text{N}_6\text{O}_2$: $M=1246.3$; Triclinic; Space Group $P\bar{1}$; $a=10.9991(32)\text{\AA}$; $b=12.5093(18)\text{\AA}$; $c=14.1828(35)\text{\AA}$; $\alpha=64.786(15)^\circ$; $\beta=75.111(21)^\circ$; $\gamma=71.091(12)^\circ$; $U=1654.0(7)\text{\AA}^3$; $Z=1$; $D_{\text{calc.}}=1.251\text{gcm}^{-3}$; $F(000)=662$; $\mu(\text{MoK}\alpha)=6.9\text{cm}^{-1}$; $R(R_w^2)=0.0854(0.2149)$.

4.7 COMPARISON OF COPPER DIMER STRUCTURES

A summary of bond lengths and angles for the copper dimers is presented in table 4.4. As more electron withdrawing alkene pendant arms are attached to the macrocycle the less basic the nitrogens become, therefore L' (Me₃TACN) with three electron donating methyl groups is the most basic and L¹² with three electron withdrawing allyl groups is the least basic. If [Cu₂L⁵(OH)₂]²⁺ is excluded, then the Cu-N bond lengths appear to follow the trend that the shorter the bond the more basic the macrocycle, although the actual differences in the bond lengths are only ~0.06Å at the most. The fact that [Cu₂L⁵(OH)₂]²⁺ has a significantly longer axial bond than the other complexes is due to the steric constraints of the ligand.

	Cu-N _{ax}	Cu-N _{eq}	Cu-O-Cu	Cu··Cu
[Cu ₂ L ⁵ (OH) ₂] ²⁺	2.358Å	2.026Å	99.6°	2.946Å
[CuL ¹⁰ (OH) ₂ CuL ¹⁰] ²⁺	2.258Å	2.028Å	101.0°	2.978Å
[CuL ¹² (OH) ₂ CuL ¹²] ²⁺	2.298Å	2.078Å	101.9°	2.988Å
[CuL ¹⁴ (OH) ₂ CuL ¹⁴] ²⁺	2.267Å	2.054Å	102.9°	3.016Å
[CuL'(OH) ₂ CuL'] ²⁺	2.238Å	2.071Å	100.1°	2.971Å

Table 4.4. *Selected bond lengths and angles for some copper dimers*

The hydroxides formed planar bridges with the two copper atoms in all of the dimers with the exception of L⁵, where the hydroxides deviated towards the xylene ring by 6°. Molecular modelling of [Cu₂L⁵(OH)₂]²⁺ using the MM+ forcefield of hyperchem predicted a deviation from planarity of 1° (figure 4.7). Hydroxide bridged copper dimers of L⁴, L⁶ and L¹⁵ were also modelled using hyperchem and are shown in figures 4.8, 4.9 and 4.10 respectively. The molecular models show that L⁴ with its *ortho*-xylene spacer unit is the least distorted from square pyramidal geometry and is best suited for the spatial requirements of a hydroxide bridged copper dimer, whereas L⁵ with its *meta*-xylene spacer is slightly distorted from the square pyramidal geometry. The *para*-xylene ligand is very distorted when coordinated to the dimeric copper centres with the aromatic ring adopting a highly unfavourable non-planar conformation, this suggests that the space between the copper atoms is too large to accommodate a hydroxide bridge and this is supported by the fact that the copper(I) complex of L⁶ was extremely slow to oxidise to the copper(II) system. The actual nature of the copper(II) complex of L⁶ has not yet been established and it's unknown if the copper(II) complex actually contains a hydroxide bridge.

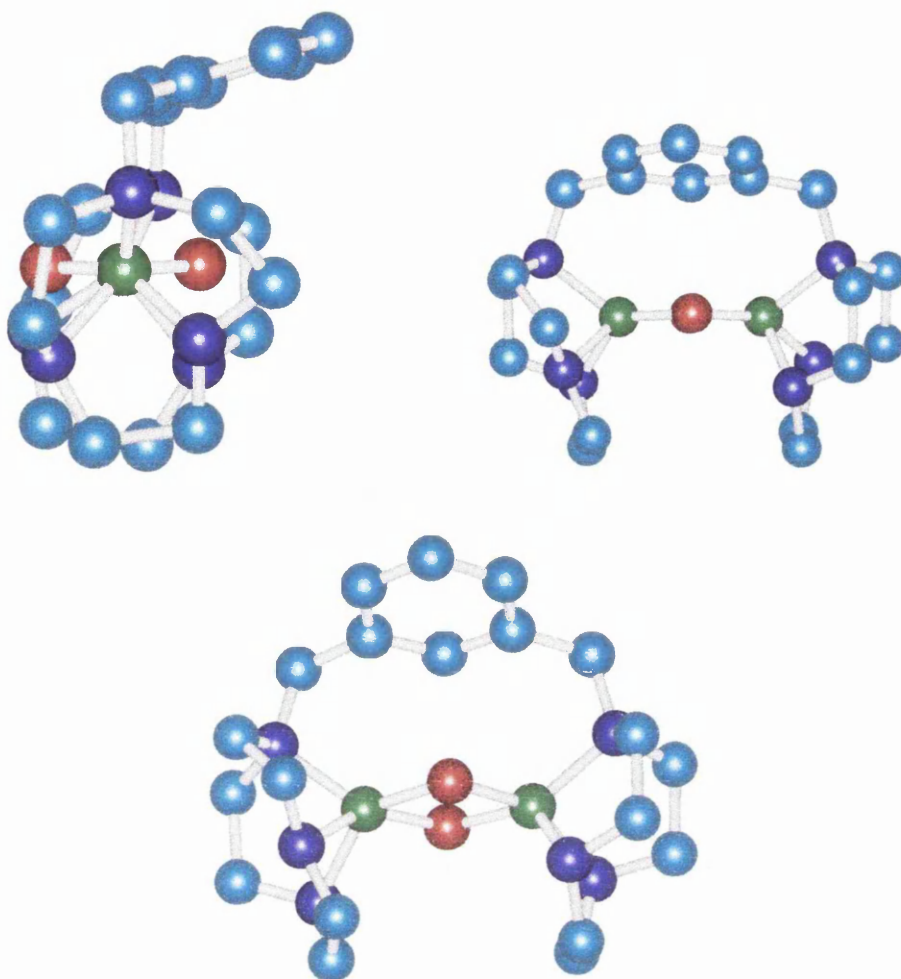


Figure 4.7. Hyperchem model of $[\text{Cu}_2\text{L}^5(\mu\text{-OH})_2]^{2+}$

	Hyperchem model	Crystal structure
Cu-N _{ax}	1.88Å	2.358Å
Cu-N _{eq}	1.88Å	2.026Å
Cu-O	1.83Å	1.929Å
Cu-Cu	2.88Å	2.946Å
Cu-O-Cu	103°	99.6°

Table 4.5. Selected bond lengths & angles for $[\text{Cu}_2\text{L}^5(\mu\text{-OH})_2]^{2+}$

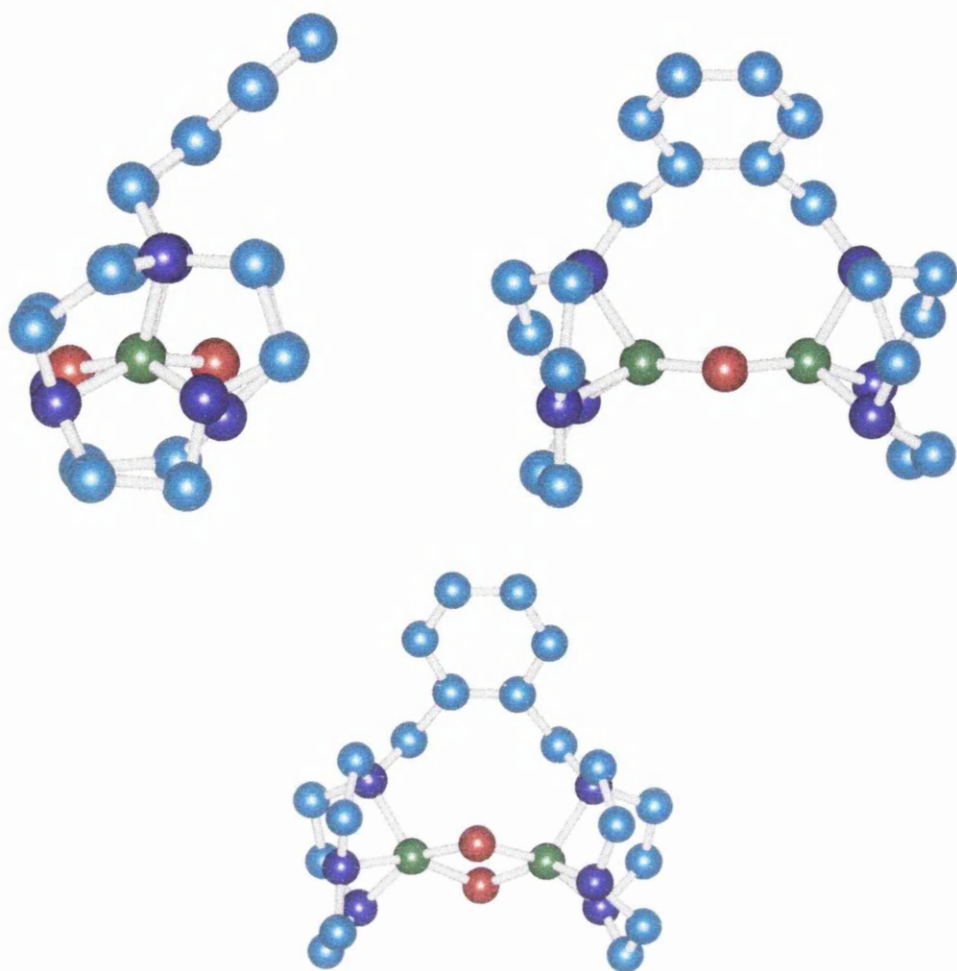


Figure 4.8. *Hyperchem model of $[\text{Cu}_2\text{L}^4(\mu\text{-OH})_2]^{2+}$*

Cu-N _{ax}	1.88Å
Cu-N _{eq}	1.88Å
Cu-O	1.83Å
Cu-Cu	2.85Å
Cu-O-Cu	102°

Table 4.6. *Selected bond lengths & angles for the model of $[\text{Cu}_2\text{L}^4(\mu\text{-OH})_2]^{2+}$*

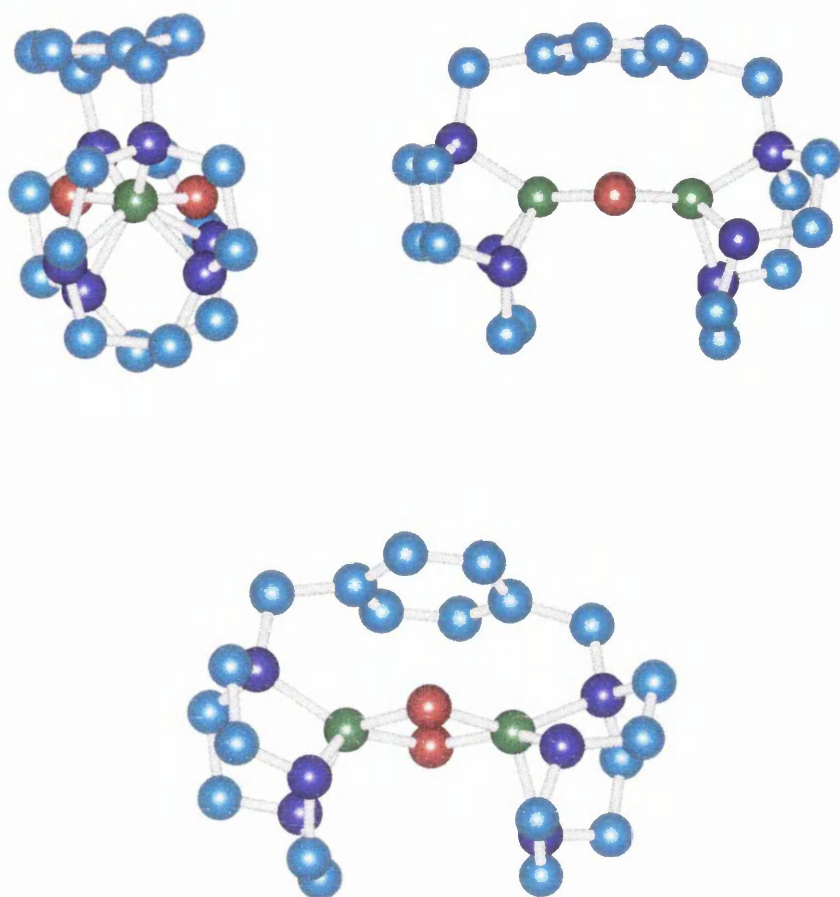


Figure 4.9. *Hyperchem model of $[\text{Cu}_2\text{L}^6(\mu\text{-OH})_2]^{2+}$*

Cu-N _{ax}	1.90 Å
Cu-N _{eq}	1.89 Å
Cu-O	1.83 Å
Cu-Cu	2.93 Å
Cu-O-Cu	105°

Table 4.7. *Selected bond lengths & angles for the model of $[\text{Cu}_2\text{L}^6(\mu\text{-OH})_2]^{2+}$*

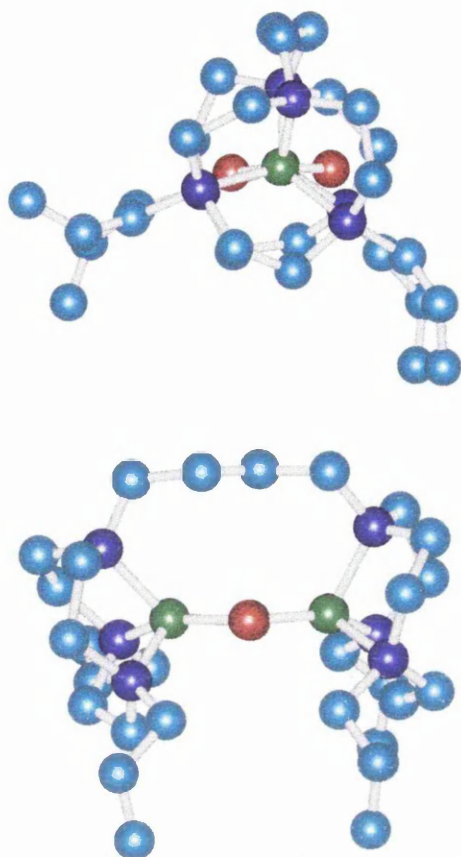


Figure 4.10. *Hyperchem model of $[\text{Cu}_2\text{L}^{15}(\mu\text{-OH})_2]^{2+}$*

Cu-N _{ax}	1.91 Å
Cu-N _{eq}	1.95 Å
Cu-O	1.87 Å
Cu-Cu	3.09 Å
Cu-O-Cu	112°

Table 4.8. *Selected bond lengths & angles for the model of $[\text{Cu}_2\text{L}^{15}(\mu\text{-OH})_2]^{2+}$*

4.8 MAGNETIC SUSCEPTIBILITY MEASUREMENTS

The temperature dependant magnetic susceptibilities of $[\text{Cu}_2\text{L}^5(\mu\text{-OH})_2]^{2+}$ and $[\text{CuL}^{12}(\mu\text{-OH})_2\text{CuL}^{12}]^{2+}$ are displayed in figures 4.11 and 4.12 respectively. The data were fitted to Bleaney-Bowers (11) expressions ($H = -2JS_1 \cdot S_2$; $S_1 = S_2 = 1/2$) giving $-2J = 318\text{cm}^{-1}$ for $[\text{Cu}_2\text{L}^5(\mu\text{-OH})_2]^{2+}$ and $-2J = 154\text{cm}^{-1}$ for $[\text{CuL}^{12}(\mu\text{-OH})_2\text{CuL}^{12}]^{2+}$, the sign of the coupling constant implying that both complexes are antiferromagnetically coupled. This was expected since the correlation between Cu-O-Cu and $2J$ discovered by Ha tfield *et al.* (12) showed that antiferromagnetic behaviour occurs when the Cu-O-Cu $> 97.6^\circ$ in $\text{Cu}(\text{OH})_2\text{Cu}$ systems. $[\text{CuL}^{12}(\text{OH})_2\text{CuL}^{12}]^{2+}$ with a Cu-O-Cu angle of 101.9° was expected to have a stronger antiferromagnetic interaction than the copper dimer of Me_3TACN ($-2J = 90\text{cm}^{-1}$) which has a Cu-O-Cu angle of 100.1° (10), since the larger the Cu-O-Cu angle the larger the interaction. The size of the exchange constant for $[\text{Cu}_2\text{L}^5(\text{OH})_2]^{2+}$ is unusual in that the complex has the smallest Cu-O-Cu angle (99.6°) of the three dimers but the largest antiferromagnetic interaction. The bent bridge can not be responsible for this behaviour since $[\text{Cu}_2(\text{bipy})_2(\text{OH})_2]^{2+}$ crystallises with a planar bridge as the NO_3^- salt and a bent bridge as the SO_4^{2-} salt, both salts having different magnetic susceptibilities and both fitting the correlation between $-2J$ and the Cu-O-Cu angle (6). The structure and magnetic susceptibilities of the other copper

dimers in the series are required before any definite conclusions can be made on the size of the Cu-O-Cu bond angle and the magnitude of the exchange constant for this type of $\text{Cu}(\text{OH})_2\text{Cu}$ system.

4.9 ^1H NMR SPECTRA OF $[\text{CuL}^{12}(\mu\text{-OH})_2\text{CuL}^{12}]^{2+}$

The use of ^1H NMR in the characterisation of copper(I) complexes is common practice, but more recently the technique has been applied to ferro- and antiferromagnetically coupled copper(II) systems (7) resulting in spectra which contain sharp resonances. It was therefore anticipated that the proton NMR spectrum of the antiferromagnetically coupled dimer $[\text{CuL}^{12}(\text{OH})_2\text{CuL}^{12}]^{2+}$ would contain sharp resonances. Characterisation would be simplified by the fact that the ligand contained C_{3v} symmetry and the structure of the complex was known. The -5 to 60ppm region of the ^1H NMR spectrum is shown in figure 4.13 with no other resonances being observed outside this region. The phenyl protons of the counter ions are observed at 6.7-7.5ppm and are unshifted relative to NaBPh_4 . The olefin protons which are furthest from the magnetic centres have been assigned to the peaks at 6.5 and 8.3ppm and are shifted slightly compared to the free ligand. The broad resonances at 25, 37 and 45ppm have been assigned to the $-\text{CH}_2-$ protons of the macrocyclic ring and pendant arms. The hydroxyl

protons are usually found between -20 and -30ppm for similar systems, but no signals were observed in that region. These results show that ^1H NMR spectra can be obtained for this system, although full assignment of the peaks will require a 2D ^1H COSY experiment and the use of a proton free counterion would make the assignment of peaks a lot simpler. Spectra for the other dimers have not been obtained due to insufficient amounts of crystalline material.

4.10 LOW TEMPERATURE OXYGEN STUDIES

All the hydroxide dimers were formed by oxidation of their corresponding copper(I) complexes at room temperature. At low temperature copper(I) complexes generally behave differently with reversible binding of molecular oxygen to form peroxo copper(II) complexes being quite common for triaza-ligands. The peroxo species are recognisable by their intense purple colour which is due to $\text{O}_2^{2-} \rightarrow \text{Cu}^{2+}$ charge transfer. Warming these peroxo species usually affords the bis(hydroxo) copper dimers, but sometimes monooxygenase activity is observed. Tolman *et al.* isolated the $\mu\text{-}\eta^2\text{:}\eta^2$ peroxo complex of $^i\text{Pr}_3\text{TACN}$ (figure 4.14a) which affords the corresponding bis(hydroxo) species on warming (13).

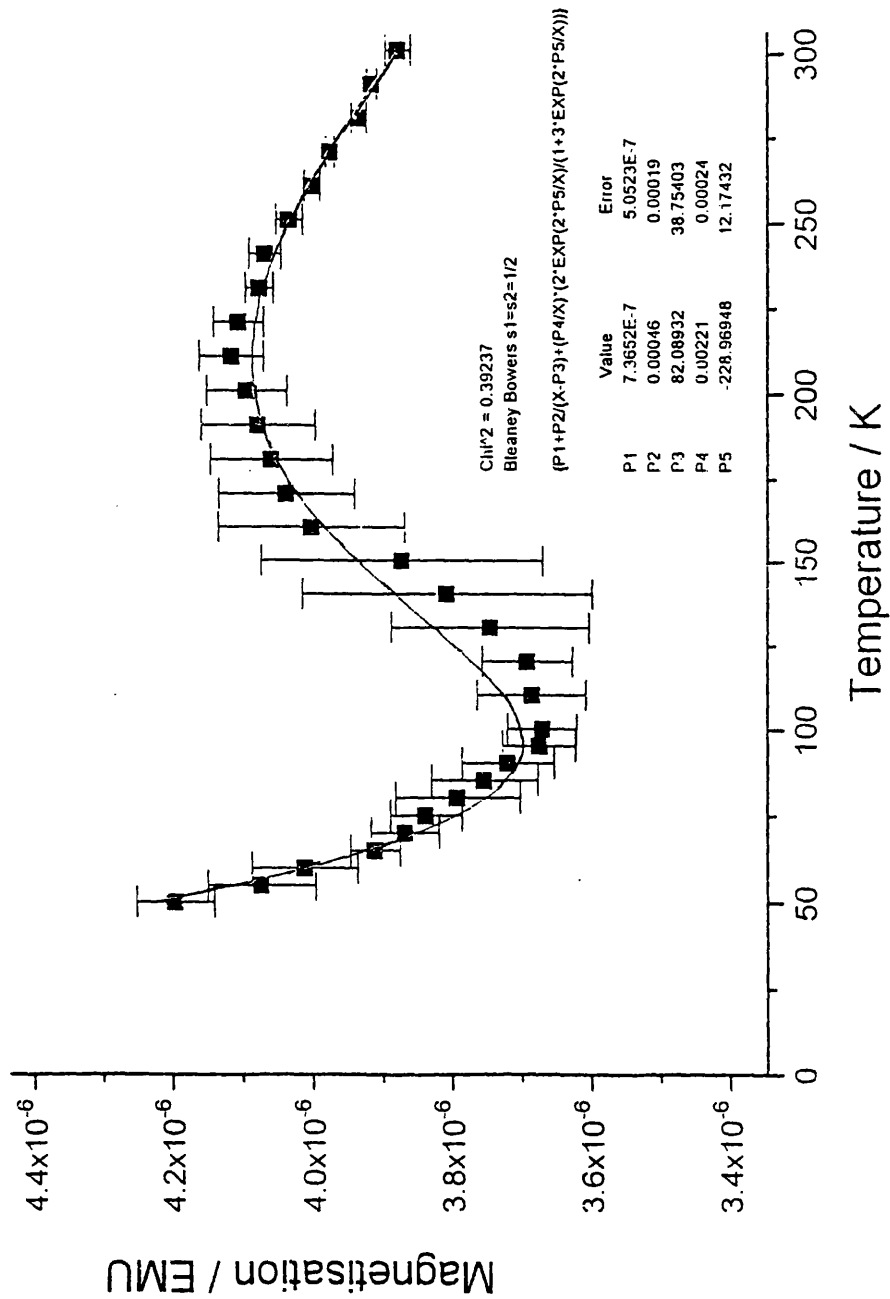


Figure 4.11. Variable temperature measurement of magnetic susceptibility for $[\text{Cu}_2\text{L}^5(\mu\text{-OH})_2][\text{BPh}_4]_2$

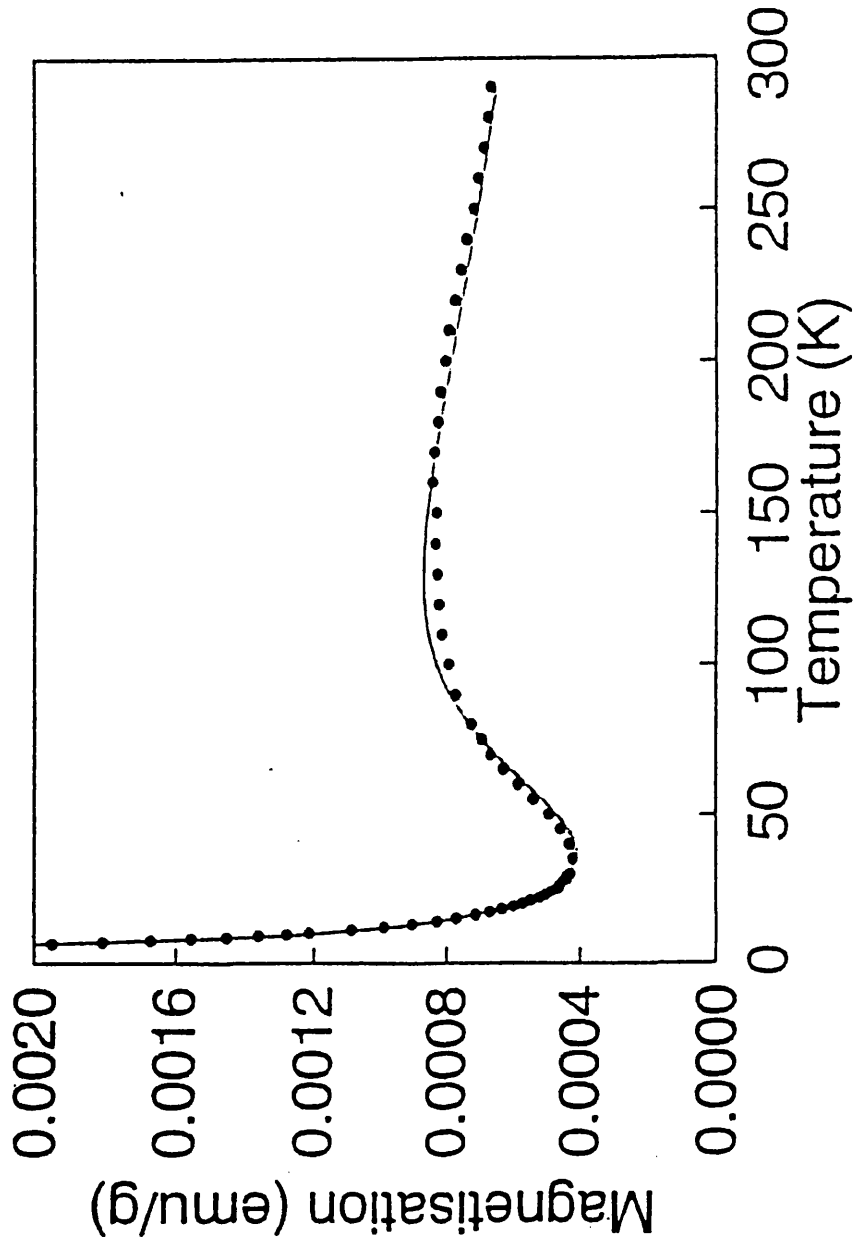


Figure 4.12. Variable temperature measurement of magnetic susceptibility for $[\text{CuL}^{12}(\mu\text{-OH})_2\text{CuL}^{12}][\text{BPh}_4]_2$

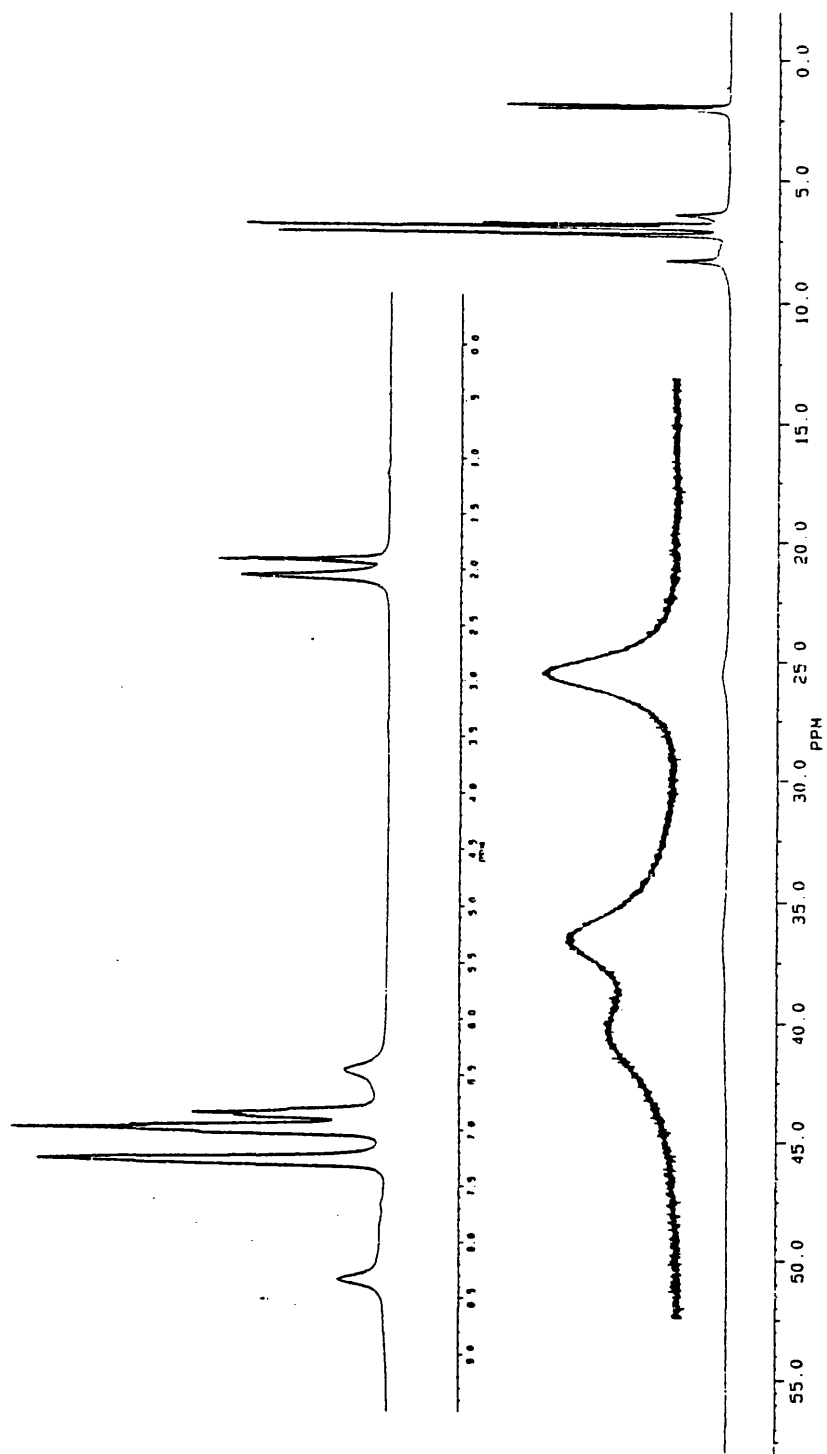
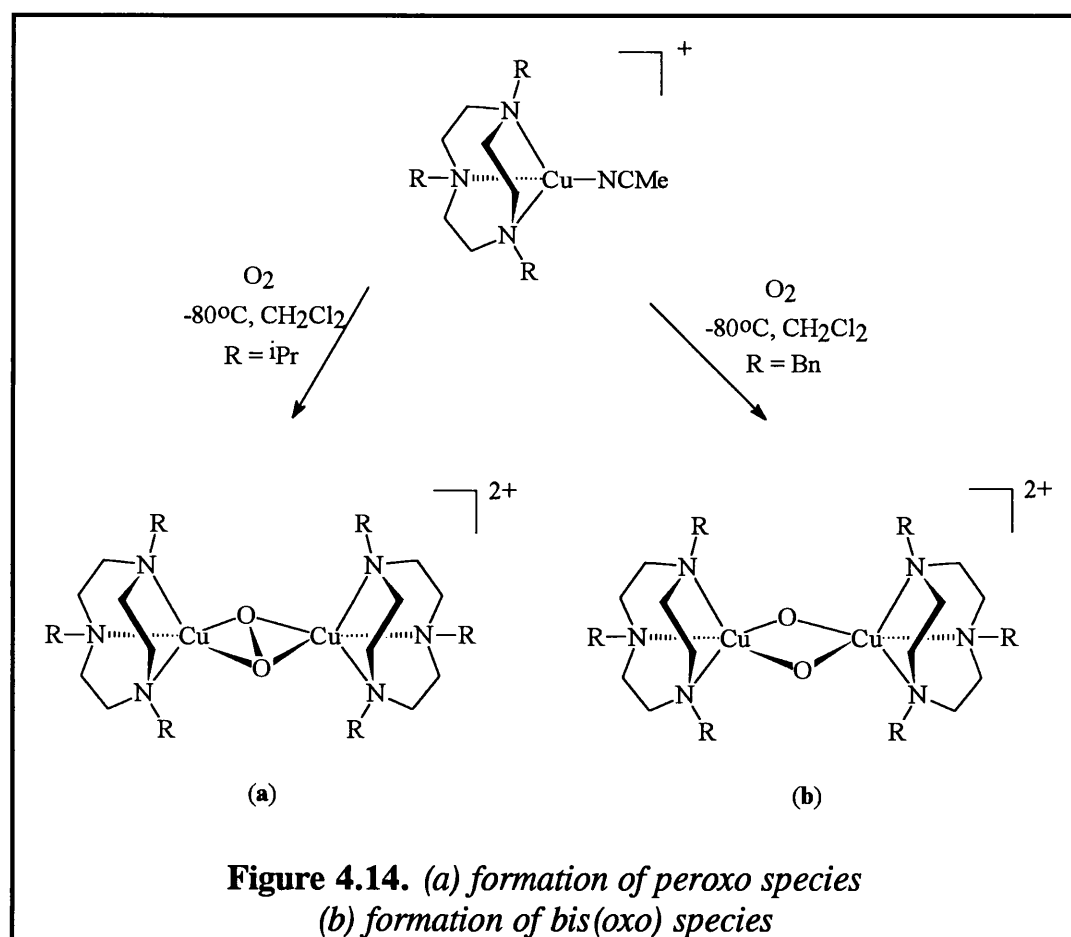
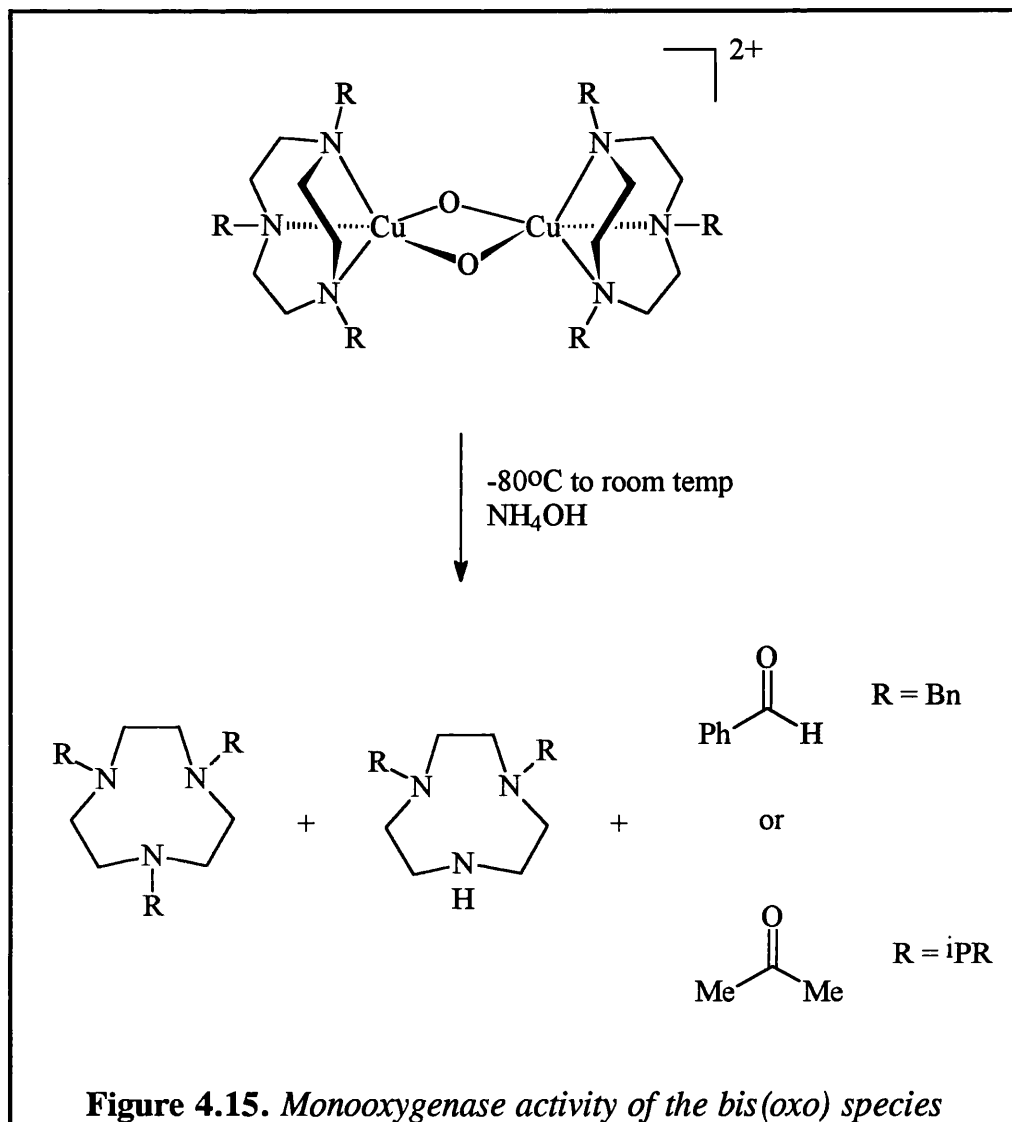


Figure 4.13. 200MHz ${}^1\text{H}$ NMR spectrum of $[\text{CuL}^{12}(\mu\text{-OH})_2\text{CuL}^{12}][\text{BPh}_4]_2$ in d_3 -acetonitrile

When the same reaction conditions were used for $[\text{Cu}(\text{Bn}_3\text{TACN})]^+$ a novel orange-brown bis(oxo) species was formed at low temperature (figure 4.14b) (14). Addition of THF to the peroxo species of $^i\text{Pr}_3\text{TACN}$ afforded the bis(oxo) species which can be converted back to the peroxo species by addition of CH_2Cl_2 . Allowing the bis(oxo) species to warm to room temperature produces bis(hydroxo) dicopper(II) complexes (15), where the copper is capped with the intact ligand and/or the *N*-dealkylated version. Removal of the copper ions from solution, showed that C-H bond activation occurred with oxidation of the pendant arms to acetone or benzaldehyde (figure 4.15) (2).





The ligands L^{3-6} , L^{12} and L^{14} are very similar in nature to Bn_3TACN and it was therefore anticipated that the observations reported by Tolman *et al.* would be true for the above ligands. Copper(I) complexes were prepared by the addition of the ligands to $\text{Cu}(\text{MeCN})_4\text{BF}_4$ in dichloromethane, the complexes were oxygenated at -78°C by bubbling pure O_2 into the solutions. All of the complexes with the exception of $[\text{CuL}^5]\text{BF}_4$ and $[\text{CuL}^6][\text{BF}_4]$ oxidised almost instantaneously to green copper(II) complexes, the colour of

the solutions indicating that peroxo or oxo species were not present. Warming the solutions under vacuum failed to reversibly bind the oxygen, suggesting the instant formation of bis(hydroxo) complexes. Changing the solvent to THF/acetonitrile (20:2) and repeating the reactions for L¹² and L¹⁴ had no effect on the colour of solution, again indicating that peroxo or oxo species did not form.

The preparation of the copper(I) complexes of L⁵ and L⁶ were unusual in that a red/brown solid was initially produced when the Cu(I) and ligand solutions were mixed at room temperature, IR data showed that the precipitated solid was not copper(II) oxide. A similar observation was reported by Churchill *et al.* (16) when copper(I) chloride complexes of *N,N,N',N'*-tetramethyl-1,3-propanediamine were oxidised at room temperature in dichloromethane by molecular oxygen. The report also showed that the formation of copper(II) carbonate species was possible if CO₂ was present in the oxidation process, with no insoluble precipitate being observed. Only after thorough degassing of the solvents and mixing at -78°C were copper(I) complexes prepared. No significant colour change was observed in the oxygenation of [CuL⁶]⁺ in CH₂Cl₂ at -78°C, but the addition of dry degassed THF at -78°C produced an instant colour change to intense green, suggestive of a bis(hydroxo) species.

Although no peroxo or oxo species were formed in the above reactions it is worth noting that the complexes studied by Tolman *et al.*

utilised ClO_4^- , SbF_6^- and CF_3SO_3^- as the counter ions. As mentioned in the previous chapter the nature of the counter ion plays an important role in the stability of copper(I) complexes, therefore repeating the oxygenation reactions using a different copper(I) salt could produce different results.

4.11 REFERENCES

1. K.D. Karlin, Y. Gultneh, *Prog. Inorg. Chem.*, 1987, **35**, 219.
2. S. Mahapatra, J.A. Halfen, W.B. Tolman, *J. Am. Chem. Soc.*, 1996, **118**, 11575.
3. D.A. Rockcliffe, A.E. Martell, *Inorg. Chem.*, 1993, **32**, 3143.
4. N. Kitajima, Y. Moro-oka, *J. Chem. Soc., Dalton Trans.*, 1993, 2665.
5. O. Kahn, *Molecular Magnetism*, VCH, New York & Cambridge, 1993.
6. D.J. Hodgson, *Prog. Inorg. Chem.*, 1975, **19**, 173.
7. J.M. Brink, R.A. Rose, R.C. Holtz, *Inorg Chem.*, 1996, **35**, 2878 and references there in.
8. L. Casella, O. Carugo, M. Gullotti, S. Garofani, *Inorg. Chem.*, 1993, **32**, 2056 and references there in.
9. M.J. Young, J. Chin, *J. Am. Chem. Soc.*, 1995, **117**, 10577
10. P. Chaudhuri, D. Ventur, K. Wieghardt, E Peters, K. Peters, A. Simon, *Angew. Chem. Int. Ed. Engl.*, 1985, **24**, 57.
11. B. Bleany, K.D. Bowers, *Proc. R. Soc. (A)*, 1952, **214**, 451.
12. K.T. McGregor, N.T. Watkins, D.L. Lewis, D.J. Hodgson, W.E. Hatfield, *Inorg. Nucl. Chem. Lett.*, 1973, **9**, 423.
13. S. Mahapatra, J.A. Halfen, E.C. Wilkinson, L. Que, W.B. Tolman, *J. Am. Chem. Soc.*, 1994, **116**, 9785.

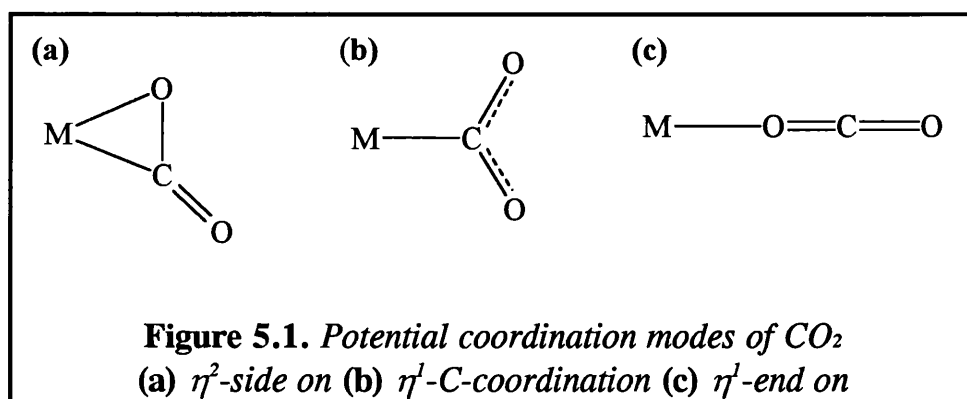
- 14.S. Mahapatra, J.A. Halfen, E.C. Wilkinson, G. Pan, C.J. Cramer, L. Que, W.B. Tolman, *J. Am. Chem. Soc.*, 1995, **117**, 8865.
- 15.S. Mahapatra, J.A. Halfen, E.C. Wilkinson, G. Pan, X. Wang, V.G. Young, C.J. Cramer, L. Que, W.B. Tolman, *J. Am. Chem. Soc.*, 1996, **118**, 11555.
- 16.M.R. Churchill, G. Davies, M.A. El-Sayed, M.F. El-Shazly, J.P. Hutchinson, M.W. Rupich, K.O. Watkins, *Inorg. Chem.*, 1979, **18**, 2296.

CHAPTER 5

COPPER(II) OXALATE COMPLEX OF L¹²

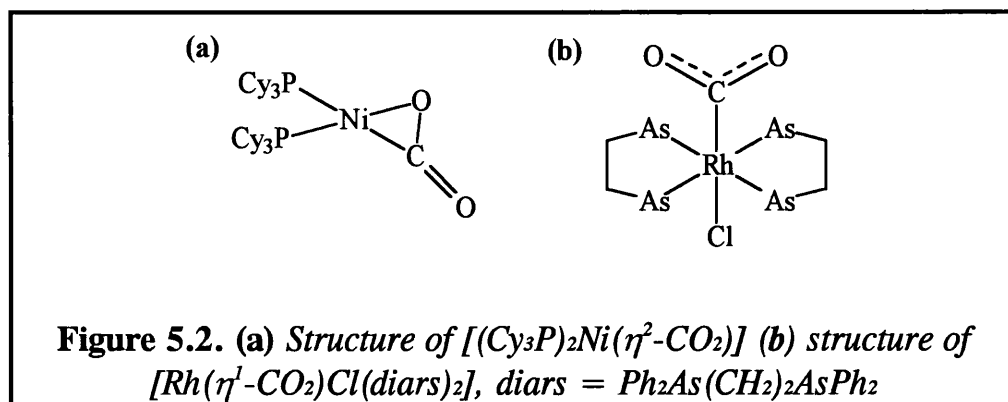
5.1 INTRODUCTION

Carbon dioxide is a molecule with several potential reactive sites: the carbon is a Lewis acid and the oxygens are weak Lewis bases, the carbon can thus be described as an electrophilic centre and the oxygens atoms as nucleophilic centres. CO₂ in its ground state also possesses two equivalent C-O π bonds that can also play a role in bonding to a transition metal centre. This polyfunctionality leads to a variety of potential transition metal CO₂ complexes (figure 5.1).

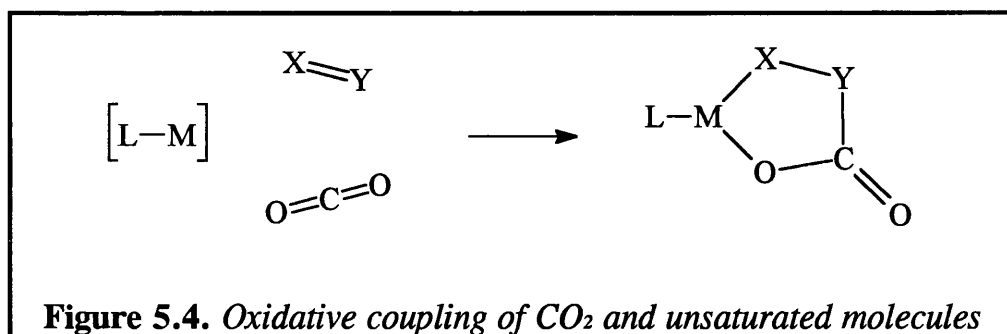
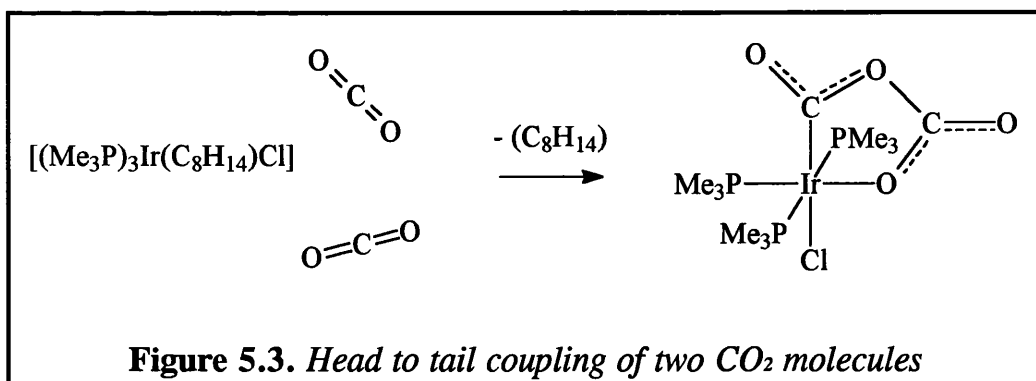


Many CO₂ complexes have been described in the literature, but earlier work used IR data to identify the coordination mode of the CO₂, which sometimes led to errors. The use of X-ray structure analysis allows clear identification of the coordination modes and the first solid state structures containing η^2 -side on and η^1 -C-coordination modes were [(Cy₃P)₂Ni(CO₂)] (1) and [Rh(CO₂)Cl(diars)₂] (2) (figure 5.2). The η^1 -end on coordination

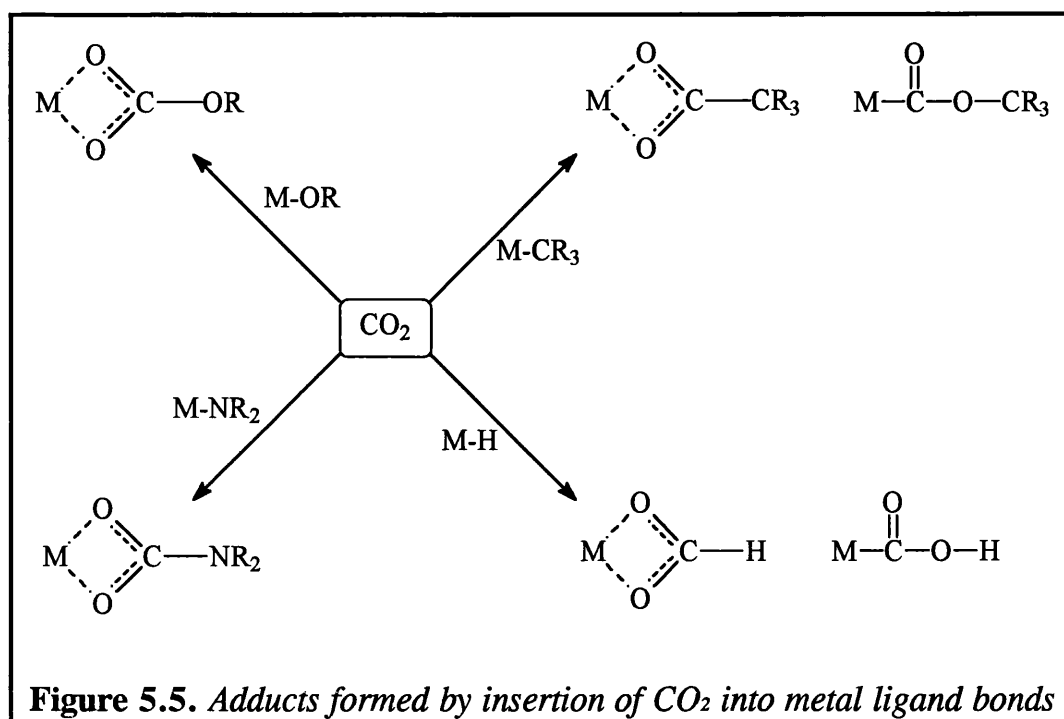
mode has been proposed as a reaction intermediate and has not been observed any solid state structure to date.



When two CO_2 molecules coordinate to the same metal, oxidative coupling can occur (3), usually with “head to tail” addition of the CO_2 molecules (figure 5.3). It has also been shown that, besides O-CO_2 bond formation, N-CO_2 and C-CO_2 bonds can be formed when the other unsaturated compound is an alkene, alkyne, aldehyde, imine or even molecular oxygen (figure 5.4) (4-6). The predominant transition metal compounds responsible for these couplings are electron rich $\text{Ni}(\text{O})$ complexes. When the addition of two CO_2 molecules is “head to head” the product is oxalate and this type of coupling is extremely rare in CO_2 coordination chemistry (7). The reduction of two CO_2 molecules to form oxalate is usually carried out by electrochemical means (8).



The insertion of CO₂ into metal-ligand bonds is well known in coordination chemistry (figure 5.5) (4, 6, 9). In many systems, the insertion is initiated by a nucleophilic attack of the ligand anion on CO₂. When the ligand anion is oxo or hydroxo, the reaction results in formation of a carbonate or bicarbonate complex and these insertions have been studied thoroughly because of their relation to the function of the zinc containing enzyme carbonic anhydrase. The enzyme catalyses the formation of HCO₃⁻ from aqueous CO₂ and it's now generally excepted that the enzymatic reaction involves nucleophilic attack of a Zn(II) bound hydroxyl group at the CO₂. The CO₂ molecule is not coordinated to the metal but is held in place by hydrogen bonds within the pocket of the protein shell of the enzyme.



5.2 CRYSTAL STRUCTURE OF $[\text{CuL}^{12}(\text{C}_2\text{O}_4)\text{CuL}^{12}][\text{BPh}_4]_2$

The structure of the oxalate bridged copper dimer of L^{12} is shown in figure 5.6, the copper atoms are in a square pyramidal environment with two oxalate oxygens and two N-allyl nitrogens as a base and an N-allyl nitrogen as the apex. The copper atoms are further coordinated by a distant acetonitrile molecule and both copper centres are related to each other by a centre of symmetry with a $\text{Cu}\cdots\text{Cu}$ distance of 5.2\AA . The $\text{Cu}\cdots\text{Cu}$ distance and other bond lengths and angles (table 5.1) are in line with other copper-oxalate bridged dimers (10, 11).

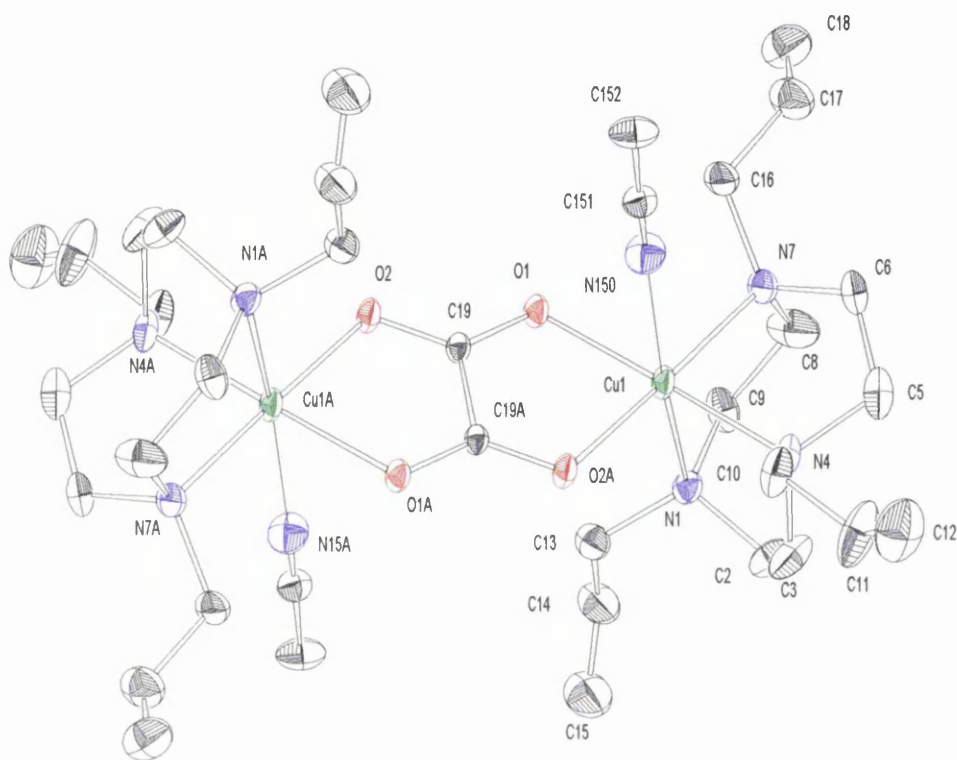


Figure 5.6. *Crystal Structure of $[\text{CuL}^{12}(\text{C}_2\text{O}_4)\text{CuL}^{12}]^{2+}$*

Crystal data for $\text{C}_{84}\text{H}_{100}\text{B}_2\text{Cu}_2\text{N}_8\text{O}_4$: $M = 1434.48$; Triclinic; Space Group $P\bar{1}$; $a = 11.2158(11)\text{\AA}$; $b = 13.1952(15)\text{\AA}$; $c = 13.8203(20)\text{\AA}$; $\alpha = 104.039(5)^\circ$; $\beta = 100.279(5)^\circ$; $\gamma = 98.024(5)^\circ$; $U = 1916.2(13)\text{\AA}^3$; $Z = 1$; $D_{\text{calc.}} = 1.243\text{gcm}^{-3}$; $F(000) = 760$; $\mu(\text{MoK}\alpha) = 6.1\text{cm}^{-1}$; $R(R_w^2) = 0.0619(0.1685)$.

Cu1-N1	2.248(5)Å	C19-O1	1.255(6)Å
Cu1-N4	2.042(5)Å	C19-O2	1.245(6)Å
Cu1-N7	2.026(5)Å	C19-C19A	1.548(7)Å
Cu1-O1	2.002(3)Å	Cu1-Cu1A	5.206(1)Å
Cu1-O2A	1.996(3)Å	Cu1-N150	2.646(6)Å
N1-Cu1-N4	84.32(18)°	N1-Cu1-O1	98.36(16)°
N1-Cu1-N7	84.92(19)°	N1-Cu1-O2A	98.31(16)°
N4-Cu1-N7	86.63(23)°	O1-Cu1-O2A	83.82(14)°
N1-Cu1-N150	176.44(17)°	Cu1-O2A-C19A	110.94(31)°
N4-Cu1-O1	176.27(18)°	Cu1-O1-C19	111.58(30)°
N7-Cu1-O2A	176.74(18)°	O1-C19-O2	126.58(45)°
C19A-C19-O1	115.70(40)°	C19A-C19-O2	117.71(42)°

Table 5.1. Selected bond lengths and angles for $[\text{CuL}^{12}(\mu\text{-C}_2\text{O}_4)\text{CuL}^{12}]^{2+}$

5.3 PREPARATION OF $[\text{CuL}^{12}(\text{C}_2\text{O}_4)\text{CuL}^{12}][\text{BPh}_4]_2 \cdot 2\text{CH}_3\text{CN}$

The oxalate complex was prepared in a similar method to the hydroxide bridged copper dimers of the previous chapter. The copper(I) complex of L^{12} was oxidised by atmospheric oxygen, in order to increase the rate of oxidation exhaled air was blown into the vessel containing the copper(I) complex for the first 15 minutes of exposure to the atmosphere. The resulting copper(II) complex was collected by filtration, evaporation of

an acetonitrile solution produced opaque green crystals. A boiling d₃-acetonitrile solution was saturated with the crude crystalline material and after standing overnight crystallographic quality crystals of $[\text{CuL}^{12}(\text{C}_2\text{O}_4)\text{CuL}^{12}][\text{BPh}_4]_2$ separated out from the solution. The crystals were originally believed to be the hydroxide bridged copper dimer of L^{12} and only after X-ray analysis was the true nature of the complex revealed.

5.4 REACTION OF $[\text{CuL}^{12}]^+$ WITH CO_2 AND CsHCO_3

The reduction of CO_2 to form oxalate by copper complexes is unknown and has only been reported for a dimeric Ti(III) complex (figure 5.7) (7). Copper(II) complexes react with CO_2 to form carbonate bridged species, the hydroxide bridged copper(II) dimers of tris(pyrazolyl)borate (12) and tris(imidazolyl)phosphine (13) exhibit remarkably high reactivity towards atmospheric CO_2 to produce carbonate bridged dimers. The reaction of copper(I) diamine complexes with O_2/CO_2 is also known and proceeds via a μ -oxo copper(II) complex to produce carbonate bridged dimers (14, 15). The oxalate observed in $[\text{CuL}^{12}(\text{C}_2\text{O}_4)\text{CuL}^{12}]^{2+}$ could only come from one plausible source, the large quantities of CO_2 in exhaled air.

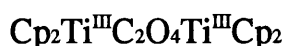


Figure 5.7. Reduction of CO_2 to $(\text{C}_2\text{O}_4)^{2-}$ by a Ti(III) complex

To prove that the oxalate originated from CO_2 several reaction conditions were applied to methanol solutions of $[\text{CuL}^{12}][\text{BPh}_4]$ (table 5.2). The reaction of $[\text{CuL}^{12}]^+$ with pure O_2 resulted in hydroxide dimer formation discussed in the previous chapter, the copper(I) complex was also stable in solution under a nitrogen atmosphere for several days. Reaction with gaseous CO_2 in dry methanol had no effect on the colour of the solution indicating that no oxidation of the Cu(I) had occurred. Oxidation of the copper(I) complex by CO_2 was achieved when wet methanol solutions of $[\text{CuL}^{12}][\text{BPh}_4]$ were used, suggesting that bicarbonate is involved in oxalate formation. A control reaction was also carried out with CuI and NaBPh_4 in methanol without the presence of L^{12} , no reaction with CO_2 was observed for this system.

Addition of L^{12} in degassed methanol to a suspension of CuI/ CsHCO_3 resulted in the suspension dissolving to give a blue solution, indicating that

the Cu(I) had been oxidised to Cu(II). The copper(II) complex was dissolved in acetonitrile and subjected to column chromatography using a silica column and acetonitrile as eluent. A slow moving yellow band separated from the absorbed complex and was collected. The complex was stripped from the column using methanol/nitromethane/2M NH_4Cl (7:1:2) and solid NaBPh_4 was added to the purified solution. Recrystallisation from nitromethane produced small green prisms of crystallographic quality.

Reaction condition	Bridging species
O_2	hydroxide
N_2	no reaction
CO_2	no reaction
$\text{H}_2\text{O} / \text{CO}_2$	oxalate and carbonate
CsHCO_3	oxalate and carbonate

Table 5.2. *Bridging ligands from different reaction conditions*

5.5 IR SPECTRA OF THE COPPER(II) COMPLEXES

The IR spectrum of a single crystal of $[\text{CuL}^{12}(\text{C}_2\text{O}_4)\text{CuL}^{12}][\text{BPh}_4]_2$ is shown in figure 5.8, the intense band at 1660cm^{-1} is due to $\nu(\text{C}=\text{O})$ of the bridging oxalate and is consistent with other dinuclear copper(II) oxalate systems (11, 16, 17). The sample of $[\text{CuL}^{12}(\text{C}_2\text{O}_4)\text{CuL}^{12}][\text{BPh}_4]_2$ also

contained a small amount of bridging carbonate which is identified by the weak band at 1580cm^{-1} . The IR spectra of the copper(II) complex formed by the reaction of $[\text{CuL}^{12}][\text{BPh}_4]$ with CO_2 is shown in figure 5.9. The spectrum is of the total solid obtained from the reaction mixture and contains bands at 1660cm^{-1} and 1580cm^{-1} indicating that bridging carbonate and bridging oxalate are present. Although the IR spectrum of $[\text{CuL}^{12}(\text{C}_2\text{O}_4)\text{CuL}^{12}][\text{BPh}_4]_2$ shows only small amounts of CO_3^- present, the sample crystallised from solution. No analysis was carried out on the solution and it may well have contained large amounts of a carbonate bridged copper(II) complex.

The IR spectra of the copper(II) complex formed by the reaction of $[\text{CuL}^{12}][\text{BPh}_4]$ with CsHCO_3 is shown in figure 5.10. The spectrum is of the total solid obtained from the reaction mixture and contains two intense bands at 1660cm^{-1} and 1580cm^{-1} indicating the presence of both bridging carbonate and oxalate. The IR spectrum of the prisms obtained from nitromethane is shown in figure 5.11 and contains an intense band at 1660cm^{-1} due to bridging oxalate and less intense band at 1580cm^{-1} due to a small amount of bridging carbonate. X-ray analysis of these prisms showed that the structure of the complex was a bridged oxalate copper dimer. The copper(II) atoms were in a square pyramidal environment and were not coordinated by acetonitrile. The IR data proves that oxalate formation is possible from the reaction of CO_2 / HCO_3^- with $[\text{CuL}^{12}]^+$, but the formation of carbonate bridged species also appears to be a major side reaction.

5.6 MECHANISM TO OXALATE FORMATION

The mechanism for the formation of oxalate by the reaction of CO_2 with $[\text{CuL}^{12}]^+$ is proposed in figure 5.12 and is by no means definite, but bicarbonate does appear to play a part in the oxalate formation. The formation of bicarbonate from CO_2 and water is a very slow process without the use of a catalyst. It is very probable that $[\text{CuL}^{12}]^+$ is oxidised to $[\text{CuL}^{12}(\text{OH})_2\text{CuL}^{12}]^{2+}$ by the trace amounts of dissolved oxygen in the reaction mixture, the dimer then has the ability to act as a catalyst in the formation of HCO_3^- from CO_2 . The formation of a bicarbonate bridged copper(I) dimer is more likely than the formation of a η^1 -end on CO_2 -copper(I) complex (figure 5.1c), since no examples of η^1 -end on coordination have been isolated to date. The instant formation of a copper(II) complex which contains oxalate, when CsHCO_3 is added to $[\text{CuL}^{12}]^+$ reinforces this idea of an intermediate bicarbonate bridged species.

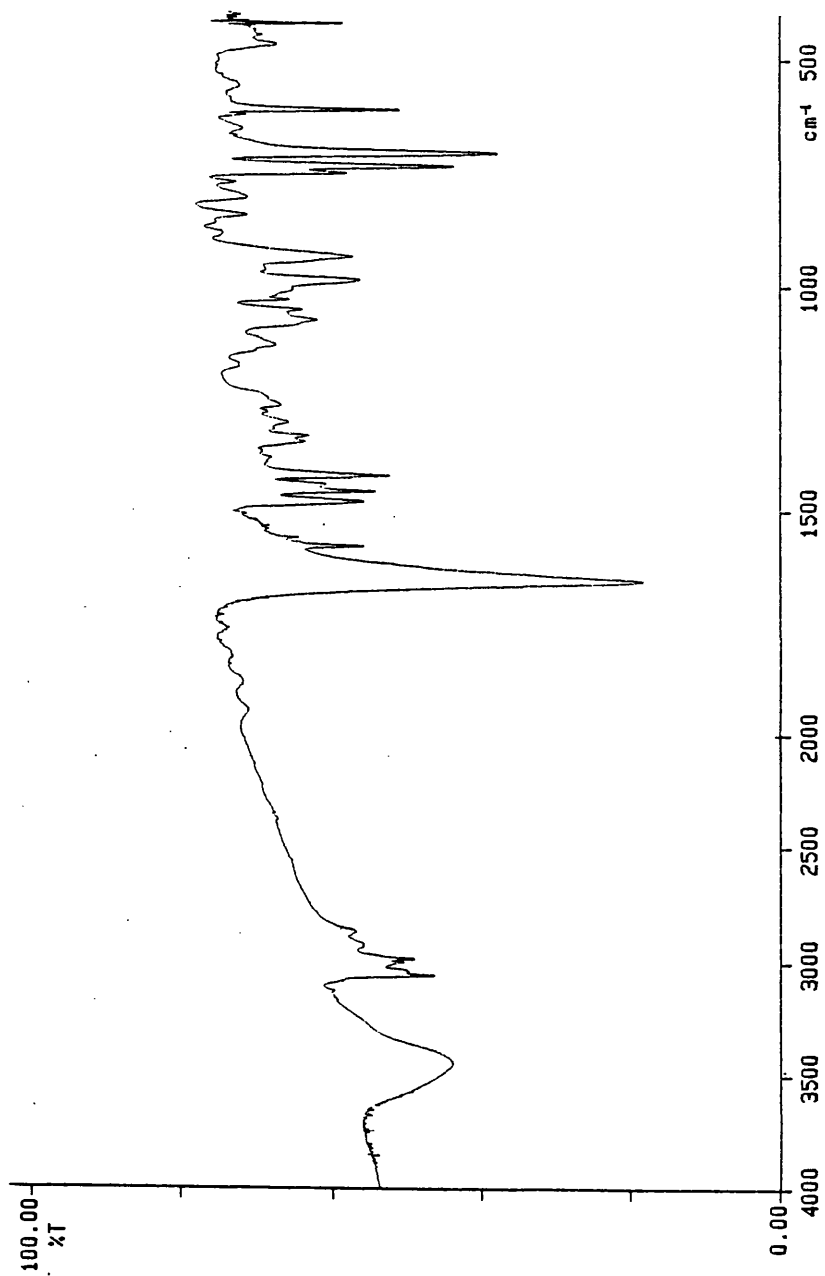


Figure 5.8. IR Spectrum of $[\text{CuL}^{12}(\text{C}_2\text{O}_4)\text{CuL}^{12}][\text{BPh}_4]_2$ (KBr disc)

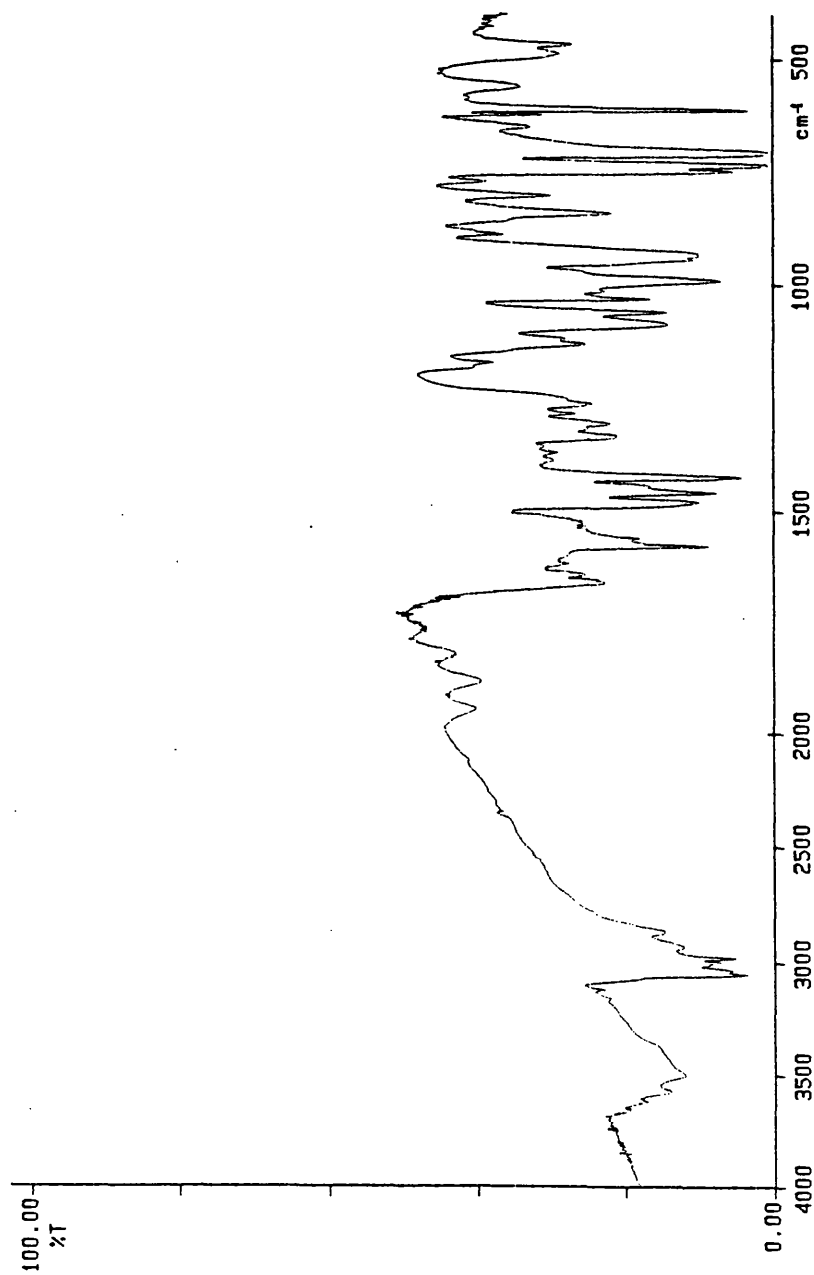


Figure 5.9. IR Spectrum of copper(II) complex from the reaction of CO₂ with [CuL¹²]/[BPh₄] (KBr disc)

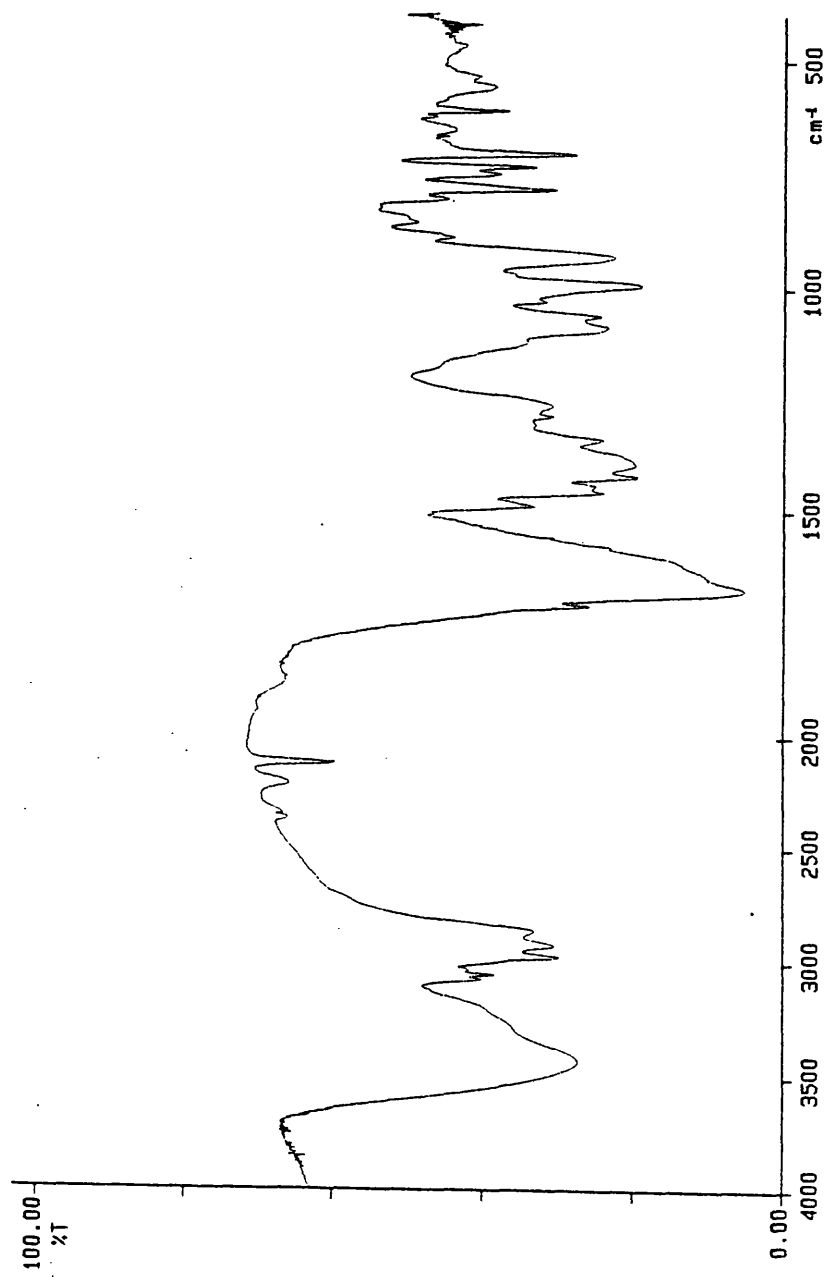


Figure 5.10. IR Spectrum of copper(II) complex from the reaction of CsHCO_3 with $[\text{CuL}^{12}]\text{I}$ (KBr disc)

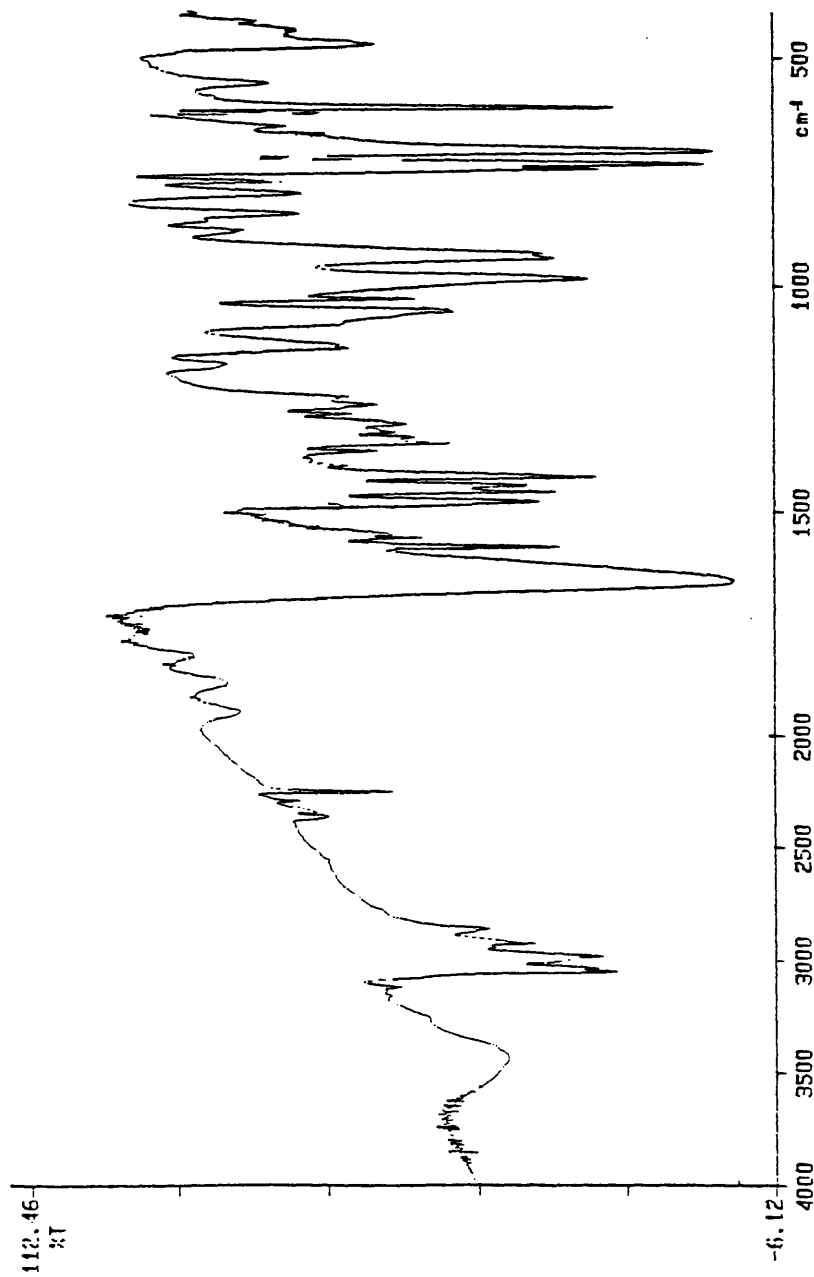


Figure 5.11. IR Spectrum of $[\text{CuL}^{12}(\text{C}_2\text{O}_4)\text{CuL}^{12}][\text{BPh}_4]_2$ obtained from the reaction of CsHCO_3 with $[\text{CuL}^{12}]\text{I}$ (KBr disc)

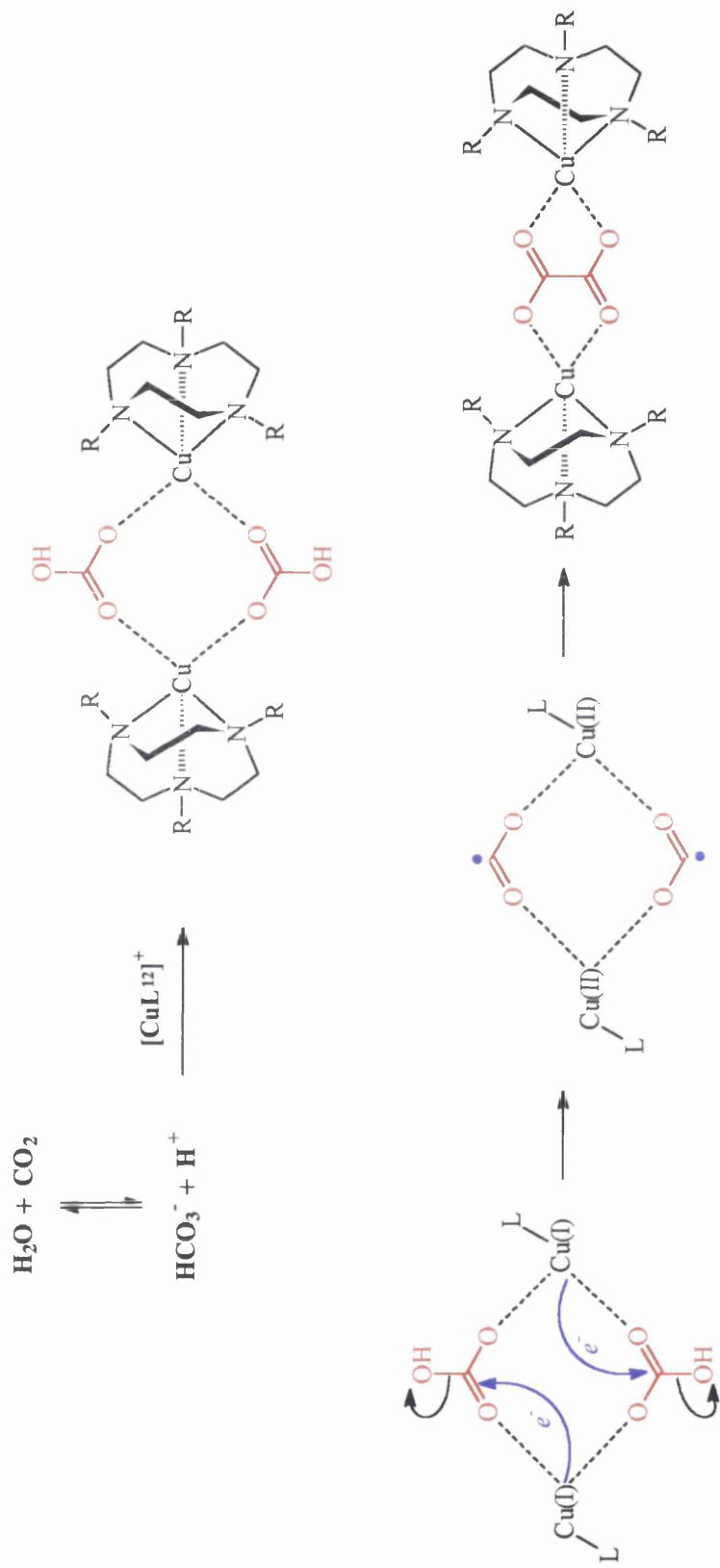


Figure 5.12. Formation of oxalate by the reaction of $[\text{CuL}^{12}]^+$ with CO_2 / HCO_3^-

5.7 REFERENCES

1. M. Aresta, C.F. Nobile, V.G. Albano, E. Forni, M. Manassero, *J. Chem. Soc., Chem. Comm.*, 1975, 636.
2. J.C. Calabrese, T. Herskovitz, J.B. Kinney, *J. Am. Chem. Soc.*, 1983, **105**, 5914.
3. T. Herskovitz, L.J. Guggenberger, *J. Am. Chem. Soc.*, 1976, **98**, 1515.
4. A. Behr, *Angew. Chem. Int. Ed. Engl.*, 1988, **27**, 661.
5. M. Aresta, E. Quaranta, I. Tommasi, P. Giannoccaro, A. Ciccarese, *Gazz. Chim. Ital.*, 1995, **125**, 509.
6. W. Leitner, *Coord. Chem. Rev.*, 1996, **153**, 257.
7. H.O Fröhlich, *Z. Chem.*, 1983, **23**, 348.
8. K. Tanka, *Adv. Inorg. Chem.*, 1995, **43**, 409.
9. D.A. Palmer, R. Van Eldik, *Chem. Rev.*, 1983, **83**, 651.
10. O. Kahn, *Angew. Chem. Chem. Int. Ed. Engl.*, 1985, **24**, 834 and references therein.
11. A. Gleizes, M. Julve, M. Verdaguer, J.A. Real, J. Faus, X. Solans, *J. Chem. Soc., Dalton Trans.*, 1992, 3209.
12. N. Kitajima, S. Hikichi, M. Tanaka, Y. Moro-oka, *J. Am. Chem. Soc.*, 1993, **115**, 5496.
13. T.N. Sorrell, W.E. Allen, P.S. White, *Inorg. Chem.*, 1995, **34**, 952.

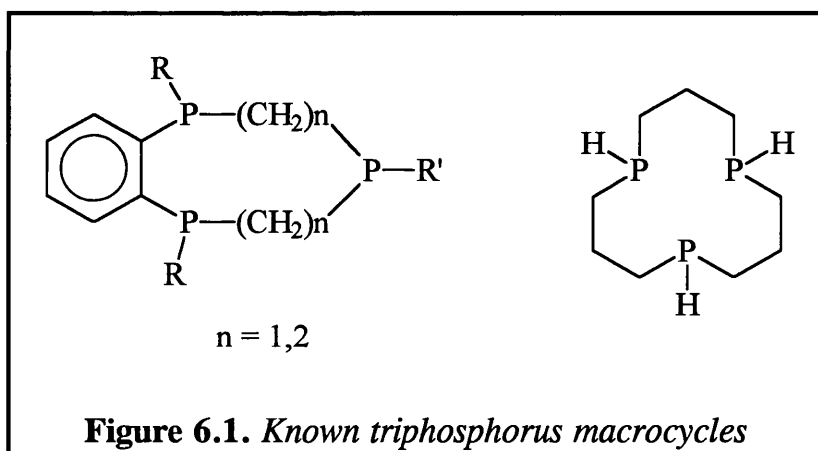
- 14.M.R. Churchill, G. Davies, M.A. El-Sayed, M.F. El-Shazly, J.P. Hutchinson, M.W. Rupich, K.O. Watkins, *Inorg. Chem.*, 1979, **18**, 2296.
- 15.M.R. Churchill, G. Davies, M.A. El-Sayed, M.F. El-Shazly, J.P. Hutchinson, M.W. Rupich, *Inorg. Chem.*, 1980, **19**, 201.
- 16.K. Nonoyama, H. Ojima, K. Ohki, M. Nonoyama, *Inorg. Chim. Acta.*, 1980, **41**, 155.
- 17.K. Nakamoto, *Infrared and Raman Spectra of Inorganic and Coordination Compounds*, 4th ed., Wiley, New York, p.244.

CHAPTER 6

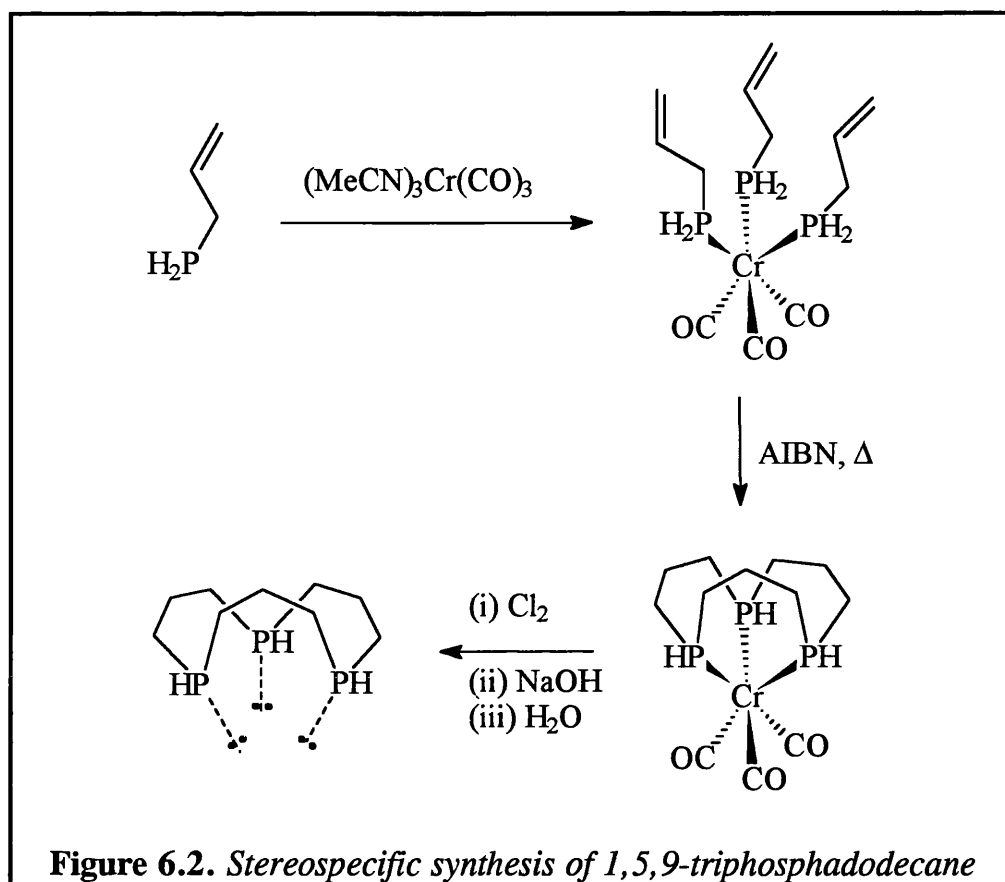
PHOSPHINE PENDANT ARM MACROCYCLES AND THEIR TRANSITION METAL COMPLEXES

6.1 INTRODUCTION

In comparison to the wide studies of nitrogen macrocycles in coordination chemistry, there are remarkably few studies of related macrocyclic phosphorus ligands. There are only two reported triphosphorus macrocyclic ligands in the literature (figure 6.1). The series of macrocyclic ligands generated from 1,2-diphosphinobenzene were prepared by Kyba *et al.* using high dilution methods which in some cases lead to non-stereospecific ligands (1). The other triphosphorus ligand 1,5,9-triphosphacyclododecane was only known on the template upon which it was prepared (2) and only recently has the free ligand been liberated (3).



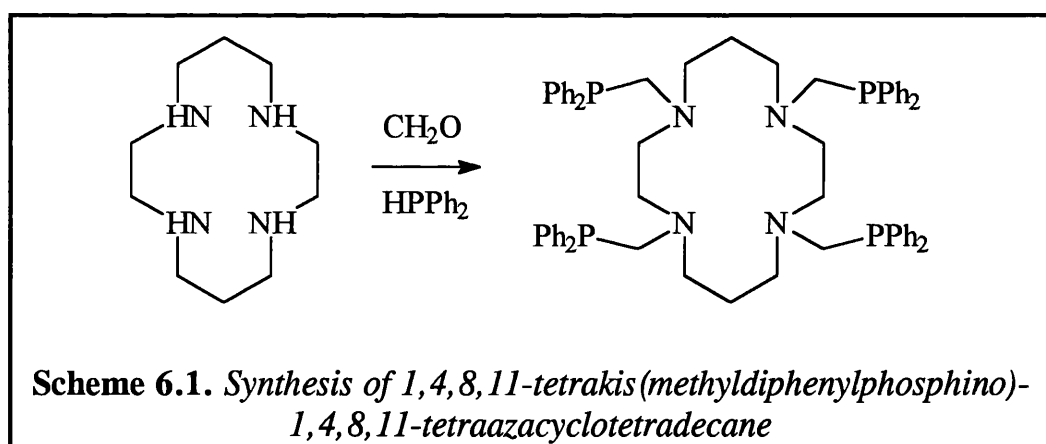
The use of a template synthesis for 1,5,9-triphosphacyclododecane (figure 6.2) means that the ligand is liberated as a single geometric conformer, unlike the high dilution methods used by Kyba *et al.*



The precursors to 1,5,9-triphosphadodecane based macrocycles can be difficult to handle due to their air-sensitive nature and the synthetic route limits the macrocyclic ring size to 12 or 15 atoms. The number of pendant arms for this synthetic route is also limited to zero or three. Therefore *N*-functionalisation of triaza macrocycles with phosphine pendant arms would allow more freedom to tune a macrocyclic phosphine ligand to a particular system, since there is a larger range of triaza macrocycle ring sizes compared to triphosphorus macrocycles. The increasing number of methods for selective *N*-protection for triaza macrocycles also allows the number of pendant arms to be changed with ease. The complication of several

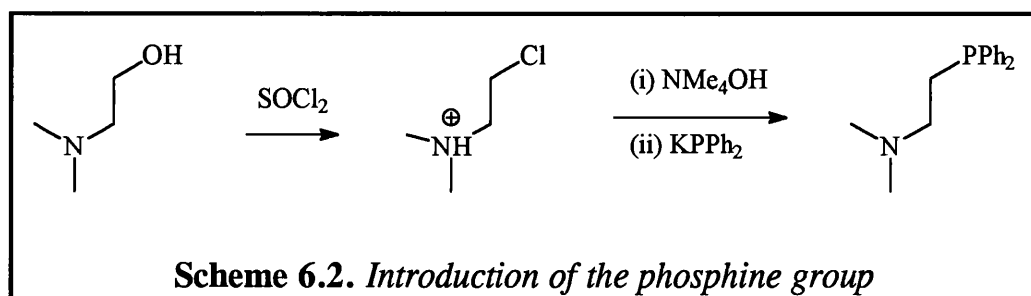
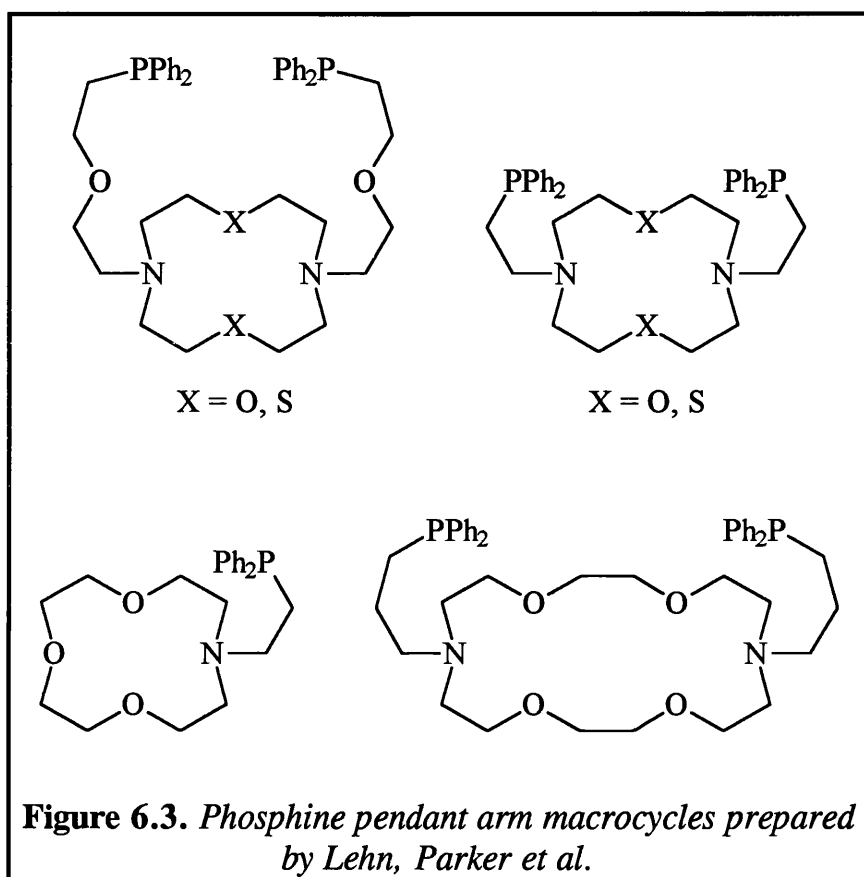
stereoisomers is not possible for triaza macrocycle systems since *N*-inversion occurs at room temperature.

The first phosphine pendant arm derivative of a polyaza macrocycle was reported by Power *et al.* (4) in the reaction of diphenylphosphine with cyclam in the presence of formaldehyde to produce 1,4,8,11-tetrakis(methyldiphenylphosphino)-1,4,8,11-tetraazacyclotetradecane (scheme 6.1). The pendant arm ligand contains phosphine donors that are separated from the nitrogen functions by one carbon atom spacers, this results in a ligand which cannot “wrap up” a metal ion and should promote polynuclear complexes. The synthetic route to this ligand should be applicable to any macrocycle with secondary nitrogen functions and with selective *N*-protection there is the possibility of derivatives with varying pendant arm numbers.



Using a different strategy Lehn, Parker *et al.* (5) reported a series of N_2O_2 , N_2S_2 , NO_3 and N_2O_4 macrocycles with phosphine pendant arms of

varying length (figure 6.3). The phosphine pendant arm macrocycles were prepared from their hydroxyl pendant arm precursors by the formation of the corresponding alkyl chloride followed by reaction with potassium diphenylphosphide (scheme 6.2).

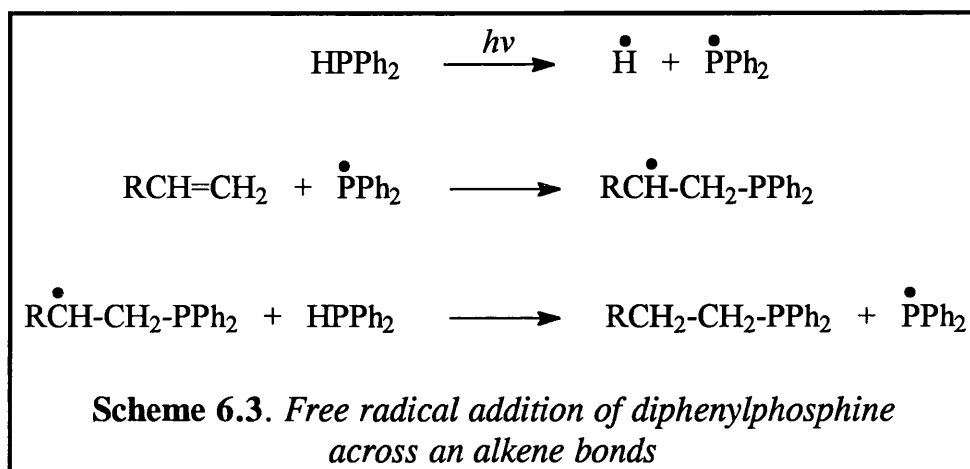


The synthetic route used by Parker and Lehn does not proceed smoothly with 1,4,7-triazacyclononane, possibly because the high basicity of the nitrogens leads to displacement of chloride and the formation of aziridinium ions (6). At the present time there is no report other than this work of a triazamacrocyclic *N*-functionalised with a phosphine group.

6.2 LIGAND PREPARATION

The ligands L^{16} - L^{21} were prepared by free-radical addition of diphenylphosphine across the alkene double bond of their corresponding alkene pendant arm derivatives (scheme 6.3). The only restriction to this scheme is that the pendant arm must contain a minimum of three carbon atoms, since a two carbon atom pendant arm is not synthetically feasible for this system. The free-radical additions were accomplished in essentially qualitative yields by photolysis under strictly anaerobic conditions using a mercury lamp. The reactants were irradiated neat, the use of solvents increased the amount of phosphine oxides in the product and were found to severely hinder the reaction rate. Free-radicals are electron deficient species and their stability decreases in the order $3^\circ > 2^\circ > 1^\circ$. The addition in scheme 6.3 is therefore strictly anti-Markovnikov since the formation of a secondary radical is preferred over the formation of a primary radical. It was originally

believed that the free amine functions in L^7 , L^{10} and L^{11} would quench the radical addition and an *N*-methylated derivative of L^7 was used as the starting alkene, but it was later found that this was not necessary. Excess diphenyl phosphine was removed from the reaction mixture by washing with 40-60 petrol or by distillation under reduced pressure.



It was anticipated that branched alkene ligands L^8 , L^9 and L^{13} would undergo free-radical addition with diphenylphosphine to produce racemic phosphine pendant arm macrocycles. The presence of a tertiary carbon centre adjacent to the terminal alkene in L^8 and L^{13} should be ideal for stabilisation of a radical intermediate in a free radical addition reaction, but the addition reaction was extremely slow and the alkene macrocycle degraded under the photolytic conditions before any significant amount of addition was achieved. No addition products were observed for L^3 and L^9 , even when radical initiators such as AIBN were added. The unreactive bridging alkene in L^3 proved to be advantageous in the synthesis of L^{21} , since

the allyl pendant arms of L^{14} could be converted to phosphine donor groups leaving the alkene bridge untouched.

6.3 METAL COMPLEXES OF L^{19}

6.3.1 Cobalt(-I / I) Complex

The reaction of $\text{Co}_2(\text{CO})_8$ with L^{19} in dichloromethane resulted in immediate effervescence indicating the release of CO. The IR spectrum of the reaction mixture contained three bands (figure 6.4). The band at 1889cm^{-1} is characteristic of $\nu(\text{CO})$ for $\text{Co}(\text{CO})_4^-$ indicating that disproportionation of $\text{Co}(0)$ to $\text{Co}(-\text{I})$ and $\text{Co}(\text{I})$ had occurred. A similar reaction was observed with *N,N',N''*-tris(propyne)-1,4,7-triazacyclononane (7) and $\text{Co}_2(\text{CO})_8$. The disproportionation of $\text{Co}_2(\text{CO})_8$ with tertiary phosphines is also known with the product being $[\text{Co}(\text{CO})_3(\text{PR}_3)_2][\text{Co}(\text{CO})_4]$ (8). The $\text{Co}(\text{I})$ complex formed with L^{19} still contained bound CO and could therefore be one of two possible types of complex; $[\text{Co}L^{19}(\text{CO})_2][\text{Co}(\text{CO})_4]$ where L^{19} was tridentate or $[\text{Co}L^{19}(\text{CO})_3][\text{Co}(\text{CO})_4]$ where L^{19} was bidentate. Stretching mode analysis showed that only $[\text{Co}L^{19}(\text{CO})_2][\text{Co}(\text{CO})_4]$ was consistent with the number of $\nu(\text{CO})$ observed in the IR spectrum. The structure is therefore probably similar to $\text{CpCo}(\text{CO})_2$ with either the three nitrogens or the three phosphines acting as the 6 electron donor.

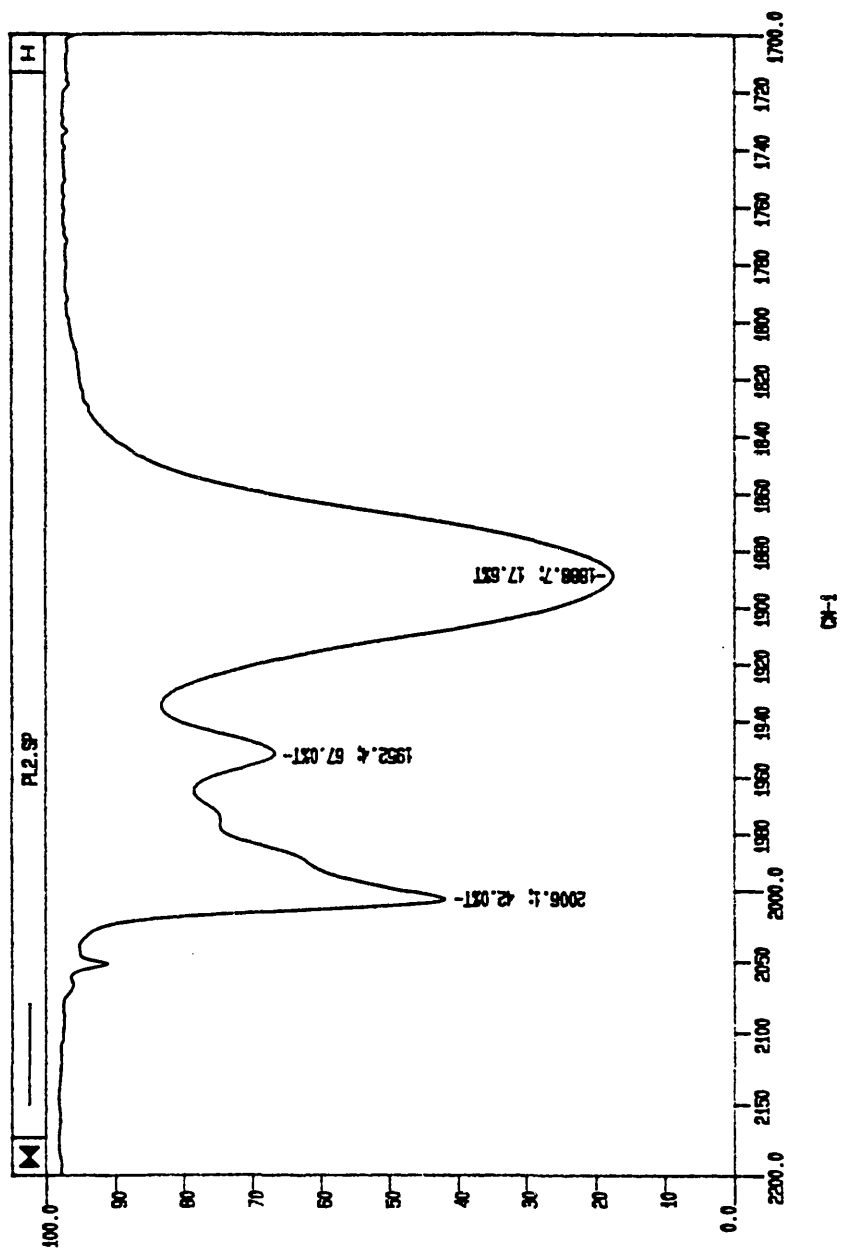


Figure 6.4. IR spectrum of $[\text{CoL}^{19}(\text{CO})_x][\text{Co}(\text{CO})_4]$ in CH_2Cl_2

6.3.2 Nickel(II) complex

L^{19} reacts with anhydrous $NiCl_2$ in ethanol to produce an intense red/purple complex, addition of $NaBPh_4$ precipitates the complex as an air/moisture sensitive microcrystalline red/brown solid. The intense red colour of the complex suggests a square planar $Ni(II)$ environment which should be diamagnetic. The electronic spectrum of the complex is shown in figure 6.5 and contains two bands at 380 and 545nm consistent with square geometry. The ^{31}P NMR spectrum of the complex (figure 6.6) contains two broad resonances at 76 (2P) and 84ppm (1P), the broadness is probably due to a paramagnetic $Ni(II)$ impurity. The ^{31}P NMR suggest a AB_2 system and the phosphines should couple to each other producing a doublet at 76ppm and a triplet at 84ppm, these splitting patterns are not observed, possibly because of the broadness of the signals. Broad resonances are also observed in the 1H NMR (figure 6.7), but no rational assignment of resonances has been attempted. The spectroscopic evidence strongly suggests a square planar environment with all three phosphine arms coordinated to the $Ni(II)$ centre and the forth site probably occupied by coordinated chloride or ethanol.

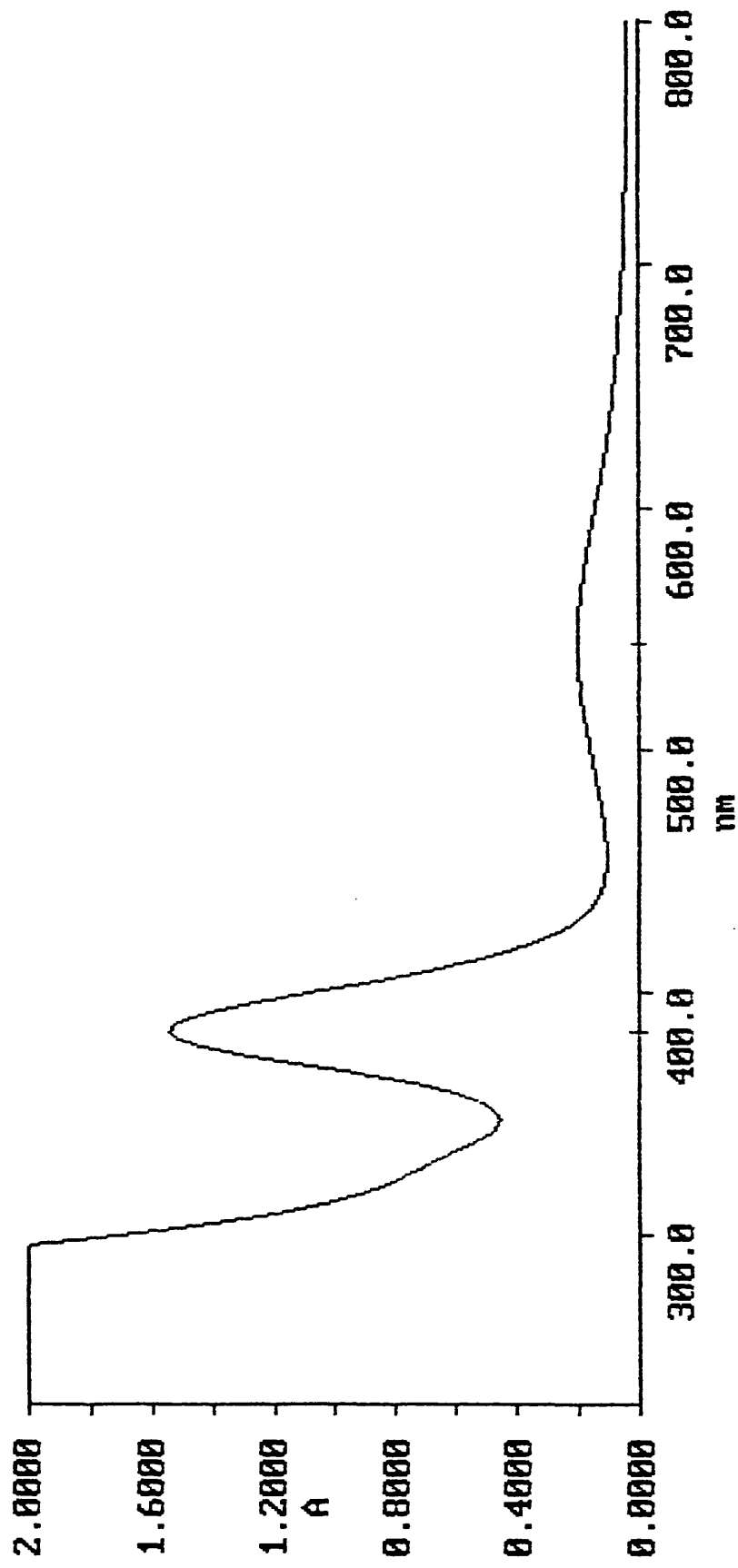


Figure 6.5. Electronic spectrum of Ni(II) complex with L¹⁹ in CH₂Cl₂

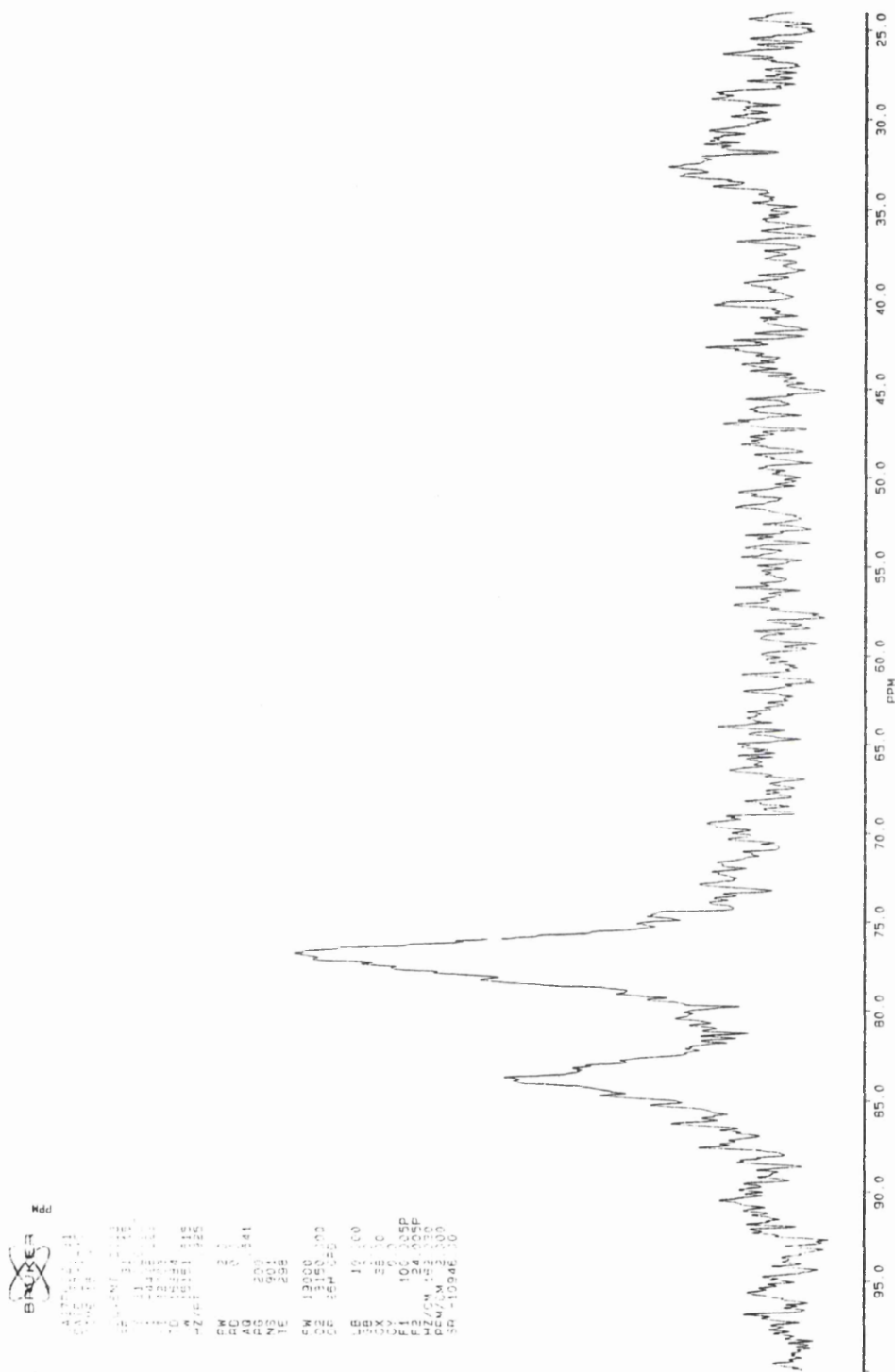


Figure 6.6. ^{31}P NMR spectrum of Ni(II) complex with L^{19} in CDCl_3

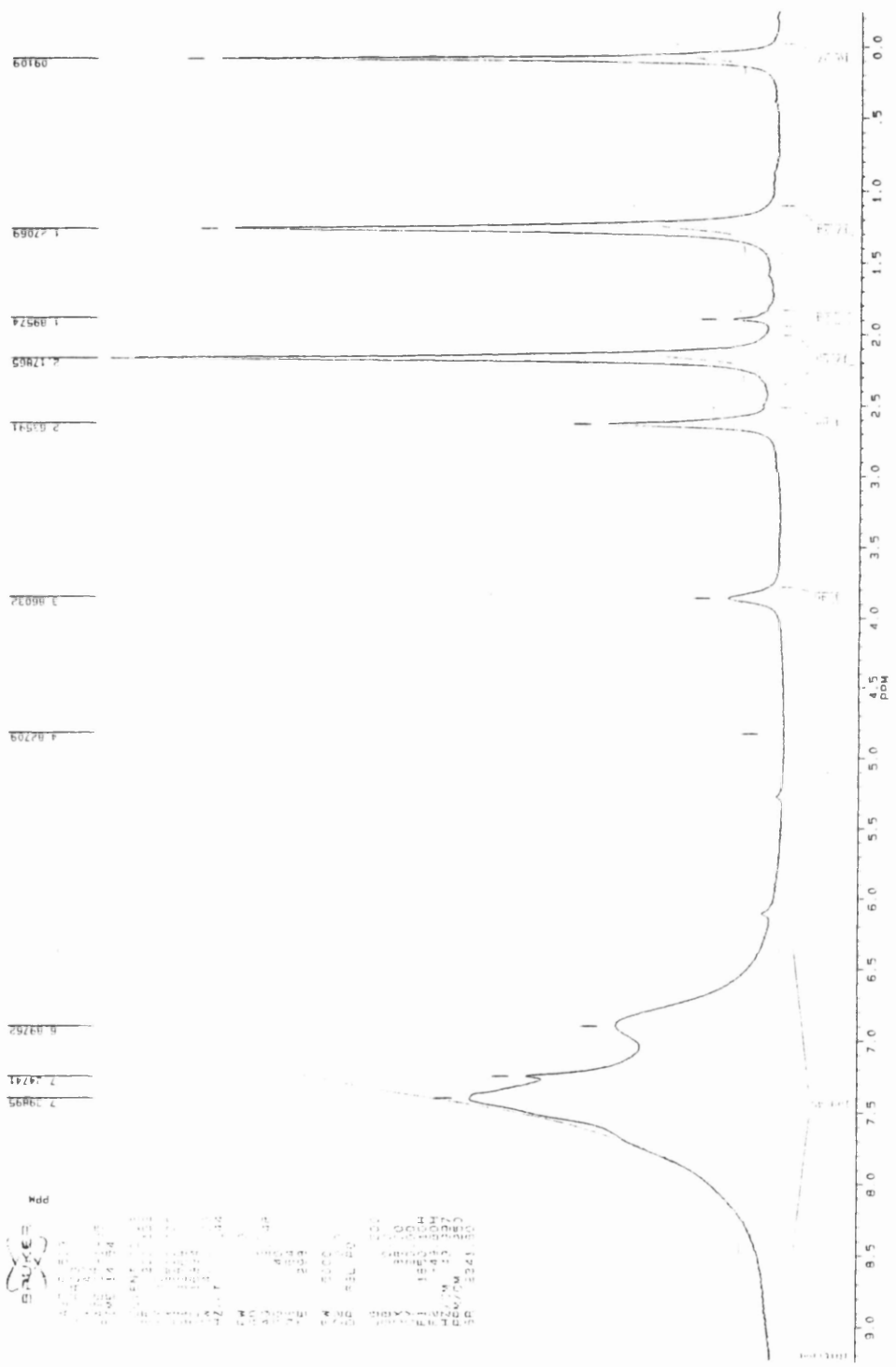


Figure 6.7. ^1H NMR spectrum of Ni(II) complex with L^{19} in CDCl_3

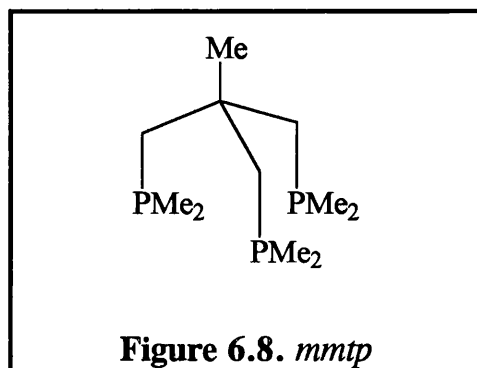
6.3.3 Molybdenum(0) complex

Mo(CO)_6 reacts with TACN (9), Me_3TACN (10), N,N',N'' -tris(propyne)-1,4,7-triazacyclononane (7) and N -3-phenoxypropyl-1,4,7-triazacyclononane (11) to produce piano stool complexes of the type LMo(CO)_3 , where all three nitrogens of the macrocycle are coordinated to the Mo centre. The basic nitrogens of the TACN rings are excellent σ -donors with no π -acceptor ability, therefore coordination of TACN ligands to Mo results in a complex which contains a high electron density on the metal centre. The carbonyls in these piano stool complexes are therefore essential for π -backbonding interactions which reduces the electron density on the metal centre and stabilises the complex. N -3-phenoxypropyl-1,4,7-triazacyclononane contains an aromatic pendant arm which has weak π -acceptor properties and N,N',N'' -tris(propyne)-1,4,7-triazacyclononane contains alkyne groups which are good π -acceptor ligands, but the pendant arm length is too short to coordinate to the Mo centre. L^{19} was expected to behave differently towards Mo(0) compared to the other pendant arm ligands, since phosphines are good π -acceptor ligands and the length of the pendant arm was sufficiently long enough to allow phosphine coordination, thus allowing displacement of some of the carbonyl groups in the piano stool complex.

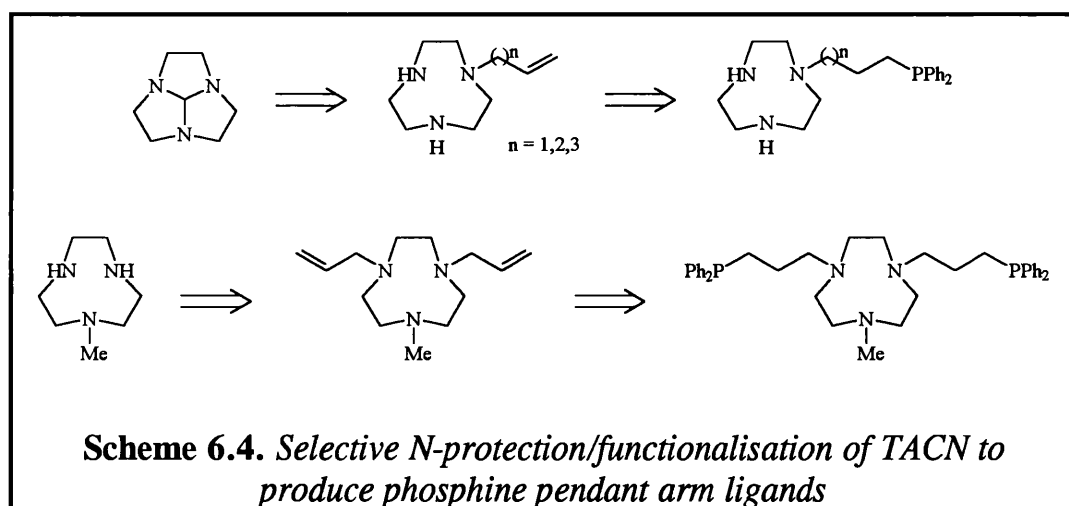
The reaction of L^{19} with $(MeCN)_3Mo(CO)_3$ showed no visible signs of effervescence, indicating that none of the carbonyls had been replaced by the phosphine groups. The IR spectrum contained three $\nu(CO)$ bands (figure 6.8) and was unlike the spectra of the other TACN systems which contained two bands (A_1 and E) consistent with C_{3v} symmetry. The lower symmetry observed in the complex is most probably due to mixed N/P donation to the metal centre and is confirmed by the ^{31}P NMR of the complex (figure 6.7) which shows resonances for uncoordinated phosphine at -16ppm and multiple resonances for coordinated phosphine at 17-31ppm. The complex was extremely unstable in solution hindering attempts to purify the sample.

Other complexes with L^{19} were prepared, but purification and identification of the complexes proved to be difficult. The reasons for this were believed to be due to the three bulky phosphine pendant arms which prevented L^{19} from being hexadentate in mononuclear complexes. The uncoordinated pendant arms in metal complexes would therefore be susceptible to oxidation, giving rise to mixtures of complexes containing phosphine/phosphine oxide pendant arms. The triphosphine ligand 1,1,1-tris(dimethylphosphinomethyl)ethane (mmtp) (figure 6.8) was shown to form an octahedral bis-ligand complex with Co(III) and mixed ligand complex $[Co(TACN)(mmtp)]^{3+}$ (12). The use of dimethylphosphine pendant arms in an analogous ligand to L^{19} should allow the ligand to be truly hexadentate

and increase the σ -donor properties of phosphine groups compared to a ligand with diphenylphosphine pendant arms. The only drawback to using dimethylphosphine donor functions is the extremely air-sensitive nature of these ligands.



Ligands with less than three phosphine donor groups were possible by the selective *N*-protection and *N*-functionalisation of TACN (scheme 6.4). These one and two pendant arm ligands should be able to coordinate to metal centres with a full donor set allowing, allowing easier characterisation and handling of the complexes.



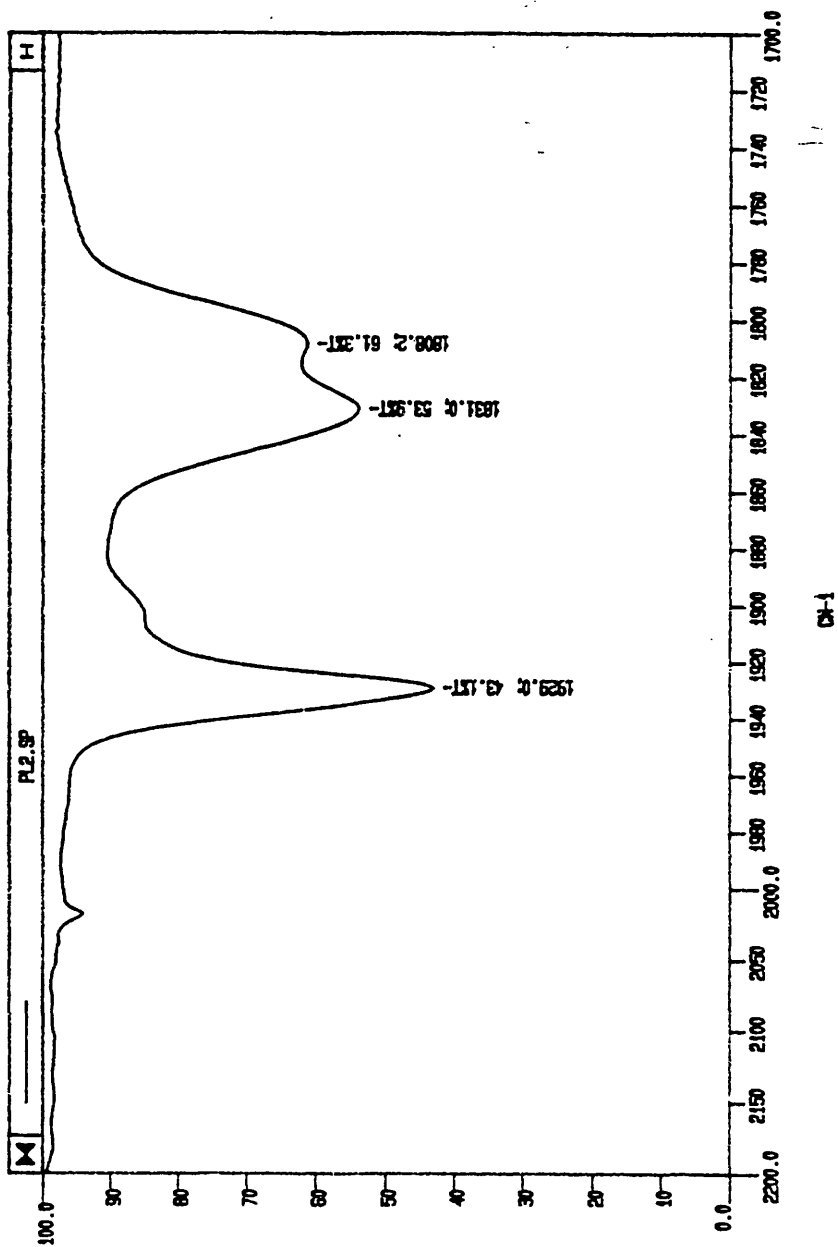


Figure 6.8. IR spectrum of $L^{19}\text{Mo}(\text{CO})_3$ in CH_2Cl_2 / MeCN

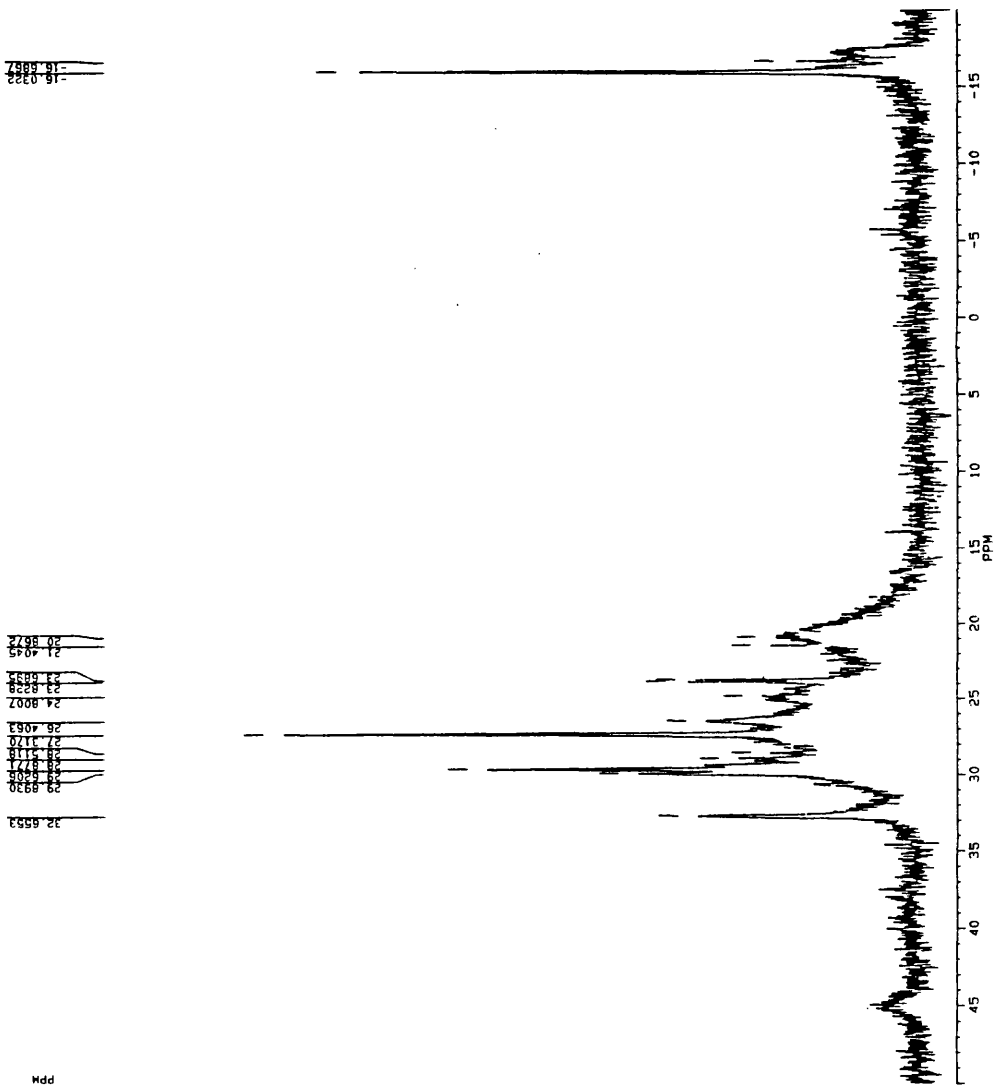


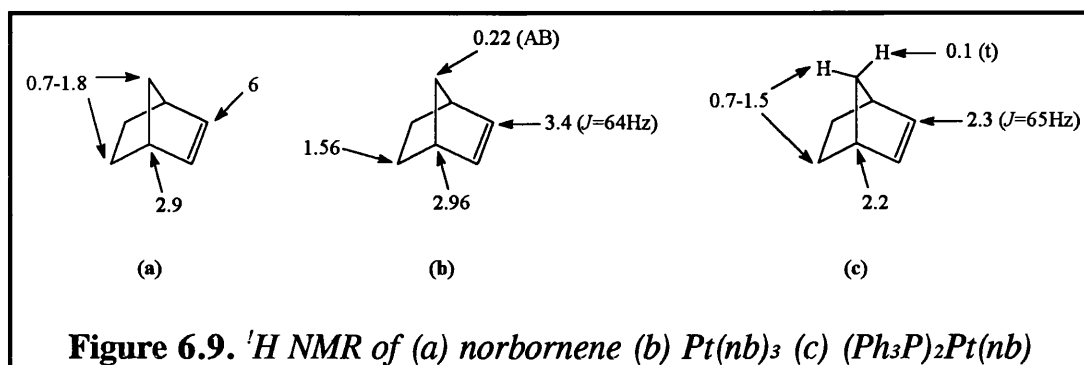
Figure 6.9. ^{31}P NMR spectrum of $L^{19}\text{Mo}(\text{CO})_3$ in CDCl_3

6.4 METAL COMPLEXES OF L²⁰

6.4.1 Platinum complex

Reaction of L²⁰ with platinum tris(norbornene) in CDCl₃ produced an orange solution. The two phosphine functions of L²⁰ were expected to replace some of the labile norbornene groups of Pt(nb)₃ producing a new Pt(0) complex. The ¹H NMR spectrum of the reaction mixture is presented in figure 6.10 and the ¹H resonances for selected norbornene compounds are shown in figure 6.9 (13, 14). The spectrum is very complex due to the variety of methylene groups in L²⁰ and norbornene and is further complicated by the presence of coordinated and uncoordinated norbornene. The resonances at 5.97 and 2.8ppm are clearly due to free norbornene and the region between 0.8-1.7ppm is due to both coordinated and free norbornene. The resonances belonging to L²⁰ are observed at 2-3ppm and 6.5-8ppm with the methylene resonances of L²⁰ obscuring the region where the coordinated olefin in L²⁰Pt(nb) would be expected. The AB type resonance at 0.25ppm is due to the methylene bridge of norbornene in L²⁰Pt(nb). The same AB splitting pattern is observed in Pt(nb)₃, but because no resonance is observed for the coordinated olefin of Pt(nb)₃ (3.36ppm) it is assumed that Pt(nb)₃ is not present. The ratio of free norbornene to coordinated olefin is 2.2:1 and was calculated by comparing the integrals of the uncoordinated olefin

resonance (5.97ppm) and the resonance due to the methylene bridge of the coordinated norbornene (0.25ppm). The ratio suggests that $L^{20}\text{Pt}(\text{nb})$ is formed releasing two moles of norbornene.



The ^{31}P NMR spectrum of the reaction mixture (figure 6.11) contains resonances at 16.7 ($J_{\text{P-Pt}}=3172\text{Hz}$) and 24.3ppm ($J_{\text{P-Pt}}=3428\text{Hz}$) with the peak at 16.7ppm being the more intense of the two. The resonances at 33ppm are due to phosphine oxides. Complexes of the type $(\text{Ph}_3\text{P})_2\text{Pt}(\text{olefin})$ have $\delta(\text{P})$ in the region 25 to 32ppm with $^1J(\text{Pt-P})$ typically 3000-3500Hz (14, 15, 16). Removing the uncoordinated norbornene from the sample results in a different ^{31}P NMR spectrum (figure 6.12). The resonance at 24.3ppm ($J_{\text{P-Pt}}=2930\text{Hz}$) is unshifted, but is more intense and the coupling to ^{195}Pt has decreased by 500Hz. The resonance at 16.7ppm has shifted +0.8ppm, is less intense and the coupling to ^{195}Pt is half that observed in the original sample. No comparison of ^{31}P chemical shifts can be made with $(\text{Ph}_3\text{P})_2\text{Pt}(\text{nb})$ since the ^{31}P NMR of this complex was not measured.

$(\text{Ph}_3\text{P})_2\text{Pt}(\text{nb})$ was reported to be unstable to olefin loss, with the olefin dissociating completely after 30 minutes (14). $\text{Pt}(\text{olefin})_3$ complexes are also known to be unstable unless an excess of olefin is present and this also appears to be true for $\text{L}^{20}\text{Pt}(\text{nb})$. Assignment of the ^{31}P chemical shifts in the $\text{Pt}(0)$ complexes of L^{20} is difficult due to the lack of similar systems in the literature. Changing a single phenyl group in Ph_3P for a methyl group can shift $\delta(\text{P})$ by 10ppm in Pt complexes (17), so ^{31}P shifts for PPh_3 complexes can only be used as a very rough guide for L^{20} . The resonance at 16.7ppm in figure 6.11 has been assigned to $\text{L}^{20}\text{Pt}(\text{nb})$ and the resonance at 24.3ppm possibly being due to $\text{L}^{20}\text{Pt}(\text{O}_2)$. Removing the uncoordinated norbornene from the sample involved washing with 2x5mL of 40/60 petrol. The petrol more than likely contained small amounts of dissolved O_2 , this small amount of oxygen would be enough to oxidise the $97\mu\text{mol}$ of $\text{L}^{20}\text{Pt}(\text{nb})$. This would explain the increase in the intensity of the resonance at 24.3ppm in figure 6.12, but does not explain the change in the magnitude of the coupling constants.

~~EXMR~~
 FIDUAL 1-20
 DATE 3-1-79
 TIME 14.24
 SOLVENT CDCl₃
 1H 100.62
 13C 101.34
 15N 101.34
 17O 101.34
 19F 101.34
 21Ne 101.34
 23Na 101.34
 25Mg 101.34
 27Al 101.34
 29Si 101.34
 31P 101.34
 33S 101.34
 35Cl 101.34
 37Ar 101.34
 39K 101.34
 41Ca 101.34
 43Sc 101.34
 45Ti 101.34
 47V 101.34
 49Cr 101.34
 51Mn 101.34
 53Fe 101.34
 55Co 101.34
 57Ni 101.34
 59Cu 101.34
 61Zn 101.34
 63Ga 101.34
 65Ge 101.34
 67As 101.34
 69Se 101.34
 71Br 101.34
 73Kr 101.34
 75Rb 101.34
 77Sr 101.34
 79Y 101.34
 81Zr 101.34
 83Nb 101.34
 85Mo 101.34
 87Tc 101.34
 89Ru 101.34
 91Rh 101.34
 93Pd 101.34
 95Ag 101.34
 97Cd 101.34
 99In 101.34
 101Sn 101.34
 103Sb 101.34
 105Te 101.34
 107I 101.34
 109Xe 101.34
 111Ba 101.34
 113La 101.34
 115Ce 101.34
 117Pr 101.34
 119Nd 101.34
 121Pm 101.34
 123Sm 101.34
 125Eu 101.34
 127Gd 101.34
 129Tb 101.34
 131Dy 101.34
 133Ho 101.34
 135Er 101.34
 137Tm 101.34
 139Yb 101.34
 141Lu 101.34
 143Hf 101.34
 145Ta 101.34
 147W 101.34
 149Re 101.34
 151Os 101.34
 153Ir 101.34
 155Pt 101.34
 157Au 101.34
 159Hg 101.34
 161Tl 101.34
 163Pb 101.34
 165Bi 101.34
 167Po 101.34
 169At 101.34
 171Rn 101.34
 173Fr 101.34
 175Ac 101.34
 177Th 101.34
 179Pa 101.34
 181U 101.34
 183Np 101.34
 185Pu 101.34
 187Am 101.34
 189Cm 101.34
 191Bk 101.34
 193Cf 101.34
 195Es 101.34
 197Fm 101.34
 199Md 101.34
 201No 101.34
 203Lr 101.34
 205Hf 101.34
 207Ta 101.34
 209W 101.34
 211Re 101.34
 213Os 101.34
 215Ir 101.34
 217Pt 101.34
 219Au 101.34
 221Hg 101.34
 223Tl 101.34
 225Pb 101.34
 227Bi 101.34
 229Po 101.34
 231At 101.34
 233Rn 101.34
 235Fr 101.34
 237Ac 101.34
 239Th 101.34
 241Pa 101.34
 243U 101.34
 245Np 101.34
 247Pu 101.34
 249Am 101.34
 251Cm 101.34
 253Bk 101.34
 255Cf 101.34
 257Es 101.34
 259Fm 101.34
 261Md 101.34
 263No 101.34
 265Lr 101.34
 267Hf 101.34
 269Ta 101.34
 271W 101.34
 273Re 101.34
 275Os 101.34
 277Ir 101.34
 279Pt 101.34
 281Au 101.34
 283Hg 101.34
 285Tl 101.34
 287Pb 101.34
 289Bi 101.34
 291Po 101.34
 293At 101.34
 295Rn 101.34
 297Fr 101.34
 299Ac 101.34
 301Th 101.34
 303Pa 101.34
 305U 101.34
 307Np 101.34
 309Pu 101.34
 311Am 101.34
 313Cm 101.34
 315Bk 101.34
 317Cf 101.34
 319Es 101.34
 321Fm 101.34
 323Md 101.34
 325No 101.34
 327Lr 101.34
 329Hf 101.34
 331Ta 101.34
 333W 101.34
 335Re 101.34
 337Os 101.34
 339Ir 101.34
 341Pt 101.34
 343Au 101.34
 345Hg 101.34
 347Tl 101.34
 349Pb 101.34
 351Bi 101.34
 353Po 101.34
 355At 101.34
 357Rn 101.34
 359Fr 101.34
 361Ac 101.34
 363Th 101.34
 365Pa 101.34
 367U 101.34
 369Np 101.34
 371Pu 101.34
 373Am 101.34
 375Cm 101.34
 377Bk 101.34
 379Cf 101.34
 381Es 101.34
 383Fm 101.34
 385Md 101.34
 387No 101.34
 389Lr 101.34
 391Hf 101.34
 393Ta 101.34
 395W 101.34
 397Re 101.34
 399Os 101.34
 401Ir 101.34
 403Pt 101.34
 405Au 101.34
 407Hg 101.34
 409Tl 101.34
 411Pb 101.34
 413Bi 101.34
 415Po 101.34
 417At 101.34
 419Rn 101.34
 421Fr 101.34
 423Ac 101.34
 425Th 101.34
 427Pa 101.34
 429U 101.34
 431Np 101.34
 433Pu 101.34
 435Am 101.34
 437Cm 101.34
 439Bk 101.34
 441Cf 101.34
 443Es 101.34
 445Fm 101.34
 447Md 101.34
 449No 101.34
 451Lr 101.34
 453Hf 101.34
 455Ta 101.34
 457W 101.34
 459Re 101.34
 461Os 101.34
 463Ir 101.34
 465Pt 101.34
 467Au 101.34
 469Hg 101.34
 471Tl 101.34
 473Pb 101.34
 475Bi 101.34
 477Po 101.34
 479At 101.34
 481Rn 101.34
 483Fr 101.34
 485Ac 101.34
 487Th 101.34
 489Pa 101.34
 491U 101.34
 493Np 101.34
 495Pu 101.34
 497Am 101.34
 499Cm 101.34
 501Bk 101.34
 503Cf 101.34
 505Es 101.34
 507Fm 101.34
 509Md 101.34
 511No 101.34
 513Lr 101.34
 515Hf 101.34
 517Ta 101.34
 519W 101.34
 521Re 101.34
 523Os 101.34
 525Ir 101.34
 527Pt 101.34
 529Au 101.34
 531Hg 101.34
 533Tl 101.34
 535Pb 101.34
 537Bi 101.34
 539Po 101.34
 541At 101.34
 543Rn 101.34
 545Fr 101.34
 547Ac 101.34
 549Th 101.34
 551Pa 101.34
 553U 101.34
 555Np 101.34
 557Pu 101.34
 559Am 101.34
 561Cm 101.34
 563Bk 101.34
 565Cf 101.34
 567Es 101.34
 569Fm 101.34
 571Md 101.34
 573No 101.34
 575Lr 101.34
 577Hf 101.34
 579Ta 101.34
 581W 101.34
 583Re 101.34
 585Os 101.34
 587Ir 101.34
 589Pt 101.34
 591Au 101.34
 593Hg 101.34
 595Tl 101.34
 597Pb 101.34
 599Bi 101.34
 601Po 101.34
 603At 101.34
 605Rn 101.34
 607Fr 101.34
 609Ac 101.34
 611Th 101.34
 613Pa 101.34
 615U 101.34
 617Np 101.34
 619Pu 101.34
 621Am 101.34
 623Cm 101.34
 625Bk 101.34
 627Cf 101.34
 629Es 101.34
 631Fm 101.34
 633Md 101.34
 635No 101.34
 637Lr 101.34
 639Hf 101.34
 641Ta 101.34
 643W 101.34
 645Re 101.34
 647Os 101.34
 649Ir 101.34
 651Pt 101.34
 653Au 101.34
 655Hg 101.34
 657Tl 101.34
 659Pb 101.34
 661Bi 101.34
 663Po 101.34
 665At 101.34
 667Rn 101.34
 669Fr 101.34
 671Ac 101.34
 673Th 101.34
 675Pa 101.34
 677U 101.34
 679Np 101.34
 681Pu 101.34
 683Am 101.34
 685Cm 101.34
 687Bk 101.34
 689Cf 101.34
 691Es 101.34
 693Fm 101.34
 695Md 101.34
 697No 101.34
 699Lr 101.34
 701Hf 101.34
 703Ta 101.34
 705W 101.34
 707Re 101.34
 709Os 101.34
 711Ir 101.34
 713Pt 101.34
 715Au 101.34
 717Hg 101.34
 719Tl 101.34
 721Pb 101.34
 723Bi 101.34
 725Po 101.34
 727At 101.34
 729Rn 101.34
 731Fr 101.34
 733Ac 101.34
 735Th 101.34
 737Pa 101.34
 739U 101.34
 741Np 101.34
 743Pu 101.34
 745Am 101.34
 747Cm 101.34
 749Bk 101.34
 751Cf 101.34
 753Es 101.34
 755Fm 101.34
 757Md 101.34
 759No 101.34
 761Lr 101.34
 763Hf 101.34
 765Ta 101.34
 767W 101.34
 769Re 101.34
 771Os 101.34
 773Ir 101.34
 775Pt 101.34
 777Au 101.34
 779Hg 101.34
 781Tl 101.34
 783Pb 101.34
 785Bi 101.34
 787Po 101.34
 789At 101.34
 791Rn 101.34
 793Fr 101.34
 795Ac 101.34
 797Th 101.34
 799Pa 101.34
 801U 101.34
 803Np 101.34
 805Pu 101.34
 807Am 101.34
 809Cm 101.34
 811Bk 101.34
 813Cf 101.34
 815Es 101.34
 817Fm 101.34
 819Md 101.34
 821No 101.34
 823Lr 101.34
 825Hf 101.34
 827Ta 101.34
 829W 101.34
 831Re 101.34
 833Os 101.34
 835Ir 101.34
 837Pt 101.34
 839Au 101.34
 841Hg 101.34
 843Tl 101.34
 845Pb 101.34
 847Bi 101.34
 849Po 101.34
 851At 101.34
 853Rn 101.34
 855Fr 101.34
 857Ac 101.34
 859Th 101.34
 861Pa 101.34
 863U 101.34
 865Np 101.34
 867Pu 101.34
 869Am 101.34
 871Cm 101.34
 873Bk 101.34
 875Cf 101.34
 877Es 101.34
 879Fm 101.34
 881Md 101.34
 883No 101.34
 885Lr 101.34
 887Hf 101.34
 889Ta 101.34
 891W 101.34
 893Re 101.34
 895Os 101.34
 897Ir 101.34
 899Pt 101.34
 901Au 101.34
 903Hg 101.34
 905Tl 101.34
 907Pb 101.34
 909Bi 101.34
 911Po 101.34
 913At 101.34
 915Rn 101.34
 917Fr 101.34
 919Ac 101.34
 921Th 101.34
 923Pa 101.34
 925U 101.34
 927Np 101.34
 929Pu 101.34
 931Am 101.34
 933Cm 101.34
 935Bk 101.34
 937Cf 101.34
 939Es 101.34
 941Fm 101.34
 943Md 101.34
 945No 101.34
 947Lr 101.34
 949Hf 101.34
 951Ta 101.34
 953W 101.34
 955Re 101.34
 957Os 101.34
 959Ir 101.34
 961Pt 101.34
 963Au 101.34
 965Hg 101.34
 967Tl 101.34
 969Pb 101.34
 971Bi 101.34
 973Po 101.34
 975At 101.34
 977Rn 101.34
 979Fr 101.34
 981Ac 101.34
 983Th 101.34
 985Pa 101.34
 987U 101.34
 989Np 101.34
 991Pu 101.34
 993Am 101.34
 995Cm 101.34
 997Bk 101.34
 999Cf 101.34
 1001Es 101.34
 1003Fm 101.34
 1005Md 101.34
 1007No 101.34
 1009Lr 101.34
 1011Hf 101.34
 1013Ta 101.34
 1015W 101.34
 1017Re 101.34
 1019Os 101.34
 1021Ir 101.34
 1023Pt 101.34
 1025Au 101.34
 1027Hg 101.34
 1029Tl 101.34
 1031Pb 101.34
 1033Bi 101.34
 1035Po 101.34
 1037At 101.34
 1039Rn 101.34
 1041Fr 101.34
 1043Ac 101.34
 1045Th 101.34
 1047Pa 101.34
 1049U 101.34
 1051Np 101.34
 1053Pu 101.34
 1055Am 101.34
 1057Cm 101.34
 1059Bk 101.34
 1061Cf 101.34
 1063Es 101.34
 1065Fm 101.34
 1067Md 101.34
 1069No 101.34
 1071Lr 101.34
 1073Hf 101.34
 1075Ta 101.34
 1077W 101.34
 1079Re 101.34
 1081Os 101.34
 1083Ir 101.34
 1085Pt 101.34
 1087Au 101.34
 1089Hg 101.34
 1091Tl 101.34
 1093Pb 101.34
 1095Bi 101.34
 1097Po 101.34
 1099At 101.34
 1101Rn 101.34
 1103Fr 101.34
 1105Ac 101.34
 1107Th 101.34
 1109Pa 101.34
 1111U 101.34
 1113Np 101.34
 1115Pu 101.34
 1117Am 101.34
 1119Cm 101.34
 1121Bk 101.34
 1123Cf 101.34
 1125Es 101.34
 1127Fm 101.34
 1129Md 101.34
 1131No 101.34
 1133Lr 101.34
 1135Hf 101.34
 1137Ta 101.34
 1139W 101.34
 1141Re 101.34
 1143Os 101.34
 1145Ir 101.34
 1147Pt 101.34
 1149Au 101.34
 1151Hg 101.34
 1153Tl 101.34
 1155Pb 101.34
 1157Bi 101.34
 1159Po 101.34
 1161At 101.34
 1163Rn 101.34
 1165Fr 101.34
 1167Ac 101.34
 1169Th 101.34
 1171Pa 101.34
 1173U 101.34
 1175Np 101.34
 1177Pu 101.34
 1179Am 101.34
 1181Cm 101.34
 1183Bk 101.34
 1185Cf 101.34
 1187Es 101.34
 1189Fm 101.34
 1191Md 101.34
 1193No 101.34
 1195Lr 101.34
 1197Hf 101.34
 1199Ta 101.34
 1201W 101.34
 1203Re 101.34
 1205Os 101.34
 1207Ir 101.34
 1209Pt 101.34
 1211Au 101.34
 1213Hg 101.34
 1215Tl 101.34
 1217Pb 101.34
 1219Bi 101.34
 1221Po 101.34
 1223At 101.34
 1225Rn 101.34
 1227Fr 101.34
 1229Ac 101.34
 1231Th 101.34
 1233Pa 101.34
 1235U 101.34
 1237Np 101.34
 1239Pu 101.34
 1241Am 101.34
 1243Cm 101.34
 1245Bk 101.34
 1247Cf 101.34
 1249Es 101.34
 1251Fm 101.34
 1253Md 101.34
 1255No 101.34
 1257Lr 101.34
 1259Hf 101.34
 1261Ta 101.34
 1263W 101.34
 1265Re 101.34
 1267Os 101.34
 1269Ir 101.34
 1271Pt 101.34
 1273Au 101.34
 1275Hg 101.34
 1277Tl 101.34
 1279Pb 101.34
 1281Bi 101.34
 1283Po 101.34
 1285At 101.34
 1287Rn 101.34
 1289Fr 101.34
 1291Ac 101.34
 1293Th 101.34
 1295Pa 101.34
 1297U 101.34
 1299Np 101.34
 1301Pu 101.34
 1303Am 101.34
 1305Cm 101.34
 1307Bk 101.34
 1309Cf 101.34
 1311Es 101.34
 1313Fm 101.34
 1315Md 101.34
 1317No 101.34
 1319Lr 101.34
 1321Hf 101.34
 1323Ta 101.34
 1325W 101.34
 1327Re 101.34
 1329Os 101.34
 1331Ir 101.34
 1333Pt 101.34
 1335Au 101.34
 1337Hg 101.34
 1339Tl 101.34
 1341Pb 101.34
 1343Bi 101.34
 1345Po 101.34
 1347At 101.34
 1349Rn 101.34
 1351Fr 101.34
 1353Ac 101.34
 1355Th 101.34
 1357Pa 101.34
 1359U 101.34
 1361Np 101.34
 1363Pu 101.34
 1365Am 101.34
 1367Cm 101.34
 1369Bk 101.34
 1371Cf 101.34
 1373Es 101.34
 1375Fm 101.34
 1377Md 101.34
 1379No 101.34
 1381Lr 101.34
 1383Hf 101.34
 1385Ta 101.34
 1387W 101.34
 1389Re 101.34
 1391Os 101.34
 1393Ir 101.34
 1395Pt 101.34
 1397Au 101.34
 1399Hg 101.34
 1401Tl 101.34
 1403Pb 101.34
 1405Bi 101.34
 1407Po 101.34
 1409At 101.34
 1411Rn 101.34
 1413Fr 101.34
 1415Ac 101.34
 1417Th 101.34
 1419Pa 101.34
 1421U 101.34
 1423Np 101.34
 1425Pu 101.34
 1427Am 101.34
 1429Cm 101.34
 1431Bk 101.34
 1433Cf 101.34
 1435Es 101.34
 1437Fm 101.34
 1439Md 101.34
 1441No 101.34
 1443Lr 101.34
 1445Hf 101.34
 1447Ta 101.34
 1449W 101.34
 1451Re 101.34
 1453Os 101.34
 1455Ir 101.34
 1457Pt 101.34
 1459Au 101.34
 1461Hg 101.34
 1463Tl 101.34
 1465Pb 101.34
 1467Bi 101.34
 1469Po 101.34
 1471At 101.34
 1473Rn 101.34
 1475Fr 101.34
 1477Ac 101.34
 1479Th 101.34
 1481Pa 101.34
 1483U 101.34
 1485Np 101.34
 1487Pu 101.34
 1489Am 101.34
 1491Cm 101.34
 1493Bk

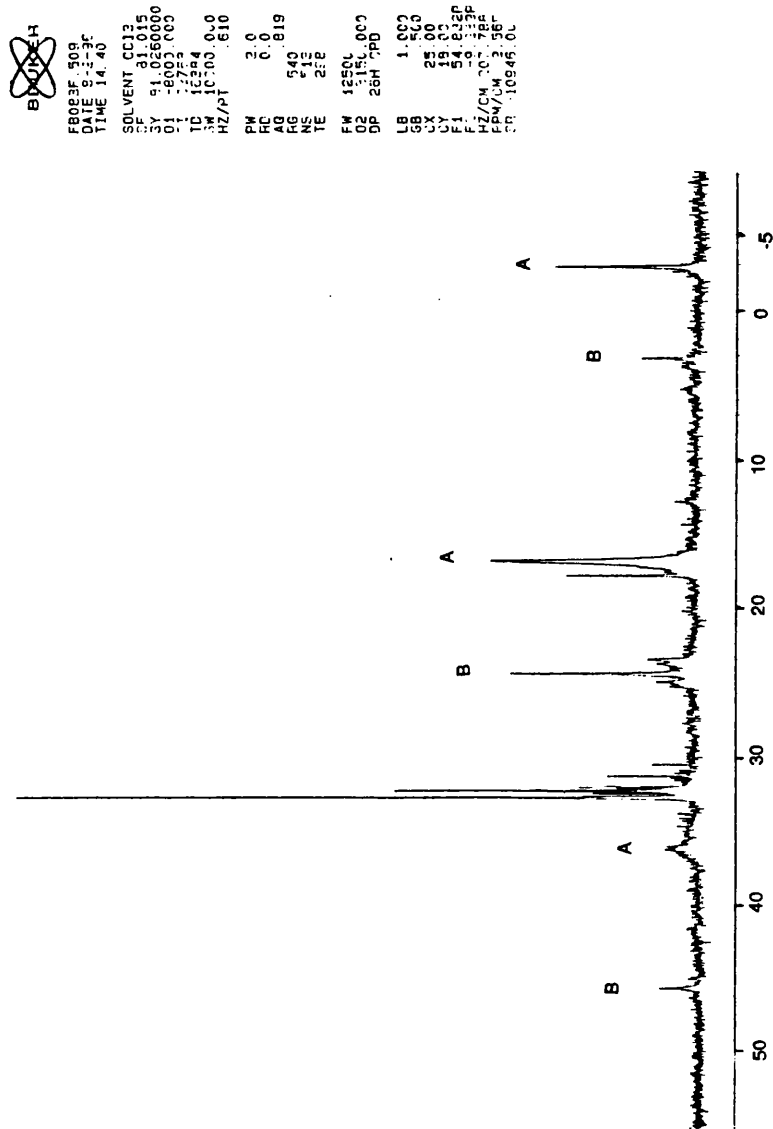


Figure 6.11. ^{31}P NMR spectrum of $\text{Pt}(\text{nb})_3 + \text{L}^{20}$ in CDCl_3

~~BRUKER~~
 F819PAL 001
 AU PROG
 LONGTERM
 DATE 20-2-96
 TIME 9.4C
 SOLVENT D2O
 SF 81.025330
 SY 81.025330
 C1 -5000.000
 S1 2768
 TD 16384
 SW 10000.000
 FZ/P1 .610
 PW 2.0
 PD 0.0
 AD 200
 RG 63000
 TE 398
 FM 12500
 D2 3150.000
 DP 25H CPD
 LB 1.000
 CB 25.00
 CY 15.00
 F1 98.020P
 F2 -25.40EP
 PZ/CM 399.376
 PCW/CA 4.817
 SR -10940.00

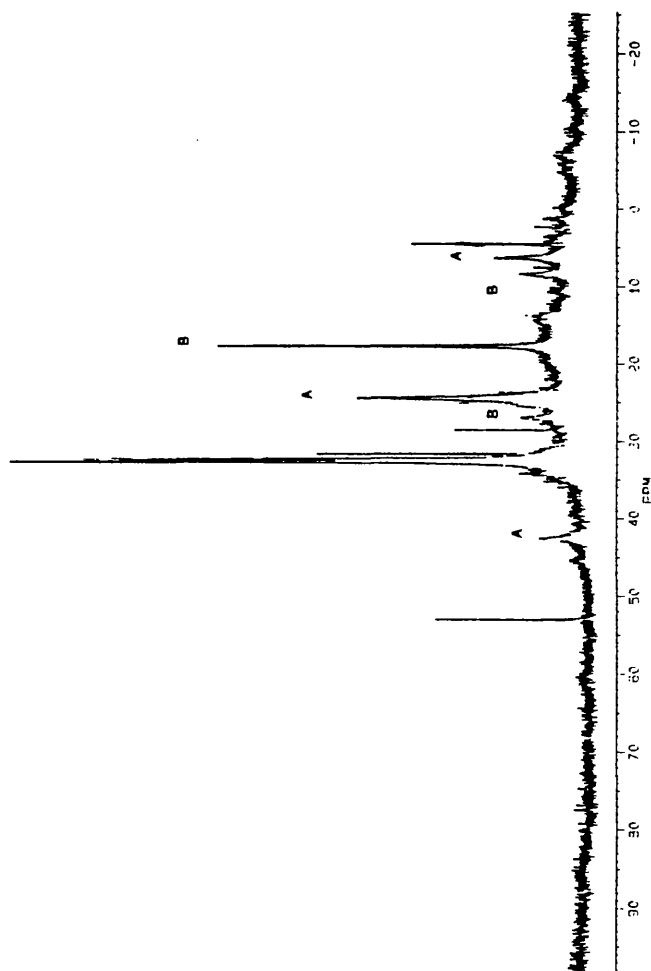


Figure 6.12. ^{31}P NMR spectrum of $\text{Pt}(\text{nb})_3 + \text{L}^{20}$ in CDCl_3 after uncoordinated norbornene has been removed

6.4.2 Gold(I) complex

The gold(I) complex of L^{20} was prepared by the slow addition of L^{20} to a solution containing two mole equivalents of AuCl. Recrystallised from chloroform/diethyl ether yielded the complex as a white microcrystalline solid. The ^{31}P NMR spectrum of the complex contained a single resonance at +28.27ppm corresponding to coordinated phosphine. The ^{31}P shift is in agreement with other gold(I) complexes of Ph_2PR ligands (**18**, **19**). Gold(I) chloride complexes of phosphine ligands generally have a linear arrangement of the phosphine and chloride around the Au centre. The structure of $L^{20}(\text{AuCl})_2$ would therefore be expected to consist of two linear AuCl centres coordinated to the phosphine arms of the macrocycle with the amine functions of the ligand remaining uncoordinated. The gold(I) complex of L^{20} reacted with $(\text{MeCN})_3\text{Mo}(\text{CO})_3$ in dichloromethane, but the complex was too unstable in solution to allow any detailed analysis.

6.5 METAL COMPLEXES OF L¹⁶

6.5.1 Zinc(II) complex

Reaction of L¹⁶ with anhydrous ZnCl₂ in ethanol followed by the addition of excess LiClO₄ precipitated [ZnL¹⁶Cl(μ-Cl)ZnL¹⁶Cl]ClO₄ which was recrystallised from acetonitrile. The crystal structure of the dimeric cation is shown in figure 6.13. The dimer is asymmetric in which both zinc atoms are coordinated by the three amine functions and the pendant phosphine arm of L¹⁶. In the Zn1 half of the dimer, the zinc is further coordinated by two chloride ions giving pseudo-octahedral geometry. The other zinc (Zn2) is formally five-coordinate, but forms a long bond with Cl2 (2.909 Å) to achieve pseudo-octahedral geometry. The Zn-N bond lengths are all unequal. The longest Zn-N bonds are to the nitrogens bearing the pendant arm, whereas the shortest Zn-N bonds are to the nitrogens *trans* to the phosphine (figure 6.14 & table 6.1). There are very few structurally characterised zinc phosphines in the literature. The closest structure to the dimer is Zn{(CH₂)₃PPh₂} in which the phosphine is part of a five membered chelate ring (20), with an average Zn-P bond length of 2.589 Å. The other relevant structures (21, 22) are [X₃ZnPPPh₃] tetrahedrons (where X=Br, Cl) and have Zn-P distances of 2.425 and 2.392 Å. The [Cl₃ZnPPPh₃] tetrahedron is part of V(THF)₂{(μ-Cl)₂ZnClPPPh₃}₂, where two of the three chloride ions

form Zn(II)-(μ-Cl)-V(II) bridges. The Zn-Cl distances for the bridging chlorides in the Zn₂V complex are 2.293 and 2.324 Å, much shorter than the corresponding distances in the zinc dimer of L¹⁶. The terminal Zn-Cl distance in the trinuclear complex (2.197 Å) is also much shorter than the corresponding distances in the zinc dimer of L¹⁶.

Zn1-N11	2.301(10) Å	Zn2-N21	2.360(13) Å
Zn1-N14	2.207(10) Å	Zn2-N24	2.0993(11) Å
Zn1-N17	2.112(10) Å	Zn2-N27	2.199(12) Å
Zn1-P1	2.518(4) Å	Zn2-P2	2.524(4) Å
Zn1-Cl1	2.378(4) Å	Zn2-Cl3	2.361(4) Å
Zn1-Cl2	2.785(5) Å	Zn2-Cl2	2.909(6) Å
N11-Zn1-N14	79.8(4)°	N21-Zn2-N24	79.6(5)°
N11-Zn1-N17	78.2(4)°	N21-Zn2-N27	78.6(5)°
N14-Zn1-N17	80.0(4)°	N24-Zn2-N27	81.1(5)°
P1-Zn1-N11	91.0(3)°	P2-Zn2-N21	87.2(3)°
P1-Zn1-N14	101.5(3)°	P2-Zn2-N27	104.9(3)°
P1-Zn1-Cl1	93.15(13)°	P2-Zn2-Cl3	94.61(13)°
P1-Zn1-Cl2	88.36(13)°		
Cl1-Zn1-Cl2	95.08(13)°		

Table 6.1. Selected bond lengths and angles for [ZnL¹⁶Cl(μ-Cl)ZnL¹⁶Cl]⁺

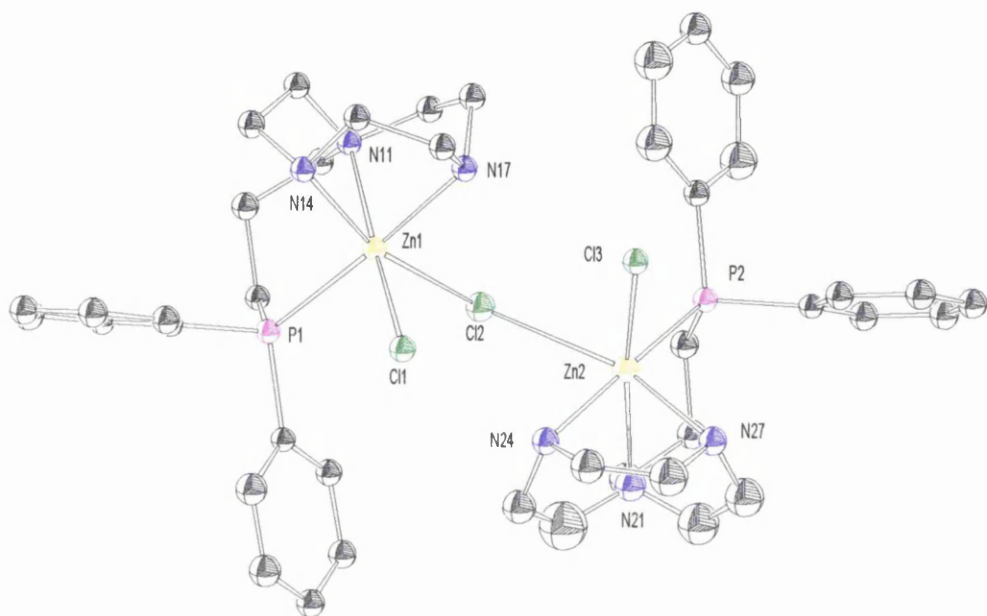


Figure 6.13. Crystal Structure of $[\text{ZnL}^{16}\text{Cl}(\mu\text{-Cl})\text{ZnL}^{16}\text{Cl}]^+$

Crystal data for $\text{C}_{42}\text{H}_{60}\text{Cl}_4\text{N}_6\text{O}_4\text{P}_2\text{Zn}_2$: $M = 1047.44$; Monoclinic; Space Group $P2_1/a$; $a = 15.806(6)\text{\AA}$; $b = 17.069(8)\text{\AA}$; $c = 17.955(4)\text{\AA}$; $\beta = 107.11(4)^\circ$; $U = 4630(3)\text{\AA}^3$; $Z = 4$; $D_{\text{calc.}} = 1.503\text{gcm}^{-3}$; $F(000) = 2176$; $R(R_w^2) = 0.109(0.368)$.

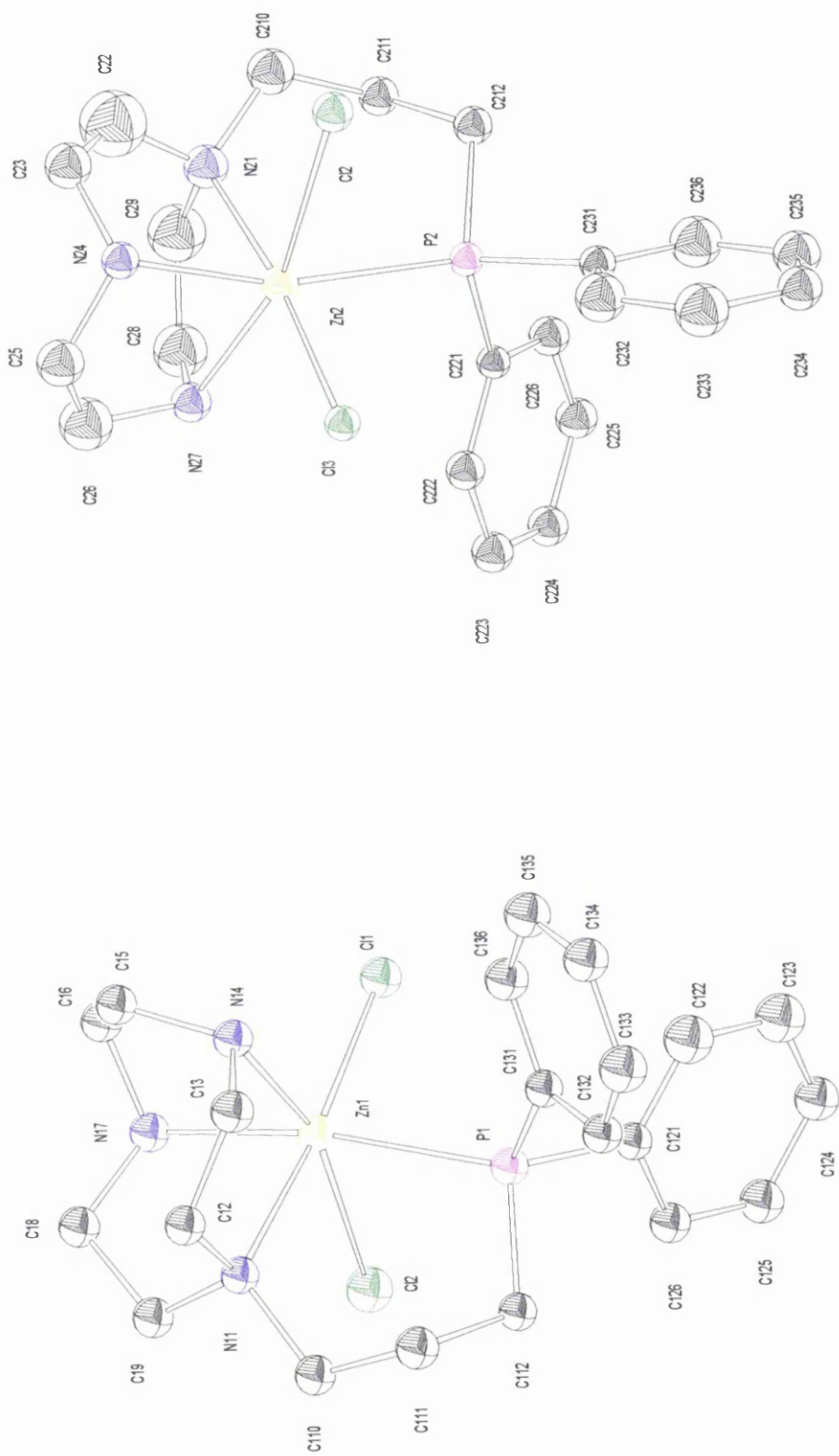


Figure 6.14. Selected views of the asymmetric halves of the zinc dimer

6.5.2 Nickel(II) complexes

Reaction of L^{16} with anhydrous $NiCl_2$ in ethanol followed by the addition of excess $LiClO_4$ produced $[NiL^{16}Cl(EtOH)]ClO_4$ (figure 6.15). The nickel atom is coordinated to the three amine functions and the phosphine pendant arm of L^{16} . An ethanol molecule and chloride ion complete the coordination sphere around the nickel centre to give a pseudo-octahedral geometry. The bonding trends in the complex are similar to those observed in the zinc dimer. The longest Ni-N bond is to the nitrogen bearing the pendant arm and the shortest Ni-N bond is to the nitrogen *trans* to the phosphine (table 6.2). The Ni-P distance is much longer than the average of Ni-PPh₃ bond lengths (2.321Å) and well above the upper quartile (2.331Å) (23).

Ni1-N1	2.137(3)Å	Ni1-P1	2.455(1)Å
Ni1-N4	2.093(3)Å	Ni1-O1	2.171(2)Å
Ni1-N7	2.094(3)Å	Ni1-Cl1	2.438(1)Å
N1-Ni1-N4	83.72(11)°	N1-Ni1-O1	170.60(10)°
N1-Ni1-N7	83.58(10)°	N4-Ni1-P1	178.43(8)°
N4-Ni1-N7	81.97(11)°	N7-Ni1-Cl1	172.67(8)°
P1-Ni1-O1	94.57(7)°	O1-Ni1-Cl1	86.18(7)°
P1-Ni1-Cl1	88.54(3)°		

Table 6.2. Selected bond lengths and angles for $[NiL^{16}Cl(EtOH)]^+$

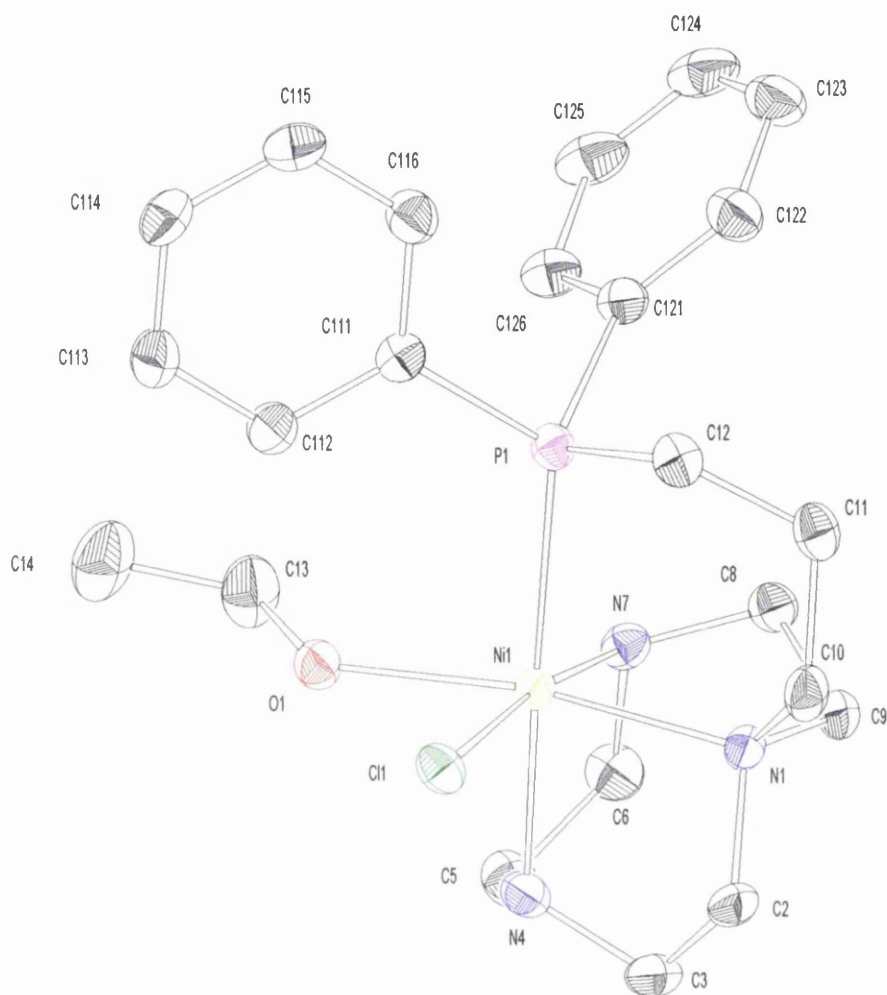


Figure 6.15. *Crystal Structure of the $[\text{NiL}^{16}\text{Cl}(\text{EtOH})]^+$ cation*

Crystal data for $\text{C}_{23}\text{H}_{38}\text{Cl}_2\text{N}_3\text{NiO}_6\text{P}$: $M=613.14$; Triclinic; Space Group $P\bar{1}$; $a=9.8208(15)\text{\AA}$; $b=11.286(2)\text{\AA}$; $c=14.2217(12)\text{\AA}$; $\alpha=107.142(9)^\circ$; $\beta=105.117(9)^\circ$; $\gamma=102.798(12)^\circ$; $U=1376(3)\text{\AA}^3$; $Z=2$; $D_{\text{calc.}}=1.480\text{gcm}^{-3}$; $F(000)=644$; $R(R_w^2)=0.0627(0.1079)$.

The addition of KSCN to $[\text{NiL}^{16}\text{Cl}(\text{EtOH})]^+$ displaced the coordinated chloride and ethanol to give a new nickel(II) complex containing two coordinated thiocyanate groups (figure 6.16). The thiocyanate coordinates to the nickel(II) via the nitrogen function of the ligand. The Ni-N bonds of the macrocycle follow the same trends observed in $[\text{NiL}^{16}\text{Cl}(\text{EtOH})]^+$, but the bond distances are slightly longer in the thiocyanate complex (table 6.3). The Ni-P bond length in $[\text{NiL}^{16}(\text{NCS})_2]$ is slightly shorter to that observed in $[\text{NiL}^{16}\text{Cl}(\text{EtOH})]^+$, but is still very much longer than those observed for Ni- PPh_3 . The closest structure to $[\text{NiL}^{16}(\text{NCS})_2]$ is the *trans* phosphine complex $[\text{Ni}(\text{NCS})_4\{\text{P}(\text{CH}_2\text{CH}_2\text{CN})_3\}_2]^{2-}$ (**24**) in which the Ni-P bond length is 2.420 Å and is only slightly longer than that in $[\text{NiL}^{16}(\text{NCS})_2]$. The Ni-NCS bond lengths of $[\text{Ni}(\text{NCS})_4\{\text{P}(\text{CH}_2\text{CH}_2\text{CN})_3\}_2]^{2-}$ are also very similar at 2.072 and 2.068 Å.

Ni1-N1	2.187(3) Å	Ni1-P1	2.4165(9) Å
Ni1-N4	2.109(3) Å	Ni1-N21	2.066(3) Å
Ni1-N7	2.128(3) Å	Ni1-N31	2.057(3) Å
N1-Ni1-N4	82.7(1)°	N1-Ni1-N21	170.3(1)°
N1-Ni1-N7	81.6(1)°	N4-Ni1-P1	176.61(9)°
N4-Ni1-N7	80.6(1)°	N7-Ni1-N31	169.0(1)°
P1-Ni1-N21	92.61(9)°	N21-Ni1-N31	95.1(1)°
P1-Ni1-N31	89.20(9)°		

Table 6.3. Selected bond lengths and angles for $[\text{NiL}^{16}(\text{NCS})_2]$

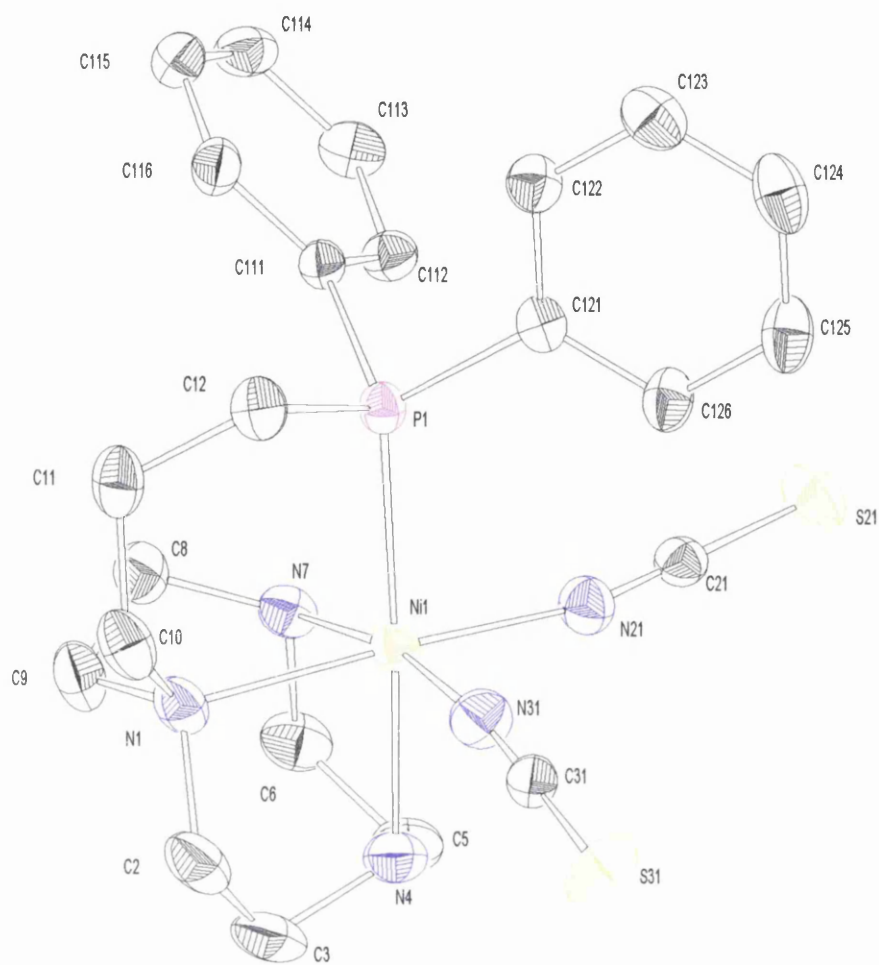


Figure 6.16. *Crystal Structure of $[\text{NiL}^{16}(\text{NCS})_2]$*

Crystal data for $\text{C}_{24}\text{H}_{33}\text{N}_6\text{NiO}_2\text{PS}_2$: $M=591.36$; Monoclinic; Space Group $C2/c$; $a=33.195(4)\text{\AA}$; $b=10.618(1)\text{\AA}$; $c=17.147(1)\text{\AA}$; $\beta=111.45(1)^\circ$; $U=5625.1(9)\text{\AA}^3$; $Z=8$; $D_{\text{calc.}}=1.397\text{gcm}^{-3}$; $F(000)=2480$; $R(R_w^2)=0.1122(0.1429)$.

6.6 METAL COMPLEXES OF L¹⁸

6.6.1 Cobalt(II) complex

The cobalt(II) complex of L¹⁸ is octahedral in methanol solution and tetrahedral in the solid state, the octahedral geometry could arise from coordinated methanol or chloride ions or a mixture of both. Ethanol solutions of the complex are blue indicating that the complex is tetrahedral. This transition between octahedral and tetrahedral geometry is common for octahedral complexes and is explained by the small energy difference between octahedral and tetrahedral cobalt(II) complexes. The cobalt(II) complex of L¹⁸ is relatively air-stable in the solid state and in solution, unlike the analogous cobalt(II) complex of L²³ which oxidises rapidly in solution.

6.6.2 Copper(I) complex

L^{18} reacts with $Cu(MeCN)_4BF_4$ in dichloromethane to give a yellow copper(I) solution. Tolman *et al.* (25) reported the synthesis and characterisation of a similar complex $[(^iPr_3TACN)Cu(PPh_3)]PF_6$ where the phosphine was not part of the macrocyclic ligand. $[(^iPr_3TACN)Cu(PPh_3)]PF_6$ was crystallised from CH_2Cl_2/Et_2O , but the copper(I) complex of L^{18} was very oxygen sensitive and oxidised to the copper(II) complex when diethyl ether was diffused into the dichloromethane solution of the complex. This air-sensitive behaviour is similar to that observed in the olefin coordinated complex $[CuL^{11}]BF_4$. Attempts at crystallising the copper(II) complex were unsuccessful.

6.7 REFERENCES

1. E.P. Kyba, C.W. Hudson, M.J. McPhaul, A.M. John, *J. Am. Chem. Soc.*, 1977, **99**, 8053.
2. B.N. Diel, R.C. Haltiwanger, A.D. Norman, *J. Am. Chem. Soc.*, 1982, **104**, 4700.
3. P.G. Edwards, J.S. Fleming, S.S. Liyanage, *Inorg. Chem.*, 1996, **35**, 4568.
4. H. Hope, M. Viggiano, B. Moezzi, P.P. Power, *Inorg. Chem.*, 1984, **23**, 2550.
5. A. Carroy, C.R. Langick, J-M. Lehn, K.E. Matthes, D. Parker, *Helv. Chim. Acta*, 1986, **69**, 580.
6. R.D. Peacock, *Personal communication*.
7. D. Ellis, *Personal communication*.
8. F.A. Cotton, G. Wilinon, *Advanced Inorganic Chemistry*, 5th ed., Wiley, New York, p739.
9. P. Chaudhuri, K. Wieghardt, Y.H. Tsay, C. Krüger, *Inorg. Chem.*, 1984, **23**, 427.
10. G. Backes-Dahmann, W. Herrmann, K. Wieghardt, J. Weiss, *Inorg. Chem.*, 1985, **24**, 485.
11. P.A. Lovatt, *B.Sc. Thesis*, 1993, University of Glasgow.

- 12.T. Ando, M. Kita, K. Kashiwabara, J. Fujita, S. Kurachi, S. Ohba, *Bull. Chem. Soc. Jpn.*, 1992, **65**, 2748.
- 13.M. Green, J.A.K. Howard, J.L. Spencer, F.G.A. Stone, *J. Chem. Soc., Dalton Trans.*, 1977, 271.
- 14.P.G. Gassman, I.G Cesa, *Organometallics*, 1984, **3**, 119.
- 15.R.G. Nuzzo, T.J. McCarthy, G.M. Whitesides, *Inorg. Chem.*, 1981, **20**, 1312.
- 16.A. Sen, J. Halpern, *Inorg. Chem.*, 1980, **19**, 1073.
- 17.J.D Kennedy, W. McFarlane, R.J. Puddephatt, P.J. Thompson, *J. Chem. Soc., Dalton Trans.*, 1976, 874.
- 18.R. Turpin, A-M. Larssonneur, J. Jaud, P. Castan, *Inorg. Chim. Acta*, 1995, **237**, 207.
- 19.B. Tzeng, W. Lo, C. Che, S. Peng, *J. Chem. Soc., Chem. Com.*, 1996, 181.
- 20.J. Dekker, J.W. Munninghoff, J. Boersma, A.L. Spek, *Organometallics*, 1987, **6**, 1236.
- 21.R.E. DeSimone, G.D. Stucky, *Inorg. Chem.*, 1971, **10**, 1808.
- 22.F.A. Cotton, S.A. Duraj, W.J. Roth, C.D. Schmulbach, *Inorg. Chem.*, 1985, **24**, 525.
- 23.A.G. Orpen, L. Brammer, F.H. Allen, O. Kennard, D.G. Watson, R. Taylor, *J. Chem. Soc., Dalton Trans.*, 1989, S1.

24.B.M. Foxman, H. Mazurek, *Inorg. Chem.*, 1979, **18**, 113.

25.J.A. Halfen, S. Mahapatra, E.W. Wilkinson, A.J. Gengenbach, V.G.

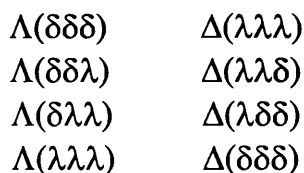
Young, L. Que, W.B. Tolman, *J. Am. Chem. Soc.*, 1996, **118**, 763.

CHAPTER 7

CHIRAL LIGANDS AND HARD PENDANT DONOR ARM MACROCYCLES

7.1 INTRODUCTION

Most of the transition metal complexes formed with hexadentate derivatives of TACN are six coordinate structures. As mentioned in chapter one, there exist two sources of chirality in a six coordinate structure and complexes of hexadentate derivatives of TACN usually exhibit both sources of chirality; the macrocyclic ring is the source of conformation isomerism and the pendant arms are the second source of chirality in the form of configurational isomerism. Thus for a complex where the ligand contains three pendant arms there are 4 possible diastereomeric molecules (and their enantiomers):

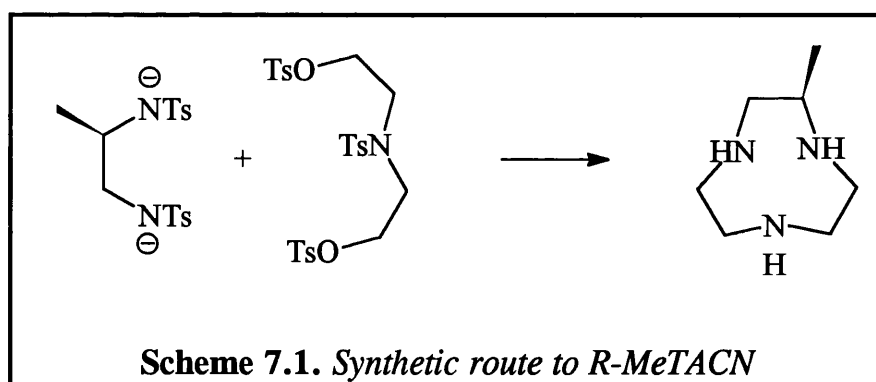


Usually one diastereoisomer is energetically more favourable and predominates, but its enantiomer will still be present in an equal amount forming a racemic mixture. If the pendant arm forms chelate rings with a twist, then the system is further complicated. Crystallisation of these complexes can be difficult due to more than one chiral species in solution, as was evident with achiral THETACN. The hexadentate ligand THETACN forms 6 coordinate complexes with a variety of metals, none of which have been characterised by X-ray crystallography to date. Introduction of an

external source of chirality such as a chiral counterion allows separation of diastereoisomers, but the simplest way to introduce chirality to the system, at least theoretically, is to use a chiral ligand. Introduction of asymmetric carbon atoms into a chelate ligand often brings about remarkable stereoselectivity in the formation of a particular optical isomer.

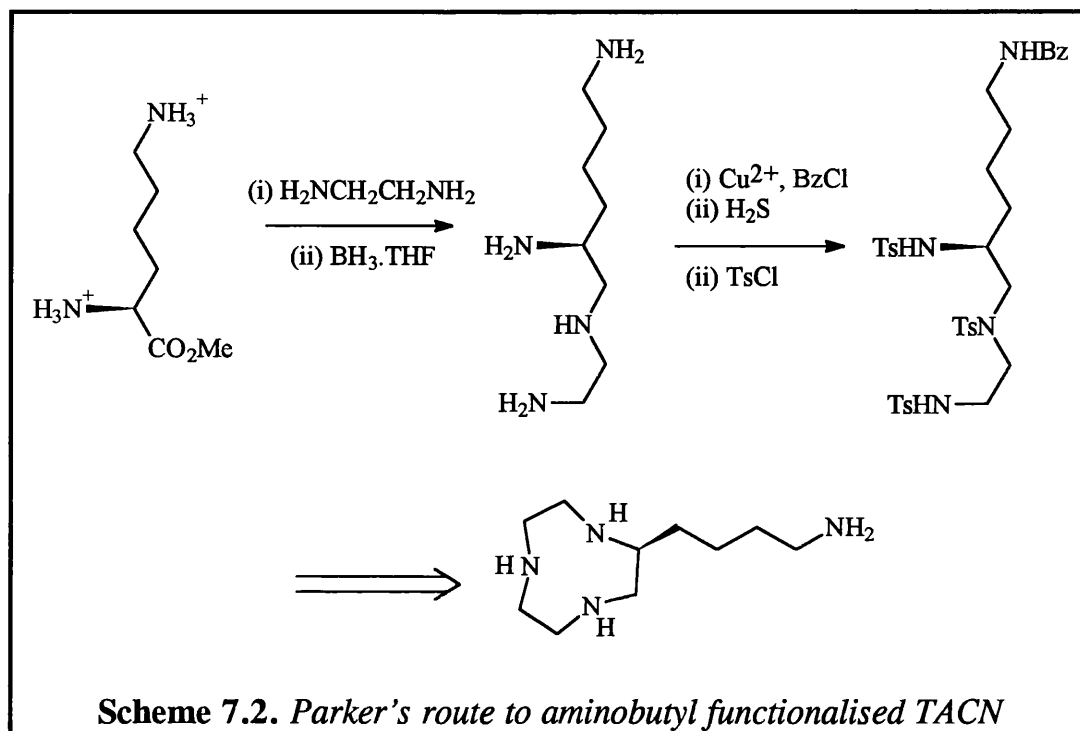
7.2 C-FUNCTIONALISED TACN DERIVATIVES

The first and simplest C-functionalised derivative of TACN was *R*-MeTACN (scheme 7.1), prepared by Mason & Peacock in 1975 (1). The cyclisation step in the ligand preparation was flawed in that it gave poor yields ($\sim 20\%$) of the required product and side reactions to linear and other cyclic products also occurred.



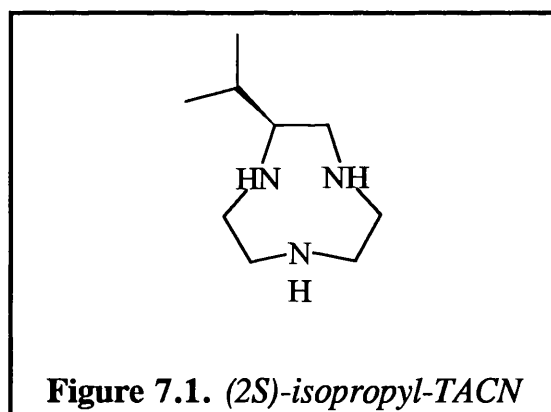
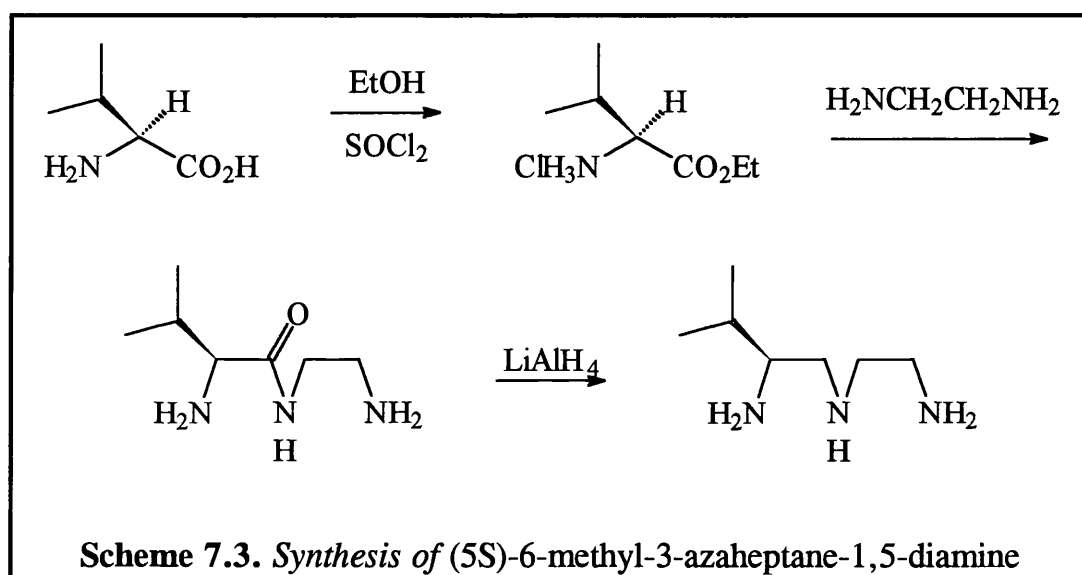
Using (2*S*)-lysine as a precursor, Parker (2) devised a route to an amino butyl derivative of TACN (scheme 7.2), the cyclisation step involved

a tosylated triamine which didn't have the polymerisation side reactions associated with scheme 7.1.



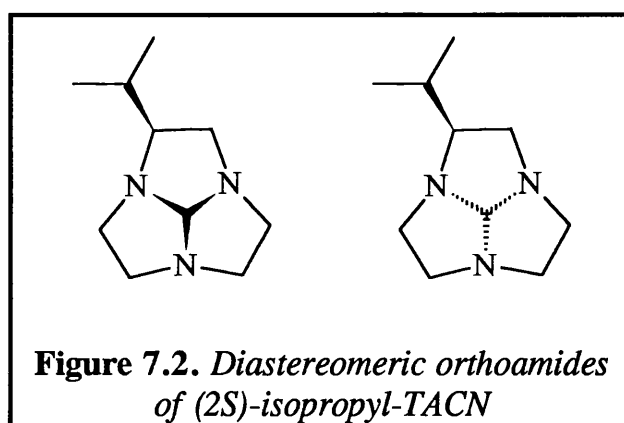
It was anticipated that modifications to Parker's scheme using small amino acids as building blocks would produce a chiral triamine, which could be cyclised to chiral TACN via a Richman-Atkins type synthesis. If possible the chiral starting materials and reducing agent were to be inexpensive so as to allow large scale production of the chiral product. Initial syntheses were concerned with the smallest chiral amino acid alanine, but the intermediate amide to the chiral amine was insoluble in THF, hindering the reduction process. Valine, although larger and more sterically hindered was successfully converted to the chiral triamine (5*S*)-6-methyl-3-azaheptane-1,5-diamine (scheme 7.3). The reaction scheme proved to be economical for

large quantities of the chiral amine and each stage in the reaction was high yielding and no further purification of the products was required. Direct application of the Richmann-Atkins synthesis should produce (2*S*)-isopropyl-TACN (figure 7.1).



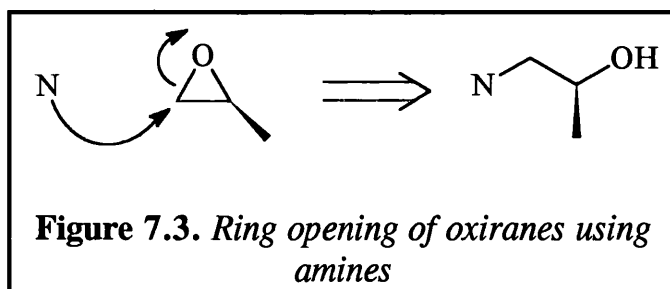
Adding chirality to the backbone of the macrocycle has its disadvantages as well as its apparent advantages. Although any ligand with three pendant arms is automatically chiral, the chirality can not be extended

to one and two pendant arm ligands, since the intermediate orthoamide required for such systems would consist of diastereoisomers (figure 7.2). Even if the diastereoisomers were separated, alkylating such an orthoamide would only lead to a horrendous mixture of products. The obvious way round this problem is to make the backbone chiral at three carbons with overall C_{3v} symmetry, but there is no easy synthetic route to such a system.

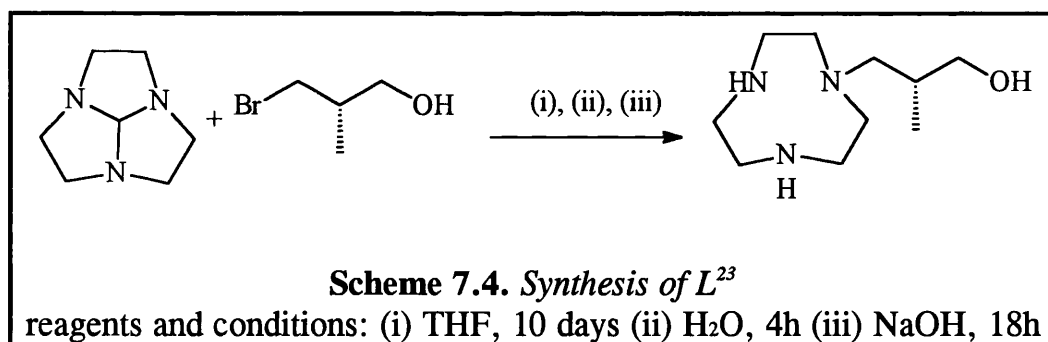


7.3 CHIRAL ALCOHOL PENDANT ARM MACROCYCLES

Using chiral oxiranes Peacock and Robb prepared (*S*) *N,N',N''*-tris(2-hydroxypropyl)-1,4,7-triazacyclononane (chapter 1). The synthetic strategy utilised the fact that for base catalysed cleavage of epoxides attack occurs at the less hindered carbon of the oxirane, resulting in a 100% regio- and stereospecific reaction (Figure 7.3).

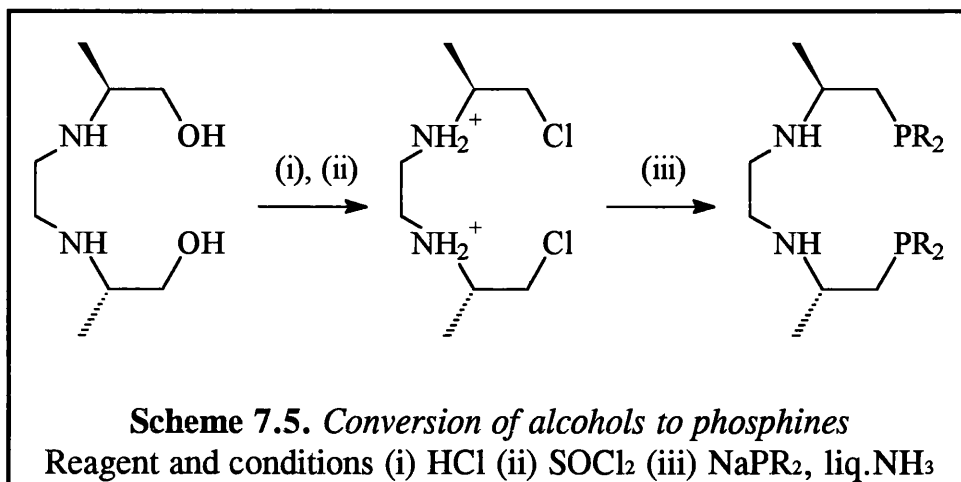


Schröder *et al.* extended this ring opening method to single and two pendant arm derivatives of TACN, but used achiral oxiranes (chapter 1). The length of the pendant arm is limited to two carbons by using oxiranes, so for longer pendant arms a different strategy is required. For L^{23} , a macrocycle with a single chiral propanol pendant arm, a different strategy was used (scheme 7.4), although the yield of the macrocycle was somewhat lower than those reported for epoxide ring opening reactions.



The conversion of these chiral alcohol pendant arms to chiral phosphine pendant arms should be possible using scheme 7.5 (3). Although L^{23} does have a distinct advantage over the shorter alcohol pendant arm ligands since the chiral centre is removed from the S_N2 reactions taking place. When a halide is part of a chiral centre racemisation may occur in the

presence of excess halide and since HCl is a side product from SOCl_2 halogenation reactions, scheme 7.5 may lead to racemisation of the chiral centre in the shorter pendant arm macrocycles.



7.4 COMPLEXES OF L^{23}

7.4.1 Cobalt Complexes of L^{23}

Cobalt complexes of tris-alcohol appended triazamacrocycles have been studied extensively over the past decade (4-8). The Co(II) complexes of TACN based ligands rapidly oxidise in air to form Co(III) , with the exception of a bridging 10 coordinate ligand which stabilises Co(II) in neutral conditions and oxidises to Co(III) at higher pH (chapter 1). Macrocyclic ring sizes of 10 or more form air-stable Co(II) complexes that are resistant to chemical oxidation. It was therefore expected that tetradentate

L^{23} would form a tetrahedral Co(II) complex which may or may not oxidise aerobically to Co(III). Under an inert atmosphere L^{23} forms an intense blue Co(II) complex, indicative of tetrahedral geometry. The solution rapidly turns intense purple when exposed to the atmosphere, suggesting that the Co(II) has oxidised to Co(III). The ^1H NMR and electronic spectra of this purple complex are presented, but do not lead to a conclusive assignment of the oxidation state or coordination number of the complex.

Octahedral Co(III) complexes have a d^6 configuration and are almost exclusively low spin, whereas tetrahedral Co(II) complexes are paramagnetic d^7 species with three unpaired electrons. Sharp, unshifted NMR spectra are therefore obtained for diamagnetic Co(III) complexes and broad, shifted spectra are obtained for Co(II) complexes. The NMR of the purple complex (figure 7.4) does contain broad resonances, but little shifting is observed when compared to the free ligand (figure 7.11). Therefore, the NMR data suggests an octahedral Co(III) complex over a tetrahedral Co(II) complex, the broadening is most probably due to a paramagnetic Co(II) impurity in the sample.

The electronic spectra of octahedral Co(III) complexes usually consist of two $d \rightarrow d$ bands in the visible region, the higher energy band is assigned to the $^1A_{1g} \rightarrow ^1T_{2g}$ transition and the other is assigned to $^1A_{1g} \rightarrow ^1T_{1g}$. Tetrahedral Co(II) complexes exhibit one transition in the visible region assigned to the $^4A_2 \rightarrow ^4T_1(P)$ transition and two bands in the near infra-red

region assigned to the ${}^4A_2 \rightarrow {}^4T_1(F)$ and ${}^4A_2 \rightarrow {}^4T_2$ transitions, although the latter is rarely observed. The electronic spectrum of the purple cobalt complex of L^{23} is shown on figure 7.5 and consists of one shouldered band at 565nm and with a molar extinction coefficient of $140\text{dm}^3\text{cm}^{-1}\text{mol}^{-1}$. The size of the extinction coefficient for the 565nm band is consistent with octahedral Co(III) with the shoulder probably due to a Co(II) impurity. The 565nm band is characteristic of the ${}^1A_{1g} \rightarrow {}^1T_{1g}$ transition for similar Co(III) complexes, but the region where the ${}^1A_{1g} \rightarrow {}^1T_{2g}$ transition would be observed is obscured by a charge transfer band.

From the ${}^1\text{H}$ NMR and electronic spectra alone, no definite oxidation and coordination number can be assigned to the cobalt complex. Previous systems with a N_3O_3 donor set and 9 membered ring may form Co(III) complexes, but it would only be speculative to conclude that L^{23} forms a octahedral Co(III) complex.

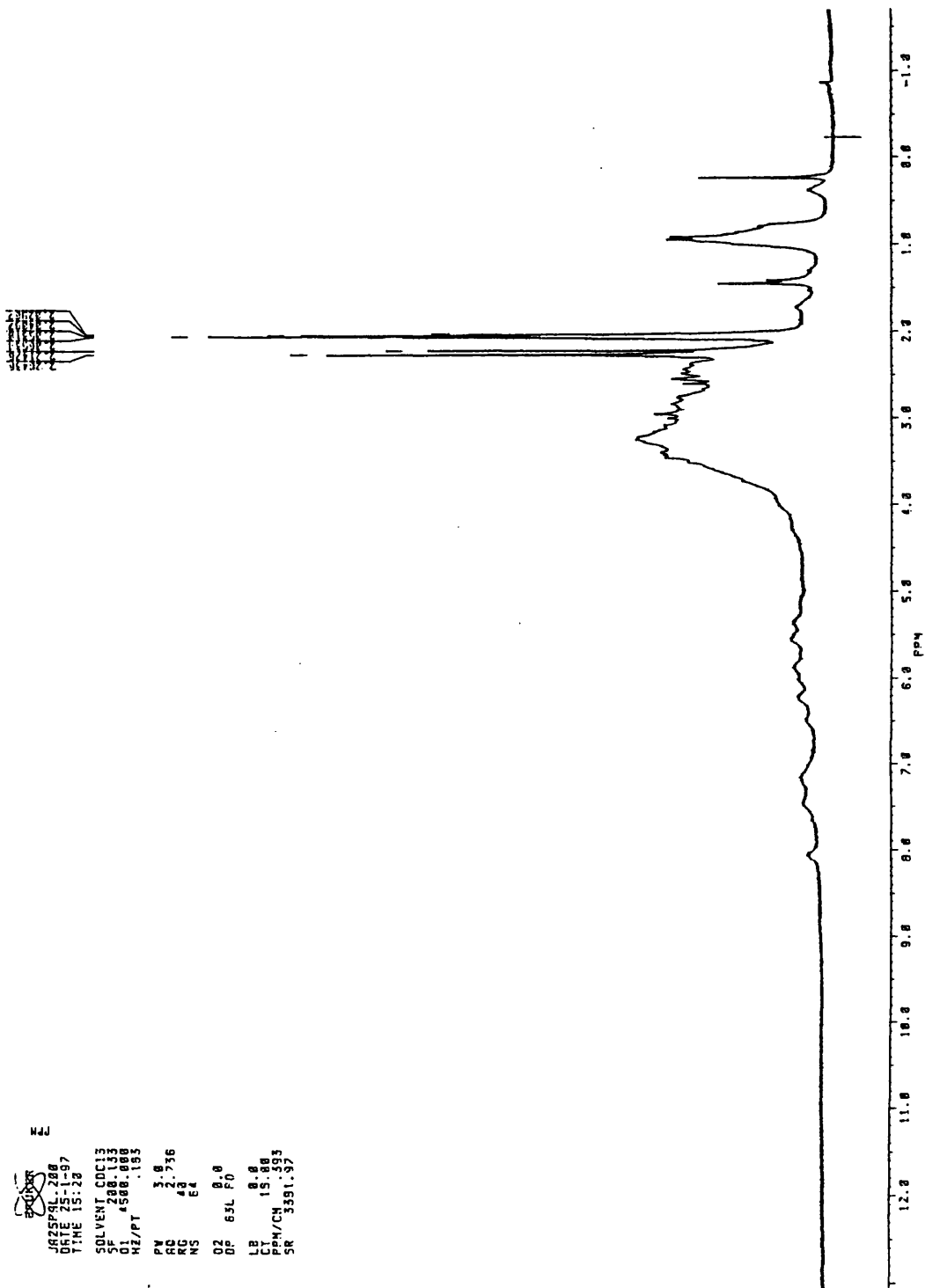


Figure 7.4. ¹H NMR spectrum of cobalt complex with L²³ in d₃-MeCN

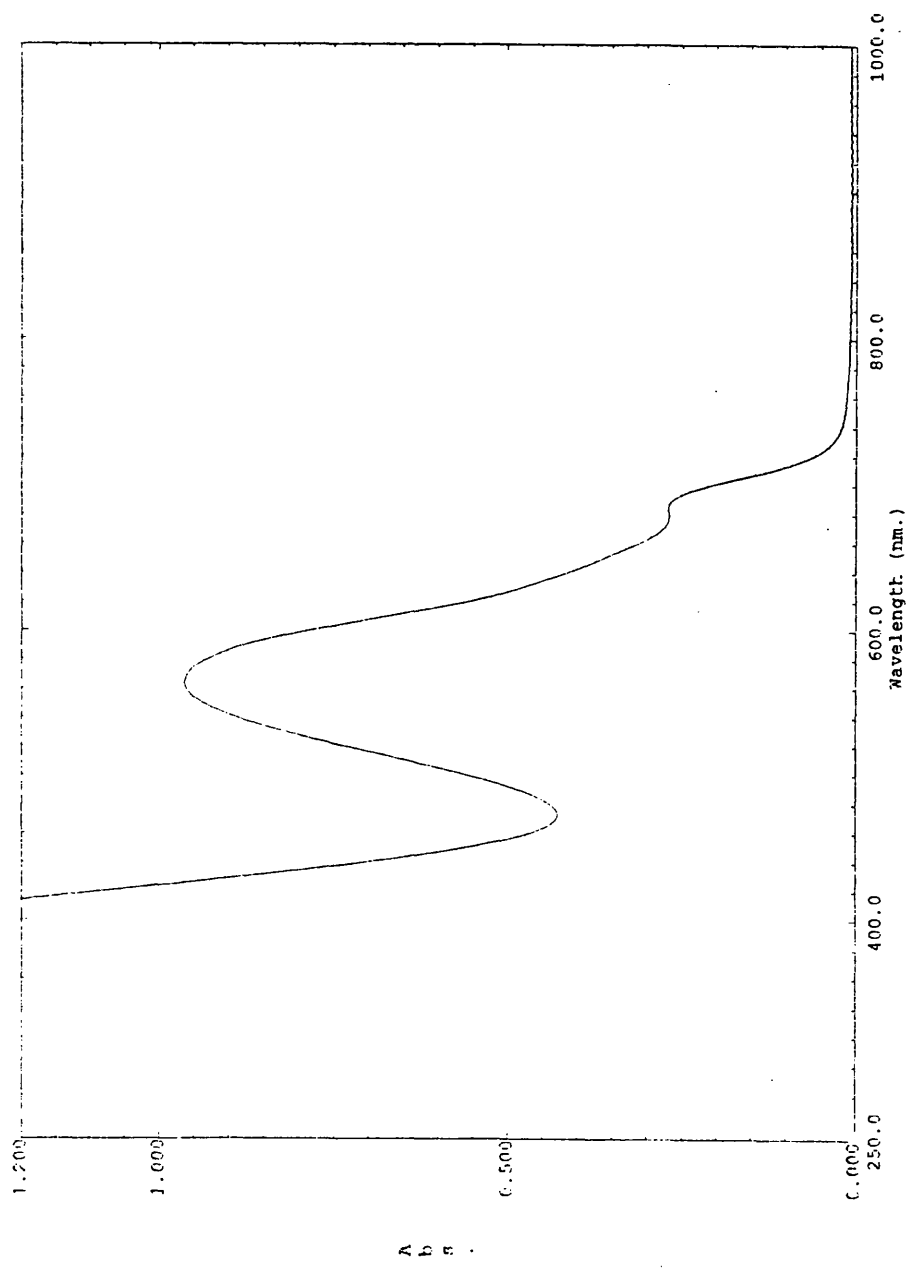


Figure 7.5. *Electronic spectrum of cobalt complex with L^{23} in acetonitrile*

7.4.2 Copper Complex of L²³

Previous chapters have discussed hydroxide bridged copper(II) dimers where the pendant arm was incapable of coordinating to the Cu(II) centre. Functionalising TACN with a single alcohol pendant arm would allow copper(II) dimers to be formed where the pendant arm could act as a bridging alkoxide unit (9, 10). Reaction of L²³ with Cu(NO₃)₂·3H₂O produced the monomeric complex [CuL²³(NO₃)](NO₃) (figure 7.6). It was anticipated that at increasing the pH would promote alkoxide bridge formation (as well as hydroxide bridge formation), but no crystalline sample was obtained from higher pH values. The copper(I) complex of L²³ was oxidised using identical conditions used for the previous copper dimers, but no pure crystalline sample could be obtained from the reaction mixture.

The structure of [CuL²³(NO₃)](NO₃) looks like a distorted octahedral geometry, but a closer inspection of the bond lengths and angles (Table 7.1) show that the Cu1-O21 bond of the coordinated nitrate is extremely long (2.567 Å) and is probably better described as an interaction. When the cation is drawn as a five coordinate species (figure 7.7), the structure is similar to the square based pyramidal dimers discussed in previous chapters, indeed the bond lengths are similar to those observed in the other copper dimers (Table 7.2).

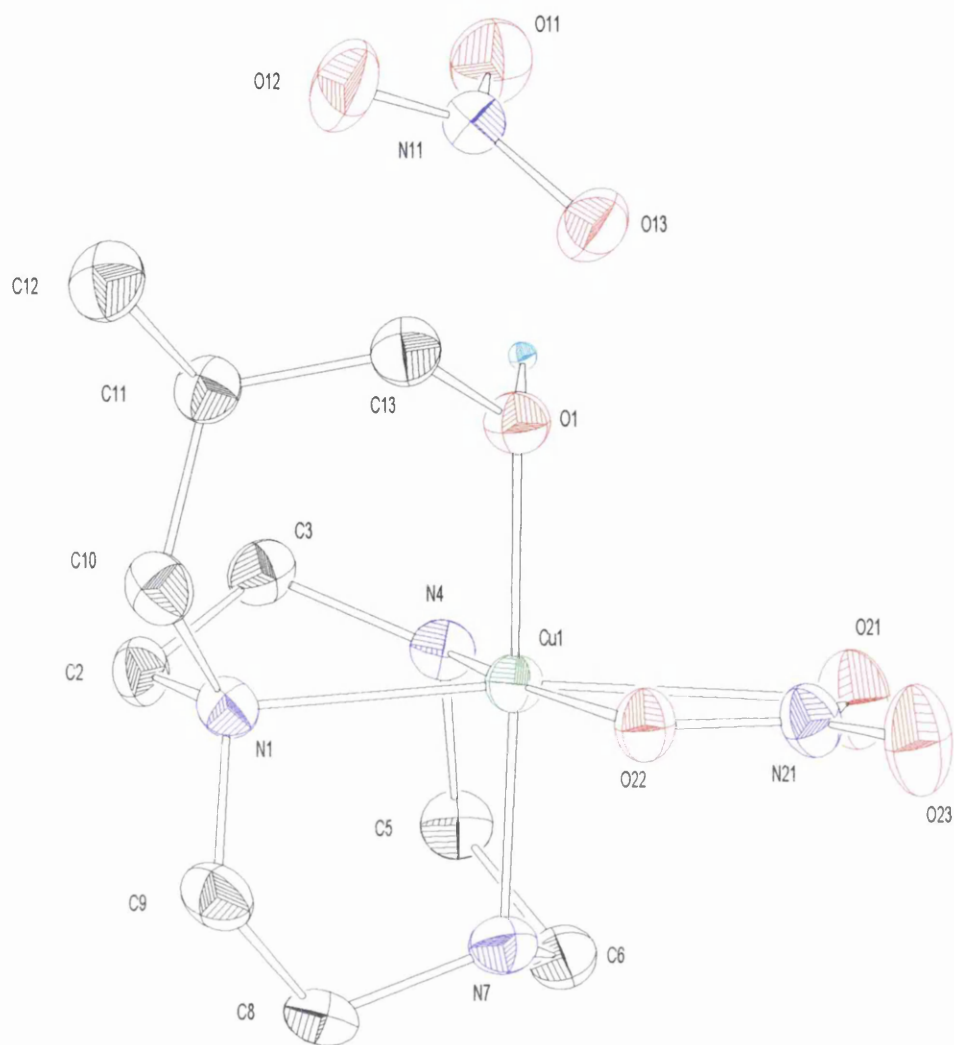


Figure 7.6. Crystal Structure of $[\text{CuL}^{23}(\text{NO}_3)][\text{NO}_3]$

Crystal data for $\text{C}_{10}\text{H}_{23}\text{CuN}_5\text{O}_7$: $M=388.9$; Orthorhombic; Space Group $P2_12_12_1$; $a=9.9140(5)\text{\AA}$; $b=11.7680(7)\text{\AA}$; $c=14.115(2)\text{\AA}$; $U=1646.7(2)\text{\AA}^3$; $Z=4$; $D_{\text{calc.}}=1.57\text{gcm}^{-3}$; $F(000)=812$; $\mu(\text{MoK}\alpha)=1.369\text{cm}^{-1}$; $R(R_w^2)=0.026(0.065)$.

Cu1-N1	2.194(2)Å	Cu1-O1	1.975(2)Å
Cu1-N4	2.037(2)Å	Cu1-O21	2.567(2)Å
Cu1-N7	1.998(2)Å	Cu1-O122	2.013(2)Å
N1-Cu1-O1	92.86(9)°	N1-Cu1-N4	85.15(9)°
N4-Cu1-O1	95.50(9)°	N1-Cu1-N7	85.30(9)°
N7-Cu1-O1	178.12(9)°	N4-Cu1-N7	84.74(10)°
N1-Cu1-O22	108.53(8)°	O1-Cu1-O22	87.41(9)°
N4-Cu1-O22	165.90(8)°	O1-H1-O13	164.98°
N7-Cu1-O22	92.80(9)°	O21-Cu-O22	54.66(9)°

Table 7.1. Selected bond lengths and angles for $[\text{CuL}^{23}(\text{NO}_3)]/[\text{NO}_3]$

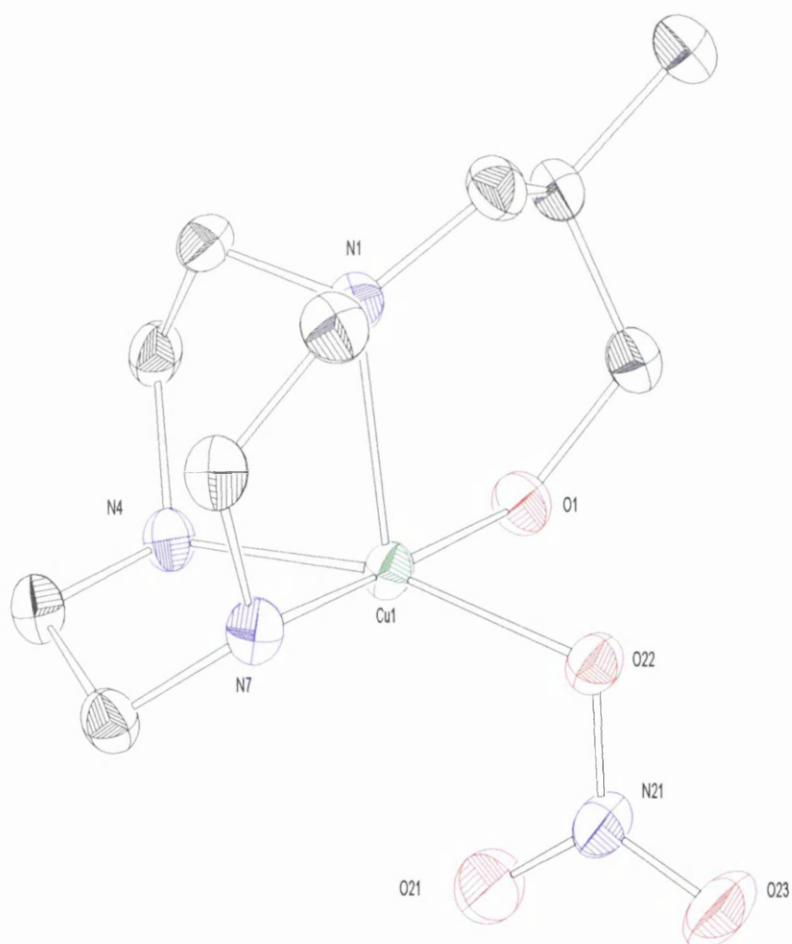


Figure 7.7. $[\text{CuL}^{23}(\text{NO}_3)]^+$ as a five coordinate copper complex

	Cu-N _{ax}	Cu-N _{eq}	Cu-O
[CuL ²³ (NO ₃)] ⁺	2.194Å	2.018Å	1.994Å
[Cu ₂ L ⁵ (OH) ₂] ²⁺	2.359Å	2.026Å	1.930Å
[CuL ¹⁰ (OH) ₂ L ¹⁰ Cu] ²⁺	2.258Å	2.029Å	1.928Å
[CuL ¹² (OH) ₂ L ¹² Cu] ²⁺	2.298Å	2.078Å	1.924Å
[CuL ¹⁴ (OH) ₂ L ¹⁴ Cu] ²⁺	2.267Å	2.054Å	1.928Å

Table 7.2. Comparison of Cu-N and Cu-O bond lengths

Divalent complexes of the shorter tris alcohol pendant arm ligands reported by Peacock contained the protonated form of the alcohol. The alcohol group of L²³ is still protonated in the complex and is hydrogen bonded to the second nitrate counter ion (H1-O13=1.84Å). The least basic tertiary nitrogen forms the longest Cu-N bond and is found at the apex of the square pyramid structure. The electronic spectrum of the complex (figure 7.8) contains two bands at 650nm ($\epsilon=97\text{dm}^3\text{mol}^{-1}\text{cm}^{-1}$) and 1160nm ($\epsilon=34\text{dm}^3\text{mol}^{-1}\text{cm}^{-1}$) which indicate a square based pyramidal environment around copper(II) ion (**11**).

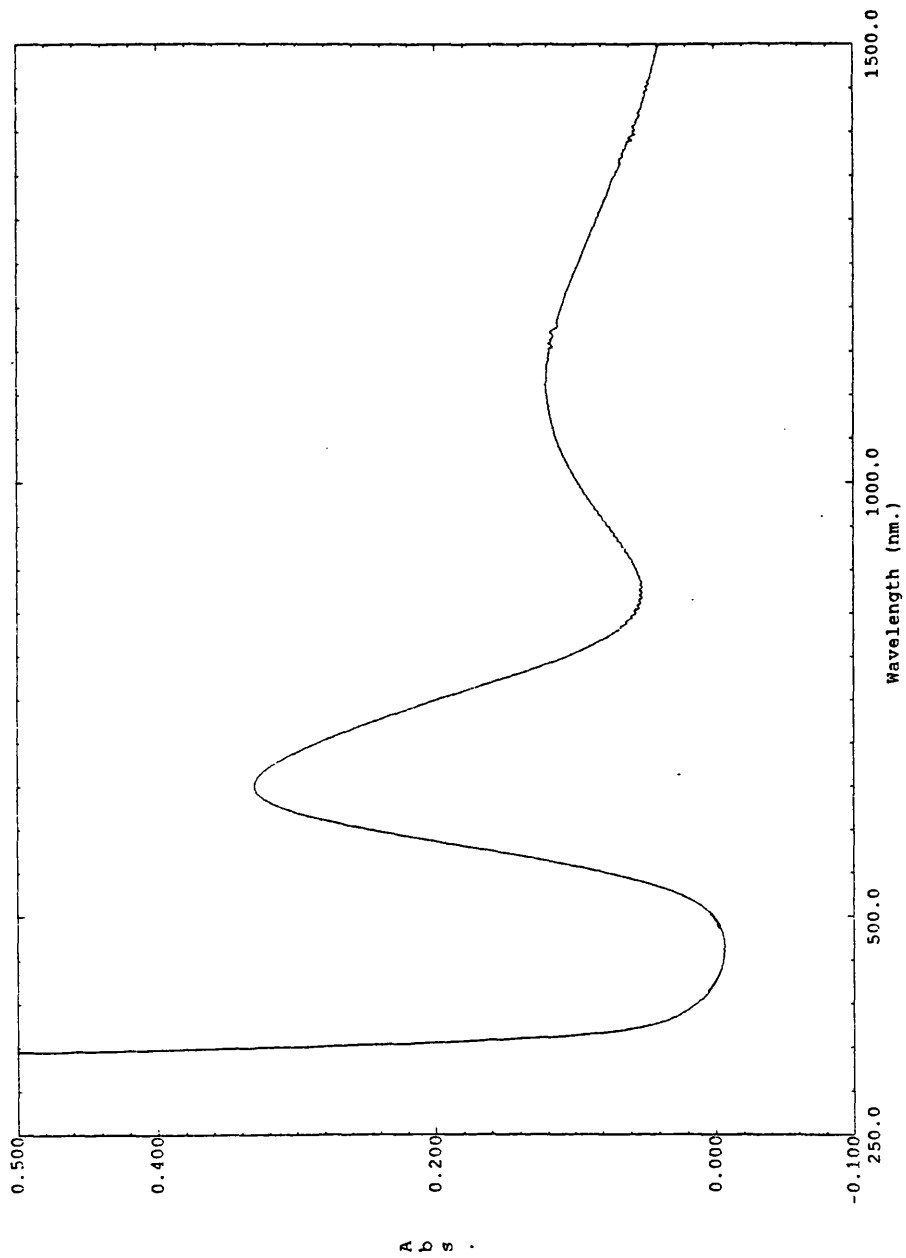


Figure 7.8. *Electronic spectrum of $[\text{CuL}^{23}(\text{NO}_3)]/[\text{NO}_3]$*

7.4.3 Zinc Complex of L²³

In the absence of LFSE it is assumed that structure of a zinc complex will be dominated by the steric requirements of the particular ligand involved. With tetradentate L²³ one would expect a tetrahedral complex, but as observed in the previous chapter, tetradentate L¹⁶ forms octahedral complexes with zinc(II) in the presence of chloride ions. Attempts to crystallise the zinc(II) complex of L²³ were unsuccessful, although the ¹H and ¹³C NMR spectra are well resolved and presented in figures 7.9 and 7.10 respectively. The methyl resonance ($\delta=0.58\text{ppm}$) in the ¹H NMR is unshifted compared to the free ligand (figure 7.11), but the remainder of the spectrum is shifted downfield and very complex. The shift of the pendant arm methylenes is of particular interest; in the free ligand both methylenes are observed as a broad doublet at 3.3ppm, but in the complex the terminal CH₂OH is shifted more downfield than -NCH₂-CH(Me)CH₂OH. This shift is unsurprising considering zinc's role in nature is to enhance the ionization of water. In the ¹³C NMR spectrum of the complex all 10 carbons are distinguished, whereas with the free ligand only 7 carbon resonances are observed (figure 7.12). No conclusions can be made on the configuration around the zinc ion, since four, five or six coordinate structures are possible with the presence of chloride and water in the system, all of which would be consistent with the NMR data.

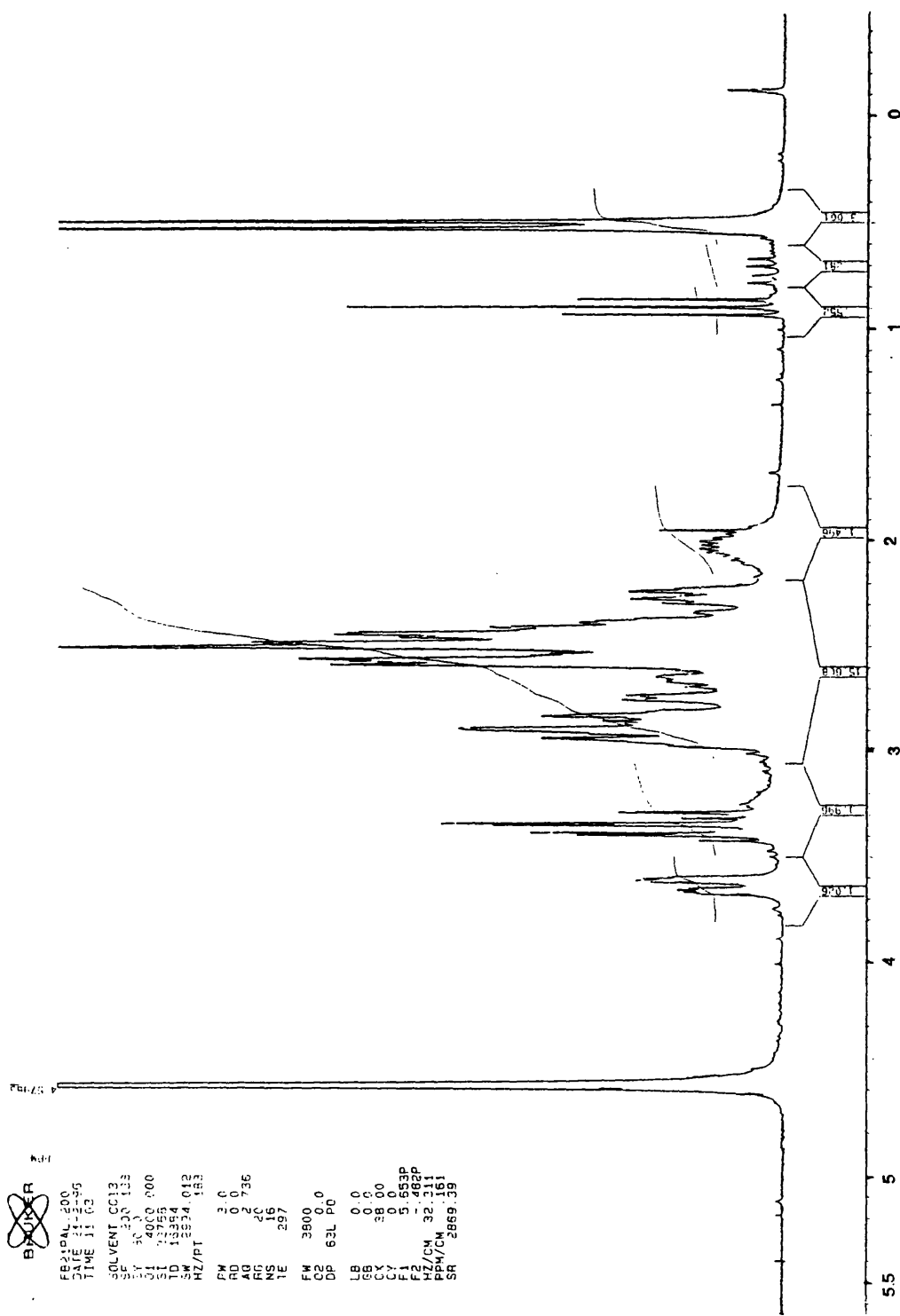


Figure 7.9. ^1H NMR of the Zn(II) complex with L^{23} in D_2O

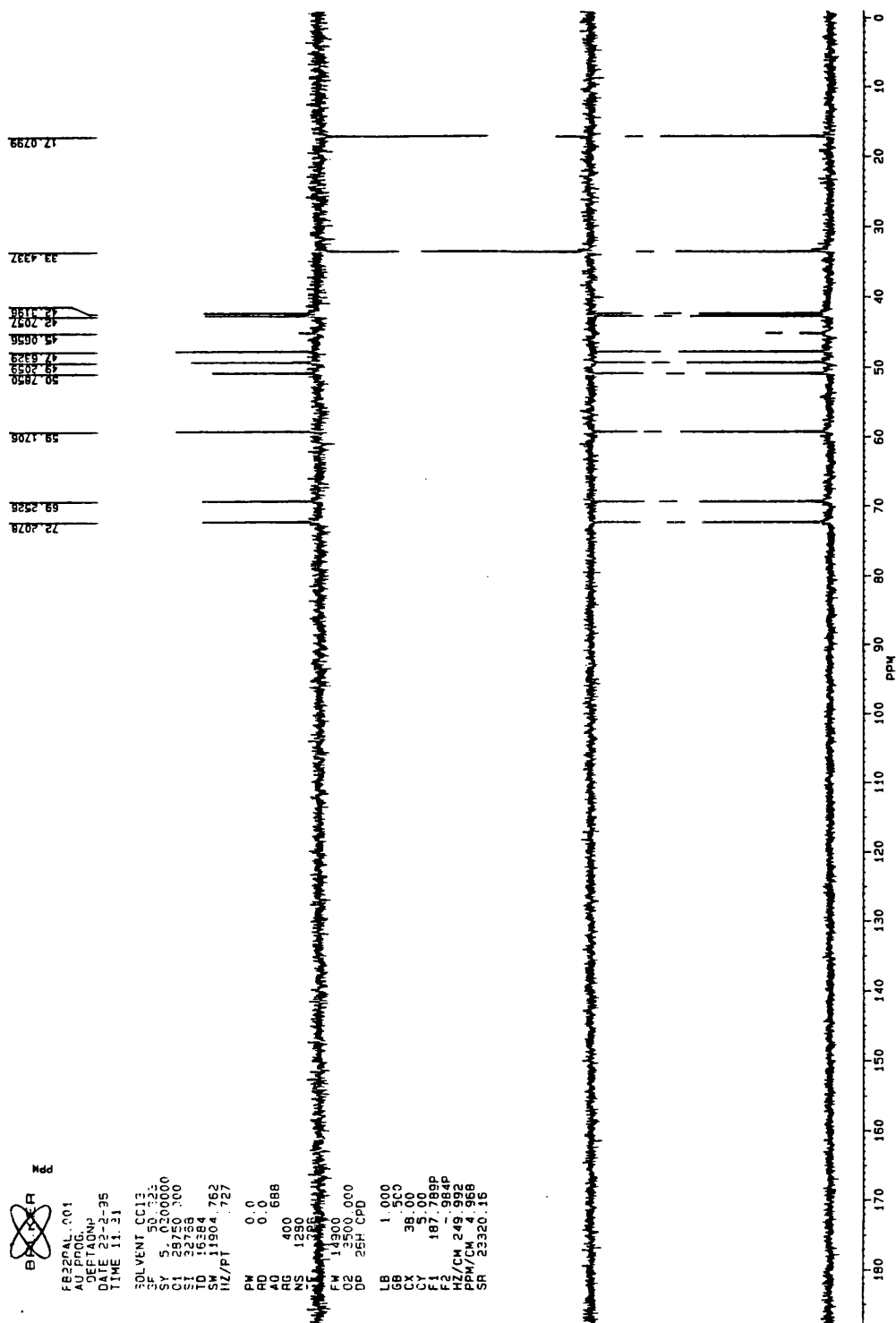


Figure 7.10. ^{13}C NMR of the Zn(II) complex with L^{23} in D_2O

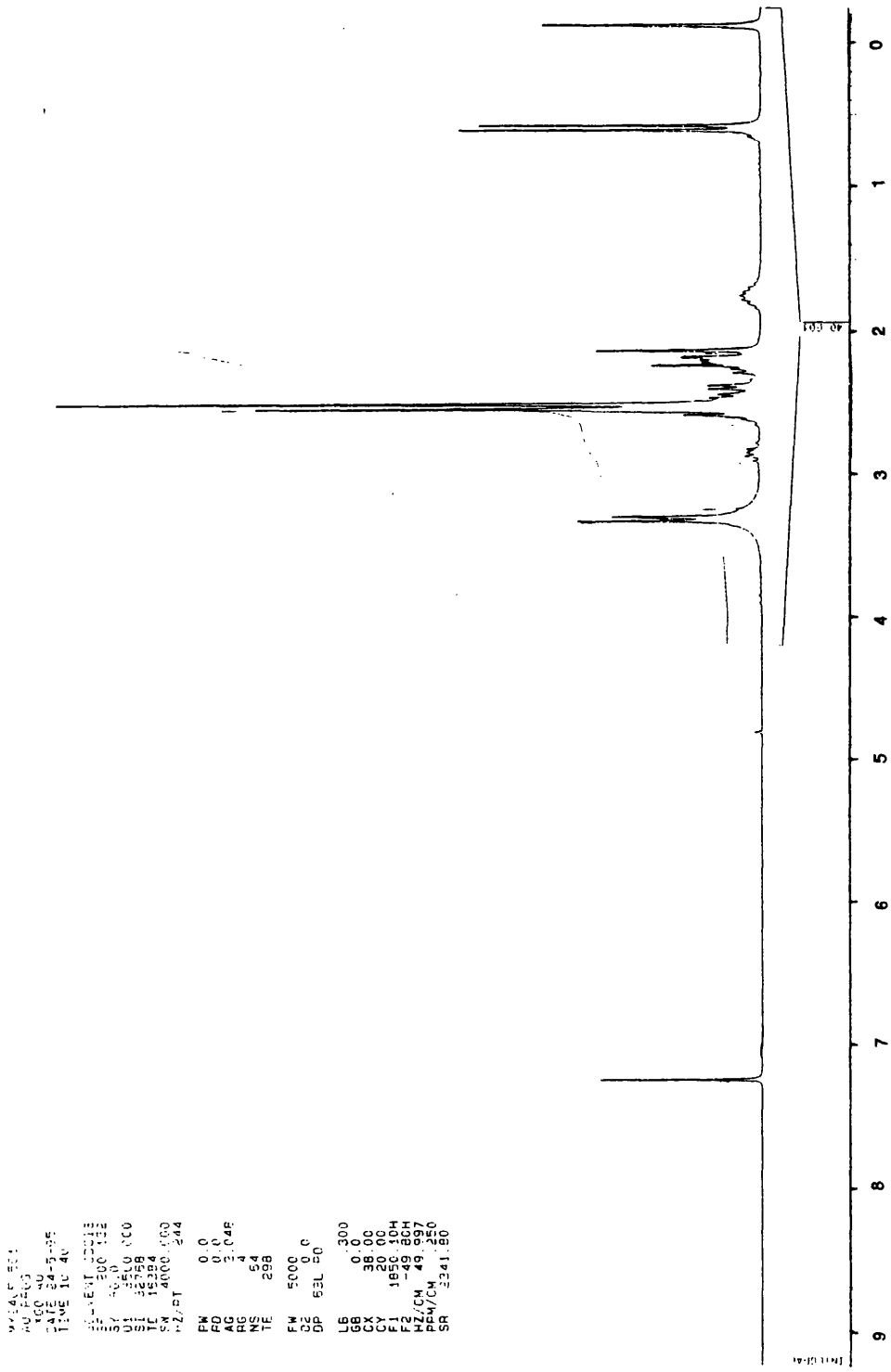


Figure 7.11. ¹H NMR of L²³ in CDCl₃

BAKER
 M241F 101
 AU 1000 AL
 DATE 1984-09-09
 TIME 11.11
 SOLVENT CDCl₃
 SF 500000.000
 SI 32768.000
 ST 32768.000
 TD 15364
 SM 12500.000
 HZ/PT 763
 PW 0.0
 RD 0.0
 AD 0.555
 RG 800
 NS 640
 TE 298
 FM 15700
 OF 3500.000
 DP 26H 00
 LB 1.000
 GB 0.0
 CX 35.00
 F1 9550.48H
 F2 -399.02H
 HZ/CM 249.987
 PPM/CM 4.985
 SR 23319.40

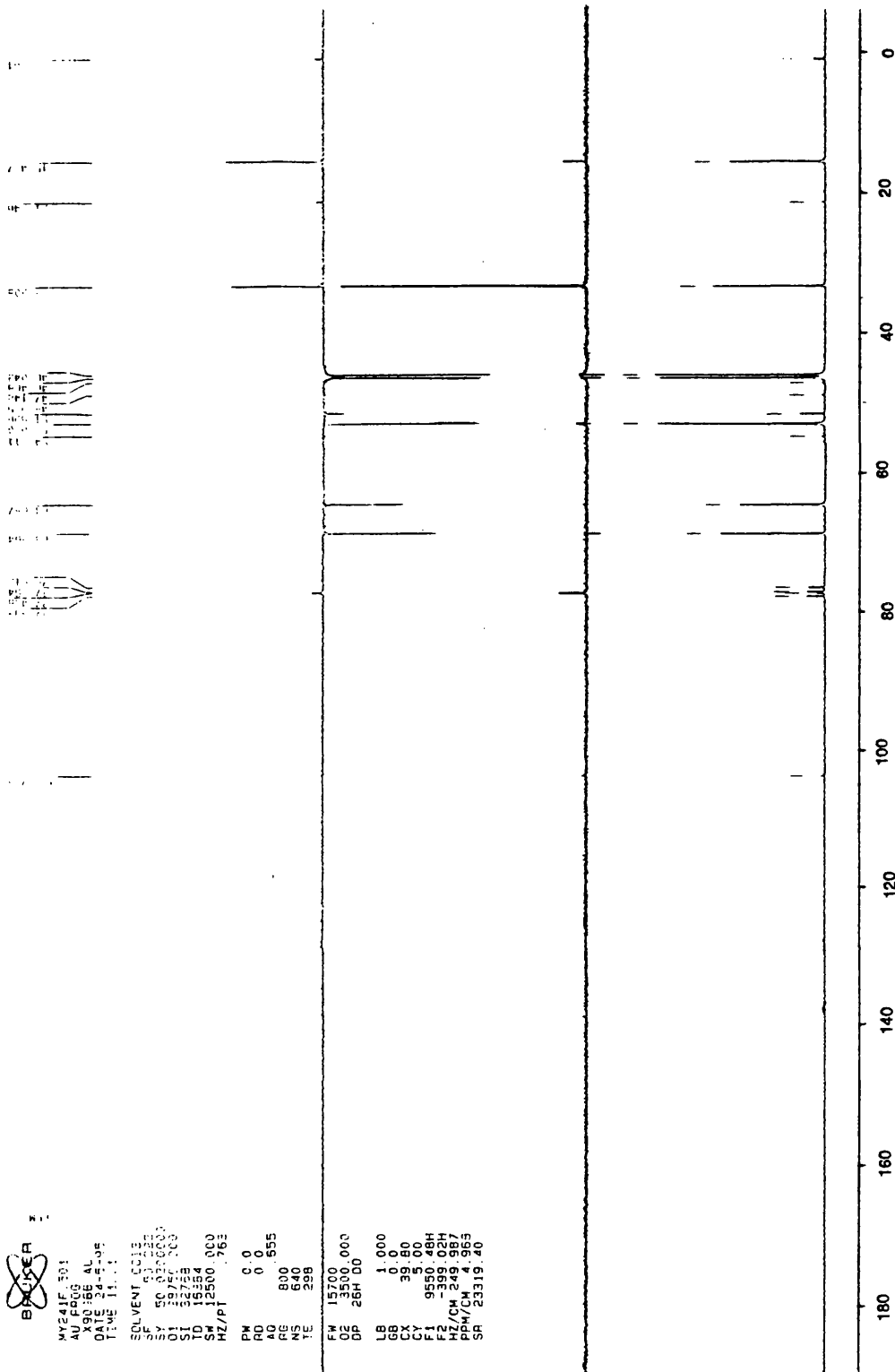
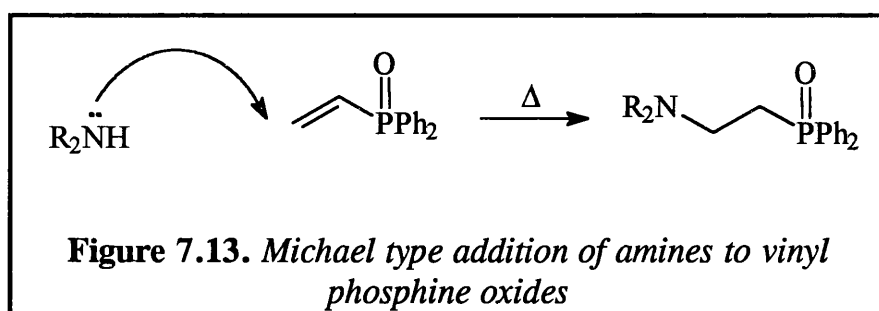


Figure 7.12. ¹³C NMR of L²³ in CDCl₃

7.5 L²² and its Cobalt(II) complex

The addition of amines to α,β -unsaturated carbonyl compounds to form amino β -amino ketones and aldehydes is well known in organic chemistry. The same addition can be carried out with vinyl phosphine oxides acting as α,β -unsaturated species, the result being a β -amino phosphine oxide (figure 7.13) (12).



As mentioned in the previous chapter, phosphine pendant arm macrocycles based on TACN can be synthesised with a pendant arm length of one, three or more carbons, but not two. Using TACN as the amine in the above reaction, it was possible to form the corresponding β -amino phosphine oxide L²². It was envisaged that the reduction of the phosphine oxide groups of L²² would produce a phosphine pendant arm macrocycle with an arm length of two carbons. The standard method of phosphine oxide reduction involves the use of silane reagents, Cl₃SiH being the most commonly used silane (13). L²² does not reduce cleanly with silanes and reduction with

LiAlH_4 is unsuitable due to the ligand's poor solubility and tendency to form gels in ethers.

Although there are numerous reports on the coordination compounds of phosphinic and phosphonic acid derivatives of TACN, there is only one report on the coordination chemistry of the phosphine oxide derivative of TACN *N,N'N''*-tris(diphenylphosphinylmethyl)-1,4,7-triazacyclononane (**14**). The ligand has one carbon less in the pendant arm than L^{22} and forms two distinct Co(II) complexes, one complex is four coordinate Co(II) where the ligand bridges two Co(II) ions and is tridentate to each cobalt, the other complex is a mononuclear octahedral complex with the ligand tetradentate.

A reaction mixture of L^{22} and CoCl_2 in ethanol with an exact ratio of 1:1 ratio forms a blue complex indicating a tetrahedral geometry round Co(II) . When a very small excess ($\sim 5\%$) of L^{22} is added to the reaction mixture an immediately colour change from blue to pink is observed. The addition of CoCl_2 does not reverse the colour change, even with gentle refluxing. The addition of NH_4PF_6 in ethanol precipitated the complex as a pink microcrystalline complex, recrystallisation was achieved by vapour diffusion of diethyl ether into an acetonitrile solution. The microanalysis results are presented below:

C 49.5% H 4.7% N 4.0% P 17.0%

These results give the ratio $C_{43}H_{49}N_3P_6$, but no combination of Co, L^{22} , PF_6 gives these results, even considering excess NH_4PF_6 , molecules of solvation and coordinating chloride ions.

The infrared of the free ligand shows $\nu(P=O)$ at 1188cm^{-1} , and on complexation to Co(II) reduces to 1141cm^{-1} with a very weak band remaining at 1188cm^{-1} . This suggests that all three pendant arms are coordinated to the Co(II), unlike the Co(II) complex reported by Kabachnik *et al.* where there was still strong absorption for the free P=O stretching frequency after complexation.

The electronic spectrum (figure 7.14) of the complex consists of two bands and is consistent with octahedral Co(II). The first band is observed at 515nm has been assigned to the ${}^4T_{1g}(F) \rightarrow {}^4T_{1g}(P)$ transition, the shoulder (540nm) has been assigned to the two electron transition ${}^4T_{1g}(F) \rightarrow {}^4A_{2g}$ and the other band observed at 1135nm has been assigned to the ${}^4T_{1g}(F) \rightarrow {}^4T_{2g}$ transition. The positions of these bands are almost identical to those observed in the octahedral Co(II) complex $[Co(NCS)_2L']$ where $L' = N,N',N''$ -tris(diphenylphosphinylmethyl)-1,4,7-triazacyclononane and was acting as a tetradentate ligand.

Although the microanalysis results prove nothing conclusive alone, it must be noted that the P content is obtained manually whereas the C H N content is determined in an automated process. Thus ignoring the phosphorus result, correct values for C H N content can be obtained for $[CoL^{22}][PF_6]_2$

(Calc. C 49.6% H 4.7% N 3.6%). It is also noteworthy to mention that the microanalysis sample was taken from a large single pink crystal (0.5cm x 0.75cm x 0.25cm) of the complex, indicating that the sample submitted was sufficiently pure and didn't contain an ambiguous amount of unknown material. Unfortunately rapid loss of solvent from this single crystal prevented structural analysis by X-ray diffraction techniques, further attempts at crystallising single X-ray quality crystals using the same conditions were unsuccessful. Thus it can be concluded that from the infrared and electronic spectra, the Co(II) is octahedral with probably all three arms coordinated to the metal, surprising considering the steric bulk of each arm.

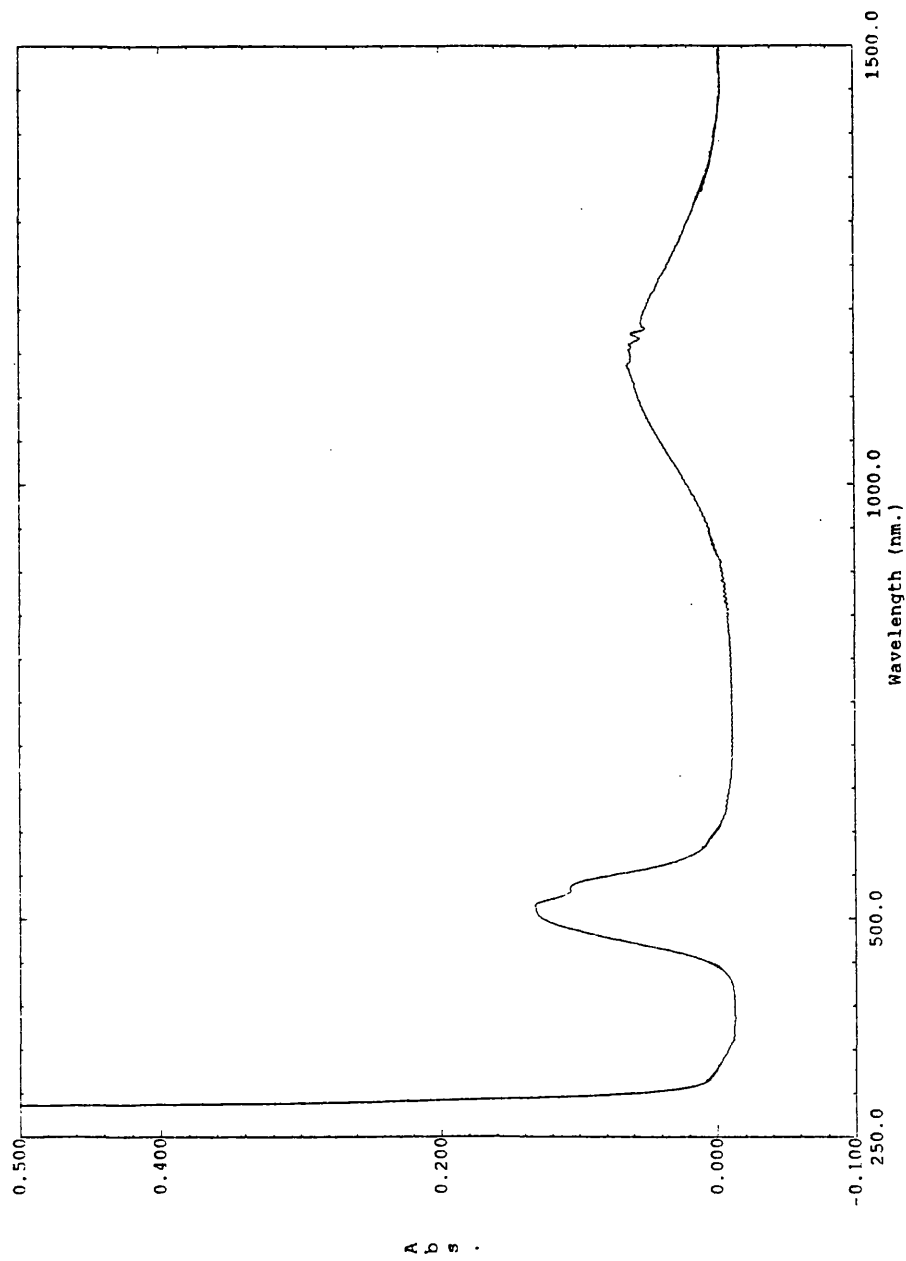


Figure 7.14. *Electronic spectrum of the Co(II) complex with L^{22} in acetonitrile*

REFERENCES

1. S.F. Mason, R.D. Peacock, *Inorg. Chim. Acta.*, 1976, **19**, 75.
2. J.P.L. Cox, A.S. Craig, I.M. Helps, K.J. Janlowski, D. Parker, M.A.W. Eaton, A.T. Millican, K. Millar, N.R.A. Beeley, B.A. Boyce, *J. Chem. Soc., Perkin Trans. 1*, 1990, 2567.
3. M. Atoh, K. Kashiwabara, J. Fujita, *Bull. Chem. Soc. Jpn.*, 1985, **58**, 3492.
4. J. Robb, *Ph.D. Thesis, University of Glasgow*, 1987.
5. I.A. Fallis, *Ph.D. Thesis, University of Glasgow*, 1992.
6. A.A. Belal, L.J. Farrugia, R.D. Peacock, *J. Chem. Soc., Dalton Trans.*, 1989, 931.
7. H. Al-Sagher, I.A. Fallis, L.J. Farrugia, R.D. Peacock, *J. Chem. Soc., Chem. Comm.*, 1993, 1499.
8. A.J. Blake, T.M. Donlevy, P.A. England, I.A. Fallis, S. Parsons, S.A. Ross, M. Schröder, *J. Chem. Soc., Chem. Comm.*, 1994, 1981.
9. S.A. Ross, *Oral Presentation, RSC Predoctoral Symposium, Glasgow 1993*.
10. D. Schulz, T. Weymüller, K. Wiegardt, C. Butzlaff, A.X. Trautwein, *Inorg. Chim. Acta.*, 1996, **246**, 387.
11. B.J. Hathaway, A.A.G. Tomlinson, *Coord. Chem. Rev.*, 1970, **5**, 1.

12. G. Maerkl, B. Merkl, *Tet. Lett.*, 1981, **22**, 4459.
13. *The Chemistry Of Organophosphorus Compounds, Volume 1*, ed. F.R. Hartely, Wiley, New York, 1990, p167.
14. M.I. Kabachnik, T.Ya. Medved, B.K. Shcherbakov, E.I. Sinyavskaya, M.Yu. Polikarpov, K.B. Yatsimirskii, *Russ. J. Inorg. Chem.*, 1985, **30**, 1463.

CHAPTER 8

GENERAL CONCLUSIONS

L^{10} and L^{11} formed extremely air sensitive Cu(I) complexes in which the amine functions and the olefin pendant arm coordinate to the Cu(I) centre. The highly basic amine functions of the ligands enhance the amount of π -backbonding in the Cu(I)-olefin bond, but also reduces the Cu(I)/Cu(II) redox potential allowing easier oxidation of the complex. L^{11} formed a complex with Ag(I), but only one nitrogen appeared to be coordinated to the metal centre and the amount of π -backbonding was less pronounced.

The dinucleating xylene ligands L^4 - L^6 formed Cu(I) complexes with the rate at which the Cu(I) complexes oxidised being proportional to the distance between the TACN units in the ligand. The ligands containing olefin pendant arms (L^{10} , L^{12} , L^{14} , L^{15}) also formed Cu(I) complexes which oxidised to Cu(II) complexes. Two Cu(II) complexes were isolated for L^{10} ; a bis-ligand Cu(II) complex and a hydroxide bridged Cu(II) dimer. The monomeric complex is Jahn-Teller distorted with an exceptionally long Cu-N axial bond. A shorter bond would result in increased steric congestion around the Cu(II) centre and a destabilisation of the complex. The second Cu(II) complex containing L^{10} was a hydroxide bridged Cu(II) dimer. Only hydroxide bridged dimers were isolated for the other ligand systems. The dimeric structures containing L^{10} , L^{12} or L^{14} showed similar geometries about the metal centre. The dimeric Cu(II) complex of L^5 showed a different geometry due to the steric demands of the ligand. Molecular models show that a hydroxide bridged Cu(II) dimer is possible for L^4 , but L^6 appears to be

to large for the spatial requirements for a $\text{Cu}(\mu\text{-OH})_2\text{Cu}$ core. None of the Cu(I) complexes bind O_2 at low temperature to form peroxo species.

The Cu(I) complex of L^{12} reductively couples two CO_2 molecules in the presence of trace amounts of water to form an oxalate bridged Cu(II) dimer. The Cu(I) complex reacted with bicarbonate to produce a similar oxalate dimer, indicating that a bicarbonate intermediate is involved in the formation of oxalate.

Phosphine pendant arm macrocycles were prepared from olefin pendant arm macrocycles by the photolytic addition of diphenylphosphine across the olefin double bond. The ligands formed complexes with metals in low or zero valance states, with the zerovalent complexes being unstable. The Zn(II) and Ni(II) complexes characterised for L^{16} have unusually long M-P distances

The hard hexadentate ligand L^{22} coordinates to Co(II) forming an octahedral complex. All three phosphine oxide pendant arms appear to be coordinated to the same metal centre, surprising considering the steric bulk of the pendant arms.

The tetradentate chiral alcohol ligand L^{23} behaves much like its hexadentate ligand analogues. Its Co(II) complex is extremely oxygen sensitive, oxidising immediately in air to form a Co(III) species. The Cu(II) complex has been structurally characterised and is monomeric with the alcohol function protonated, the geometry around the metal centre is very

similar to that observed in the hydroxide bridged Cu(II) dimers mentioned earlier.